

UNCLASSIFIED

AD NUMBER
AD822349
NEW LIMITATION CHANGE
TO Approved for public release, distribution unlimited
FROM Distribution authorized to U.S. Gov't. agencies and their contractors; Critical Technology; SEP 1967. Other requests shall be referred to Army Missile Command, Attn: AMSMI-RR, Redstone Arsenal, AL, 35809.
AUTHORITY
usamc ltr, 4 jun 1973

THIS PAGE IS UNCLASSIFIED

AD822349



REPORT NO. RK-TR-67-7

**SOLID PROPELLANT ROCKET MOTOR INTERNAL
BALLISTICS COMPUTER PROGRAM
(PROGRAM MANUAL)**

Prepared By
The Boeing Company
Seattle, Washington

Under
Contract No. DA-01-021-AMC-15557(Z)

For
ARMY MISSILE COMMAND
REDSTONE ARSENAL, ALABAMA
September 1967

This document is subject to special export controls and each
transmittal to foreign governments or foreign nationals may be
made only with prior approval of *Att: AMSM - RR*



U.S. ARMY MISSILE COMMAND

Redstone Arsenal, Alabama 35809

PREFACE

This document is volume one (D2-125286-1) of three volumes. It describes a FORTRAN IV digital computer program developed for analysis of solid rocket motor internal ballistics. Volume one, "Program Manual," explains the theory and describes the mathematical model, program capabilities and information necessary for program maintenance and revision. Volume two, "User's Guide," (D2-125286-2) describes program options, preparation of program input data and program output. Volume three, "Sample Case Results and Program Listings," (D2-125286-3) contains the sample case results and complete program listings of the computer program. The document is divided into three volumes for handling convenience. Section numbering is continuous through the three volumes. A complete table of contents appears in each volume.

CONTENTS

	<u>PAGE</u>
VOLUME 1 (D2-125286-1)	
Preface	viii
Abstract	xii
Key Words	xiii
Acknowledgements	xiv
Definition of Terms	xv
List of Illustrations	xvii
1.0 Introduction	1
1.1 General Information	1
1.2 History of Program Development	3
1.3 References	4
2.0 Program Capabilities and Limitations	5
2.1 Program Capabilities	5
2.1.1 Program Output	7
2.1.2 Program Assumptions	7
2.2 Limitations	8
3.0 Method of Solution	11
4.0 Gas Dynamic Equation Development	16
4.1 Gas Dynamics for Incremental Control Volumes	16
4.1.1 Steady Flow Gas Dynamics	19
4.1.2 Non-Steady Flow Gas Dynamics	23
4.1.3 Non-Steady Flow Gas Dynamics with Acceleration	33
4.2 Complete Motor Gas Dynamics	36
4.2.1 Fore-Head Pressure Convergence	36
4.2.2 Nozzle Gas Dynamics	37
4.3 Propellant Characteristics and Burning Rate Model	41
4.3.1 Propellant Gas Properties	41
4.3.2 Propellant Burning Rate Model	42
4.3.3 Anisotropic Propellant Burning	44
5.0 Geometrical Definition of Propellant Grain	56
5.1 Grain Cross Section Geometry	56

	<u>PAGE</u>
5.1.1 General Forked Wagon Wheel	56
5.1.2 Slotted-Cone	67
5.2 Grain Longitudinal Geometry	77
5.2.1 Head-End with Web, Fore-Head Section	77
5.2.2 Cylindrical Section	92
5.2.3 Straight-Through Grain, Motor End Sections	94
5.3 Moments of Inertia and CG Location	106
5.3.1 Roll Moment of Inertia	107
5.3.2 Pitch Moment of Inertia	108
5.3.3 CG of Sections	110
6.0 Detailed Programming Information	150
6.1 Subroutine Description	151
6.1.1 Subroutine Descriptions	151
6.1.2 Subroutine Linkage Table	161
6.2 Flow Charts	171
6.3 Storage Allocation and Computer System	188
6.4 Diagnostic Tools	206
6.5 Nomenclature	207
7.0 Results	254

VOLUME 2 (D2-125286-2)

Preface	vi
List of Illustrations	xvii
8.0 User's Guide	1
8.1 Description of Input Data	2
8.1.1 Grain Geometry	2
8.1.2 Propellant Properties	8
8.1.3 Nozzle Configuration	11
8.1.4 Internal Gas Dynamics	12
8.2 Preparation of Input Data	14
8.3 Output Description	47
8.3.1 Input Data Printout	47
8.3.2 Initial Geometry Printout	47

	<u>PAGE</u>
8.3.3 Geometry Table Printout	47
8.3.4 Inert Sliver Summary Printout	47
8.3.5 Internal Ballistic Solution Printout	48
8.3.6 Expanded Increment Dividing Plane Printout	51
8.3.7 Burnout Printout	52
8.4 Sample Cases	54
8.4.1 Base Case One and Variations Description	54
8.4.2 Base Case Two and Variations Description	55
8.5 Operating Information	57
VOLUME 3 (D2-125286-3)	
Preface	xii
List of Illustrations	xvi
9.0 Sample Case Results and Program Listings	1
9.1 Sample Case Results	1
9.2 Program Listings	313

ABSTRACT

This report describes a FORTRAN IV digital computer program developed to calculate internal ballistic performance of solid propellant rocket motors with high burning rates, short burning durations, and high vehicle accelerations. Forked wagon wheel, conventional wagon wheel, standard star, slotted-cone, and circular port monolithic and segmented grain designs may be considered. Accurate description of an inert sliver in the cylindrical section is allowed for all but the forked wagon wheel grain design. The effects of anisotropic burning of the propellant may be considered. The storage of mass and momentum (capacitance effects) and vehicle acceleration are included in the internal gas dynamic equations. Ignition transients may be calculated. Tabular input of the motor grain description is available for special grain configurations that cannot be described by the program geometry constants. Motor performance parameters such as delivered and vacuum thrust and total impulse, fore-head and aft-head total pressure, nozzle discharge flow, fore-head and aft-head total pressure integrals, pitch and roll moments of inertia, center of gravity locations, burn surface area, and weight of propellant remaining are printed for each time interval.

This report is divided into three volumes. Volume one is the Program Manual, volume two is the User's Guide, and volume three is the Sample Case Results and Program Listings.

KEY WORDS

The following Key Words identify the major program capabilities:

- Internal Ballistics
- Solid Propellant Rocket Motor
- Monolithic Grain
- Segmented Grain
- One-Dimensional Gas Dynamics
- Steady Flow Gas Dynamics
- Non-Steady Flow Gas Dynamics
- Isotropic Propellant Burning
- Anisotropic Propellant Burning
- Vehicle Acceleration
- Ignition Transient Interval
- Web-Time Interval
- Tail-Off Interval
- Fore-Head Section
- Aft-Head Section
- Cylindrical Section
- Center of Gravity
- Moment of Inertia
- Grain Geometry
- Nozzle

ACKNOWLEDGEMENTS

Acknowledgement is given to the Thiokol Chemical Corporation, Redstone Division, for the original SCAT machine language program from which this program was developed (References 1 and 2), and to the Thiokol Chemical Corporation, Wasatch Division, for the documentation of the grain geometry calculations from which the description of the mathematical model was developed (Reference 3).

DEFINITION OF TERMS

The following general definitions apply throughout this document:

Internal Ballistics: Analysis of the burning characteristics and progression of the propellant surface, dynamics of the gas flow, and the gas generation in the interior of solid propellant rocket motors.

Performance Characteristics: Parameters that specify motor performance, e.g., thrust vs time, maximum chamber pressure, specific impulse, and burn time.

Gas Dynamics: Study of the generation and flow of combustion products along the propellant grain and through the nozzle.

Steady Flow Gas Dynamics: Mass, energy, and momentum within a control volume are constant with time.

Non-Steady Flow Gas Dynamics: Mass, energy, and momentum within a control volume are not constant with time.

Grain Design: The cross sectional grain configuration of the propellant.

Monolithic Grain: The propellant grain is one single piece.

Segmented Grain: The propellant grain is divided up into a number of longitudinal segments.

Slots: The region between the segments which does not contain propellant.

Web: The minimum distance between the grain surface and the case wall.

Core: The region occupied by the combustion gases.

Reference Planes: The stations in the cylindrical section of a motor where the grain design is specified.

Incremental Dividing Planes: The stations in the cylindrical section of the motor where the solution of the internal gas dynamic equations is obtained.

Mass Addition Region: The region between incremental dividing planes.

Ignition Transient Interval: The time required to obtain motor operating pressure.

Web-Time Interval: The time required to burn through the web.

Tail-off Interval: The time interval after web burn through.

Isotropic Propellant Burning: Where the burning rate characteristics are independent of distance burned.

Anisotropic Propellant Burning: Where the burning rate characteristics are dependent on distance burned.

LIST OF ILLUSTRATIONS

<u>FIGURE NUMBER</u>	<u>TITLE</u>	<u>PAGE</u>
2.1	Grain Design Options	9
2.2	Typical Motor Configurations	10
3.1	Reference Plane and Increment Dividing Plane Identification	14
3.2	Macroscopic Flow Chart	15
4.1	Mathematical Model of Mass Addition Region Control Volume	50
4.2	Mathematical Model of Slot Between Grain Segments	51
4.3	Reference Plane and Increment Dividing Plane Identification	52
4.4	Anisotropic Propellant Burning Configuration Near Case Wall Before Web Burnout	53
4.5	Anisotropic Propellant Burning Configuration Near Case Wall and Inert Sliver Before Web Burnout	54
4.6	Anisotropic Propellant Burning Configuration Near Case Wall After Web Burnout	55
5.1	Grain Design Options	112
5.2	One-Half Fork of General Modified Wagon Wheel Configuration	113
5.3	Part of Calculated Constants for One-Half Fork of General Modified Wagon Wheel Configuration by PLNCNS Subroutine	114
5.4	Part of Calculated Constants for One-Half Fork of General Modified Wagon Wheel Configuration Produced by PLNCNS Subroutine	115
5.5	Sector Definition	116
5.6	Slotted-Cone	117

<u>FIGURE NUMBER</u>	<u>TITLE</u>	<u>PAGE</u>
5.7	Slotted-Cone Addition to Standard Star Showing Location of Fixed Geometry Points	118
5.8	Complete Slotted-Cone Burning Surface for τ Less than R_2	119
5.9	Slotted-Cone Burning Surface Addition for τ Greater than R_2 and Less than $T_{6\max}$	120
5.10	Slotted-Cone Burning Surface Addition for τ Greater than $T_{6\max}$ and Less than $T_{7\max}$	121
5.11	Slotted-Cone Burning Surface Addition for τ Greater than $T_{7\max}$ and Less than T'_{V7} with T'_{V7} Less than T'_{V6}	122
5.12	Slotted-Cone Burning Surface for τ Greater than T'_{V7} with T'_{V7} Less than T'_{V6}	123
5.13	Slotted-Cone Burning Surface for τ Greater than T'_{V6} with T'_{V6} Less than T'_{V7}	124
5.14	Head-End with Web, Motor Fore-Head	125
5.15	Sectors for Block No. 1	126
5.16	Head-End with Web Plane Definition	127
5.17	Head-End with Web, Block 1 Plane Definition	128
5.18	Plane for Block 1 Analysis	129
5.19	γ_1 for Subroutine GAMSUB	130
5.20	γ_2 for Subroutine GAM2S	131
5.21	P_0 for Subroutine POSUB	132
5.22	P_3 for Subroutine P3SUB	133
5.23	Planes for Block 1 Analysis	134
5.24	Planes Produced in Sectors 3A and 3B or in Sectors 11A and 11B	135
5.25	Area for Block No. 2A and 2B	136
5.26	A_{1g} for Subroutine AIGSUB	137

<u>FIGURE NUMBER</u>	<u>TITLE</u>	<u>PAGE</u>
5.27	Sectors for Block 2B of Fore-Head Section	138
5.28	Sector for Block 2B	139
5.29	Distribution of Volume In Radial Burning Section	140
5.30	Motor Case Longitudinal Constants	141
5.31	Straight Through Grain Configuration	142
5.32	Sector Definition	143
5.33	Zone Definition	144
5.34	Sector Parameters, Zones B, C, and Web	145
5.35	Circular Arc Sector 3 Zone A	146
5.36	Element of Incremental Area for Zone B	147
5.37	Head-End Section, Volume Elements for MOI and CG Calculations	148
5.38	Cylindrical Section Volume Elements for MOI and CG Calculations	149
7.1	HIBEX Forehead Chamber Pressure Trace	255
7.2	Influence of Internal Flow and Burning Rate Model	256
8.1	Program Model	62
8.2	Typical Motor Configurations	63
8.3	Straight Through Grain Configuration	64
8.4	Straight Through Grain Configuration Inputs	65
8.5	Head-End Web	66
8.6	Grain Configuration Options	67
8.7	Reference Plane and Increment Dividing Plane Identification	68
8.8	General Forked Wagon Wheel Configuration Inputs	69

<u>FIGURE NUMBER</u>	<u>TITLE</u>	<u>PAGE</u>
8.9	Calculated Plane Constants	70
8.10	Calculated Plane Constants	71
8.11	LA Definition	72
8.12	Wagon Wheel Configuration Inputs	73
8.13	Star Grain Configuration Inputs	74
8.14	Slotted-Cone Grain Configuration Inputs	75
8.15	Circular Port Configuration Inputs	76
8.16	Nozzle Configuration Inputs	77
8.17	Motor Case Longitudinal Inputs and Constants	78
8.18	Base Case One	79
8.19	Base Case Two, Monolithic Grain	80
8.20	Base Case Two, Segmented Grain	81

LIST OF FLOW CHARTS - VOLUME 1

<u>FLOW CHART NUMBER</u>	<u>TITLE</u>	<u>PAGE</u>
1	MAIN Program	172
2	Subroutine MNCHN1	173
3	Subroutine MNCHN2	174
4	Compute Plane Constants	175
5	Subroutine AESUB	176
6	Subroutine MNCHN3	178
7	Subroutine SCI	179
8	Subroutine SCTOR1	180
9	Subroutine SCTOR2	181
10	Subroutine MNCHN4	182

<u>FLOW CHART NUMBER</u>	<u>TITLE</u>	<u>PAGE</u>
11	Subroutine SEGSUB	183
12	Subroutine SETPH	185
13	Subroutine TISUB	186
14	Check for Case Termination	187

1.0

INTRODUCTION

This report describes a FORTRAN IV digital computer program, developed by The Boeing Company for operation on an IBM 7094 computer with an IBSYS version 13 monitor system from an earlier Thiokol Chemical Corporation program, to perform dynamic analyses of solid propellant rocket motor internal ballistics. A complete description of the mathematical model, the engineering equation development, the method of solution, and detailed programming information is presented to explain program principles and theory and to facilitate program maintenance and revision.

This program was developed under contract from the Army Missile Command Propulsion Laboratory, Redstone Arsenal, Alabama, contract number DA-01-021-AMC-15557(Z) by the Engineering Digital Computing Organization 2-2640, with support from the Missile and Information Systems Division, Flight Technology Propulsion Organization 2-5711 of The Boeing Company.

1.1

General Information

The report is divided into three volumes. Volume I, the Program Manual, provides a technical explanation of the theory, mathematical model, program capabilities and information necessary for program maintenance and revision. Volume II, the User's Guide, describes program options, preparation of input data and program output. Volume III, the Sample Case Results and Program Listings, contains the complete program listings of the computer program. The following paragraphs describe briefly the sections of the report comprising each volume.

Volume I

The Program Capabilities and Limitations, Section 2.0, indicates the capability the program has to evaluate grain designs and internal ballistics and the program limitations that exist in these areas.

The Method of Solution, Section 3.0, describes the method the program uses to obtain the internal ballistic solutions and the organization of major program sections which divide the solution into logical blocks or core loads that reside in core at separate times.

The Gas Dynamic Equation Development, Section 4.0, presents the development of the equations for the non-steady flow gas dynamics for both segmented and monolithic motors, propellant description, and for an accelerating reference system. In general, this section describes modifications made to the original Thiokol Chemical Corporation program for conducting design studies of solid propellant configurations (Reference 1) to simulate the

Internal ballistics of high burning rate propellants with characteristically short burn durations. These modifications were made specifically to include the storage of mass and momentum in the gas dynamic equations, to consider the effects of very high vehicle acceleration on the internal ballistics, and to study anisotropic propellant burning. As a result of these modifications, ignition transients may be calculated.

The Geometry Equation Development, Section 5.0, explains in detail the setup and solution of the grain geometry equations which determine the perimeter length, cross sectional area, burn surface area, moments of inertia, and center of gravity location of the various grain options and longitudinal configurations. The equation development and figures presented in this section were obtained from References 1 and 3.

The Detailed Programming Information, Section 6.0, presents a brief description of all program subroutines, macroscopic program logic flow charts, a description of the computing system and program storage allocation, program diagnostic aids, and a list of the program nomenclature. Appropriate comments are placed throughout the program listings as a supplement to the subroutine flow charts to assist in program maintenance and revision.

The Results, Section 7.0, presents a comparison of a computer prediction with three full scale HIBEX motor firings. Dimensionless fore-head pressure traces are shown for the computer prediction and the motor firings.

Volume II

The User's Guide, Section 8.0, presents an explanation of the required program inputs, sample cases showing the available program options, a description of the output format, and the required control cards to permit effective program use and operation without knowledge of the program technical aspects. This section is arranged to be complete without reference to the program manual technical sections and may be used independent of the program manual.

Volume III

The Listings, Section 9.0, contains the sample case results and program listings of the computer program.

1.2

History of Program Development

In March 1960, work was initiated at the Thiokol Chemical Corporation, Redstone Division, under the auspices of Systems Analysis Laboratory, Army Rocket and Guided Missile Agency, Redstone Arsenal, Alabama, for the development of a solid propellant rocket motor design program (References 1 and 2). In 1962, The Boeing Company received a copy of this program, and in 1963 developed a segmented motor version. In 1964, the Saturn Branch of the Aerospace Division of Boeing at New Orleans converted the SCAT machine language program to FORTRAN II for operation on the IBM 7094 computer. In 1965, The Boeing Aerospace Division in Seattle, Washington, converted the FORTRAN II version to FORTRAN IV for operation on the SRU 1107 and made the modifications discussed in Section 1.1 for the HIBEX contract to add the transient capability. In May 1966, The Boeing Company proposed to the Army Missile Command to segment the existing SRU 1108 program, perform the necessary conversion for operation on the IBM 7094, and completely document the advanced program version. A contract was received in July 1966 from the Army Missile Command for a 6 month development effort to perform the required conversion.

1.3

References

1. Control No. U-A-61-28A, "Final Report Design Study of Solid Propellant Configurations," Thiokol Chemical Corporation, Redstone Division, July 1961.
2. Control No. U-A-62-18A, "Final Report, Design Study of Solid Propellant Configuration," Thiokol Chemical Corporation, Alpha Division, May 1962.
3. T263206, "Generalized Wagon Wheel Grain Design Study," Thiokol Chemical Corporation, Wasatch Division, June 1962.
4. D2-99598-1, "HIBEX Rocket Motor Performance, Design and Development Analysis (U)," Confidential, Aero-Space Division, The Boeing Company, March 1966.
5. D2-125060-2, "Small High Performance Interceptor Research (U)," Confidential, Aero-Space Division, The Boeing Company, December 1966.
6. Leipmann, H. W., and Roshko, A., Elements of Gas Dynamics, GALCIT Aeronautical Series, John Wiley and Sons, Inc., Third Printing, February 1960.
7. Shapiro, Ascher H., The Dynamics and Thermodynamics of Compressible Fluid Flow, Volume I, The Ronald Press Co., 1953.
8. Baumeister, Theodore, Mark's Mechanical Engineer's Handbook, Sixth Edition, McGraw-Hill Book Company, 1958.
9. Univac 1107 Fortran Programmers Guide, U-3540, August 1963.

2.0

PROGRAM CAPABILITIES AND LIMITATIONS

This computer program was developed to calculate solid propellant rocket motor internal ballistics. Because of its development from earlier grain design and ballistic performance programs, additional capabilities are present. Throughout the development effort, all prior program capabilities have been retained so that a general program exists with both grain design and internal ballistic evaluation capability.

2.1

Program Capabilities

The basic propellant grain design is the forked wagon wheel, however, the grain design equations are general so that the conventional wagon wheel, standard star and circular port as well as the slotted-cone may be described by variations in the input data. Figure 2.1 shows the five grain design options. Other more complicated grain designs may be evaluated by describing the perimeter length and burn area as a function of distance burned and input to the computer program as tabular data.

The propellant grain configuration may be either monolithic or segmented with up to 11 slots. The propellant case and port cavity may be either cylindrical or tapered. The fore-head section configuration may be a straight through grain or may contain a complete web. Figure 2.2 shows the various motor configuration options. The aft-head section configuration is a straight through grain.

The propellant characteristics are described by definitive properties of the combustion gases and a generalized burning rate equation. The propellant gas properties may be held constant or may be varied as a function of the static pressure in the port cavity. The burning rate model includes erosive burning and will allow either isotropic or anisotropic burning of the propellant surface.

Either steady or non-steady flow gas dynamics are available to obtain the internal ballistic solution. The steady flow gas dynamics solve the momentum and continuity equations without consideration of time dependent terms such that there is no storage of mass or momentum (no capacitance effects). The non-steady flow gas dynamics solve the momentum and continuity equations with respect to time so that the storage of mass and momentum is considered and the start transient and tail-off intervals may be determined.

The effects of vehicle acceleration on the internal ballistic solution may be considered. The acceleration term is included in the momentum equation.

The effect of a tapered inert sliver may be considered in the cylindrical section for all but the forked wagon wheel grain design.

2.1

Program Capabilities (Continued)

The following is a summary of the program capabilities:

1.0 Grain Design

- A. Circular Port
- B. Standard Star
- C. Slotted-Cone
- D. Conventional Wagon Wheel
- E. Forked Wagon Wheel
- F. Tables of Perimeter and Burn Area as a Function of Distance Burned can be Input

2.0 Motor Configuration

- A. Cylindrical Section
 - 1) Monolithic grain
 - 2) Segmented grain
 - 3) Tapered inert sliver
- B. Fore-head Section
 - 1) Straight through grain
 - 2) Complete web (head-end with web)
- C. Aft-head Section
 - 1) Straight through grain
 - 2) Burning on aft face

3.0 Propellant Characteristics

- A. Isotropic Propellant Burning
- B. Anisotropic Propellant Burning
- C. Erosive Burning
- D. Variable Gas Properties (function of static pressure)

4.0 Internal Ballistics

- A. Steady Gas Flow
- B. Non-Steady Gas Flow
 - 1) Ignition transient interval
 - 2) Web-time interval
 - 3) Tail-off interval
- C. Vehicle Acceleration

2.1.1

Program Output

The program provides the following output:

1.0 Motor

- A. Delivered Thrust
- B. Vacuum Thrust
- C. Fore-head Total Pressure
- D. Nozzle Total Pressure
- E. Fore-head Total Pressure Time Integral
- F. Nozzle Total Pressure Time Integral
- G. Delivered Total Impulse
- H. Vacuum Total Impulse
- I. Nozzle Discharge Flow Rate
- J. Polar and Rectangular Moment of Inertia
- K. Center of Gravity

2.0 Propellant Characteristics

- A. Weight of Propellant Remaining
- B. Forward Tangent Plane Propellant Burning Rate
- C. Aft Tangent Plane Propellant Burning Rate
- D. Total Weight of Propellant Expended

3.0 Grain Geometry

- A. Cylindrical Section Burn Area
- B. Fore-head Section Burn Area
- C. Aft-head Section Burn Area
- D. Grain Segment Face Burn Area
- E. Total Motor Burn Area

4.0 Nozzle Characteristics

- A. Throat Area
- B. Effective Expansion Ratio (flow separation accounted for)
- C. Pressure Ratio Across Nozzle
- D. Momentum Portion of Thrust Coefficient

2.1.2

Program Assumptions

The following assumptions were made to translate the physical system into the one-dimensional gas dynamic model:

1. Propellant burning during ignition and steady state operation occurs normal to the grain surface.
2. The burn rate in the fore-head and aft-head sections is assumed to be constant over the burning surface of the entire section.

2.1.2

Program Assumptions (Continued)

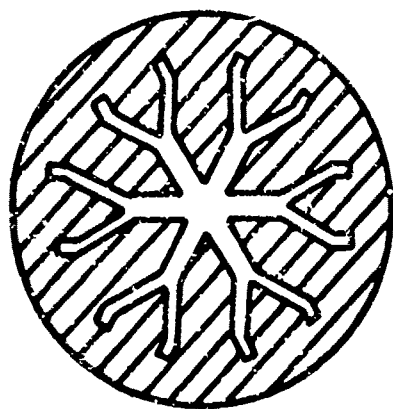
3. Mass addition occurs instantaneously with no velocity component along the motor's longitudinal axis ($dZ/dt = 0$).
4. The products of combustion obey the perfect gas law.
5. The gas flow is one-dimensional and adiabatic.
6. The combustion temperature is constant throughout the motor.
7. The heat capacity of the combustion gases is constant.
8. The friction forces of the combustion gases in the port cavity are negligible.
9. The moments of inertia about the pitch and yaw axis are equal.

2.2

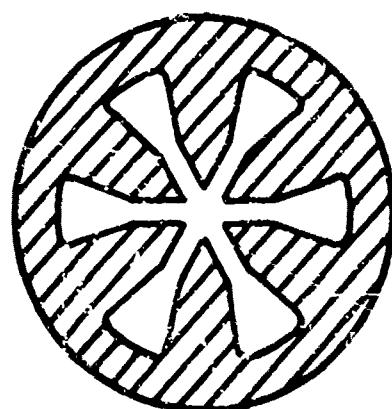
Limitations

The program has the following limitations:

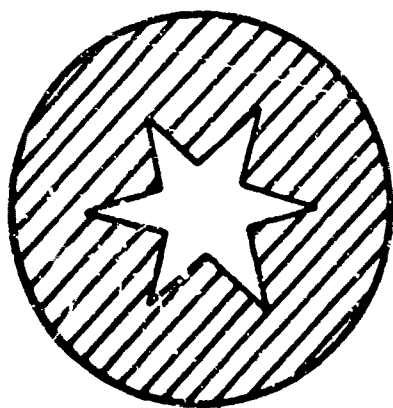
1. A maximum of 11 reference planes are allowed in the cylindrical section to describe the grain design.
2. A maximum of 100 increment dividing planes are allowed in the cylindrical section to define the mass addition regions. If this restriction is exceeded by defining a ΔZ too small, the case execution will be terminated and an appropriate comment will be printed.
3. A maximum of 11 slots are allowed for segmented motors.
4. The slotted-cone grain design is applicable only to the cylindrical section. Burn area tables must be input for the forward and aft domes when this grain design is used.
5. The inert sliver option is restricted to the cylindrical section and does not apply to either end section.
6. The effects of an accelerating reference system can be determined only for non-steady flow gas dynamics.



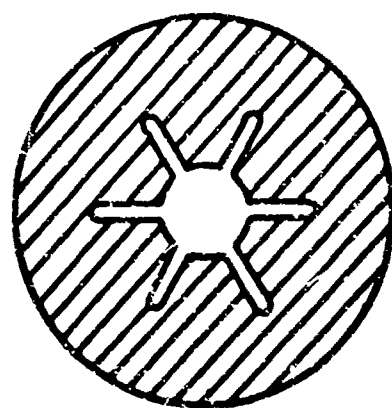
Forked Wagon Wheel



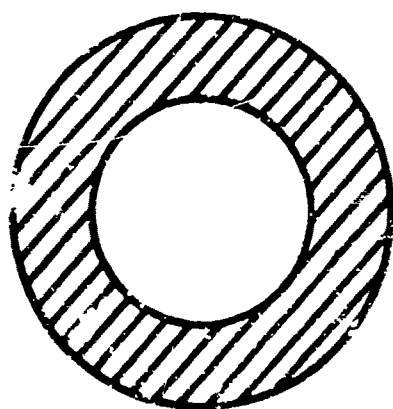
Conventional Wagon Wheel



Standard Star

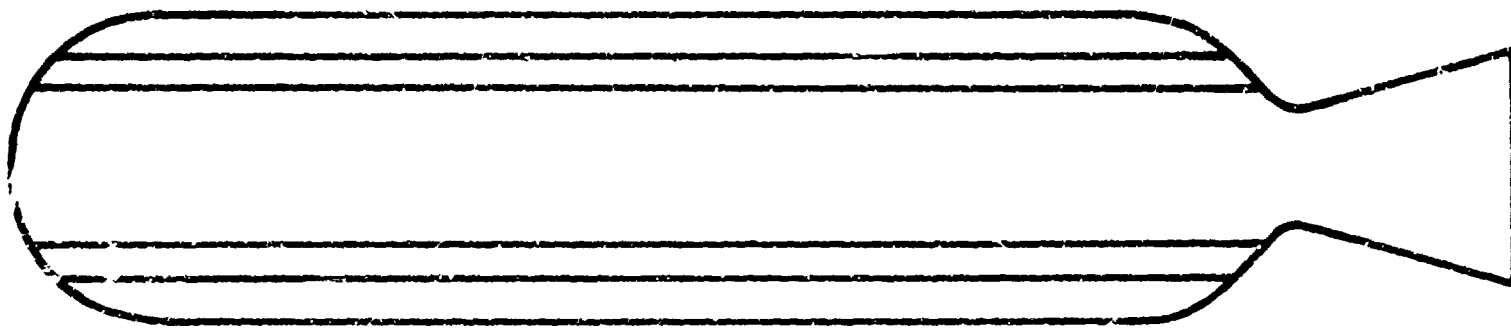


Slotted-Cone

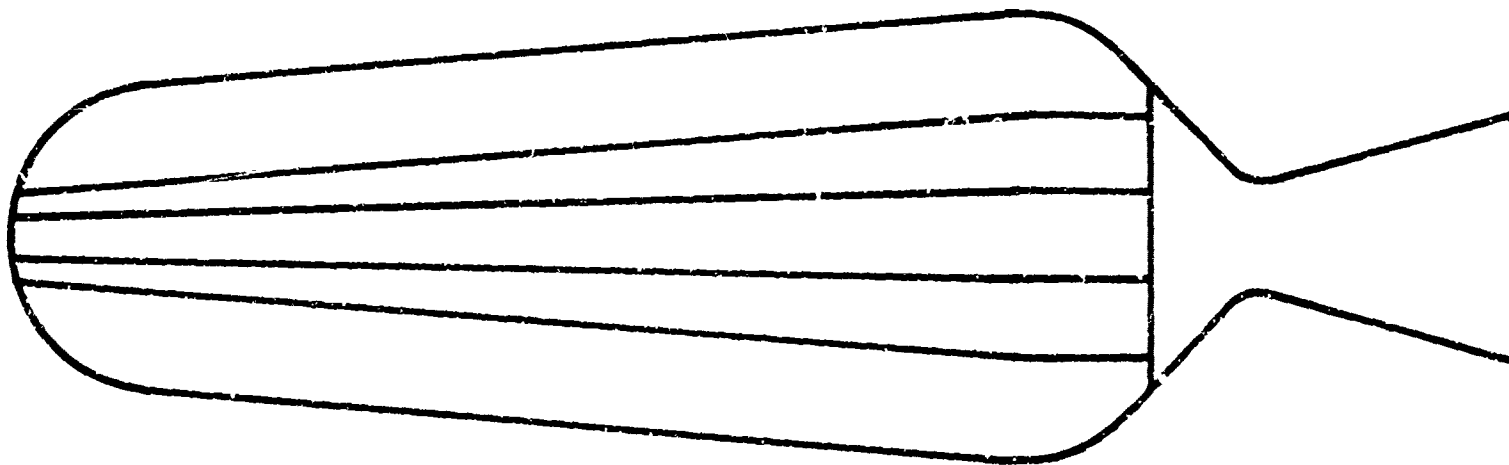


Circular Port

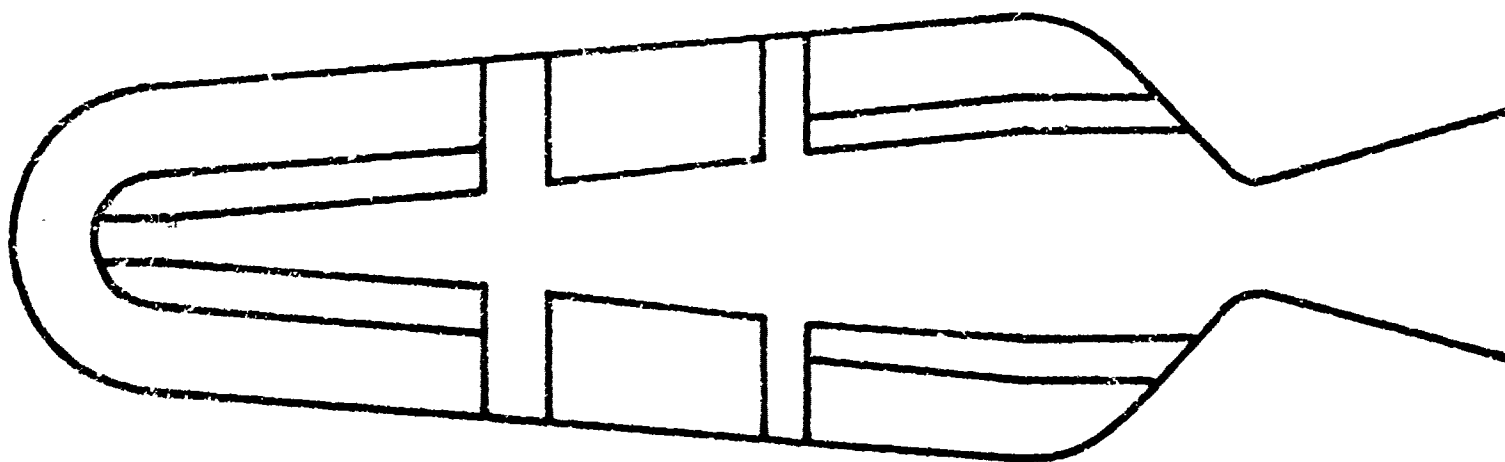
Figure 2.1. Grain Design Options



Monolithic Grain With Cylindrical Case



Monolithic Grain with Tapered Case
and Propellant Cutback in Aft-end



Segmented Grain with a Head-end with Web and Tapered Case

Figure 2.2. Typical Motor Configurations

The program calculations are based on the geometrical model shown in Figure 3.1. The motor configuration is divided into three sections: the head-end section (forward dome), the cylindrical section, and the aft-head section (aft dome) or nozzle. The grain geometry is described by input reference planes within the cylindrical section. The cylindrical section, which may contain either a monolithic or a segmented grain, is further divided into a number of increments or mass addition regions by the location of increment dividing planes, at each reference plane and at specified intervals (ΔZ) from each reference plane until either a segment slot interface or the next reference plane is passed. During the computer solution of the gas dynamics, port perimeter, port cross sectional area and moments of inertia are determined at each increment dividing plane by linear interpolation between adjacent reference planes. Mass addition is assumed to occur as a step process between two increment dividing planes.

The program method of solution is divided into four separate computer core loads linked together by a main control program and a common data region. Each core load is unique, but dependent on preceding core loads for generated data. The flow chart shown in Figure 3.2 presents the macroscopic program order of solution with the separate core loads linked together.

The first computer core load contains the subroutines required to read the input data, initialize the data cells, compute the input reference plane constants, locate the increment dividing planes, check for input data errors, and print the program inputs and computed constants.

The second computer core load contains the geometry subroutines required to compute the initial propellant cross section area and perimeter length for the cylindrical section reference planes, the aft-head and straight through grain fore-head sections burn area and initial propellant volume as a function of distance burned. The moments of inertia and centers of gravity for the aft-head and straight through grain fore-head sections and the radius of gyration for the cylindrical section are also calculated. The computed values for each section are stored in tables for use during the solution of the internal ballistics in the fourth core load.

The third computer core load contains the geometry subroutines required to compute the initial propellant volume, burn area, moments of inertia, and CG location tables of the head-end with

web. The third core load is loaded only if a head-end with web is required after the cylindrical section and aft-head section geometry calculations have been completed in the second core load.

After the grain geometry calculations are performed in the first, second, and third core loads and the perimeter and area tables have been established, the internal ballistic solution is initiated in the fourth core load by determining the geometry values of each reference plane and each end section from a table look-up procedure in the geometry tables. For steady flow conditions, an initial estimate of the fore-head pressure is made, and the burning rate (which is assumed to be constant over the entire head-end section) is determined as described in Section 4.1.1. With this burn rate and the tabular value of the fore-head burn area, the instantaneous value of mass addition is determined for the fore-head section. The state and gas dynamic properties of the propellant at the forward tangent plane, the first increment dividing plane, are determined from the simultaneous solution of the momentum and continuity equations assuming perfect gas relationships.

The grain geometry at the first increment dividing plane is then determined and stored in temporary locations for future reference. The grain geometry of increment dividing plane two is determined. The increment section mass generation rate is determined from the perimeter lengths of increment dividing planes one and two, the increment length, and the burning rates at the upstream adjacent increment dividing planes. The propellant properties and mass flow at increment dividing plane two are then determined by a simultaneous solution of the momentum and continuity equations for either steady or non-steady flow conditions.

The above procedure is repeated for each cylindrical section mass addition region. Once the cylindrical section is complete, the same general calculations are performed for the aft-head section. The port cross sectional area and perimeter length and burning rate are assumed to be constant in the aft-head section and identical to the values at the aft tangent plane.

The nozzle throat area is compared to the maximum value that will maintain subsonic flow in the port. If this maximum value is exceeded, the program prints an error comment and terminates the case. If this maximum value is not exceeded, the flow rate of propellant discharge through the nozzle is computed on the basis of isentropic flow. This flow rate is compared to the flow rate of propellant discharged from the grain. If these two values do not agree within .1 percent, the fore-head pressure is adjusted and the program returns to the fore-head and repeats until

3.0

Method of Solution (Continued)

convergence is attained. Once equilibrium is reached, additional ballistic properties are computed and the performance data is printed.

Following the performance printout, the thickness burned in each increment dividing plane and slot interface is then determined from the previous web thickness. A check is then made to see if burnout has occurred at any of the increment dividing planes. If burnout occurs, a comment is printed that the increment dividing plane has burned out. The progression of the slot interfaces for segmented motors is indicated by a printout of the increment dividing plane longitudinal location.

The time is then incremented by the computed time interval and the program returns to the fore-head to compute new equilibrium conditions and determine new values of the perimeter length and port cross section area at each increment dividing plane and burn area for each end section. This process is then repeated until the termination option is exceeded.

The general program solution of the internal ballistics outlined above is modified for non-steady flow conditions. When the start transient interval is computed, the fore-head pressure is defined by tabular input of the fore-head pressure as a function of time, or the burn rate coefficient is defined by tabular input of the burn rate coefficient as a function of distance burned. When the fore-head pressure is input for the start transient, the burn rate coefficient is varied to obtain convergence; and when the burn rate coefficient is input for the start transient, the fore-head pressure is varied, as for steady flow conditions, to obtain convergence. When the fore-head pressure is input for the start transient, an initial estimate of the burn rate coefficient is made by computing a first guess of the burn rate coefficient from the motor configuration parameters and the fore-head pressure variation. With this burn rate coefficient, the instantaneous value of mass addition and mass discharge is determined for the head-end section. The propellant gas properties for the first increment dividing plane are then determined from a simultaneous solution of the non-steady gas flow equations as above. The remainder of the ballistic solution is unchanged.

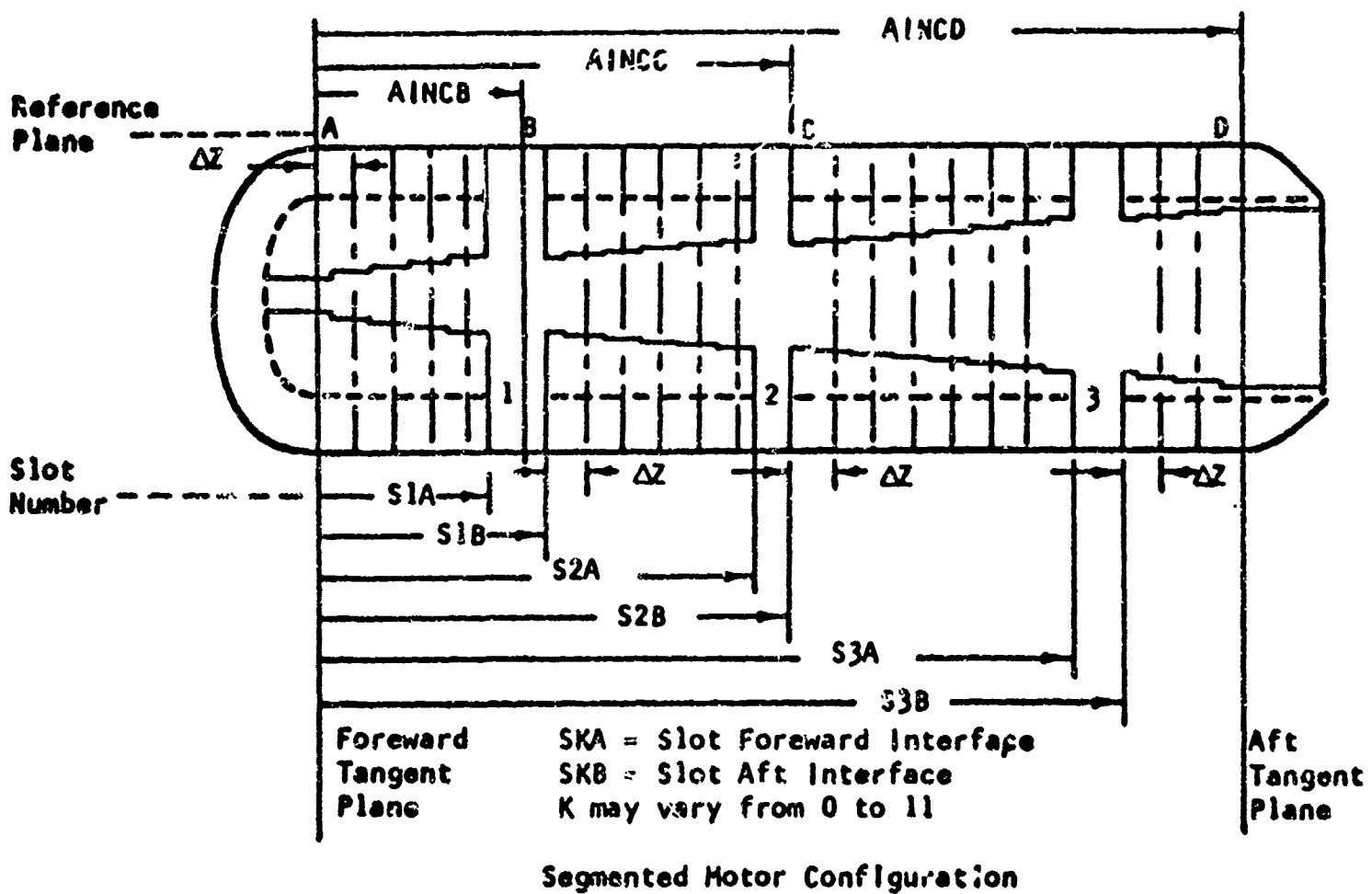
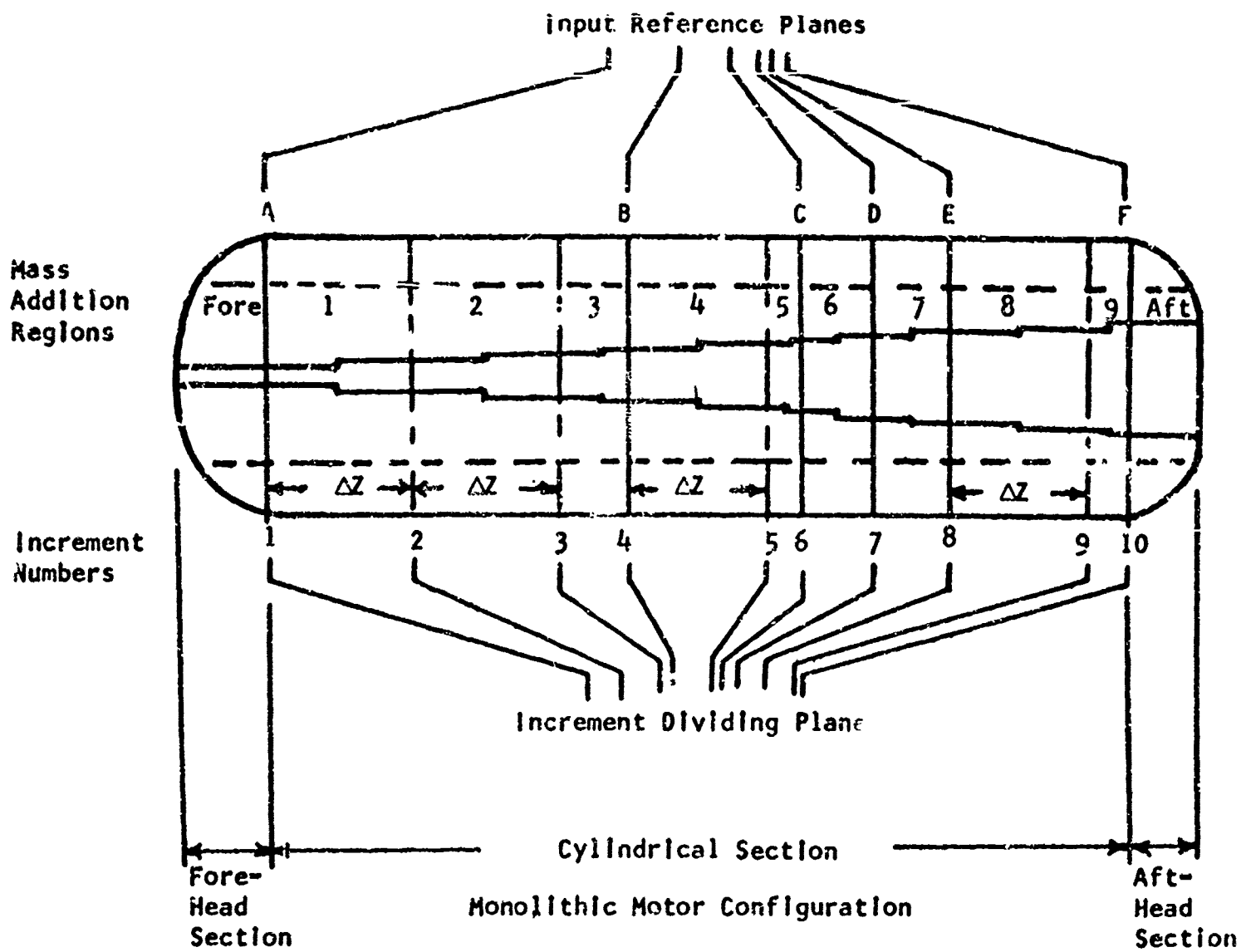


Figure 3.1 Reference Plane and Increment Dividing Plane Identification

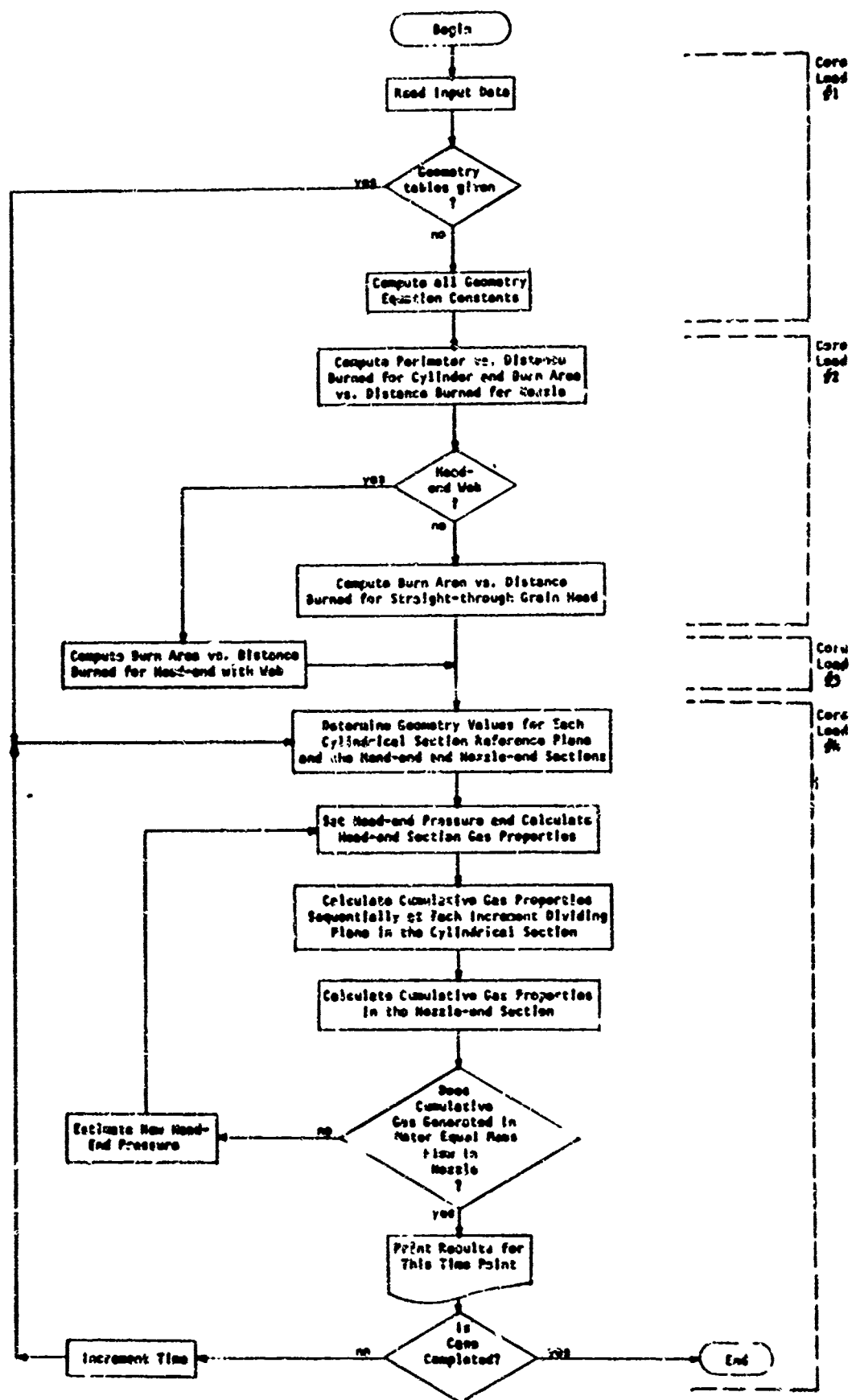


Figure 3.2 Macroscopic Flow Chart

4.0

GAS DYNAMIC EQUATION DEVELOPMENT

The static and total pressure, temperature, velocity, and flow rate of the gas along the length of the propellant grain and through the nozzle are required to determine the progression of the propellant burning surface and motor performance parameters such as chamber pressure, thrust, and total impulse. These parameters are obtained from an iterative solution of the perfect gas law and the equations of continuity, momentum, and energy for one-dimensional gas flow. The gas flow along the propellant grain is determined by dividing the grain into a number of increments which are termed mass addition regions. Two control volumes are shown in Figures 4.1 and 4.2 which define the mass addition regions for the monolithic and segmented motor configurations shown in Figure 4.3. The gas dynamic equations, which are solved for each mass addition region along the propellant grain, are described in the following sections. The isotropic and erosive burning rate equation, anisotropic mass generation model, and propellant gas properties required for the calculations are also described.

4.1

Gas Dynamics for Incremental Control Volumes

The solution of the continuity, momentum, and energy equations for the mass addition regions along the propellant grain and through the nozzle are described in this section. Steady flow, non-steady flow, or non-steady flow with acceleration may be selected.

The following assumptions are basic to the development of the gas dynamic equations:

1. Mass addition occurs as an instantaneous process with no velocity component parallel to the motor axis ($dZ/dt = 0$).
2. The products of combustion obey the perfect gas law.
3. The gas flow is one-dimensional and adiabatic.
4. The combustion temperature, specific heat ratio, and molecular weight are constant throughout the motor.
5. The friction forces of the combustion gases in the port cavity are negligible.
6. The static pressure is constant across the fore-head section, i.e., no static pressure loss resulting from mass addition or area change.
7. The port area and perimeter are constant across the aft-head section from the aft tangent plane to the grain exit, i.e., constant area duct.

4.1

Gas Dynamics for Incremental Control Volumes (Continued)

The control volume or mass addition region inlet is defined as station 1 and outlet is defined as station 2 as shown in Figures 4.1 and 4.2. The analysis of the mass addition regions along the grain segments is accomplished in subroutines AIBSUB and AIBST to obtain the solution for the discharge pressure, temperature, and flow rate from known inlet conditions at station 1 and a known value of the instantaneous mass generation rate. The instantaneous mass generation rate is determined from the port perimeters, upstream burning rates, and mass addition region incremental length as follows:

$$\dot{dW} = \frac{(L_{p1} R_{b1} + L_{p2} R_{b2})}{2} \Delta Z \rho_f$$

where

- \dot{dW} = mass generation rate, lb/sec
- L_{p1} = port perimeter at station 1, in
- L_{p2} = port perimeter at station 2, in
- ΔZ = mass addition region length, in
- ρ_f = solid propellant density, lb/in³
- R_{b1} = burning rate at station 1, in/sec
(determined from conditions at adjacent upstream increment dividing plane)
- R_{b2} = burning rate at station 2, in/sec
(determined from conditions at adjacent upstream increment dividing plane)

A mass balance for the slots between the grain segments is obtained in subroutine SLOT. The instantaneous mass generation rate at each slot interface is determined as follows:

$$\dot{dW} = A_f \rho_f a P^n$$

where

- A_f = burning area at slot interface, in²
- P = slot interface static pressure, lb/in²
- a = slot burn rate coefficient
- n = slot burn rate coefficient pressure exponent

The general energy equation and the perfect gas law are applied at station 2 to obtain the state properties:

4.1

Gas Dynamics for Incremental Control Volumes (Continued)

$$U = \left[\frac{2 g_o R \gamma (T_o - T)}{\gamma - 1} \right]^{1/2} \quad (\text{general energy})$$

$$P = 12 \rho R T \quad (\text{perfect gas})$$

The continuity and momentum equations are iterated to obtain the discharge pressure, P_2 , and flow rate, \dot{W}_2 , for each mass addition region. For steady flow conditions, the basic equations are as follows:

$$12 \rho_1 A_1 U_1 + d\dot{W} = 12 \rho_2 A_2 U_2 \quad (\text{continuity})$$

$$\begin{aligned} P_1 A_1 + \frac{P_1 + P_2}{2} (A_2 - A_1) - P_2 A_2 \\ = \frac{12 \rho_1 A_1 U_1}{g_o} (U_2 - U_1) + \frac{U_2 d\dot{W}}{g_o} \end{aligned} \quad (\text{momentum})$$

For non-steady flow conditions, the basic equations are as follows:

$$\dot{W}_2 = \dot{W}_1 + d\dot{W} - \frac{d\dot{W}}{dt} \quad (\text{continuity})$$

$$\frac{d\dot{W}}{dt} = \frac{\partial}{\partial t} \left[\left(\frac{P_1 + P_2}{T_1 + T_2} \right) \frac{V}{12R} \right] \quad (\text{perfect gas})$$

$$\begin{aligned} \frac{\partial}{\partial t} \int_1^2 \frac{(\rho U A)}{g_o} dx + \frac{(\rho_2 U_2^2 A_2 - \rho_1 U_1^2 A_1)}{g_o} \\ = P_1 A_1 - P_2 A_2 + \frac{P_1 + P_2}{2} (A_2 - A_1) \end{aligned} \quad (\text{momentum})$$

where

P = static pressure, lb/in²

U = velocity, ft/sec

\dot{W} = flow rate, lb/sec

4.1

Gas Dynamics for Incremental Control Volumes (Continued)

T = static temperature, $^{\circ}\text{R}$

A = port cross sectional area, in^2

V = port volume of mass addition region, in^3

ρ = density, lb/in^3

R = gas constant, $^{\circ}\text{R}/\text{ft}$

4.1.1

Steady Flow Gas Dynamics

The original program developed by the Thiokol Chemical Corporation (references 1 and 2) based the internal gas dynamics on steady flow. Continuity and momentum equations were iterated to obtain mass addition region discharge pressure, temperature, and velocity. This capability is retained in subroutine AIBSUB. The steady flow solution for a segment slot is obtained in subroutine SLOT by neglecting the time dependent terms of the non-steady flow equations. Therefore the steady flow option can be exercised for both monolithic and segmented grain motor designs.

The solution of the steady flow gas dynamics is obtained from an iterative solution of the continuity and momentum equations with the general energy equation and perfect gas law applied at the discharge section to obtain the density and temperature of the combustion gases. The discharge flow rate is obtained from the sum of the mass generation rate and inlet mass flow. An initial value of the discharge velocity is then obtained from the momentum equation, assuming $P_2 = P_1$, and a starting value of the discharge density is obtained from the continuity equation. With the initial value of the discharge density, the following iterative procedure is employed to converge the steady flow equations.

Initially, a guess of the discharge velocity U_2 is obtained from the momentum equation by assuming no pressure loss, $P_2 = P_1$, as follows:

$$\frac{12 \rho_1 A_1 U_1}{g_0} (U_2 - U_1) + \frac{U_2 d\dot{W}}{g_0} = 0$$

or

$$\frac{\dot{W}_1 U_2}{g_0} - \frac{\dot{W}_1 U_1}{g_0} + \frac{U_2 d\dot{W}}{g_0} = 0$$

4.1.1

Steady Flow Gas Dynamics (Continued)

and

$$\dot{W}_1 U_1 = \dot{W}_1 U_2 + U_2 \dot{W} = \dot{W}_2 U_2$$

From the perfect gas law and continuity equation:

$$U_2 = \frac{\dot{W}_1 U_1}{\dot{W}_2} = \frac{\dot{W}_1 U_1}{\rho_2 A_2 U_2} = \frac{\dot{W}_1 U_1}{\frac{P_2 A_2 U_2}{12 RT_2}}$$

or

$$U_2^2 = \dot{W}_1 U_1 \frac{12 RT_2}{P_2 A_2}$$

Using the general energy equation:

$$\frac{2g_o R \gamma (T_o - T_2)}{\gamma - 1} = \dot{W}_1 U_1 \frac{12 RT_2}{P_2 A_2}$$

Multiplying both sides of the above equation by $-2A_2$ and adding like terms to eliminate T_2 yields:

$$\begin{aligned} \frac{-2g_o R \gamma (T_o - T_2)}{\gamma - 1} 2A_2 + (A_1 + A_2)g_o R T_o - (A_1 + A_2)g_o R T_o \\ + (A_1 + A_2)g_o R T_2 - (A_1 + A_2)g_o R T_2 = \frac{-2A_2 \dot{W}_1 U_1 RT_2}{P_2 A_2} \end{aligned}$$

Rearranging and combining terms yields:

$$\left[\frac{-2g_o \gamma (T_o - T_2)}{\gamma - 1} 2A_2 + (A_1 + A_2)g_o R (T_o - T_2) \right] + \left[(A_1 + A_2)g_o R T_2 + \frac{2A_2 \dot{W}_1 U_1 RT_2}{P_2 A_2} \right] - (A_1 + A_2)g_o R T_o = 0$$

Multiplying through by \dot{W}_2 and again rearranging terms yields:

4.1.1

Steady Flow Gas Dynamics (Continued)

$$\dot{W}_2 \frac{2g_o \gamma (T_o - T_2)}{\gamma - 1} \left[-2A_2 + \frac{(\gamma - 1)(A_1 + A_2)}{2\gamma} \right] + \left[(A_1 + A_2)g_o RT_2 + \frac{2A_2 \dot{W}_1 U_1 RT_2}{P_2 A_2} \right] \dot{W}_2 - (A_1 + A_2)g_o RT_o \dot{W}_2 = 0$$

The terms in the second set of brackets may be rearranged with the perfect gas law, remembering that $P_2 = P_1$:

$$\dot{W}_2 \frac{2g_o \gamma (T_o - T_2)}{\gamma - 1} \left[-2A_2 + \frac{(\gamma - 1)(A_1 + A_2)}{2\gamma} \right] + \left[(A_1 + A_2)g_o P_1 A_2 + 2A_2 \dot{W}_1 U_1 \right] U_2 - (A_1 + A_2)g_o RT_o \dot{W}_2 = 0$$

Thus, from the general energy equation:

$$-\dot{W}_2 U_2^2 \left[2A_2 - \left\{ \frac{\gamma(A_1 + A_2)}{2\gamma} - \frac{(A_1 + A_2)}{2\gamma} \right\} \right] + \left[(A_1 + A_2)g_o A_2 P_1 + 2A_2 \dot{W}_1 U_1 \right] U_2 - (A_1 + A_2)T_o R g_o \dot{W}_2 = 0$$

The above equation is solved for U_2 using the quadratic formula as follows:

$$CAA = -\dot{W}_2 \left[2A_2 - \left\{ \frac{\gamma(A_1 + A_2)}{2\gamma} - \frac{(A_1 + A_2)}{2\gamma} \right\} \right]$$

$$CBB = (A_1 + A_2)g_o A_2 P_1 + 2A_2 \dot{W}_1 U_1$$

$$CC = -(A_1 + A_2)T_o R g_o \dot{W}_2$$

$$RAD = CBB^2 - (4CC)CAA$$

$$Temp_6 = 1 - \frac{RAD^{1/2}}{CBB}$$

$$U_{Tmp} = \frac{CBB Temp_6}{2 CAA}$$

4.1.1

Steady Flow Gas Dynamics (Continued)

where U_{tmp} is based on the assumption of $P_2 = P_1$ and is used only once in calculating the initial value of ρ_{tmp} .

The continuity and momentum equations are iterated by converging on the discharge density as follows:

$$1. \quad \rho_{tmp} = \frac{\dot{W}_2}{12 A_2 U_{tmp}} \quad (\text{continuity})$$

$$\text{where } \dot{W}_2 = \dot{W}_1 + d\dot{W}$$

$$2. \quad U_{tmp} = \dot{W}_2 / 12 A_2 \rho_{tmp}$$

$$3. \quad T_{tmp} = T_o - \frac{(\gamma-1) U_{tmp}^2}{2 g_o R \gamma} \quad (\text{general energy})$$

$$4. \quad P_{tmp} = P_1 - \frac{2 (\dot{W}_2 U_{tmp} - \dot{W}_1 U_1)}{g_o (A_1 + A_2)} \quad (\text{momentum})$$

$$5. \quad \rho_2 = \frac{P_{tmp}}{12 R T_{tmp}} \quad (\text{perfect gas})$$

$$6. \quad T_{tmp} = \rho_{tmp} - \rho_2$$

$$7. \quad \text{If } \frac{|T_{tmp}|}{\rho_{tmp}} \leq .0001 \quad \text{go to 8, otherwise set } \rho_{tmp} = \rho_2$$

and return to 2.

$$8. \quad \begin{aligned} P_2 &= P_{tmp} \\ T_2 &= T_{tmp} \\ U_2 &= U_{tmp} \end{aligned}$$

9. Determine discharge mach number,

4.1.1

Steady Flow Gas Dynamics (Continued)

$$M_2 = \left[\frac{2(T_o - T_{Tnp})}{(\gamma-1)T_{Tnp}} \right]^{1/2}$$

4.1.2

Non-Steady Flow Gas Dynamics

The non-steady flow gas dynamic equations were developed to predict ignition and tail-off transients. The non-steady gas flow equations account for mass, momentum, volume, and pressure within the control volume varying with time. The fundamental equations of momentum and continuity along with the perfect gas law are expressed in partial differential form and then integrated across the control volume describing an incremental mass addition region using the technique of finite differences.

The gas dynamic solution for the mass addition regions is obtained by iterating the continuity and momentum equations for the discharge pressure, temperature, and flow rate. When the solution of the above discharge parameters have converged, the discharge values of mach number, density, and total pressure are determined. The derivation of the time dependent momentum equation and discharge flow rate and pressure equations are presented in the following sections for a mass addition region, Figure 4.1, and a segment slot, Figure 4.2.

4.1.2.1

Mass Addition Region

This section develops gas dynamic equations and solutions for a mass addition region as shown in Figure 4.1. The equation development from fundamental engineering principles to obtain the discharge conditions is taken from reference 6 and is presented below. The discharge pressure,

$$P_2 = \left[\frac{\dot{W}_1 U_1}{g_o} - \frac{\dot{W}_2 U_2}{g_o} + P_1 A_1 + \frac{P_1 + P_2}{2} (A_2 - A_1) - \frac{(P_1 + P_2)(U_1 + U_2)(V - V')}{24 g_o R (T_1 + T_2) \Delta t} - \frac{V(U_1 + U_2)(P_1 + P_2 - P_1' - P_2')}{24 g_o R (T_1 + T_2) \Delta t} \right] / A_2 + \left[\frac{(P_1 + P_2)(A_1 + A_2) a \Delta z}{24 R (T_o + T_2) g_o} \right] / A_2$$

4.1.2.1

Mass Addition Region (Continued)

and discharge flow rate,

$$\dot{W}_2 = \dot{W}_1 + d\dot{W} - \frac{(P_1 + P_2)}{12R(T_1 + T_2)} \frac{V - V^1}{\Delta t} - \frac{V(P_1 + P_2 - P_1^1 - P_2^1)}{12R(T_1 + T_2)\Delta t}$$

where

V = current port volume, in^3

V^1 = one past time increment volume, in^3

P_1^1 = Inlet past time increment pressure, lb/in^2

P_2^1 = discharge past time increment pressure, lb/in^2

Δt = time increment, sec

a = vehicle longitudinal acceleration, ft/sec^2

are iterated in subroutine AIBST to obtain the solution of the gas dynamic equations for a mass addition region. Total pressure, static temperature, mach number, and density are then calculated at the discharge station 2.

The derivation of the above equations and method of convergence follows:

Starting with the continuity equation:

$$1. \quad \frac{\partial}{\partial x} (\rho U A) + \frac{\partial}{\partial t} (\rho A) = 0 \quad (\text{continuity equation})$$

Integrating with respect to x between station 1 and 2 gives:

$$2. \quad \rho_2 U_2 A_2 - \rho_1 U_1 A_1 + \frac{\partial}{\partial t} \int_1^2 \rho A dx = 0$$

The first two terms are the discharge and inlet mass flow rates, \dot{W}_1 and \dot{W}_2 , respectively. The integral is the rate of change of mass between the stations 1 and 2 and may be evaluated as follows:

$$3. \quad \frac{\partial}{\partial t} \int_1^2 \rho A dx = \frac{\partial}{\partial t} \rho_m V - d\dot{W}$$

where

4.1.2.i

Mass Addition Region (continued)

$$V = \int_1^2 A \, dx, \text{ in}^3$$

$$\rho_m = \text{average density, lbm/ft}^3$$

$$d\dot{W} = \text{mass flow generated in the section, lb/sec}$$

and upon differentiation:

$$4. \quad \frac{\partial}{\partial t} (\rho_m V) = \rho_m \frac{dV}{dt} + V \frac{d\rho_m}{dt}$$

Combining terms and using finite differences with the perfect gas law yields from the continuity equation the solution of the discharge mass flow in terms of the pressures and control volume:

$$5. \quad \dot{W}_2 = \dot{W}_1 + d\dot{W} - \frac{P_1 + P_2}{12R(T_1 + T_2)} \frac{V - V'}{\Delta t} - \frac{V}{12R(T_1 + T_2)} \frac{P_1 + P_2 - P'_1 - P'_2}{\Delta t}$$

Euler's fluid acceleration equation for unit mass is:

$$6. \quad \frac{\partial U}{\partial t} + U \frac{\partial U}{\partial x} = - \frac{g_o}{\rho} \frac{\partial P}{\partial x}$$

Multiplying Euler's equation (6) by ρA and the continuity equation (1) by U gives:

$$7. \quad \rho A \frac{\partial U}{\partial t} + \rho U A \frac{\partial U}{\partial x} = -g_o A \frac{\partial P}{\partial x}$$

and

$$8. \quad U \frac{\partial}{\partial t} (\rho A) + U \frac{\partial}{\partial x} (\rho U A) = 0$$

Adding equations (7) and (8), and combining appropriate terms, yields the one-dimensional momentum equation:

$$9. \quad \frac{\partial}{\partial t} \left(\frac{\rho U A}{g_o} \right) + \frac{\partial}{\partial x} \left(\frac{\rho U^2 A}{g_o} \right) = -A \frac{\partial P}{\partial x} = - \frac{\partial}{\partial x} (PA) + P \frac{\partial A}{\partial x}$$

4.1.2.1

Mass Addition Region (Continued)

Then, integrating equation (9) with respect to x between station 1 and 2 gives:

$$10. \quad \frac{\partial}{\partial t} \int_1^2 \frac{(\rho U A)}{g_o} dx + \frac{(\rho_2 U_2^2 A_2 - \rho_1 U_1^2 A_1)}{g_o} = (P_1 A_1 - P_2 A_2) + \int_1^2 P dA$$

The last integral may be evaluated by defining a mean pressure, P_m , thus:

$$11. \quad \int_1^2 P dA = P_m (A_2 - A_1)$$

The first integral of equation (10) is the rate of change of momentum from nonstationary changes between stations 1 and 2 and may be evaluated by defining a mean density, ρ_m , and a mean velocity, U_m , and integrating with respect to x , thus:

$$12. \quad \frac{\partial}{\partial t} \int_1^2 \frac{(\rho U A)}{g_o} dx = \frac{\partial}{\partial t} \frac{(\rho_m U_m V)}{g_o}$$

and upon differentiation:

$$13. \quad \frac{\partial}{\partial t} \frac{(\rho_m U_m V)}{g_o} = \frac{\rho_m U_m}{g_o} \frac{dV}{dt} + \frac{\rho_m V}{g_o} \frac{dU_m}{dt} + \frac{U_m V}{g_o} \frac{d\rho_m}{dt}$$

Letting $\frac{dU_m}{dt} = 0$ and combining terms using finite differences with the perfect gas law yields from the momentum equation the solution of the discharge pressure in terms of the mass flows and pressures:

$$14. \quad P_2 = \left[\frac{\dot{W}_1 U_1}{g_o} - \frac{\dot{W}_2 U_2}{g_o} + P_1 A_1 + \frac{P_1 + P_2}{2} (A_2 - A_1) - \frac{(P_1 + P_2)(U_1 + U_2)(V - V')}{24 g_o R (T_1 + T_2) \Delta t} - \frac{V(U_1 + U_2)(P_1 + P_2 - P_1' - P_2')}{24 g_o R (T_1 + T_2) \Delta t} \right] / A_2$$

The acceleration term to be added to equation 14 is derived in Section 4.1.3.

4.1.2.1

Mass Addition Region (Continued)

Equations (5) and (14) are iterated in subroutine AIBST to solve for discharge temperature, pressure, and flow rate at each mass addition region as follows:

1. Estimate a starting value of the discharge pressure and temperature using the influence coefficient equations for constant specific heat and molecular weight, reference 7.

$$DT = T_1(\gamma-1) \left[\frac{(1+\gamma M_1^2) M_1^2 d\dot{W}}{(1-M_1^2) \dot{W}_1} \right]$$

$$a) T_{2\text{guess}} = T_1 - DT$$

$$DP = P_1 d\dot{W} 2\gamma M_1^2 \left[\frac{1 + \frac{(\gamma-1) M_1^2}{2}}{\dot{W}_1 (1-M_1^2)} \right]$$

$$b) P_{2\text{guess}} = P_1 - DP$$

2. Determine the gas storage:

$$\frac{dW}{dt} = \left[\frac{(P_1 + P_{2\text{guess}})(2V - V') - V(P_1' + P_2')}{12 R (T_1 + T_{2\text{guess}}) \Delta t} \right]$$

3. Determine the discharge flow rate:

$$\dot{W}_2 = \dot{W}_1 + d\dot{W} - \frac{dW}{dt}$$

4. Determine the discharge velocity:

$$U_2 = \frac{\dot{W}_2 R T_{2\text{guess}}}{P_2 A_2}$$

4.1.2.1

Mass Addition Region (Continued)

5. Determine the discharge pressure (equation 14 above):

$$P_2 = \left\{ \frac{\dot{W}_1 U_1}{g_0} - \frac{\dot{W}_2 U_2}{g_0} + P_1 A_1 + \frac{(P_1 + P_{2\text{guess}})}{2} (A_2 - A_1) \right. \\ \left. - \left[V(U_1 + U_2) (P_1 + P_{2\text{guess}} - P_1^i - P_2^i) \right. \right. \\ \left. \left. + (P_1 + P_{2\text{guess}}) (U_1 + U_2) (V - V^i) \right] \right\} / \left[24 g_0 R \right. \\ \left. (T_1 + T_{2\text{guess}}) \Delta t \right] / A_2$$

6. If an accelerating reference system is considered (see Section 4.1.3 for derivation):

If $\frac{a}{g_0} > 0$, determine acceleration term:

$$\text{Temp} = \left[(P_1 + P_{2\text{guess}}) (A_1 + A_2) \frac{a}{g_0} \Delta z \right] / \left[24 R (T_1 + T_{2\text{guess}}) A_2 \right]$$

$$P_2 = P_2 + \text{Temp}$$

7. If $\left| \frac{P_2 - P_{2\text{guess}}}{P_{2\text{guess}}} \right| \leq .001$, go to step 8, otherwise obtain

new value of $P_{2\text{guess}}$ using method of false position and return to step 1(h).

8. Determine U_2 based on converged P_2 :

$$U_2 = \frac{\dot{W}_2 R T_{2\text{guess}}}{P_2 A_2}$$

9. Determine the discharge temperature using the general energy equation:

$$T_2 = T_0 - \frac{(\gamma - 1) U_2^2}{2 g_0 \gamma R}$$

4.1.2.1 Mass Addition Region (Continued)

10. If $\left| \frac{T_{2\text{guess}} - T_2}{T_{2\text{guess}}} \right| \leq .001$, go to step 11, otherwise obtain new value of $T_{2\text{guess}}$ using method of false position and return to step 1(a).

11. Solution is converged, determine discharge mach number, gas density, and total pressure:

$$M_2 = U_2 / \left[g_0 \gamma R T_2 \right]^{1/2}$$

$$\rho_2 = \frac{\dot{W}_2}{12 A_2 U_2}$$

$$P_{02} = P_2 \left(\frac{T_0}{T_2} \right)^{\frac{\gamma}{\gamma-1}}$$

4.1.2.2 Segment Slot Mass Addition

The development of the gas dynamic equations for the region between grain segments of segmented motors (referred to as a slot) is similar to the non-steady gas flow equation development for a mass addition region, Section 4.1. The control volume for a slot is defined from the forward slot interface to the aft slot interface with mass addition occurring at each interface and not within the control volume. The control volume for a slot is shown in Figure 4.2.

The following assumptions are made in subroutine SLOT (including the assumptions of Section 4.1):

- The static pressure and temperature at the slot interface is the same as the port static pressure, $P_1 = P_2$, $P_3 = P_4$, $T_1 = T_2$, and $T_3 = T_4$.
- The mass flow generated at the slot interface is a function of the port static pressure only and is determined from the following burn rate equation:

$$\dot{W} = A_f \rho_f a P^n$$

4.1.2.2

Segment Slot Mass Addition (Continued)

where:

- \dot{dW} = generated mass flow, lb/sec
- A_f = burn area at slot interface, in²
- ρ_f = solid propellant density, lb/in³
- P = slot interface static pressure, lb/in²
- a = burn rate coefficient
- n = burn rate equation pressure coefficient.

- c. Static pressure at station 3 is a function of the area change (dA/dx), and the capacitance effects (dP/dt and dV/dt) between stations 2 and 3, and acceleration of the vehicle.

The solution of the gas dynamics within a slot is obtained from the above assumptions and the equations developed in Section 4.0 as follows:

1. Determine the mass generation rate at the forward slot interface (station 2) from the static pressure at station 1 (port cavity discharge)

$$\dot{dW}_f = A_f \rho_f a P^n$$

2. Determine the inlet flow rate, velocity, and mach number:

$$\dot{W}_2 = \dot{W}_1 + \dot{dW}_f$$

$$U_2 = \frac{\dot{W}_2 R T_1}{P_1 A_2}$$

$$M_2 = \frac{U_2}{\left[g_0 k R T_1 \right]^{1/2}}$$

3. Determine the current slot volume and rate of change of volume:

$$V = \frac{A_2 + A_3}{2} (z_3 - z_2)$$

where

4.1.2.2

Segment Slot Mass Addition (Continued)

Z_3 = aft interface station location, in.

Z_2 = forward interface station location, in.

$$\frac{dV}{dt} = \frac{\pi}{2\Delta t} \left[\tau_f (R_{f2}^2 + R_{SLOTf}^2) + \tau_a (R_{f3}^2 + R_{SLOTa}^2) \right]$$

where:

τ_f = current value of forward slot interface distance burned in.

τ_a = current value of aft slot interface distance burned in.

4. Guess the value of the slot aft interface static pressure and temperature using the influence coefficient equations for constant specific heat and molecular weight, reference 7.

$$dT = \frac{T_1 (\gamma - 1) (1 + \gamma M_2^2) M_2^2 d\dot{w}_f}{(1 - M_2^2) \dot{w}_2}$$

$$dP = \frac{P_1 d\dot{w}_f + g_o M_2^2 (1 + \frac{\gamma - 1}{2} M_2^2)}{\dot{w}_2 (1 - M_2^2)}$$

$$P_{3\text{guess}} = P_2 - dP$$

$$T_{3\text{guess}} = T_1 - dT$$

5. Determine the mass generation rate at the aft slot interface (station 3) from the guessed static pressure at station 3:

$$\dot{d\dot{w}}_a = A_a a P_{3\text{guess}}^n$$

6. Determine the stored gas in the slot

$$\frac{dW}{dt} = \frac{(P_2 + P_{3\text{guess}})}{12 R (T_1 + T_{3\text{guess}})} \frac{dV}{dt} + \frac{V}{12 R (T_1 + T_{3\text{guess}})} \frac{(P_2 + P_{3\text{guess}} - P_2^i - P_3^i)}{\Delta t}$$

SHEET

4.1.2.2

Segment Slot Mass Addition (Continued)

where

$$\frac{dW}{dt} = \frac{\partial}{\partial t} \left(\frac{P V}{12 RT} \right)$$

7. Determine the discharge flow rate and velocity:

$$\dot{W}_3 = \dot{W}_2 + \frac{dW}{dt}$$

$$U_3 = \frac{\dot{W}_3 R T_{3\text{guess}}}{P_{3\text{guess}} A_3}$$

8. Determine the aft slot interface static pressure (see Section 4.1.2.1, equation 14).

$$P_3 = \left[\frac{\dot{W}_2 U_2}{g_0} - \frac{\dot{W}_3 U_3}{g_0} + P_2 A_2 + \frac{P_2 + P_{3\text{guess}}}{2} (A_3 - A_2) - \frac{(P_2 + P_{3\text{guess}})(U_2 + U_3)}{24g_0 R(T_{3\text{guess}} + T_1)} \frac{dV}{dt} - \frac{V(U_2 + U_3)(P_2 + P_{3\text{guess}} - P_2^i - P_3^i)}{24g_0 R(T_{3\text{guess}} + T_1) \Delta t} \right] / A_3 + \left[\frac{(P_2 + P_{3\text{guess}})(A_2 + A_3) \Delta Z}{24g_0 R(T_2 + T_{3\text{guess}})} \right] / A_3$$

9. if $\left| \frac{P_3 - P_{3\text{guess}}}{P_3} \right| \leq \text{CRP}$, go to step 10, otherwise obtain new

value of $P_{3\text{guess}}$ using method of false position and return to step 5. If CRP is not input the program will set CRP equal to .001.

10. Determine the slot aft interface static temperature from the general energy equation:

4.1.2.2

Segment Slot Mass Addition (Continued)

$$T_3 = T_0 - \frac{(\gamma - 1) U_3^2}{2 g_0 \gamma R}$$

11. If $\left| \frac{T_3 - T_{3\text{guess}}}{T_3} \right| \leq \text{CRT}$, go to step 12, otherwise obtain new value of $T_{3\text{guess}}$ using method of false position and return to step 7. If CRT is not input the program will set CRT equal to .001.
12. Determine the slot discharge velocity, mach number, density, and total pressure:

$$U_4 = \frac{\dot{W}_3 R T_3}{P_3 A_4}$$

$$M_4 = \frac{U_4}{[g_0 \gamma R T_3]^{1/2}}$$

$$\rho_4 = \frac{\dot{W}_3}{12 A_4 U_4}$$

$$P_0 = P_3 \left(\frac{T_0}{T_3} \right)^{\frac{\gamma}{\gamma-1}}$$

4.1.3

Non-Steady Flow Gas Dynamics with Acceleration

The effects of longitudinal acceleration of the vehicle on the internal ballistic solution is considered in this section. In conventional gas dynamic studies, the effects of gravitational forces are not considered because, for compressible fluids, gravitational forces are significantly less than surface forces. Recent development of missiles for low level ICBM intercept may require boost accelerations that are of significant magnitude to affect motor internal pressures and temperatures. In an accelerating reference system, the force field which results from the acceleration is equivalent to a gravitational force field in a nonaccelerating reference system.

4.1.3

Non-Steady Flow Gas Dynamics with Acceleration

The acceleration effects are considered only on the gas dynamic equations in the port cavity of the motor and not in the nozzle. Effect of acceleration on a nozzle is to move the sonic point upstream of the throat. The effect of acceleration on the motor internal ballistics is to reduce the pressure drop along the propellant grain as well as fore-head pressure.

The resulting acceleration term is added to the momentum equation as follows:

$$\frac{\partial}{\partial t} \int_1^2 \frac{(\rho U A)}{g_0} dx + \frac{(\rho_2 U_2^2 A_2 - \rho_1 U_1^2 A_1)}{g_0} \\ = (P_1 A_1 - P_2 A_2) + \int_1^2 P dA + \frac{(\rho_m A_m a \Delta Z)}{g_0}$$

where

- a = vehicle longitudinal acceleration, ft/sec^2
- ΔZ = length between increments, ft
- ρ_m = average gas density in increment, lb/ft^3
- A_m = average cross sectional area in increment, ft^2
- g_0 = conversion constant, 32.174 lbm/slug

The acceleration term is developed as follows:

1. From Newton's Second Law of motion:

$$F_{bf} = \frac{W}{g_0} a$$

where

- F_{bf} = body force, lbf
- W = weight, lbf
- a = acceleration, ft/sec^2

4.1.3

Non-Steady Flow Gas Dynamics with Acceleration

2. The body force exerted on the gas within a mass addition region is:

$$F_{bf} = \frac{\rho_m A_m \Delta Z}{g_o} a$$

3. Assuming perfect gas relationships, the body force may be written as:

$$F_{bf} = \frac{(P_1 + P_2) (A_1 + A_2) \Delta Z a}{24 g_o R (T_1 + T_2)}$$

4. and from $P = F/A$:

$$\Delta P = \frac{(P_1 + P_2) (A_1 + A_2) \Delta Z}{24 (T_1 + T_2) A_2} \frac{a}{g_o}$$

where

ΔP = pressure change resulting from acceleration, lb/in^2

The pressure change resulting from vehicle acceleration is added to the discharge pressure of a mass addition region as shown in Section 4.1.2.1, step 6, for the iteration of the discharge pressure and flow rate.

4.2

Complete Motor Gas Dynamics

Solution of overall motor gas dynamics or internal ballistics from fore-head to nozzle exit is described in this section.

4.2.1

Fore-Head Pressure Convergence

Solution of motor internal ballistics for each time point is obtained by an iteration process which converges on fore-head pressure, P_H , (Figure 3.1). An initial estimate is made for fore-head pressure either from the input value P_{H1} at time = 0, or from the previous time solution of P_H at time > 0. The fore-head section mass balance is obtained in subroutine MNCHN4 (flow chart No. 10) after geometry values have been determined. Then parameters necessary to solve cylindrical section mass addition regions in subroutine SEGSUB (flow chart number 11) are determined. When the cylindrical section is complete, the aft-head section mass balance is obtained in subroutine MNCHN4 and the fore-head pressure is checked for convergence in subroutine SETPH (flow chart number 12).

The fore-head pressure convergence check in subroutine SETPH is made as follows:

1. Determine the throat critical pressure ratio:

$$\frac{P_s}{P_0} = \left(\frac{2}{\gamma+1} \right)^{\frac{\gamma}{\gamma-1}}$$

2. Determine the nozzle total pressure:

$$P_{ON} = P \left(\frac{T_0}{T} \right)^{\frac{\gamma}{\gamma-1}}$$

where

P = aft-head section discharge static pressure,
lbs/in²

T = aft-head section discharge static temperature, °R

3. If $P_{ON} \left(\frac{P_s}{P_0} \right) \geq P_a$, the nozzle is choked. Determine the sonic nozzle flow rate:

4.2.1

Fore-Head Pressure Convergence (Continued)

$$DIS = \frac{g_o NN A_t P_{ON}}{C^*}$$

where

NN = number of nozzles

Go to 5.

4. If $P_{ON} \left(\frac{P_s}{P_o} \right) < P_a$, the nozzle is not choked. Determine the subsonic nozzle flow rate:

$$SDIS = NN P_{ON} A_{EE} \left(\frac{P_a}{P_{ON}} \right)^{\frac{1}{\gamma}} \left[\frac{2\gamma g_o}{T_o R(\gamma-1)} \left(1 - \left(\frac{P_a}{P_{ON}} \right)^{\frac{\gamma-1}{\gamma}} \right) \right]^{1/2}$$

where

A_{EE} = nozzle exit plane area.

DIS = SDIS

5. If $\left| \frac{\dot{W} - DIS}{DIS} \right| > CRW$, estimate new fore-head pressure as follows (\dot{W} = grain discharge flow rate): If CRW is not input the program will set CRW equal to .005.

a) $WD = \frac{\dot{W} - WDB}{P_H - P_{Hold}}$

where P_{Hold} = previous iterative value of P_H , psi

WDB = previous iterative value of WD, lb/sec

\dot{W} = grain discharge flow rate, lb/sec

b) $DEED = \frac{DIS - DISB}{P_H - P_{Hold}}$

where DISB = previous iterative value of DIS

4.2.1

Fore-Head Pressure Convergence (Continued)

c) If $DEED = WD$ or if $DEED = 0$:

$$\Delta P = P_H \left[\left(\frac{\dot{W}}{DIS} \right)^{1.4} - 1 \right]$$

d) If $DEED \neq WD$:

$$\Delta P = \frac{\dot{W} - DIS}{DEED - WD}$$

e) $WDJ = \dot{W}$

$$DISB = DIS$$

f) If $\dot{W} \leq DIS$, $P_{min} = P_H$

g) If $\dot{W} > DIS$, $P_{max} = P_H$

h) $P_{Hguess} = P_H + \Delta P$

i) If $P_{Hguess} \leq P_{min}$ and $P_{min} = 0$

$$P_{Hguess} = 5.0 \text{ lbs/in}^2$$

j) If $P_{Hguess} \leq P_{min}$ and $P_{min} \neq 0$

$$P_{Hguess} = 2.0 P_H$$

k) If $P_{min} < P_{Hguess} \geq P_{max}$:

$$P_{Hguess} = .9(P_{max} - P_{min}) + P_{min}$$

Return to fore-head section with $= P_{Hguess}$.

4.2.1

Fore-Head Pressure Convergence (Continued)

- 1) If $P_{\min} < P_{\text{Hguess}} < P_{\max}$, return to fore-head section with $P_H = P_{\text{Hguess}}$.
6. If $\left| \frac{\dot{W} - \text{DIS}}{\text{DIS}} \right| \leq \text{CRW}$, convergence has been attained. If CRW is not input the program will set CRW equal to .005.

4.2.2

Nozzle Gas Dynamics

After the fore-head pressure convergence criterion has been satisfied (step 5 and 6 of the previous section), the nozzle gas dynamics in subroutine SETPH are determined as follows:

1. Determine the nozzle exit area:

$$A_{EE} = \frac{\pi D_E^2}{4}$$

2. Determine the nozzle expansion ratio:

$$\epsilon_G = \frac{A_{EE}}{A_t}$$

3. Iterate the following equation for $\frac{P_E}{P_{ON}}$ using the method of false position:

$$\frac{P_E}{P_{ON}} = \left[\left(\frac{1}{\gamma} \right)^{1/\gamma} \left(\frac{2}{\gamma+1} \right)^{\frac{1}{\gamma-1}} / \epsilon_G \right] / \left[1 - \left(\frac{P_E}{P_{ON}} \right)^{\frac{\gamma-1}{\gamma}} \right]^{\frac{\gamma}{2}}$$

4. Determine the momentum portion of the thrust coefficient:

$$C_{fo} = \left[\frac{2\gamma^2}{\gamma-1} \left(\frac{2}{\gamma+1} \right)^{\frac{\gamma+1}{\gamma-1}} \left\{ 1 - \left(\frac{P_E}{P_{ON}} \right)^{\frac{\gamma-1}{\gamma}} \right\} \right]^{1/2}$$

4.2.2

Nozzle Gas Dynamics (Continued)

5. Determine the delivered vacuum thrust coefficient:

$$C_{foL} = (C_{fo} \lambda_n + \frac{P_E}{P_{ON}} \epsilon_G) C_m$$

6. Determine the delivered thrust at P_a for sonic flow:

$$F = (C_{foL} P_{ON} A_t - P_a \epsilon_G A_t) NN$$

7. Determine the delivered thrust for subsonic flow:

$$V_E = \left[\frac{2\gamma T_o R g_o}{\gamma-1} \left\{ 1 - \left(\frac{P_a}{P_{ON}} \right)^{\frac{\gamma-1}{\gamma}} \right\} \right]^{1/2}$$

$$F = \frac{V_E \lambda_N \dot{W} C_m NN}{g_o}$$

8. Determine the fore-head pressure-time integral:

$$\int P_H dt = \int P_i dt + (P_{Hold} + P_H) \frac{\Delta t}{2}$$

9. Determine the nozzle total pressure-time integral:

$$\int P_{ON} dt = \int P_{ON} dt + (P_{ONold} + P_{ON}) \frac{\Delta t}{2}$$

10. Determine the nozzle discharge flow-time integral:

$$\int \dot{W}_N dt = \int \dot{W}_N dt + (\dot{W}_{Nold} + \dot{W}_N) \frac{\Delta t}{2}$$

11. Determine the total impulse:

$$IT = IT + (F + F_{old}) \frac{\Delta t}{2}$$

4.2.2

Nozzle Gas Dynamics (Continued)

The above iterative procedure is allowed to continue for no more than 11 iterations. If the fore-head pressure has not converged within 11 iterations, a summary of the last iteration is printed followed by a complete program data dump and the next case is set up. When convergence has been attained, the program output is printed and the next time increment solution is initiated by setting $P_{H\text{guess}}$ equal to the previous time increment solution of P_H . Program execution for each case continues until termination options are satisfied.

4.3

Propellant Characteristics and Burning Rate Model

The characteristics of the propellant are represented by a mathematical model of the burning rate and properties of the products of combustion. Basic assumptions of a perfect gas, constant combustion temperature and constant specific heat allow the propellant gas properties to be described by the characteristic velocity, C^* , the combustion temperature, T_0 , the specific heat ratio, γ , and the gas constant, R .

The propellant burning rate model allows either isotropic or anisotropic burning of the propellant surface. Isotropic burning is defined as uniform combustion occurring normal to the propellant surface. In anisotropic burning, the burn rate varies with distance burned as well as with conditions at the gas-propellant interface. It results from non-homogeneous dispersion of propellant additives near the case wall and core during propellant casting.

4.3.1

Propellant Gas Properties

The propellant gas properties may be held constant or may be varied as a function of the static pressure in the port cavity. If the gas properties are to be held constant, the parameters T_0 , C^* , γ , and R are input. If the gas properties are to be varied, tables of the combustion temperature (TCOMB), the molecular weight (AMWG), the specific heat ratio (GAMAG), and the characteristic velocity (CSTR), are input as a function of static pressure (PRESS).

When the gas tables are input, a spline interpolation procedure is used in subroutine CSTRSB to obtain the gas properties for the static pressure at the increment dividing plane. The spline interpolation procedure sets up a series of piecewise cubics between the table values to obtain an interpolated value corresponding to this static pressure.

4.3.2

Propellant Burning Rate Model

The propellant burning rate model may include the effects of erosive burning. Erosive burning is defined as the change in the local burning rate resulting from gas velocity parallel to the burning surface.

The propellant burning rate, R_B , at any increment dividing plane is determined from the following parameters at the adjacent upstream increment dividing plane:

1. Static pressure	P
2. Gas velocity	U
3. Mass velocity per unit area	G
4. Distance from stagnation point	h_{RB}
5. Burning rate	R_{BII}
6. Solid propellant density	ρ_f

With the exception of ρ_f , these values are not input but are calculated within the program.

Fifty-one constants are available to define the burning rate equation. Only the constants that are required for the particular burning rate equation to be used are input. These constants are as follows:

KG1 through KG5
 KU1 through KU5
 KR1 through KR39
 KSL0T1 through KSL0T2

Prior to calculating burning rate, critical values of velocity, UCR, and mass velocity per unit area, GCR, are obtained as follows:

$$UCR = KU1 + (KU2) P^{(KU3)} + (KU4) P^{(KU5)}$$

$$GCR = KG1 + (KG2) P^{(KG3)} + (KG4) P^{(KG5)}$$

Propellant burning rate is then calculated in one of two ways:

If G is greater than or equal to GCR, and U is greater than or equal to UCR, the following relation is used:

$$R_B = KR1 + (KR2) P^{(KR3)} + (KR4) P^{(KR5)} + (KR6) U^{(KR7)} \\ + (KR8) U^{(KR9)} + (KR10) G^{(KR11)} + (KR12) G^{(KR13)}$$

4.3.2

Propellant Burning Rate Model

$$\begin{aligned}
 & + (KR14) P^{(KR15)} U^{(KR16)} + (KR17) P^{(KR18)} U^{(KR19)} \\
 & + (KR20) P^{(KR21)} G^{(KR22)} + (KR23) P^{(KR24)} G^{(KR25)} \\
 & + \frac{KR26}{(KR27) P^{(KR28)} + (KR29) P^{(KR30)}} \\
 & + (KR31) \frac{G^{(KR32)}}{R_B^{(KR33)}} e^{-\left[\frac{(KR34) R_{BHI} D_f}{G} \right]}
 \end{aligned}$$

If the value of G is less than GCR or if the value of U is less than UCR, then the following relation is used:

$$R_B = KR35 + (KR36) P^{(KR37)} + (KR38) P^{(KR39)}$$

To prevent the values of GCR and UCR from being used simultaneously for choosing the burning rate model, one of these values must always be equal to zero. This is accomplished by setting the values of constants KG1, KG2, and KG4 or the values of constants KU1, KU2, and KU4 equal to zero. The program will automatically stop if any of the terms KG1, KG2, or KG4 are not equal to zero when any of the terms KU1, KU2, or KU4 are also not equal to zero. In such cases, the program will print-out a statement that the GCR or UCR coefficients are invalid. If KR26 is not zero, then neither KR27 nor KR29 can be negative or simultaneously equal to zero; if this restriction is exceeded, the program will stop and print-out a statement of invalid KR27 or KR29.

The burning rate at the segment slot face is calculated by

$$RBSLOT = (KSLOT1) P^{(KSLOT2)}$$

where P is the static pressure in the port at the segment interface.

4.3.3

Anisotropic Propellant Burning

Anisotropic propellant burning capability, where burn rate depends on distance burned, was added to the program because of Boeing's experience with the HIBEX motor. Anisotropic burning occurred during both ignition and tail-off. It appeared to be the result of two effects: 1) variation in the alignment of the staples between the bulk of the propellant at the case wall and the core interface, and 2) the burning distance required to develop "coning" about the staples. Anisotropic burning is most easily represented by variation of the constant "a" as a function of distance burned in the burn rate equation, $r = aP^n$. During ignition, mass generation is determined by multiplying the port perimeter by the anisotropic burning rate. During tail-off, regions exist where both isotropic and anisotropic burning occur. The port perimeter is subdivided accordingly. The total mass generation is then the sum of the individual mass generation rates.

The following assumptions have been made in developing the mathematical model:

1. The anisotropic region at both the core interface and the case wall is of uniform thickness along the motor length.
2. The thickness of the anisotropic region is the same at both the core interface and the case wall.
3. The burn rate variation through the anisotropic region is a function only of distance burned and local static pressure, $r = a(\tau)P^n$.
4. The anisotropic burn rate increases from the core interface toward the isotropic propellant and decreases from the isotropic propellant toward the case wall.
5. The fore-head and aft-head burning rate during motor tail-off is the same as the adjacent tangent plane isotropic burning rate.

The following limitations apply to the program:

1. Anisotropic burning cannot be considered for propellants with wagon wheel grain configurations during tail-off.
2. Anisotropic burning may be considered for non-steady flow options only during ignition and tail-off.

Program simulation of anisotropic burning is accomplished by altering normal program solution during the ignition transient interval to solve for the burn rate coefficient with a fixed

4.3.3

Anisotropic Propellant Burning (Continued)

value of the fore-head pressure at each time increment. The burn rate coefficient is stored in a table as a function of distance burned at a desired location within the cylindrical section (Input NINCPL). A program option is available to input this anisotropic burn rate coefficient table and solve for fore-head pressure as discussed in Section 4.2.1. The burning rate within the fore-head and aft-head sections may be specified by inputs KRH and KRW or by the anisotropic burning rate table inputs. During the tail-off interval, when the burning surface is within the anisotropic propellant region, the burning rate at each increment dividing plane in sectors 6, 7, and 8 becomes a function of the distance from the case wall within the sector as shown in Figures 4.4, 4.5, and 4.6.

The program method of solution for anisotropic burning during the ignition transient interval, when the fore-head pressure trace is input, is altered to converge on the burn rate coefficient, KRST. At each time increment, an estimate of the burn rate coefficient is determined in subroutine RBSTSB from the fore-head pressure rise rate and the motor configuration as follows:

From the perfect gas law using finite differences:

$$1. \quad \frac{dP_H}{dt} = \frac{\partial}{\partial t} \left[\frac{12 W_H R T}{V} \right] = \frac{12 R T}{V} \frac{dW_H}{dt}$$

and,

$$2. \quad \frac{dW_H}{dt} = \dot{W}_{in} - \dot{W}_{out}$$

where

$$\begin{aligned} \dot{W}_{in} &= \text{generated weight flow rate, lb/sec} \\ \dot{W}_{out} &= \text{nozzle discharge flow rate, lb/sec} \\ V &= \text{free volume, in}^3 \end{aligned}$$

The nozzle discharge flow rate is determined from the nozzle geometry:

$$3. \quad \dot{W}_{out} = \frac{g_o A_t P_{0N}}{C^*}$$

where

4.3.3

Anisotropic Propellant Burning (Continued)

$$\begin{aligned}
 g_o &= \text{gravitational constant, ft/sec}^2 \\
 A_t &= \text{nozzle throat area, in}^2 \\
 P_{ON} &= \text{nozzle total pressure, lb/in}^2 \\
 C^* &= \text{characteristic velocity, ft/sec}^2
 \end{aligned}$$

and the generated weight flow rate is determined from the motor configuration:

$$4. \quad \dot{W}_{in} = R_b A_b \rho_f$$

where

$$\begin{aligned}
 R_b &= \text{burn rate, in/sec} \\
 A_b &= \text{total burn area, in}^2 \\
 \rho_f &= \text{propellant density, lb/in}^3
 \end{aligned}$$

$$5. \quad RT = \frac{\Gamma^2 C^{*2}}{g_o}$$

where

$$\Gamma^2 = \gamma \left(\frac{2}{\gamma+1} \right)^{\frac{\gamma+1}{\gamma-1}}$$

Therefore:

$$6. \quad \frac{dP_H}{dt} = \dot{P}_H = \frac{12 \Gamma^2 C^{*2}}{V g_o} (R_b A_b \rho_f) - \frac{12 \Gamma^2 C^*}{V} (P_{ON} A_t)$$

Combining and arranging terms with $P_{ON} = (TPR) P_H$, where TPR is an input estimate of the port pressure drop, we have:

$$7. \quad R_b = \frac{\dot{P}_H + \frac{(12 \Gamma^2 C^*) (A_t TPR P_H)}{V}}{\frac{12 \Gamma^2 C^{*2} A_b \rho_f}{g_o V}}$$

and

4.3.3

Anisotropic Propellant Burning (Continued)

$$8. \quad KRST = \frac{R_b}{P_H^n}$$

After the initial estimate of KRST is made, the ballistic solution is converged for the fixed fore-head pressure obtained from the input pressure trace using the convergence procedure outlined in Section 4.2.1. When the anisotropic burn rate coefficient table is input, the method of solution remains unchanged except that the burn rate coefficient which depends on distance burned at location NINCPL from the forward tangent plane is determined from the input table at each time increment.

The ignition transient interval is terminated when the value of time exceeds the last table value of the input fore-head pressure trace independent variable TIMEPH(NPH), or when the burn rate table is input, the termination option TST. The steady state interval will then continue with the last table value of the burn rate coefficient dependent variable AARTAU(NAKRST) or the burn rate coefficient inputs KR(2) and KR(36) (depending on choice of inputs) in the general burning rate equation.

As the burning surface progresses toward the case wall, the anisotropic region is first exposed in the region of sector 8 as shown in Figure 4.4. This results in a non-uniform burning rate along the propellant burning surface during the tail-off interval.

Three burning rates are determined for the burning surface: R_{b8} which is determined from the anisotropic burning distance in sector 8, R_{b7} which is determined from an integration along the anisotropic perimeter of sector 7 between the isotropic and anisotropic burning distances using the anisotropic burn rate coefficient table, and the normal isotropic burn rate, R_b .

Two separate burn distances are defined: the isotropic burn distance in sectors 1 through 7, TAUZ(III), and the anisotropic burn distance in sectors 7 and 8, TAUZTO(III). The anisotropic burn rate becomes progressively less during motor tail-off, resulting in an anisotropic burn distance less than the isotropic burn distance and producing burning that is not normal to the grain surface.

Figures 4.4, 4.5, and 4.6 show the configurations of the anisotropic propellant region that can exist at the case wall for a standard star configuration with an inert sliver. The angles η_2 , η_{22} , and "ANGLE" are used to determine the anisotropic pro-

4.3.3

Anisotropic Propellant Burning. (Continued)

pellant perimeter lengths, AL_7 and AL_8 , during motor tail-off. Angle η_2 is subtended from the R_5 radius and locates the intersection of the anisotropic propellant region with the isotropic propellant region. Angle η_{22} is subtended from the motor axis to the same intersection point for η_2 . "ANGLE" is subtended from the motor axis and identifies the point of intersection of the isotropic burn distance vector, swung from R_5 , with the case wall.

Subroutine LPT0 contains the geometry calculations to determine the sector perimeter length of the anisotropic propellant for each reference plane during motor tail-off. The anisotropic propellant perimeter length in sector 8 is identified as AL_8 , and in sector 7 is identified as AL_7 . The perimeter length of sector 7 anisotropic propellant (AL_7) is assumed to be a straight line between the point determined by the intersection of the isotropic propellant with the anisotropic propellant and the anisotropic burning distance with the case wall or with sector 8.

The distance burned of the anisotropic propellant in sectors 7 and 8 is computed from the burn rate of the anisotropic propellant in Sector 8 (RB_8) in Subroutine SEG SUB. Once sector 8 has burned out, RB_8 is determined from the first table value of the anisotropic burn rate coefficient (the minimum value). The progression of the intersection of the propellant with the case wall is assumed to proceed at the minimum burn rate.

The mass flow generated is determined in subroutine SEG SUB from the perimeter lengths of the anisotropic burning propellant (AL_7 and AL_8), and the isotropic burning propellant (ALP) and their corresponding burn rates as follows:

$$\dot{m}_7 = N_0 \rho_f \Delta Z (AL_7 R_{B7} + AL_{7HI} R_{B7HI})$$

$$\dot{m}_8 = N_0 \rho_f \Delta Z (AL_8 R_{B8} + AL_{8HI} R_{B8HI})$$

$$\dot{m} = \left[\frac{\rho_f \Delta Z}{2} (ALP_{HI} - AL_{TOHI}) RB_{HI} + (ALP - AL_{TE}) R_B \right] + \dot{m}_7 + \dot{m}_8$$

where

$$AL_{TO} = (AL_7 + AL_8) 2N_0$$

4.3.3

Anisotropic Propellant Burning (Continued)

and subscripted "H" values are at the inlet to the mass addition region. The non-subscripted ones represent the outlet to the mass addition region.

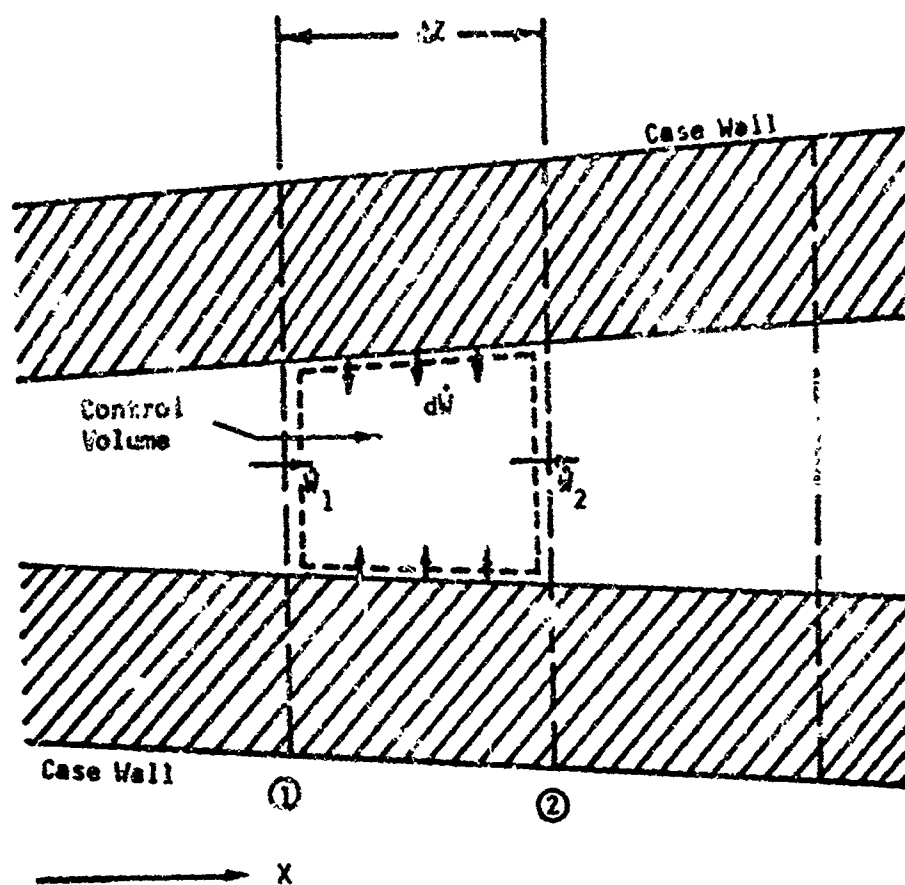
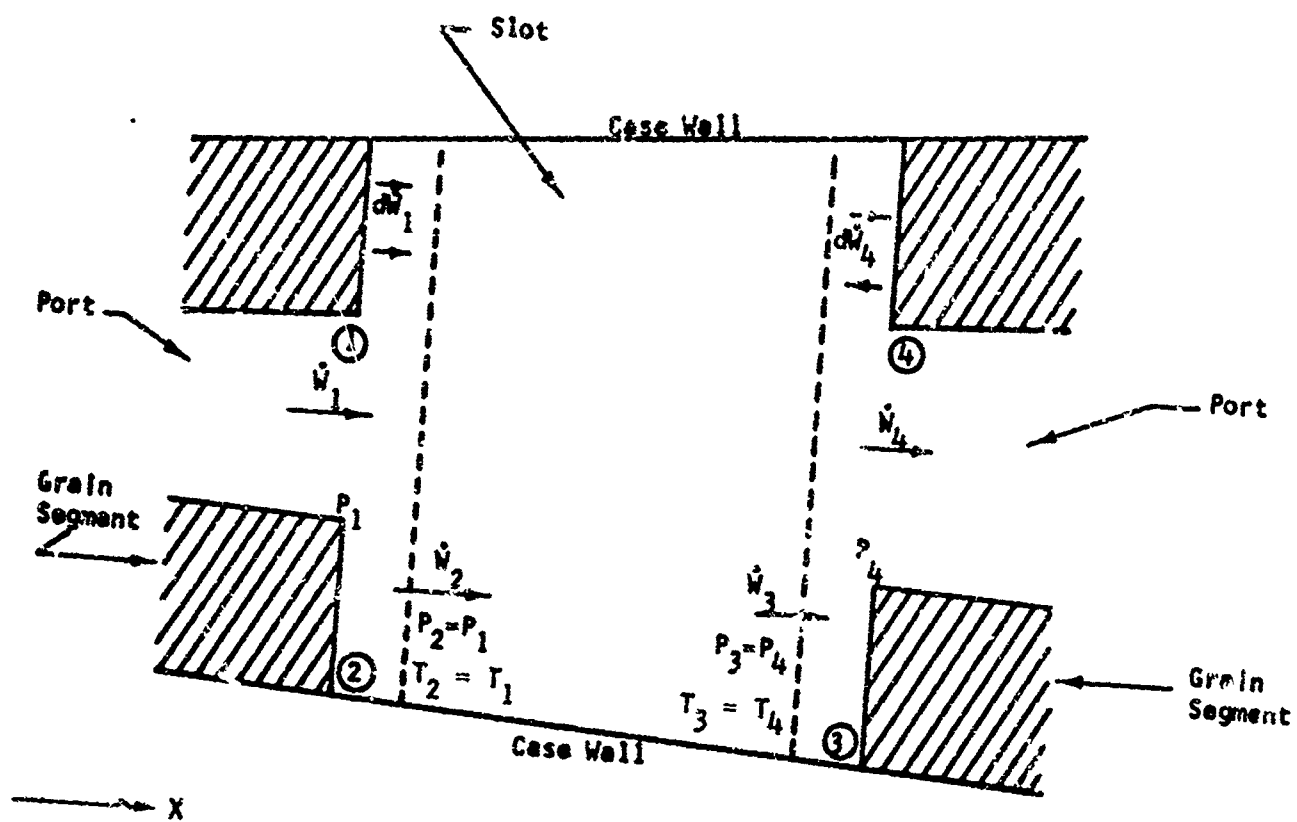


Figure 4.1. Mathematical Model of Mass Addition Region Control Volume



- ① Slot forward Interface
- ② Slot forward Interface mass addition region
- ③ Slot aft Interface mass addition region
- ④ Slot aft Interface

Figure X.2. Mathematical Model of Slot Between Grain Segments

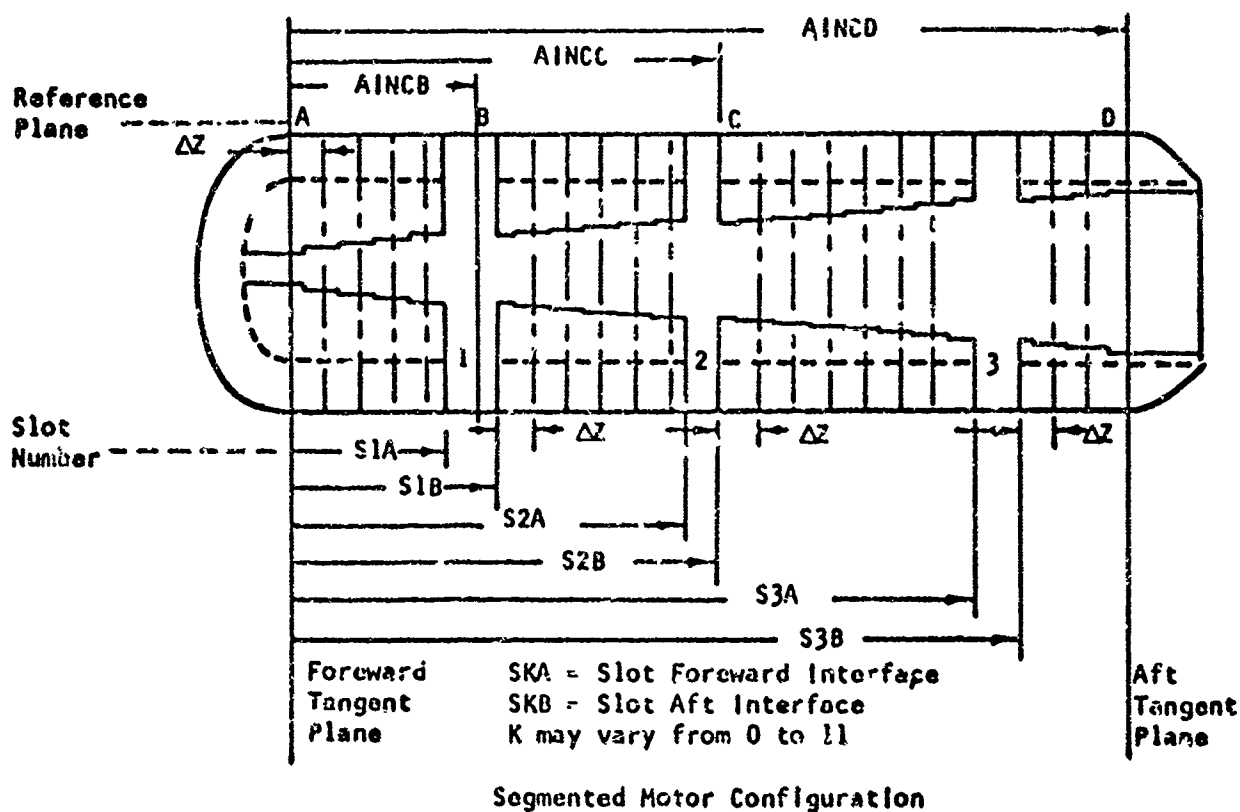
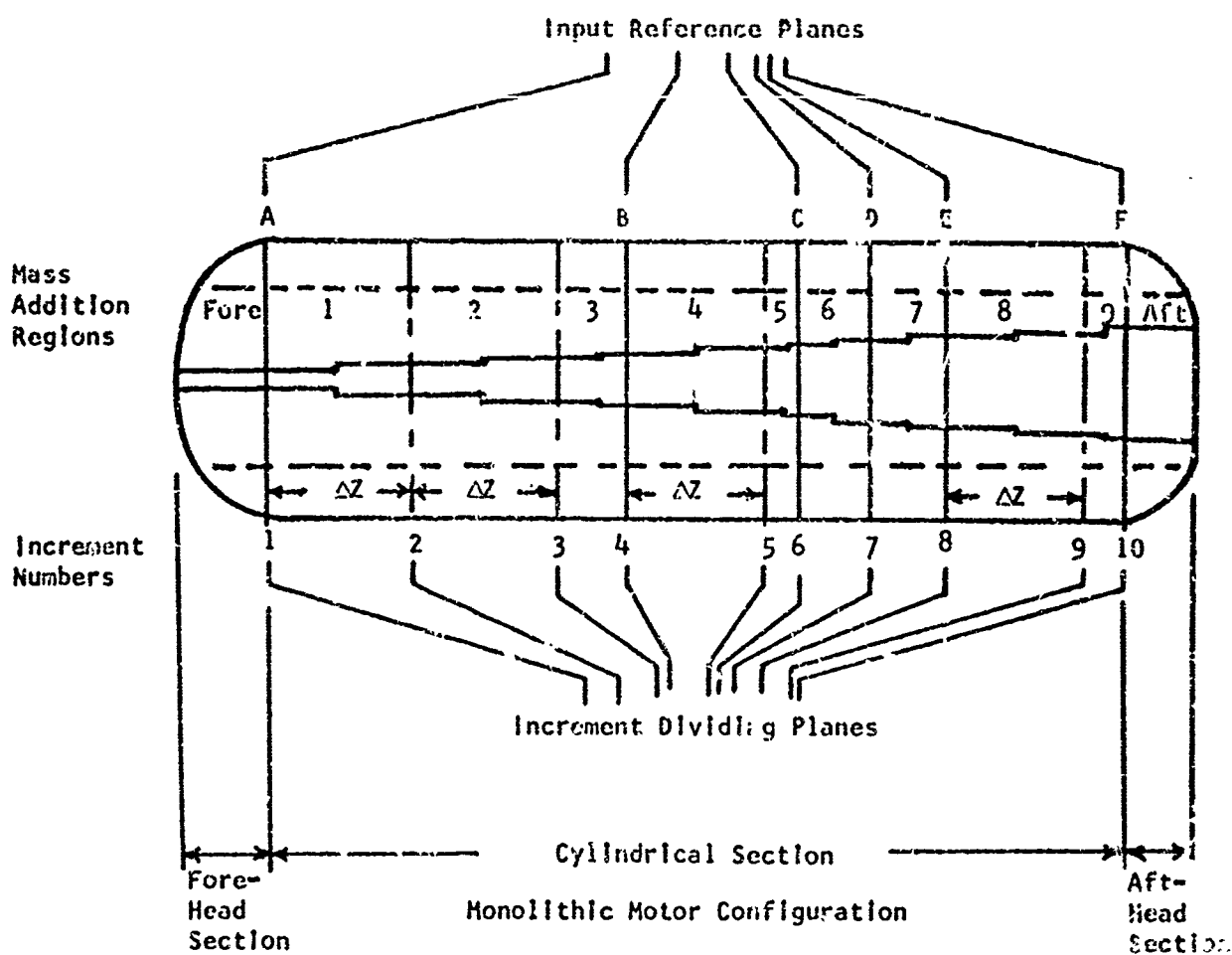


Figure 4.3 Reference Plane and Increment Dividing Plane Identification

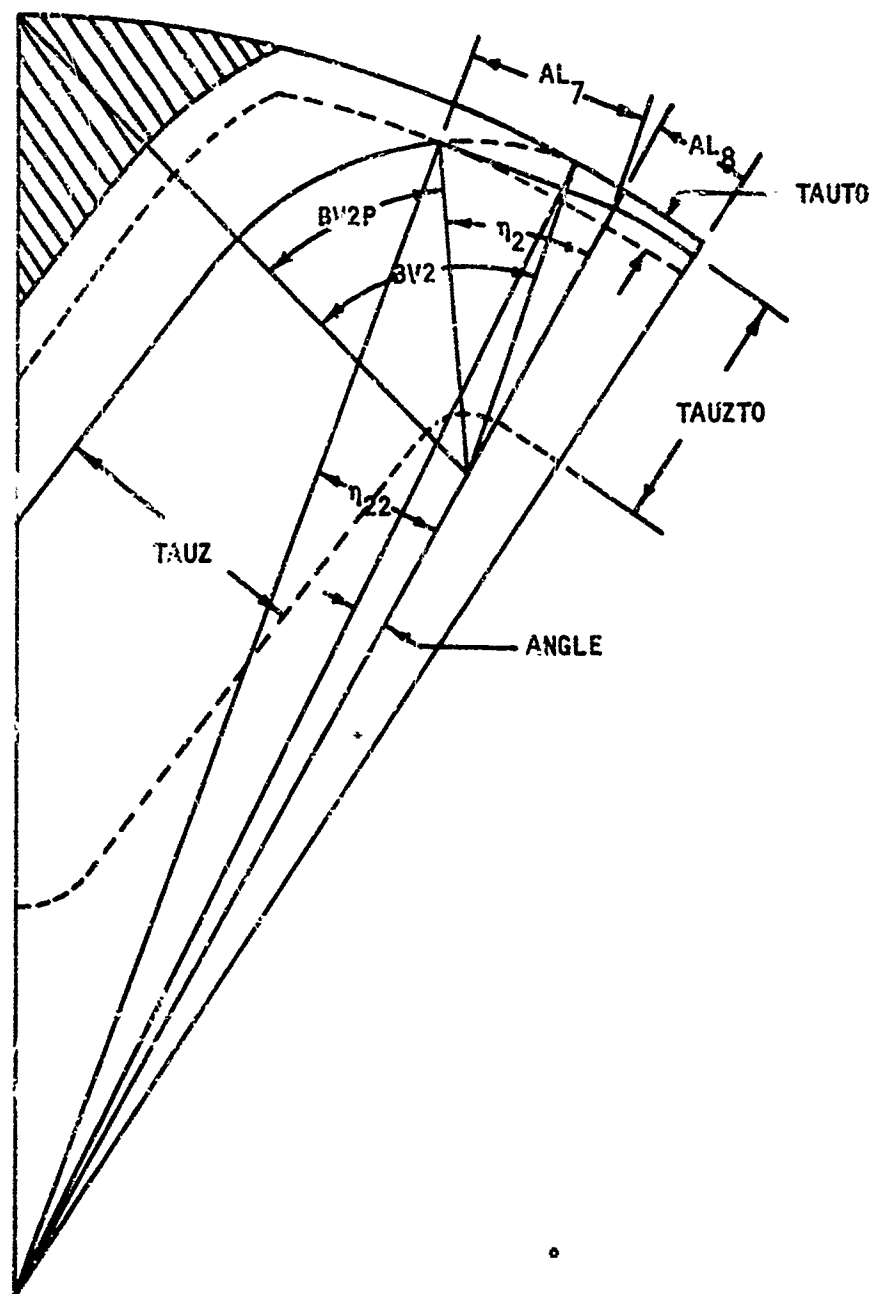


Figure 4.4. Anisotropic Propellant Burning Configuration Near Case Wall Before Web Burnout

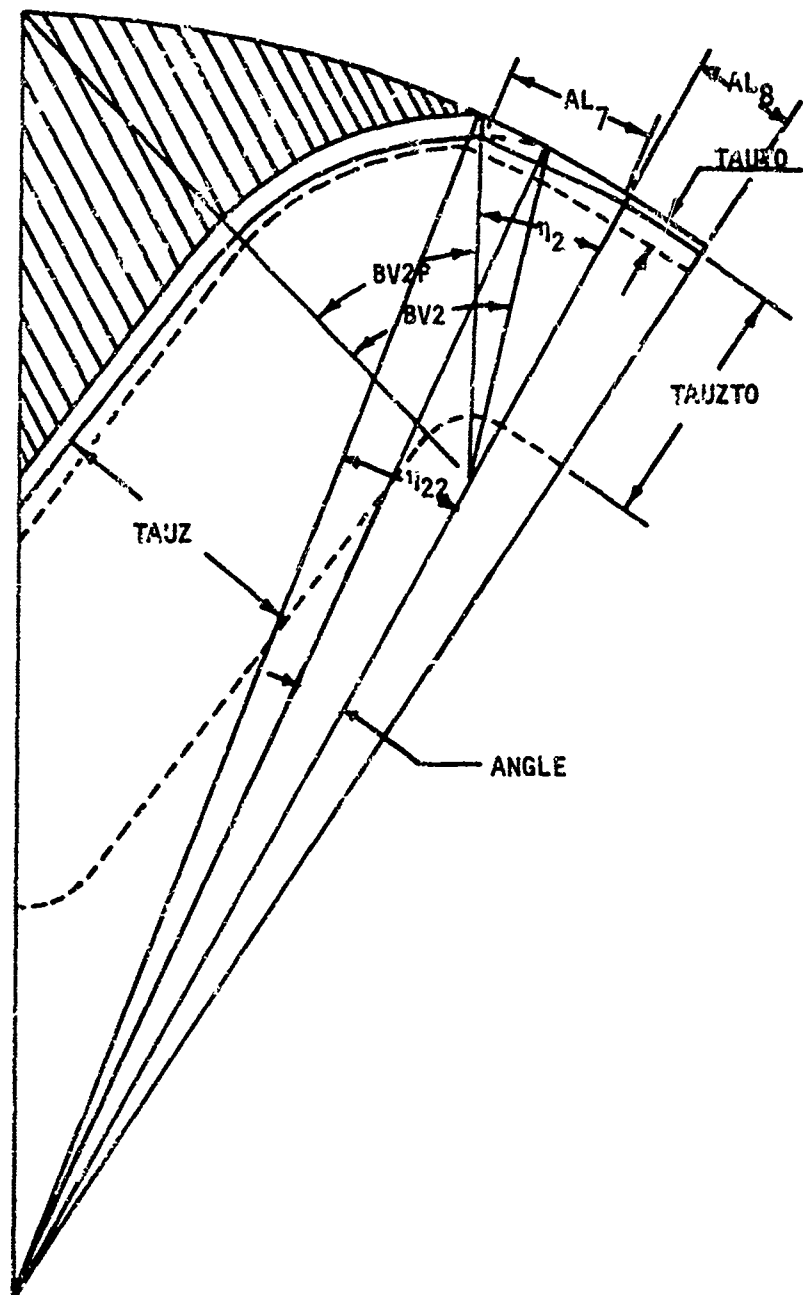


Figure 4.5. Anisotropic Propellant Burning Configuration Near Case Wall and Inert Sliver Before Web Burnout

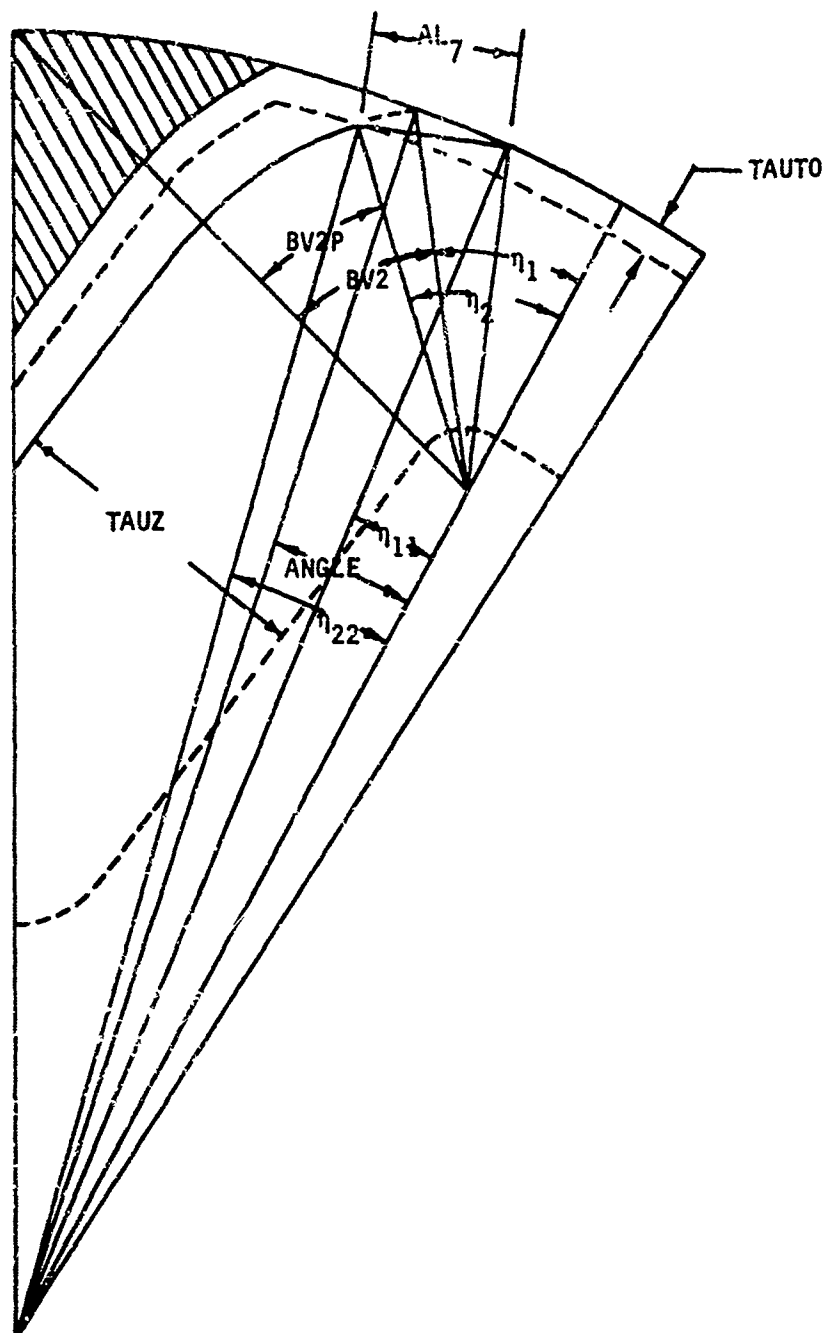


Figure 4.6. Anisotropic Propellant Burning Configuration
Near Case Wall After Web Burnout

5.0

GEOMETRICAL DEFINITION OF PROPELLANT GRAIN

For geometrical analysis, the motor is divided longitudinally into three sections: fore-head section, cylindrical section, and aft-head section. The fore-head section may incorporate a head-end with web or it may be defined in a manner similar to the aft-head section which is a straight through grain. The following describes subroutines and equations used to calculate burning surface area, port cross sectional area, propellant volume, center of gravity and moment of inertia for the fore-head, cylindrical, and aft-head sections.

5.1

Grain Cross Section Geometry

Propellant grain cross section options which are programmed for the computer are shown in Figure 5.1. The grain design may vary from the more complicated forked wagon wheel to the standard star, or to the circular port. The slotted-cone grain design is a modification of the standard star. Variations in the input parameters for the forked wagon wheel, which are shown in Figure 5.2, will produce the five basic grain design patterns. The basic parameters required to describe the grain cross section are input for reference planes located at specified distances from the forward tangent plane of the motor, Figure 4.3. The reference planes describing the propellant cross section may be placed at any desired location within the cylindrical section, thus allowing accurate descriptions of the propellant configuration for either monolithic or segmented motors.

5.1.1

General Forked Wagon Wheel

Cross-sectional geometry constants are required to determine the perimeter length and port area of each input reference plane. These basic geometry constants are determined in the first core load. Once these plane constants have been computed and stored for each input reference plane, the perimeter length for all values of distance burned and the initial port area are determined for each reference plane in the second core load and stored in tables for use during the internal ballistic solution in the fourth core load. The reference plane constants for the forked wagon wheel grain configuration are determined by subroutine PLNCNS from the geometry inputs, Figure 5.2. These plane constants are shown in Figures 5.3 and 5.4. A total of 45 constants are generated and stored for each reference plane:

Subroutine PLNCNS Reference Plane Constants

$$R_1 = R_f - \tau_w - L_{S1}$$

$$R_9 = R_f - \tau_w - L_{S2}$$

5.1.1

General Forked Wagon Wheel (Continued)

$$\theta_1 = \frac{\pi}{N_0}$$

$$\tau_{2\max} = R_2 + L_A \frac{\sin \alpha_{01}}{\cos \alpha_{01}}$$

$$\tau_{4\max} = \tau_{2\max} + L_B \frac{\sin \alpha_{02}}{\cos \alpha_{02}}$$

$$\tau_{5\max} = (\tau_{4\max} + R_4) \frac{\cos \alpha_{02}}{\cos \alpha_{03}} - R_4$$

$$x_{45} = (\tau_{5\max} + R_5) \cos \alpha_{03}$$

$$y_{45} = R_1 + R_2(1 - \sin \alpha_{01}) + L_A \cos \alpha_{01} + \tau_{2\max}(\sin \alpha_{01} - \sin \alpha_{02}) \\ + L_B \cos \alpha_{02} + R_4(\sin \alpha_{03} - \sin \alpha_{02}) - R_5 \sin \alpha_{03}$$

$$L_C = \left[(R_f - \tau_w - R_5)^2 - (x_{45} \cos \alpha_{03} - y_{45} \sin \alpha_{03})^2 \right]^{1/2} \\ - x_{45} \sin \alpha_{03} - y_{45} \cos \alpha_{03}$$

$$x_{03} = (\tau_{2\max} - R_3) \left[\cos \alpha_{01} + \tan \left(\frac{\alpha_{01} - \alpha_{02}}{2} \right) \sin \alpha_{01} \right]$$

$$y_{03} = R_1 + R_2 + (R_3 - R_2) \sin \alpha_{01} + \left[(\tau_{2\max} - R_3) \tan \frac{\alpha_{01} - \alpha_{02}}{2} \right. \\ \left. + L_A \right] \cos \alpha_{01}$$

$$R_{03} = \left[x_{03}^2 + y_{03}^2 \right]^{1/2}$$

$$x_{05} = (\tau_{5\max} + R_4) \cos \alpha_{03}$$

5.1.1

General Forked Wagon Wheel (Continued)

$$Y_{05} = Y_{45} + (R_5 - R_4) \sin \alpha_{03}$$

$$R_{05} = [X_{05}^2 + Y_{05}^2]^{1/2}$$

$$X_{07} = X_{45} + L_C \sin \alpha_{03}$$

$$Y_{07} = Y_{45} + L_C \cos \alpha_{03}$$

$$R_{07} = [X_{07}^2 + Y_{07}^2]^{1/2}$$

$$\tau_{6\max} = \tau_{5\max} + L_C \frac{\sin \alpha_{03}}{\cos \alpha_{03}}$$

$$\tau_{7\max} = [X_{07}^2 + (R_f - Y_{07})^2]^{1/2} - R_5$$

$$\tau_{12\max} = R_8 + L_E \frac{\sin \alpha_{05}}{\cos \alpha_{05}}$$

$$X_{76} = (\tau_{12\max} + R_6) \cos \alpha_{04}$$

$$Y_{76} = R_9 + R_8(1 - \sin \alpha_{05}) + L_E \cos \alpha_{05} + \tau_{12\max}(\sin \alpha_{05} - \sin \alpha_{04}) - R_6 \sin \alpha_{04}$$

$$L_D = [(R_f - \tau_w - R_6)^2 - (X_{76} \cos \alpha_{04} - Y_{76} \sin \alpha_{04})^2]^{1/2} - X_{76} \sin \alpha_{04} - Y_{76} \cos \alpha_{04}$$

$$X_{09} = X_{76} + L_D \sin \alpha_{04}$$

$$Y_{09} = Y_{76} + L_D \cos \alpha_{04}$$

5.1.1

General Forked Wagon Wheel (Continued)

$$R_{09} = [X_{09}^2 + Y_{09}^2]^{1/2}$$

$$X_{011} = (\tau_{12\max} - R_7) \left[\tan \frac{\alpha_{05} - \alpha_{04}}{2} \sin \alpha_{05} + \cos \alpha_{05} \right]$$

$$Y_{011} = R_9 + R_8 + (R_7 - R_8) \sin \alpha_{05} + \left[(\tau_{12\max} - R_7) \tan \left(\frac{\alpha_{05} - \alpha_{04}}{2} \right) + L_E \right] \cos \alpha_{05}$$

$$R_{011} = [X_{011}^2 + Y_{011}^2]^{1/2}$$

$$\tau_{10\max} = \tau_{12\max} + L_D \frac{\sin \alpha_{04}}{\cos \alpha_{04}}$$

$$\tau_{9\max} = [X_{09}^2 + (R_f - Y_{09})^2]^{1/2} - R_6$$

$$\theta_2 = \arccos \left(\frac{Y_{07}}{R_{07}} \right)$$

$$\theta_3 = \arccos \left(\frac{Y_{09}}{R_{09}} \right)$$

$$\theta_4 = \theta_1 - \theta_2 - \theta_3$$

$$\beta_{71\max} = \arccos \left[\frac{(\tau_{7\max} + R_5)^2 - (R_f - Y_{07})^2}{(\tau_{7\max} + R_5)^2} \right]^{1/2} / (\tau_{7\max} + R_5) - \alpha_{03}$$

$$\beta_{72\max} = \frac{\pi}{2} + \theta_2 - \beta_{71\max} - \alpha_{03}$$

$$\beta_{91\max} = \arccos \left[\frac{(\tau_{9\max} + R_6)^2 - (R_f - Y_{09})^2}{(\tau_{9\max} + R_6)^2} \right]^{1/2} / (\tau_{9\max} + R_6)$$

5.1.1

General Forked Wagon Wheel (Continued)

$$\beta_{92\max} = \frac{\pi}{2} + \theta_3 - \beta_{91\max} - \alpha_{04}$$

$$\tau_{\max} = \tau_{7\max}, \text{ or } \tau_{9\max}, \text{ whichever is larger.}$$

If θ_0 is input, determine τ_{\max} for slotted-cone geometry as follows (Figure 5.7):

$$\angle AJB = \arcsin \left[\frac{(R_f - R_5 - \tau_w) \sin(\theta_2)}{R_{6M} + R_5} \right]$$

$$\angle ABC = \pi - \theta_2 - \angle AJB$$

$$\angle ACB = \arcsin \left[\frac{(R_f - R_5 - \tau_w) \sin(\angle ABC)}{R_f} \right]$$

$$\angle BAC = \pi - \angle ABC - \angle ACB$$

$$\angle GFE = \frac{\pi}{2} - \alpha_{01}$$

$$\angle AFE = \frac{\pi}{2} + \alpha_{01}$$

$$\angle AEF = \arcsin \left[\frac{(R_1 + R_2) \sin(\angle AFE)}{R_f} \right]$$

$$\angle GAE = \pi - \angle AFE - \angle AEF$$

$$\text{If } \theta_0 \geq \angle GAE, \tau_{\max} = R_f - R_1$$

$$\text{If } \theta_0 < \angle GAE,$$

$$BH = [R_f^2 + (R_f - R_5 - \tau_w)^2 - 2R_f(R_f - R_5 - \tau_w) \cos(\theta_0 + \theta_2)]^{\frac{1}{2}}$$

$$\text{If } (\theta_0 + \theta_2) \geq \angle BAC,$$

$$\angle AHB = \arcsin \left[\frac{(R_f - R_5 - \tau_w) \sin(\theta_0 + \theta_2)}{BH} \right]$$

$$\angle ABH = \pi - \angle AHB - \theta_0 - \theta_2$$

$$\angle HBC = \angle ABC - \angle ABH$$

$$BH' = BH \cos(\angle HBC)$$

5.1.1

General Forked Wagon Wheel (Continued)

$$\tau_{\max} = (R_f - R_1) \text{ or } (BH' - R_5), \text{ whichever is smaller.}$$

$$\text{If } (\theta_0 + \theta_2) < \angle BAC,$$

$$\tau_{\max} = (R_f - R_1) \text{ or } (BH - R_5), \text{ whichever is smaller.}$$

The calculated plane constants appear on the printout and allow the user a means of checking if the proper grain design is being analyzed. Although the program is designed to solve the general configuration shown in Figure 5.2, there are certain variations of this configuration that exceed the mathematical limits of the analysis. To obtain a program solution, all of the following conditions must exist for each reference plane used:

R_1	must be greater than or equal to zero
R_3	must be less than or equal to $\tau_{2\max}$
R_7	must be less than or equal to $\tau_{12\max}$
R_9	must be greater than or equal to zero
L_C	must be greater than or equal to zero
L_D	must be greater than or equal to zero
β_{71M}	must be greater than or equal to zero
β_{91M}	must be greater than or equal to zero
α_{01}	must be less than 90°
α_{02}	must be greater than or equal to zero
α_{03}	must be less than 90°
α_{04}	must be greater than or equal to zero
α_{05}	must be less than 90°
θ_4	must be greater than or equal to zero

If any of these restrictions are exceeded for any of the input reference planes, the program will automatically stop and print the reference plane dimensions along with a statement of the exceeded restriction. Although the program is self-checking for these mathematically invalid configurations, there are some physically invalid configurations for which there is no such check.

Special attention should be given to the manner in which input lengths L_A , L_B , and L_E are defined. The length L_A is measured along a common tangent to the arcs generated by radii R_2 and R_3 (Figure 5.2). One of the points that defines this length is the point of tangency with the arc generated by the radius R_2 . How-

5.1.1

General Forked Wagon Wheel (Continued)

ever, the other point that defines length L_A is not the point of tangency with the arc generated by radius R_3 . This end limit of length L_A is determined by bisecting the included angle between lengths L_A and L_B , and extending this bisector until it intersects the axis of symmetry of the grain sector. From this intersection point, a line perpendicular to L_A is drawn. The intersection of this perpendicular and the line L_A is the point which defines the end of length L_A . Line lengths L_B and L_F are defined in a similar manner.

The perimeter length and initial port area of the grain cross section for each reference plane are determined in the second core load for incremental distances burned before and after web burn-out specified by input. The geometry plane constants of each reference plane are moved from storage into working locations in subroutine LPDAPS and the perimeter length and initial port area are determined for each sector of the cross section (shown in Figures 5.2, 5.3, and 5.4) at the specified DTAU increments by subroutine AFPSUB.

Subroutine LPDAPS

Subroutine LPDAPS sets up the parameters required to determine the perimeter length, L_p , and the cross-sectional propellant area, A_{FF} , for both the primary and secondary propellant tips of the forked wagon wheel. Initially, the parameters required to determine the secondary propellant tip are set and subroutine AFPSUB is used to evaluate the perimeter length and the area of propellant for each sector, and then the parameters for the primary propellant tip are set. Figure 5.5 shows the boundaries of the sectors for the forked wagon wheel grain.

The perimeter length and propellant area of sector 8 are then determined and summed with the values determined from sectors 1-7 and 9-13. The total perimeter of the grain configuration is obtained by multiplying the sum by 2N0. The port area is obtained by summing the cross sectional area of the propellant sectors, multiplying by N0, and subtracting the result from the area of a circle of radius R_f .

Subroutine AFPSUB

Subroutine AFPSUB determines the port perimeter length of one-

5.1.1

General Forked Wagon Wheel (Continued)

half of a symmetrical section and propellant cross sectional area of a symmetrical section of all sectors except sector 8. The plane constants required for each sector are set by subroutines MNCHN2 and LPDAPS.

The perimeter and area of the cross section for all grain configurations are calculated from basic trigonometric formulas. Required angles and line lengths are computed from known dimensions using the law of sines and the law of cosines. Propellant cross sectional area is determined by adding and subtracting areas of circular sectors and triangles. All configurations contain only straight lines and circular arcs.

Initially, the constants to determine the initial area and perimeter length for sectors 9 through 13, Figure 5.5, are set by subroutine LPDAPS, and then the sectors 1 through 7 are set such that $L_{13} = L_1$, $L_{12} = L_2$, $L_{11} = L_3$, $L_{10} = L_4$, and $L_9 = L_7$. The sector perimeter length, L , and initial propellant cross sectional areas, AFP , are determined as follows:

1. If $\tau < R_2$,

$$L_1 = (R_2 - \tau) \left(\frac{\pi}{2} - \alpha_{01} \right)$$

$$AFP_1 = (R_2 - \tau) L_1$$

2. If $\tau \geq R_2$,

$$L_1 = 0$$

$$AFP_1 = 0$$

3. If $\tau < R_3$,

$$\Delta L_3 = (\tau_{2\max} - R_3) \tan \left(\frac{\alpha_{01} - \alpha_{02}}{2} \right)$$

$$AFD = (R_3 + \tau_{2\max} - 2\tau) \Delta L_3$$

5.1.1

General Forked Wagon Wheel (Continued)

4. If $\tau \geq R_3$ and if $\tau < \tau_{2\max}$

$$\Delta L_3 = (\tau_{2\max} - \tau) \tan \left(\frac{\alpha_{01} - \alpha_{02}}{2} \right)$$

$$AFD = (\tau_{2\max} - \tau) \Delta L_3$$

5. If $\tau \geq R_3$ and if $\tau \geq \tau_{2\max}$

$$L_2 = 0$$

$$\Delta L_3 = 0$$

$$AFD = 0$$

6. If $\tau \leq R_2$,

$$L_2 = L_A + \Delta L_3$$

$$AFP_2 = (R_2 - 2\tau + \tau_{2\max}) L_A + AFD$$

7. If $\tau > R_2$,

$$L_2 = L_A \left[\frac{(\tau_{2\max} - \tau)}{(\tau_{2\max} - R_2)} \right] + \Delta L_3$$

$$AFP_2 = (\tau_{2\max} - \tau) (L_2 + \Delta L_3) + AFD$$

8. If $\tau < R_3$,

$$L_3 = (R_3 - \tau) (\alpha_{01} - \alpha_{02})$$

$$AFP_3 = L_3 (R_3 - \tau)$$

9. If $\tau \geq R_3$,

$$L_3 = 0$$

$$AFP_3 = 0$$

5.1.1

General Forked Wagon Wheel (Continued)

$$10. \text{ If } \tau < \tau_{2\max}$$

$$L_4 = L_B + \Delta L_3$$

$$AFP_4 = (\tau_{2\max} - 2\tau + \tau_{4\max}) L_B + \Delta L_3 D$$

$$11. \text{ If } \tau_{2\max} \leq \tau < \tau_{4\max}$$

$$L_4 = (\tau_{4\max} - \tau) L_B / (\tau_{4\max} - \tau_{2\max})$$

$$AFP_4 = (\tau_{4\max} - \tau) L_4$$

$$12. \text{ If } \tau_{2\max} \leq \tau \leq \tau_{4\max},$$

$$L_4 = 0$$

$$AFP_4 = 0$$

$$13. \text{ If } \tau < \tau_{4\max}$$

$$L_5 = (R_4 + \tau) (\alpha_{03} - \alpha_{02})$$

$$AFP_5 = (R_4 + \tau_{5\max}) (R_4 + \tau_{4\max}) \sin(\alpha_{03} - \alpha_{02}) - L_5 (R_4 + \tau)$$

$$14. \text{ If } \tau_{4\max} \leq \tau < \tau_{5\max},$$

$$L_5 = (R_4 + \tau) \alpha_{03} - \arccos \left[\frac{(R_4 + \tau_{4\max}) \cos(\alpha_{02})}{(R_4 + \tau)} \right]$$

$$AFP_5 = (R_4 + \tau_{5\max}) (R_4 + \tau) \sin \left[\frac{L_5}{(R_4 + \tau)} \right] - (R_4 + \tau) L_5$$

$$15. \text{ If } \tau_{4\max} \leq \tau \leq \tau_{5\max},$$

$$L_5 = 0$$

$$AFP_5 = 0$$

5.1.1

General Forked Wagon Wheel (Continued)

16. If $\tau \leq \tau_{5\max}$,

$$L_6 = L_C$$

$$AFP_6 = (\tau_{5\max} - 2\tau + \tau_{6\max}) L_C$$

17. If $\tau_{5\max} < \tau < \tau_{6\max}$, L_C

$$L_6 = L_C (\tau_{6\max} - \tau) / (\tau_{6\max} - \tau_{5\max})$$

$$AFP_6 = (\tau_{6\max} - \tau) L_6$$

18. If $\tau_{5\max} < \tau \geq \tau_{6\max}$,

$$L_6 = 0$$

$$AFP_6 = 0$$

19. If $\tau \leq \tau_{6\max}$,

$$\beta_{71} = \beta_{71\max}$$

$$AFP = (R_5 + \tau_{7\max})(R_5 + \tau_{6\max}) \sin(\beta_{71}) - \beta_{71} (R_5 + \tau)^2$$

20. If $\tau_{6\max} < \tau < \tau_{7\max}$,

$$\beta_{71} = \beta_{71\max} + \alpha_{03} - \arccos \left(\frac{X_{07}}{(\tau + R_5)} \right)$$

$$AFP = (R_5 + \tau_{7\max})(R_5 + \tau) \sin(\beta_{71}) - \beta_{71} (R_5 + \tau)^2$$

21. If $TSLVR > 0$,

$$\beta_{VX} = \arcsin \left[\frac{R_7 \sin(\theta_2)}{R_5 + \tau_{7\max}} \right] - \arcsin \left[\frac{R_7 \sin(\theta_2 - \theta_{SLV})}{(R_5 + \tau_{SLVR})} \right] - \theta_{SLVR}$$

$$Temp = \tau_w^2 + (R_5 + \tau_{7\max})^2 - 2 \tau_w (R_5 + \tau_{7\max})$$

$$\cos \left[\arcsin \left(\frac{R_7 \sin \theta_2}{R_5 + \tau_{7\max}} \right) \right]$$

5.1.1

General Forked Wagon Wheel (Continued)

$$\text{Temp}_a = \arcsin \left[\frac{R_7 \sin \theta_2}{R_5 + \tau_{7\max}} \right]$$

$$\text{Temp}_b = \pi - \arcsin \left[\frac{R_7 \sin \theta_2}{\text{Temp}} \right]$$

$$\text{Temp}_c = \arcsin \left[\frac{\text{Temp} \sin(\text{Temp}_b)}{(T_{\text{SLVR}} + R_5)} \right]$$

$$\beta_{\text{VXX}} = \text{Temp}_c - \text{Temp}_a$$

$$\begin{aligned} A_{\text{SLVR}} = & \theta_2 R_f^2 - (R_f - \tau_w) R_7 \sin \theta_2 - (\theta_2 - \theta_{\text{SLV}}) R_f^2 \\ & + (T_{\text{SLVR}} + R_5) R_7 \sin \left\{ \pi - \theta_2 + \theta_{\text{SLV}} \right. \\ & \left. - \arcsin \left[R_7 \sin(\theta_2 - \theta_{\text{SLV}}) / (T_{\text{SLVR}} + R_5) \right] \right\} \\ & - \text{Temp} (T_{\text{SLVR}} + R_5) \sin(\pi - \text{Temp}_c - \text{Temp}_b) \\ & - (\beta_{\text{VXX}} + \beta_{\text{VX}}) (T_{\text{SLVR}} + R_5)^2 \end{aligned}$$

22. If $\tau \leq \tau_w$

$$\beta_{72} = \beta_{72\max}$$

$$A_{P7} = A_{P7} + \theta_2 R_f^2 - R_f R_7 \sin \theta_2 - \beta_{72} (R_5 + \tau)^2$$

$$L_7 = (\beta_{71} + \beta_{72}) (R_5 + \tau)$$

23. If $\tau > \tau_w$

$$\begin{aligned} \beta_{72} = & \arccos \left\{ \frac{(\tau + R_5)^2 + (R_f - \tau_w - R_5)^2 - R_f^2}{2(\tau + R_5)(R_f - \tau_w - R_5)} \right\} \\ & - \beta_{71\max} - \alpha_{03} - \frac{\pi}{2} + \theta_2 \end{aligned}$$

5.1.1

General Forked Wagon Wheel (Continued)

$$\begin{aligned}
 AFP_7 &= AFP + \theta_2 R_f^2 - R_f R_7 \sin \theta_2 + R_7 (R_5 + \tau) \sin(\beta_{72\max} - \beta_{72}) \\
 &\quad - R_f^2 \arccos \left\{ 1 - \left(\frac{R_5 + \tau (\sin(\beta_{72\max} - \beta_{72}))^2}{R_f} \right)^{1/2} \right\} \\
 &\quad - \beta_{72} (R_5 + \tau)^2 \\
 L_7 &= (\beta_{71} + \beta_{72}) (R_5 + \tau)
 \end{aligned}$$

24. If $\tau < \tau_{SLVR}$,

$$L = L_1 + L_2 + L_3 + L_4 + L_5 + L_6 + L_7$$

$$AFP = AFP_1 + AFP_2 + AFP_3 + AFP_4 + AFP_5 + AFP_6 + AFP_7 - ASLVR$$

25. If $\tau \geq \tau_{SLVR}$,

$$L = 0$$

$$AFP = 0$$

5.1.2

Slotted-Cone

The slotted-cone configuration is an addition to the standard star in which a segment of propellant, represented by angle θ_c , has been inserted as shown in Figure 5.6. The insert of propellant results in additions to the perimeter and area calculations for a standard star which requires the determination of three basic angles, QAG, RAG, and SAG, shown in Figures 5.9, 5.10, and 5.11, respectively. Nine points, A, B, C, C', E, F, G, J, and H are defined in Figure 5.7, and are used in the following analysis to determine line lengths and angles. Four moving points, P, Q, R, and S on the burning perimeter are identified in Figures 5.8 through 5.13.

Point A lies on the motor axis (Figure 5.7). Point B coincides with the center of the input radius R_5 and point F coincides with the center of the input radius R_2 . Point G is located on the case

5.1.2

Slotted-Cone (Continued)

wall at the point where a line through points A and F intersect the case. Points C and E are located on the case wall where a line perpendicular to side L_c at the intersection of side L_c with radius R_5 intersects the case and where a line perpendicular to side L_c at the intersection of side L_c with radius R_2 intersects the case. Point H lies on the case wall at the angle θ_0 from point G. Point C' defines the point where side L_c of the standard star disappears as a result of the progression of the burning surface of the slotted cone insert.

Perimeter length QR, Figure 5.9, defines the addition to side L_c of the standard star, resulting from the addition of the central angle θ_0 of the slotted-cone. Perimeter length PQ defines the length of the arc subtended from the radius, $(R_1 + \tau)$, and intersecting with length QR. When the burning distance, τ , is less than or equal to the input radius R_2 , only the perimeter length PQ is present. When the burning distance is greater than R_2 , but less than or equal to the geometry constant T_{6max} , as shown in Figure 5.9, both perimeter lengths PQ and QR are present.

Perimeter length RS defines the addition to the arc subtended from the point of the input radius R_5 (geometry point B). Whenever T_{V7}^i is greater than T_{7max} , and T_{7max} is greater than T_{6max} (Figure 5.10), and τ is greater than T_{6max} but less than or equal to T_{7max} , geometry point S lies on the line AG and perimeter lengths PQ, QR, and RS are present.

Whenever τ is greater than T_{7max} but less than T_{V7}^i , perimeter length RS is defined as in Figure 5.11.

Whenever τ is greater than T_{V7}^i , as shown in Figures 5.12 and 5.13, geometry point R and perimeter length QR do not exist and only perimeter lengths PQ and QS remain.

The angle θ_0 is allowed to vary on input between 0° and 90° . Should θ_0 be less than the angle QAG shown in Figure 5.9, then the perimeter length PQ does not exist and point Q then lies on the line AH. Should θ_0 be less than the angles QAG and RAG, then the perimeter lengths PQ and QR and the points P and Q do not

5.1.2

Slotted-Cone (Continued)

exist and the point R lies on the line AH. When angle SAG exceeds θ_0 , complete burnout has occurred.

The following are the port perimeter and propellant cross sectional area equations for this addition to the standard star configuration. Figures 5.8 through 5.13 show the progression of the burning surface and the geometric figures required for each equation.

1. If $\tau \leq R_2$ (Figure 5.8),

$$\text{Perimeter} = \theta_0 (R_1 + \tau)$$

$$\text{Area} = \theta_0 \left[R_f^2 - (R_1 + \tau)^2 \right]$$

2. If $\tau > R_2$ (Figure 5.9),

$$\angle AJB = \arcsin \left[\frac{(R_f - R_5 - \tau_w)}{T_{6\max} + R_5} \sin \theta_2 \right]$$

$$\angle ABC = \pi - \theta_2 - \angle AJB$$

$$\angle ACB = \arcsin \left[\frac{(R_f - R_5 - \tau_w)}{R_f} \sin \angle ABC \right]$$

$$\angle BAC = \pi - \angle ABC - \angle ACB$$

$$BC = R_f \frac{\sin \angle BAC}{\sin \angle ABC}$$

$$T_{V6}^i = BC - R_5$$

$$T_{V7}^i = \frac{(R_f - R_5 - \tau_w)^2 - R_1^2 - R_5^2 - 2(R_f - R_5 - \tau_w)R_5 \cos \angle ABC}{2R_1 - 2R_5 + 2(R_f - R_5 - \tau_w) \cos \angle ABC}$$

$$\text{Temp}_{76} = \text{minimum of } T_{V7}^i \text{ and } T_{V6}^i$$

5.1.2

Slotted-Cone (Continued)

3. If $R_2 < \text{Temp}_{76}$, and if $\tau \leq T_{6\text{max}}$ (Figure 5.3),

$$FR = \frac{(\tau - R_2)}{\sin \alpha_{01}}$$

$$AR = R_1 + R_2 + FR$$

$$\angle RQA = \pi - \arcsin \left[\frac{AR \sin \alpha_{01}}{R_1 + \tau} \right]$$

$$\angle QAR = \pi - \angle RQA - \alpha_{01}$$

$$QR = (R_1 + \tau) \frac{\sin \angle QAR}{\sin \alpha_{01}}$$

$$\angle QAG = \arcsin \left[\frac{QR \sin \alpha_{01}}{(R_1 + \tau)} \right]$$

a. and $\angle QAG \geq \theta_0$,

$$\text{Perimeter} = \frac{AR \sin \theta_0}{\sin(\pi - \alpha_{01} - \theta_0)}$$

$$\text{Area} = \theta_0 R_f^2 - (\text{Perimeter}) AR \sin \alpha_{01}$$

b. Or $\angle QAG < \theta_0$,

$$PQ = (R_1 + \tau)(\theta_0 - \angle QAG)$$

$$\text{Perimeter} = PQ + QR$$

$$\text{Area} = \theta_0 R_f^2 - (\theta_0 - \angle QAG)(R_1 + \tau)^2 - QR AR \sin \alpha_{01}$$

5.1.2

Slotted-Cone (Continued)

4. If $R_2 < \tau < \text{Temp}_{76}$ and if $T_{6\max} < \tau \leq T_{7\max}$ (Figure 5.10),

$$\angle ASB = \arcsin \left[\frac{(R_f - R_5 - \tau_w) \sin \theta_2}{(R_5 + \tau)} \right]$$

$$\angle SBA = \pi - \theta_2 - \angle ASB$$

$$\text{Area}_1 = \theta_0 R_f^2 + (R_f - R_5 - \tau_w)(R_5 + \tau) \sin \angle SBA$$

a. And $\angle RAG \geq \theta_0$

$$\angle BRA = \arcsin \left[\frac{(R_f - R_5 - \tau_w) \sin(\theta_2 + \theta_0)}{(R_5 + \tau)} \right]$$

$$\angle RBA = \pi - \angle BRA - \theta_2 - \theta_0$$

$$\angle RBS = \angle SBA - \angle RBA$$

$$RS = \angle RBS(R_5 + \tau)$$

$$\text{Perimeter} = RS$$

$$\text{Area} = \text{Area}_1 - (R_f - R_5 - \tau_w)(R_5 + \tau) \sin \angle RBA - \angle RBS(R_5 + \tau)^2$$

b. Or $\angle RAG < \theta_0$

$$\text{Area}_2 = \text{Area}_1 - \angle RBS(R_5 + \tau)^2 - (R_f - R_5 - \tau_w)(R_5 + \tau) \sin \angle ABC$$

(1) And if $\angle QAG \geq \theta_0$

$$\angle QAR = \theta_0 - \angle RAG$$

$$\angle AQR = \pi/2 + \angle ARB - \angle QAR$$

$$QR = \frac{AR \sin \angle QAR}{\sin \angle AQR}$$

$$\text{Perimeter} = QR + RS$$

5.1.2

Slotted-Cone (Continued)

$$\text{Area} = \text{Area}_2 - QR \, AR \sin(\pi/2 - \angle ARB)$$

$$(2) \text{ Or if } \angle QAG < \theta_0$$

$$\angle PAQ = \theta_0 - \angle QAG$$

$$PQ = \angle PAQ (R_1 + \tau)$$

$$QR = \frac{(R_1 + \tau) \sin \angle RAQ}{\sin(\pi/2 - \angle ARB)}$$

$$\text{Perimeter} = PQ + QR + RS$$

$$\text{Area} = \text{Area}_2 - QR \, AR \sin(\pi/2 - \angle ARB) - \angle PAQ (R_1 + \tau)^2$$

5. If $R_2 < \tau < \text{Temp}_{76}$, and if $T_{6\max} < \tau < T_{7\max}$ (Figure 5.11),

$$\angle SAB = \arccos \left[\frac{R_f^2 + (R_f - R_5 - \tau_w)^2 - (R_5 + \tau)^2}{2 R_f (R_f - R_5 - \tau_w)} \right]$$

$$\angle SAG = \angle SAB - \theta_2$$

$$AR = \left[(R_5 + \tau)^2 + (R_f - R_5 - \tau_w)^2 - 2(R_5 + \tau)(R_f - R_5 - \tau_w) \cos \angle ABC \right]^{1/2}$$

$$\angle RAB = \arcsin \left[\frac{(R_5 + \tau) \sin \angle ABC}{AR} \right]$$

$$\angle RAG = \angle RAB - \theta_2$$

$$\angle ARB = \pi - \angle ABC - \angle RAB$$

$$\angle ARQ = \frac{\pi}{2} - \angle ARB$$

$$\angle AQR = \pi - \arcsin \left[\frac{AR \sin \angle ARQ}{(R_1 + \tau)} \right]$$

$$\angle QAR = \pi - \angle AQR - \angle ARQ$$

$$\angle QAG = \angle QAR + \angle RAG$$

5.1.2

Slotted-Cone (Continued)

a. And $SAG \geq \theta_0$

Complete burnout has occurred.

Perimeter = 0.0

Area = 0.0

b. Or $SAG < \theta_0$

$$\angle ASB = \arcsin \left[\frac{(R_f - R_5 - \tau_w) \sin(\theta_2 + \angle SAG)}{(R_5 + \tau)} \right]$$

$$\angle SBA = \pi - \theta_2 - \angle SAG - \angle ASB$$

$$Area_1 = (\theta_0 - \angle SAG) R_f^2 + R_f (R_f - R_5 - \tau_w) \sin(\theta_2 + \angle SAG)$$

$$\angle RQA = \pi - \arcsin \left[\frac{AR \sin(\pi/2 - \angle ARB)}{(R_1 + \tau)} \right]$$

$$\angle RAQ = \frac{\pi}{2} + \angle ARB - \angle RQA$$

$$\angle QAG = \angle RAQ + \angle RAG$$

$$\angle RBS = \angle SBA - \angle ABC$$

$$RS = \angle RBS (R_5 + \tau)$$

(1) and if $\angle RAG \geq \theta_0$ go to 4a(2) or if $\angle RAG < \theta_0 \leq \angle QAG$ go to 4b(1)(3) or if $\angle RAG < \theta_0 > \angle QAG$ go to 4b(2)6. If $R_2 < \tau \geq \text{Temp}_{76}$, and if $T_{V6}^1 = T_{V7}^1$

Complete burnout has occurred.

Perimeter = 0.0

Area = 0.0

5.1.2

Slotted-Cone (Continued)

7. if $R_2 < \tau \geq \text{TEMP}_{76}$, and if $T_{V6} > T_{V7}$, and $\tau \leq \tau_w$ (Figure 5.12),

$$\angle QAB = \arccos \left[\frac{(R_{V1} + \tau)^2 + (R_f - R_5 - \tau_w)^2 - (R_5 + \tau)^2}{2(R_1 + \tau)(R_f - R_5 - \tau_w)} \right]$$

$$\angle AQB = \arcsin \left[\frac{(R_f - R_5 - \tau_w) \sin(\angle QAB)}{(R_5 + \tau)} \right]$$

$$\angle ABQ = \pi - \angle AQB - \angle QAB$$

$$\angle ASB = \arcsin \left[\frac{(R_f - R_5 - \tau_w) \sin(\theta_2)}{(R_5 + \tau)} \right]$$

$$\angle ABS = \pi - \theta_2 - \angle ASB$$

$$\angle QAG = \angle QAB - \theta_2$$

a. and $\angle QAG \geq \theta_0$

$$\angle AQB = \arcsin \left[\frac{(R_f - R_5 - \tau_w) \sin(\theta_2 + \theta_0)}{(R_5 + \tau)} \right]$$

$$\angle ASQ = \pi - \theta_2 - \theta_0 - \angle AQB$$

$$\angle QBS = \angle ABS - \angle ABQ$$

$$\text{PERIM} = \angle QBS (R_5 + \tau)$$

b. or $\angle QAG < \theta_0$

$$\text{PERIM} = (\angle ABS - \angle ABQ) (R_5 + \tau) + (\theta_0 - \angle QAG) (R_1 + \tau)$$

5.1.2

Slotted-Cone (Continued)

8. If $R_2 \leq \tau \leq \text{Temp}_{76}$, and if $T_{V6}^1 > T_{V7}^1$ and $\tau > \tau_w$ (Figure 5.12),

$$\angle SAB = \arccos \left[\frac{R_f^2 + (R_f - R_5 - \tau_w)^2 - (R_5 + \tau)^2}{2 R_f (R_f - R_5 - \tau_w)} \right]$$

$$\angle SAG = \angle SAB - \theta_2$$

a. and $\angle SAG \geq \theta_0$

Complete burnout has occurred.

Perimeter = 0.0

Area = 0.0

b. Or $\angle SAG < \theta_0$

$$\angle QAB = \arccos \left[\frac{(R_1 + \tau)^2 + (R_f - R_5 - \tau_w)^2 - (R_5 + \tau)^2}{2 (R_1 + \tau) (R_f - R_5 - \tau_w)} \right]$$

$$\angle QAG = \angle QAB - \theta_2$$

$$\angle ABS = \arccos \left[\frac{(R_f - R_5 - \tau_w)^2 + (R_5 + \tau)^2 - R_f^2}{2 (R_f - R_5 - \tau_w) (R_5 + \tau)} \right]$$

(1) and if $\angle QAG \geq \theta_0$

$$\angle AQB = \arcsin \left[\frac{(R_f - R_5 - \tau_w) \sin(\theta_2 + \theta_0)}{(R_5 + \tau)} \right]$$

$$\angle ABQ = \pi - \theta_2 - \theta_0 - \angle AQB$$

$$\angle QBS = \angle ABS - \angle ABQ$$

$$QS = \angle QBS (R_5 + \tau)$$

$$\text{Perimeter} = QS$$

$$\text{Area} = (\theta_2 + \theta_0 - \angle SAB) R_f^2 + R_f (R_f - R_5 - \tau_w) \sin \angle SAB$$

$$- (R_5 + \tau)^2 \angle QBS - (R_f - R_5 - \tau_w) (R_5 + \tau) \sin \angle ABQ$$

5.1.2

Slotted-Cone (Continued)

(2) Or if $\angle QAG < \theta_0$

$$\angle ABQ = \arccos \left[\frac{(R_f - R_5 - \tau_w)^2 + (R_5 + \tau)^2 - (R_1 + \tau)^2}{2(R_f - R_5 - \tau_w)(R_5 + \tau)} \right]$$

$$\angle QBS = \angle ABS - \angle ABQ$$

$$QS = \angle QBS (R_5 + \tau)$$

$$\angle PAQ = \theta_2 + \theta_0 - \angle QAB$$

$$PQ = \angle PAQ (R_1 + \tau)$$

$$\text{Perimeter} = PQ + QS$$

$$\begin{aligned} \text{Area} = & (\theta_2 + \theta_0 - \angle SAB) R_f^2 + R_f (R_f - R_5 - \tau_w) \sin \angle SAB \\ & - (R_5 + \tau)^2 \angle QBS - (R_1 + \tau) (R_f - R_5 - \tau_w) \sin \angle QAB \\ & - (\theta_2 + \theta_0 - \angle QAB) (R_1 + \tau)^2 \end{aligned}$$

9. If $R_2 < \tau \geq \text{Temp}_{76}$ and if $T_{V6} < T_{V7}$ (Figure 5.13),

$$AT = \left[(R_f - R_5 - \tau_w)^2 + (R_5 + \tau)^2 - 2(R_f - R_5 - \tau_w)(R_5 + \tau) \cos \angle ABC \right]^{1/2}$$

$$\angle ATB = \arcsin \left[\frac{(R_f - R_5 - \tau_w) \sin \angle ABC}{AT} \right]$$

$$\angle STA = \pi/2 - \angle ATB$$

$$\angle AST = \pi - \arcsin \left[\frac{AT \sin \angle STA}{R_f} \right]$$

$$\angle TAB = \pi - \angle ABC - \angle ATB$$

$$\angle SAT = \pi - \angle AST - \angle STA$$

$$\angle SAG = \angle SAT + \angle TAB - \theta_2$$

a. And $\angle SAG \geq \theta_0$

Complete burnout has occurred.

5.1.2

Slotted-Cone (Continued)

$$\text{Perimeter} = 0.0$$

$$\text{Area} = 0.0$$

$$\text{b. Or } \angle \text{SAG} < \theta_0$$

$$\angle \text{QSA} = \pi - \angle \text{AST}$$

$$\angle \text{AQS} = \pi - \arcsin \left[\frac{R_f \sin \angle \text{QSA}}{(R_1 + \tau)} \right]$$

$$\angle \text{QAS} = \pi - \angle \text{AQS} - \angle \text{QSA}$$

$$\angle \text{QAG} = \angle \text{SAG} + \angle \text{QAS}$$

$$(1) \text{ And If } \angle \text{QAG} \geq \theta_0$$

$$\angle \text{QAS} = \theta_0 - \angle \text{SAG}$$

$$\angle \text{AQS} = \pi - \angle \text{QAS} - \angle \text{QSA}$$

$$\text{QS} = \frac{R_f \sin \angle \text{QAS}}{\sin \angle \text{AQS}}$$

$$\text{Perimeter} = \text{QS}$$

$$\text{Area} = \angle \text{QAS } R_f^2 - R_f \text{ QS } \sin \angle \text{QSA}$$

$$(2) \text{ Or If } \angle \text{QAG} < \theta_0$$

$$\angle \text{PAQ} = \theta_0 - \angle \text{QAG}$$

$$\text{PQ} = (R_1 + \tau) \angle \text{PAQ}$$

$$\text{QS} = R_f \frac{\sin \angle \text{QAS}}{\sin \angle \text{AQS}}$$

$$\text{Perimeter} = \text{PQ} + \text{QS}$$

$$\begin{aligned} \text{Area} = & (\angle \text{PAQ} + \angle \text{QAS}) R_f^2 - \text{QS } R_f \sin \angle \text{QSA} \\ & - \angle \text{PAQ} (R_1 + \tau)^2 \end{aligned}$$

5.2 Grain Longitudinal Geometry

Representative longitudinal configurations which can be accommodated by the computer program have been shown in Figure 2.2. Many configurations are possible: monolithic or segmented grains in the cylindrical section of the motor; head-end with web or a straight through grain in the fore-head section; straight through grain in the aft-head; external and internal taper; and elliptical contour fore-head and aft-head motor sections are examples. Grain cross sectional geometry can be varied within the cylindrical section of the motor.

5.2.1 Head-End with Web, Fore-Head Section

This section describes the analysis of the head-end with web which is solved in the third core load of the computer program. Description of the head-end with web calculations are based on the motor fore-head section shown in Figure 5.14. Grain geometry within the fore-head section is based on the input geometrical cross section at the forward tangent plane.

The burning surface area for all distances burned and the initial propellant volume are obtained by separating the analysis into four blocks. Each block performs the following function:

Block 1 calculates the surface area versus distance burned and the initial volume of the propellant tip. The volume and area are obtained by integrating elemental areas and volumes consisting of trapezoids and parallelograms.

Block 2A calculates the surface area of the pseudoellipsoid minus the igniter opening using the Theorem of Pappus. Block 2B calculates the volume of propellant between the inner and outer ellipsoids and the surface area on the pseudo ellipsoid which is covered by the propellant tip. The volume and area are obtained by integrating elemental areas and volumes using the Theorem of Pappus.

Block 3 calculates the initial total propellant volume. The volume between the inner and outer ellipsoids is determined from the difference in volume of two oblate spheroids. The volume of the tip is obtained by adding the volumes of cylindrical segment elements.

Total surface area, A , versus distance burned is obtained by combining the blocks:

$$A = A_{\text{Block 1}} + A_{\text{Block 2A}} - A_{\text{Block 2B}}$$

The initial propellant volume is calculated in two ways, one

5.2.1 Head-End with Web, Fore-Head Section (Continued)

method as in Block 3 and the other by:

$$\text{Volume} = V_{\text{Block 1}} + V_{\text{Block 2B}}$$

The initial volumes are compared in subroutine VOLSUB and a correction factor, A_R , is obtained which is added to the total burning surface area. This is due to the assumption that the difference is caused by the integration method in the Block 1 analysis.

Subroutine HDNSUB

Subroutine HDNSUB is the control routine which sets up the correct variables and equations to perform the block 1, 2A, 2B, and 3 analysis.

5.2.1.1 Block 1 Analysis

The generalized forked wagon wheel grain configuration is divided into 13 sectors (1, 2, 3, 3A, 3B, 4, 5, 6, 7, 9, 10, 11, 11A, 11B, 12, 13) as shown in Figure 5.15. Sectors (1, 2, 4, 5, 6, 7, 9, 10, 12 and 13) share a common analysis, as do sectors (3 and 11) and (3A, 3B, 11A, and 11B); however, some of the sectors have special equations for line segments and angles. The sector boundaries used for the head-end with web analysis, Figure 5.15, are different than sector boundaries used for the straight through grain analysis, Section 5.2.3 and Figure 5.32.

Subroutine SCI is the control routine to determine the surface area versus distance burned and initial volume of the propellant tip for the block 1 analysis and is called from subroutine HDNSUB with an argument L to indicate the sector to be computed. The analysis for sectors 1 and 3 will be explained in detail since the analysis for the other sectors is similar.

Figure 5.16 shows geometric constructions and calculation control planes used to obtain elemental burn surface areas and propellant volumes in the propellant tip. Also shown is part of a forked wagon wheel grain and the required constructions. For clarity, only one tip is shown. Two planes, "A" and "B", control volume and area calculations for the propellant tip. These two planes are generated as follows: The intersection of the surface of the propellant tip with the forward tangent plane, i.e., the tangent plane perimeter, Figure 5.16b, is divided into incremental lengths, ΔL . Lines, spaced ΔL apart, perpendicular to the tangent plane, are run from the tangent plane along the side of the propellant tip to intersect the inner ellipsoid. These intersections locate points P_{oa} and P_{ob} .

5.2.1.1

Block 1 Analysis (Continued)

Perpendiculars to the side of the propellant tip from points P_{oa} and P_{ob} locate points P_{1a} and P_{1b} on the plane of symmetry or on the outer ellipsoid depending on the initial location of each $\Delta L0$ along the propellant tip perimeter in the tangent plane. Figure 5.16a shows P_{1a} and P_{1b} on the plane of symmetry. Perpendiculars to the inner ellipsoid at points P_{oa} and P_{ob} locate points P_{2a} and P_{2b} on the outer ellipsoid. Points P_{oa} , P_{1a} , P_{2a} , P_{ob} , P_{1b} , and P_{2b} define the A and B planes. Points P_{3a} and P_{3b} lie in the A and B planes and are located on the outer ellipsoid.

The trapezoid formed by $\Delta L0$ on the perimeter of the tip at the tangent plane and points P_{oa} and P_{ob} is the area calculation element.

Perpendiculars, in "x-z" planes, for these same four points form the volume calculation elements which are bounded by the trapezoidal area elements as shown in Figure 5.16. The $\Delta L0$ spacing on the propellant tip perimeter which governs plane placement varies in value along the perimeter as follows:

The $\Delta L0$ spacing, Figure 5.16b, is calculated first as:

a) $\Delta L0_1$ of each sector is:

$$\Delta L0_1 = \left(\frac{\Delta L}{R_f} \right) R_f$$

where $\frac{\Delta L}{R_f}$ is an input parameter.

b) $\Delta L0$ is then modified by:

$$\Delta L0 = \frac{K(\Delta L0_{\text{previous}})}{(D_{pr} + D_{ps})}$$

where

D_{pr} and D_{ps} are the distances between planes A and B, Figure 5.17.

The starting value of $\Delta L0$ previous is $\Delta L0_1$.

5.2.1.1 Block 1 Analysis (Continued)

The factor K , an input variable, is the major parameter in determining the distance between the two planes. The incremental distance ΔL_0 is stepped along the sector perimeters from $L_x = 0$ to $L_x = L_p$.

5.2.1.1.1 Sector 1 (Figure 5.15)

Subroutines ASUBC, BSUBC, RASUBB, XRSUBB, THETAR, GAMSUB, GAMA2S, POSUB, PLSUB, P3SUB, ROPSB, and VSTRSB are used to obtain the surface area and initial volume for sector 1.

The distance D_{03} between the points P_0 and P_3 on the inner ellipsoid are shown in Figure 5.18 for planes that are located at increments of one-tenth the perimeter length of a sector. A minimum perimeter length, HOLDR, is set equal to the perimeter length in which the distance D_{03} for the plane is greater than the burn distance, τ . The first plane is located at the perimeter length HOLDR and subsequent planes are spaced the distance ΔL_0 apart. HOLDR is initialized to the perimeter length for plane B on subsequent iterations.

After the minimum perimeter length, HOLDR, is determined, the distance D_{03} for a plane located at the total perimeter $AL(1)$ for the sector is determined. The parameter TDMAX is initialized to the maximum value of TDMAX or D_{03} for the sector and then checked with the maximum permissible burn distance, TAUM. If TDMAX equals or exceeds TAUM, an error condition exists and execution is terminated. If all D_{03} 's are less than TAUM, the radial burning surface area between the planes and the burning surface area on the propellant tip are determined.

Radial burning surface area, Figure 5.17:

$$ASI = \frac{(L_{TA} + L_{TB})(D_{pr} + D_{ps})}{L}$$

Propellant tip burning surface area:

$$ASI = \frac{(L_p - HOLDR)(R_2 - \tau)(Y_{OA} + Y_{OB})}{2R_2}$$

where Y_0 is defined in Figure 5.21.

5.2.1.1.1 Sector 1 (Figure 5.15) (Continued)

L_p is the perimeter length along the initial grain perimeter measured from the beginning of a sector to a general point.
HOLDR is the prior incremental value of L_p .

The initial volume is determined from the following equation:

$$V_{STR} = \frac{(Y_{3A} + Y_{0B})(L_p - HOLDR)R_2}{4}$$

Subroutine ASUBC

Subroutine ASUBC sets up the correct variables and equations to determine the coordinates (X, Y, and Z) of the points P_{0a} , P_{1a} , and P_{3a} for planes located at increments of one-tenth L_p along the perimeter of the sector. Subroutines RASUBB, XRSUBB, THETAR, GAMSUB, GAMA2S, POSUB, PISUB, P3SUB, and TRAN are called to determine the coordinates.

Subroutine RASUBB

Subroutine RASUBB determines the length of the radius vector, R_{aT} , from the motor axis to a general point in a sector. The perimeter length from the beginning of the sector to a general point is required in calculating a value of R_{aT} for each sector, Figure 5.19.

Subroutine XRSUBB

Subroutine XRSUBB determines the X-coordinate, X_{ra} , for a point located on the perimeter of a sector. The parameter R_{aT} from the RASUBB subroutine is required to obtain the coordinate. A separate equation is required for each sector, Figure 5.15.

Subroutine THETAR

Subroutine THETAR determines the angle, θ_r , between the Z-axis and the line segment R_{aT} . The parameters X_{ra} and R_{aT} are required to obtain θ_r , Figure 5.15.

Subroutine GAMSUB

Subroutine GAMSUB determines the angle γ_1 between the line normal to the perimeter in the XZ-plane, and a line normal to the line segment R_{aT} , Figure 5.19. The perimeter length of the sector and the angle θ_r are required to obtain γ_1 . A separate equation for each of the 16 individual sectors is required. γ_1 for sector 3A is not equal to γ_1 for sector 3B (also true for sectors 11A and 11B).

5.2.1.1.1 Sector 1 (Figure 5.15) (Continued)

Subroutine GAMA2S

Subroutine GAMA2S determines the angle γ_2 between the Y-axis and a line normal to the ellipse $\left(\frac{Y}{B_{oe}}\right)^2 + \left(\frac{Z'}{A_{oe}}\right)^2 = 1$, which is defined by the ellipse ratio β_{oe} , at the point $Z' = RAT$. Although γ_2 is in the rotated YZ' -plane and not in the YZ -plane, because of the symmetry of the ellipsoid about the Y-axis, computation can occur in the YZ -plane, Figure 5.20.

Subroutine POSUB

Subroutine POSUB determines the coordinates X , Y , and Z of the point P_0 which is located at the intersection of the inner ellipse and a line extended along the propellant surface parallel to the tip from a general point on the perimeter, Figures 5.16 and 5.21.

The parameters R_{aT} and θ_r are required to determine the coordinates. The coordinates X_0 and Z_0 are obtained by trigonometry from R_{aT} and θ_r , Figure 5.21. The equation of the ellipsoid:

$$\left(\frac{Y_0}{B_{oe}}\right)^2 + \left(\frac{X_0^2 + Z_0^2}{A_{oe}^2}\right) = 1$$

yields the coordinate Y_0 .

The remaining points defining the plane (P_1 , P_2 , and P_3) are obtained from P_0 . Radial burning in the plane originates at P_0 .

Subroutine PISUB

Subroutine PISUB determines the coordinates (X_1 , Y_1 , and Z_1) of the point P_1 which is located on the Y-Z plane or on the outer ellipse along a line through point P_0 and normal to the sector perimeter as shown in Figure 5.22. P_1 is normally located on the Y-Z plane; however, for sectors 7 and 9, when the angle γ_1 exceeds β_{7max} in sector 7 or β_{9max} in sector 9, the point P_1 is located on the outer ellipse and is coincident with P_3 . The line segment Z_{1aT} shown in Figure 5.19 is used to flag subroutine P3SUB that P_1 is coincident with P_3 whenever Z_{1aT} is non-zero.

5.2.1.1.1 Sector 1 (Figure 5.15) (Continued)

$\beta_{91\max}$ and $\beta_{71\max}$ are geometry plane constants discussed in Section 5.1.1.

Subroutine P3SUB

Subroutine P3SUB determines the coordinates (X_3 , Y_3 , and Z_3) of the point P_3 that is located on the outer ellipse. If Z_{1aT} , determined in subroutine P1SUB, is not equal to zero, P_3 is coincident with P_1 and the coordinates of P_3 are set equal to the coordinates of P_1 . If Z_{1aT} is equal to zero, then P_3 is in the Y-Z plane and the coordinates of P_3 are determined from the angle ϕ shown in Figure 5.22.

Subroutine ROPSB

Subroutine ROPSB sums the values of the Y axis coordinate of P_0 (Y_{0A} and Y_{0B}) or P_0' (Y_{0A}' and Y_{0A} or Y_{0B}' and Y_{0B}) in planes A and B which are used in subroutine SCI to compute the surface area along the grain face. If the burn distance τ is greater than the maximum permissible burn distance for the sector, then the value of the sum is set to zero.

Subroutine BSUBC

Subroutine BSUBC sets up the correct variables and equations to determine the coordinates (X , Y , and Z) of the points P_{0b} , P_{1b}' , and P_{3b} located at increments of ΔL_0 along the perimeter of sector 1, Figure 5.15. The A plane coordinates are initialized to the prior B plane coordinates during the integration along the perimeter.

Subroutine VSTRSB

Subroutine VSTRSB determines the initial volume of the sectors. The incremental volume for each sector is determined from the incremental cross-sectional areas of the sectors and the average of the P_0 point Y-coordinates of the A and B planes.

5.2.1.1.2 Sector 3

Subroutines HASUBC, HBSUBC, HAPSUBC, HBPSBC, STUPRS, STUPPS, DFRASB, RASUBB, XRSUBB, THETAR, GAMSUB, GAMAZS, POSUB, P1SUB, P3SUB, and ROPSB are used to obtain the surface area and initial

5.2.1.1.2 Sector 3 (Continued)

volume for sectors 3, 3A, and 3B. As in sector 1, two planes are used to obtain the surface area. The distance between the planes A and B is determined by ΔL_0 in the same manner as for sector 1. The analysis for the surface area in sector 3 is similar to the analysis for the surface area in sector 1 except that the A and B planes will cross as shown in Figure 5.23 for sectors 3 and 11 and in Figure 5.24 for sectors 3A, 3B, 11A, and 11B.

The perimeter length of sector 3A (AL_{3A}) is determined from the geometry constants, and the coordinates of points P_0 , P_1 , and P_3 for both planes A and B. Since the surface area of sector 3B is identical with the surface area of sector 3A, the grain surface areas of both sectors between the planes are determined simultaneously by stepping the B plane an increment ΔL_0 along the sector 3A perimeter. The surface area along the grain between the planes is determined from the following equation:

$$ASI = \frac{(Y_0 + Y_0')}{2} \left[(X_0 - X_0')^2 + (Z_0 - Z_0')^2 \right]^{1/2}$$

The surface area along the tip for sector 3 is determined from the following equation after the integration for sector 3A is complete:

$$ASI = L_3 \frac{(R_2 - \tau)}{R_2} \frac{(Y_{0A} + Y_{0B})}{2}$$

where L_3 is the initial sector 3 perimeter length.

The initial volume of sector 3, and sectors 3A and 3B, is determined at the beginning of subroutine SCTOR1 after completion of the block 1 analysis as follows:

$$V_{STR} = \frac{(Y_{0A} + Y_{3A} + Y_{0B} + Y_{3B})(\tau_{2max} + R_3)}{4} + \frac{(\alpha_{01} - \alpha_{02})(Y_{0B} + Y_{3B})R_3^2}{4}$$

Subroutines RASUB3, XRSUBB, THETAR, GAMSUB, CAMA2S, POSUB, PLSUB, PJSUB, and ROPSB have been explained in Section 5.2.1.1.1 for sector 1. Therefore, only the subroutines unique to sector 3 are explained in this section.

5.2.1.1.2 Sector 3 (Continued)

Subroutines HASUBC, HBSUBC, HAPSUBC, and HBPSUBC

The function of these subroutines is the same as the function of subroutines ASUBC and BSUBC for sector 1; the correct variable and equations are set up to determine the coordinates (X, Y, and Z) of the points P_0 , P_1 , and P_3 for planes located at increments of $\Delta L0$ along the perimeter of the sector. Subroutine HASUBC deals with plane A, subroutine HBSUBC deals with plane B, subroutine HAPSBC deals with plane A', and subroutine HBPSBC deals with plane B', Figure 5.24.

Subroutines STUPRS and STUPPS

These subroutines store the variables that define the planes produced in sector 3A. Subroutine STUPRS is called in subroutine SCI after the A and B planes have been defined by subroutines HASUBC and HBSUBC. Subroutine STUPPS is called in subroutine SCI after the A' and B' planes have been defined by subroutines HAPSBC and HBPSBC. The stored variables are then used in subroutine SCI to determine the area along the grain face.

Subroutine DPRASB

Subroutine DPRASB determines the distance between the points P_{ra} and P'_{ra} and between P_{sa} and P'_{sa} that lie on the planes produced in sector 3A as shown in Figure 5.24. These distances DP_{ra} and DP_{sa} are used in subroutine SCI to alter the distance between the planes ($\Delta L0$) for each successive iteration as explained in Section 5.2.1.1 for sector 1.

5.2.1.2 Block 2A Analysis

Subroutine SCTOR1 is the control routine to determine the surface area of the pseudoellipsoid for the block 2A analysis and is called from subroutine HDNSUB. The initial volume of propellant for sectors 3A, 3B, 11A, and 11B is determined prior to the integration for the pseudoellipsoid surface area.

Points P_0 and P_1 that are used in Block 2A are not the same plane points used in the Block 1 analysis. Points P_0 and P_1 lie on the inner ellipsoid and are spaced a distance DS along the ellipsoid, Figure 5.25, starting at the igniter opening. The spacing of P_0 and P_1 are determined as follows:

5.2.1.2 Block 2A Analysis (Continued)

First

$$\Delta R = \left(\frac{\Delta R_v}{R_f} \right) l_{if}$$

where

$$\frac{\Delta R_v}{R_f} \quad \text{Is an input parameter}$$

R_f grain radius at the forward tangent plane.

Then each successive increment is

$$\Delta R = \frac{KK}{DS} \Delta R$$

where KK is an input.

Initially, if the motor has an igniter hole in the head end, Z_{p0} , which is the Z-coordinate of the point, P_0 , is set equal to R_{ig} . Otherwise, Z_{p0} is set equal to zero. ΔR is then added to Z_{p0} to obtain Z_{p1} , which is the Z coordinate of the point P_1 . Subroutine YPSUB is then called to obtain the Y coordinate of points P_0 and P_1 . The radius of curvature ρ_1 at the point P_1 on the pseudoellipsoid, the length, b , of the Y-intercept of the normal line to the ellipse at P_0 , and the Z coordinate Z_i are then determined to obtain the arc length, L_0 . Using these values, the incremental strip surface area is determined. This procedure is then repeated by setting $Z_{p0} = Z_{p1}$, and $Z_{p1} = Z_{p0} + \Delta R$ until $Z_{p1} = R_c - \tau_w$. The area adjacent to the igniter hole is then determined and added to the incremental sum.

Subroutines YPSUB, POEISB, LBSUB, ZISUB, and AIGSUB are used to determine the surface area of the pseudoellipsoid. The surface area for an incremental strip, as shown in Figure 5.25, is determined by the following equation:

$$ASI = \frac{\pi L_0}{2NO} (Z_{p1} + \tau \sin \alpha_{rc1} + Z_{p0} + \tau \sin \alpha_{rc0})$$

5.2.1.2

Block 2A Analysis (Continued)

The surface area for the entire pseudoellipsoid, including the igniter hole, is obtained by summing the incremental areas. The surface area around the igniter hole is added to the sum of the incremental areas. The lateral surface area of the igniter hole is assumed to be a non-burning inhibited surface.

Subroutine YPSUB

Subroutine YPSUB determines the Y coordinate of a point on the pseudoellipsoid. The angles α_{rc0} and α_{rc1} of the points P_{0a} and P_{0b} as shown in Figure 5.25 are also determined.

Subroutine ROELSB

Subroutine ROELSB determines the radius of curvature ρ_1 at the point P_0 on the inner ellipsoid. The radius of curvature is determined by the standard equation:

$$\rho_1 = \frac{[1 + (z')^2]^{3/2}}{z''}, \text{ where}$$

$$z' = \frac{dz}{dy}, \quad z'' = \frac{d^2z}{dy^2}$$

Subroutine LBSUB

Subroutine LBSUB determines the length b of the Y-intercept of the line normal to the inner ellipse at P_0 , Figure 5.25. The length is used in subroutine ZISUB to obtain the coefficients of the ellipse equation which defines the pseudoellipsoid.

Subroutine ZISUB

Subroutine ZISUB determines the Z-coordinate produced by the intersection of the outer ellipse:

$$\left(\frac{Y}{B_{1e}}\right)^2 + \left(\frac{Z}{A_{1e}}\right)^2 = 1$$

and the normal line to the ellipse at P_1 .

5.2.1.2

Block 2A Analysis (Continued)

Subroutine AIGSUB

Subroutine AIGSUB determines the surface area around the igniter opening. The area is obtained by finding the surface area of revolution which requires an angle π/N_0 , an arm length

$$\frac{\tau \sin \alpha_{rN}}{2} + R_{Ig}, \text{ and an arc length } \tau \alpha_{rN}, \text{ Figure 5.26.}$$

Initially, the Y-intercept of a line normal to the inner ellipse at the igniter radius is obtained,

$$Y_{NO} = \left[B_{OE}^2 - \frac{R_{Ig}^2}{P_{OE}^2} \right]^{1/2}$$

from which the angle between the Y-axis and the igniter opening on the inner ellipse is obtained,

$$\alpha_{rN} = \frac{\pi}{2} - \arccos \left[\frac{R_{Ig}}{\left[(B_{OE}^2 - Y_{NO}^2)^2 + R_{Ig}^2 \right]^{1/2}} \right]$$

and then the surface area of revolution is determined (Theorem of Pappus)

$$A_{Ig} = (2R_{Ig} + \tau \sin \alpha_{rN}) \frac{\pi \tau \alpha_{rN}}{2 N_0}$$

5.2.1.3

Block 2B Analysis

Subroutine SCTOR2 is the control routine to determine the surface area on the pseudoellipsoid that is covered by the propellant tips for the block 2B analysis. The surface area is determined by dividing the cross-sectional grain configuration into 12 sectors in subroutine HDNSUB, as shown in Figure 5.27. The surface area on the pseudoellipsoid for each sector is then determined by subroutine S2SK. Summing the surface areas for all sectors, and subtracting this area from the area obtained in blocks 1 and 2A, yields the total surface area of the head-end with web for any value of τ .

5.2.1.3

Block 2B Analysis

Subroutine S2SK

Subroutine S2SK determines the sector surface area on the pseudoellipsoid and is called from subroutine SCTOR2 with an argument to indicate the current sector. Each sector is set up to determine the incremental surface area contributed by that sector. Thus, in sector 3, Z_{p0} is set equal to R_{p2} , then R_{p3} is obtained and θ_{r0} is set equal to θ_{r1} . ΔR is then added to Z_{p0} to obtain Z_{p1} as shown in Figure 5.28. Y_{p0} , Y_{p1} and DS are then determined. The spacing for ΔR is calculated in the same manner as was done in Block 2A.

Finally, the parameters L_{pp} , X_{r1} , θ_{r0} , θ_{r1} , α_{rc0} , α_{rc1} , ρ_1 , b , Z_1 , and L_Q are determined and the incremental surface area for the sector is obtained from the equation, Figure 5.25:

$$L_Q = (\rho_1 + \tau)(\alpha_{rc1} - \alpha_{rc0})$$

and

$$AS = L_Q(Z_{p1} + \tau \sin \alpha_{rc1} + Z_{p0} + \tau \sin \alpha_{rc0}) \frac{(\theta_{r1} + \theta_{r0})}{4}$$

Z_{p0} is then set to Z_{p1} and the procedure repeated until Z_{p1} equals maximum radius of the sector.

The initial volume between the inner and outer ellipsoids for each sector is determined as follows (see Figure 5.25):

$$V_{JTO} = \left[(\rho_1 + D_{WB})^2 - \rho_1^2 \right] (\theta_{r1} + \theta_{r0})(\alpha_{rc1} - \alpha_{rc0}) \frac{Z_G N_0}{2}$$

where:

$$D_{WB} = \frac{Z_1 - Z_{p1}}{\sin \alpha_{rc1}}$$

$$D_{S1} = \rho_1(\alpha_{rc1} - \alpha_{rc0})$$

$$D_{S2} = (\rho_1 + D_{WB})(\alpha_{rc1} - \alpha_{rc0})$$

5.2.1.3

Block 2B Analysis (Continued)

$$X_{WB} = \frac{(2D_{S2} + D_{S1}) D_{WB}}{3(D_{S2} + D_{S1})}$$

$$Z_G = \frac{(Z_{P0} + Z_{P1})}{2} + X_{WB} \ln \left[\frac{\alpha_{rc1} + \alpha_{rc0}}{2} \right]$$

Subroutines YPSUB, XRTHR, ROELSB, LBSUB, and ZISUB are used to obtain the surface area. All of these subroutines except XRTHR have been explained in Section 5.2.1.2 for the block 2A analysis.

Subroutine XRTHR

Subroutine XRTHR is a set-up subroutine that uses subroutine XRSUBB to obtain the x-coordinate of a point located on the perimeter of a sector shown in Figure 5.28. The angle θ_{r1} between the Z axis and a line from the motor axis to the point on the sector is also determined.

5.2.1.4

Block 3 Analysis

Subroutine VOLSUB is the control routine which determines the initial propellant volume for the block 3 analysis. Initially, the volume present in the web region is determined from the volume produced by the difference of volumes of two oblate spheroids minus the volume of the igniter hole as follows:

$$V_{EH} = \frac{2}{3} \pi (B_{ie} A_{ie}^2 - B_{oe} A_{oe}^2) - \pi R_{ig}^2 (B_{ie} - B_{oe})$$

Next, the volume of the propellant tips is determined by dividing the grain configuration into 12 sectors as was done in block 2B, Figure 5.27. The volume contributed by each sector (subroutine VSEC) is then added to V_{EH} to obtain the total volume of propellant in the head-end, V_{FH} .

Finally, the surface area generated by radial burning from the line of intersection of the propellant tip with the head-end web, A_R , is approximated in the following manner:

The propellant volume in the radial burning portion is determined,

$$V_R = V_{FH} - V_{EH} + V_{STO} - 2 V_{STR} N_0$$

5.2.1.4

Block 3 Analysis (Continued)

The value for thickness burned at which the maximum surface area of this radial burning portion occurs is assumed to be the thickness at which the initial burnout of the web portion of the head-end web begins (for most cases this is very nearly correct). The curve for surface area versus thickness burned for this fuel volume is assumed to have the following equations (Figure 5.29):

$$A_R = \begin{cases} \frac{(T_{MAX} - \tau_{WH})^q \tau}{\tau_{WH}} & \text{for } \tau \leq \tau_{WH} \\ (T_{MAX} - \tau)^q & \text{for } \tau_{WH} < \tau < T_{MAX} \\ 0 & \text{for } \tau \geq T_{MAX} \end{cases}$$

where

T_{MAX} = maximum burn distance in the head-end section

τ_{WH} = maximum web thickness in the head-end section

q = calculated exponent

The maximum thickness burned in the head-end web is determined,

$$\text{If } B_{IE} - B_{OE} > \tau_W, \quad \tau_{WH} = \tau_W$$

$$\text{If } B_{IE} - B_{OE} \leq \tau_W, \quad \tau_{WH} = B_{IE} - B_{OE}$$

The radial burning volume is matched to the following integral ($V_R = V_{RX}$) by an iteration process to determine the exponent q ,

$$V_{RX} = \int_0^{\tau_{WH}} \frac{(T_{MAX} - \tau_{WH})^q}{\tau_{WH}} \tau d\tau + \int_{\tau_{WH}}^{T_{MAX}} (T_{MAX} - \tau)^q d\tau$$

or

5.2.1.4 Block 3 Analysis (Continued)

$$V_{RX} = \frac{(TDMAX - \tau_{WH})^q \tau_{WH}}{q} + \frac{(TDMAX - \tau_{WH})^{q+1}}{q+1}$$

The above integral represents the area beneath the curve shown in Figure

The radial burning area A_R is added to the total surface area, AS , at the completion of the block 3 analysis in subroutine VOLSUB.

Subroutine VSEC

Subroutine VSEC determines the initial volume of the tips that are present in the fore-head and is called from subroutine VOLSUB with an argument to indicate the sector to be computed. The same subroutines used in the block 2B analysis to obtain the incremental surface area of a pseudoellipsoid are used in this subroutine to obtain the incremental sector volumes. An arc length L_Q is obtained from the expression

$$L_Q = Z_{P1} - Z_{P0}$$

and the incremental volume within a sector is obtained from the expression

$$\Delta V = NO L_Q (Z_{P1} + Z_{P0}) (\theta_{r1} + \theta_{r0}) (Y_{P0} + Y_{P1}) / 4$$

5.2.2 Cylindrical Section

The longitudinal cylindrical section is that portion of the motor between the forward and aft tangent planes, Figure 4.3. Its length is designated as h_{CO} and the radius as R_f as shown in Figure 5.30. It may be either straight or tapered and may contain either a monolithic or segmented grain with or without a tapered port.

The longitudinal cylindrical section is first divided into incremental mass addition regions by locating increment dividing planes every delta Z distance, starting at the forward tangent plane and proceeding to the aft tangent plane. A maximum of 100 increment dividing planes is allowed.

The longitudinal cylindrical section is then divided by a number of reference planes. A minimum of two is required, one at each of the tangent planes. A maximum of eleven, A through K, is allowed to indicate changes in the cross-sectional grain geometry at specified locations within the section as shown in Figure 4.3. The cross sectional grain geometry is described at each reference plane used, by the port perimeter, L_p , the case radius, R_f , the port area, A_p , the propellant area, A_{pp} , the radius of gyration, K_{gy} , and the distance to the inert sliver, T_{SLVR} . If the inert

5.2.2 Cylindrical Section (Continued)

sliver option is used.

In segmenting propellant grains, the location of the slots, which separates the grain segments, is determined by defining the distance of the slot forward and aft interfaces from the forward tangent plane of the motor. This is shown by the values $S1A$, $S1B$, $S2A$, $S2B$, etc., Figure 4.3. The increment dividing planes, in this case, are determined as above, but with each segment treated as having a forward and aft tangent plane. The reference planes may be located within a slot, within a grain segment, or on a slot interface. The restrictions on the number of increment dividing planes and reference planes is also 100 and 11 respectively.

The following describes the subroutines which determine the longitudinal geometry for the cylindrical section:

Subroutine MNCHN4

Subroutine MNCHN4 contains the program control logic required to obtain the internal ballistic solution and the control logic used to initialize the working reference planes for subroutine SEGSUB. During burning, the distance burned at each reference plane for each time increment is determined by linear interpolation between adjacent increment dividing planes. When the reference plane is located within a slot, the increment dividing planes located within the grain segment are used for extrapolation to obtain the reference plane distance burned. When the distance burned has been determined for each input reference plane, the perimeter length, port area, and radius of gyration for each reference plane, and the burn area and CG location for each head section is determined from a table look-up procedure in the geometry tables.

During the internal ballistic solution for each time point the cylindrical section working reference planes (X and Y) are set up for successive input reference planes (A-B, R-C, etc.).

Subroutine SEGSUB

Subroutine SEGSUB contains the program control logic which determines the perimeter length, cross sectional propellant and port area, propellant volume, and mass generation at each increment dividing plane or mass addition region. The control logic is set to check for the existence of a slot forward interface between adjacent increment dividing planes, to check the location of the current upstream (X) and downstream (Y) working reference planes, and to set the parameters required in performing the gas dynamic solution for the slots and mass addition regions. Each increment dividing plane case radius, perimeter length, sliver radius, fuel area and port area and radius of gyration are obtained by linear interpolation between each reference plane.

5.2.3

Straight Through Grain, Motor End Sections

The following is applicable to motor aft-head or fore-head sections with straight through grains. A straight through grain is shown in Figure 5.31. The E subscript shown is set to N for analysis of the aft-head and to H for the fore-head.

Basic geometry constants required for analysis are calculated prior to determination of burn surface area versus distance burned and propellant volume. These constants are calculated in subroutine ENDCSB and are shown in Figure 5.30.

5.2.3.1

Geometry Constants

Subroutine ENDCSB

Initially, the case opening radius is determined from the input parameter DE1:

$$R_{E1} = \frac{D_{E1}}{2}$$

Then the angle between the tangent to the ellipse section at the radius R_{E1} and the motor axis is determined:

$$\alpha_{ER} = \arccos R_{E1} / [(R_f^2 - R_{E1}^2) \beta_E^2 + R_{E1}^2]^{1/2}$$

where R_f and β_E are input parameters.

If α_{ER} is less than or equal to the maximum allowable angle, α_{DEmax} , defined by input, then α_{DEmax} is set to α_{ER} , R_{E2} is set to R_{E1} and h_{E1} is set to zero. If, however, α_{ER} is greater than α_{DEmax} , then

$$R_{E2} = \frac{\cos(\alpha_{DEmax}) R_f \beta_E}{[\cos(\alpha_{DEmax})^2 \beta_E^2 - \cos(\alpha_{DEmax})^2 + 1.0]^{1/2}}$$

and

$$h_{E1} = (R_{E2} - R_{E1}) \frac{\sin(\alpha_{DEmax})}{\cos(\alpha_{DEmax})}$$

Next, the length of the head elliptical section is determined:

$$h_{E2} = [R_f^2 - R_{E2}^2]^{1/2} / \beta_E$$

5.2.3.1 Geometry Constants, Subroutine ENDCSB (Continued)

and the length of the end section is computed:

$$h_{EO} = h_{E1} + h_{E2}$$

If h_{EO} is less than the maximum burn distance at the adjacent tangent plane, τ_{max} , determined in Section 5.1, Geometry Constants, the end section is lengthened to the maximum burned distance:

$$h_{ER} = \tau_{max}$$

If, however, h_{EO} is greater than or equal to τ_{max} , then $h_{ER} = h_{EO}$. Finally, the maximum burn distance in the conical section and the end section is determined:

$$\tau_{E1} = [(R_{E2} - R_{E1})^2 + h_{E1}^2]^{1/2}$$

$$\tau_{EO} = [(R_f^2 - R_{E1})^2 + h_{EO}^2]^{1/2}$$

The complete end section case volume is determined from:

$$V_{CE} = (h_{ER} - h_{EO}) \pi R_f^2 + \frac{1}{3} \left[3 \frac{R_f^2}{\beta_E} - h_{E2}^2 \right] [\pi h_{E2} \beta_E^2] \\ + (R_{E2} R_{E1} + R_{E1}^2 + R_{E2}^2) \pi \frac{h_{E1}}{3}$$

The following coefficients are calculated for use in subroutine RCSUB when the burning distance $\tau > \tau_{E1}$. They are the coefficients of a fourth degree equation of the intersection of an ellipse and a circle and are used to compute the location of intersection of the burning surface and the case wall.

$$CAE = (\beta_E^2 - 1)^2$$

$$CBE = -(\beta_E^2 - 1)^2 \beta_E^2 R_{E1}^4$$

$$CCCE = [\beta_E^4 R_{E1}^2 3 + (\beta_E^4 + \beta_E^2) h_{EO}^2 + R_f^2 (\beta_E^2 - 1) - R_E^2 \beta_E^2] 2$$

$$CCVE = 2(\beta_E^4 - \beta_E^2)$$

$$CDCE = [(h_{EO}^2 + R_{E1}^2) \beta_E^2 + R_f^2 \beta_E^2] 4R_{E1}$$

5.2.3.1

Geometry Constants, Subroutine ENDCSB (Continued)

$$CDVE = 4 R_{E1} \beta_E^4$$

$$CECE = R_f^4 + (R_{E1}^2 - h_{EO}^2) \beta_E^2 R_f^2 + (R_{E1}^2 + h_{EO}^2) \beta_E^4$$

$$CEVE = (h_{EO}^2 \beta_E^2 + R_{E1}^2 \beta_E^2 + R_f^2) 2 \beta_E^2$$

5.2.3.2

Calculation Sectors and Zones

The cross-sectional grain geometry in motor end sections is based on the geometry at the forward and aft tangent planes. Figures 5.32 and 5.33 define sectors and zones used for burn-surface area and propellant volume calculations. The general forked wagon wheel grain in Figure 5.32 is divided into 13 sectors. Depending on the exact grain geometry, more than one sector may exist in a zone. This is the case for zone A, Figure 5.33 and initial sectors 1, 2, 3, and 4 in Figure 5.32. The opposite may exist where only a portion of a sector is bounded by a zone boundary.

Four zones can exist in the end section. Their boundaries are defined as:

Zone A is that region between the minimum propellant radius, R_1 , and the case opening, R_{E1} . Burning will occur along the side of the propellant tip and on the end face.

Zone B is that region between the case opening, R_{E1} , and where the end-burning surface intersects the case, R_c . Burning will occur along the propellant tip and on the toroidal end face.

Zone C is that region between where the end-burning surface intersects the case, R_c , and the web, $\tau_w = \tau$. Burning will occur only along the side of the propellant tip or in the valley.

Web Zone is that region between the radius $R_f = \tau_w + \tau$ and the radius of the case R_f . Burning will occur along the perimeter of sector 8 and along the end face if the case opening, R_{E1} , is greater than the radius to the web, $R_f = \tau_w + \tau$.

The sectors that are in zones B, C, and web are subdivided into smaller elements. The sectors in zone A are not subdivided. Sector boundaries and zones which the sectors occupy are recalculated as the burning surface regresses.

5.2.3.2

Calculation Sectors and Zones (Continued)

Subroutine ASESUB

Subroutine ASESUB is the control routine to determine the total burning surface area and initial volume of the end sections. The grain cross-section at the adjacent tangent plane is divided into sectors, Figure 5.32. The correct equations from subroutines XRSUB and RASUB are set up and the proper values for the coordinates of the origin of the circular arc, X_{OV} , Y_{OV} , the radius of curvature of the sector, R_T , the angle between the bisector of the propellant tip and the straight side sectors, α_V , and the perimeter length, L_X , are assigned for each sector. After the required parameters have been set for a sector, the sector burning area and volume are determined in subroutine AESUB.

Subroutine AEPSUB

Subroutine AEPSUB tests for the existence of a sector and is called from subroutine ASESUB. If a sector has burned out or was not present in the initial grain configuration, control is returned to subroutine ASESUB; otherwise, control proceeds to subroutine AESUB. After the sector burning area and volume have been determined in subroutine AESUB, the sector values are added to the sum of the values for the previous sector and control is returned to subroutine ASESUB.

Subroutine AESUB

Subroutine AESUB determines the total burning surface area and initial volume of the sectors. A test is made at the beginning of each zone to determine if the sector exists in that zone.

The parameters X_{RO} , R_{AO} , and Y_{AO} are associated with the beginning coordinates of a sector perimeter, and the parameters X_{RX} , R_{AX} , Y_{AX} and L_X are associated with the end coordinates of a sector perimeter as shown in Figure 5.32. These parameters are determined by subroutines XRSUB and RASUB from the Pythagorean Theorem. The beginning and end points of a sector may not be the beginning and end points of the area to be computed should a sector exist in more than one zone. The beginning coordinates of an area are then subscripted min and the end coordinates are subscripted max instead of 0 and X, respectively. The perimeter length is then defined as L_R . Figure 5.34 shows an example of the min and max coordinates that are used in the following zone A analysis. When an integration scheme is employed, zones B, C, and Web, the min and max coordinates of each increment are determined to compute sector surface area.

5.2.3.2

Calculation Sectors and Zones (Continued)

Subroutine RCSUB

Subroutine RCSUB obtains the radius vector from the motor axis to the intersection of the aft burning surface with the case wall, R_c , Figure 5.33. The intersection is determined from the equation of a straight line when $\tau \leq \tau_{E1}$, and from the equation for the aft-dome configuration (circle or ellipse) when $\tau > \tau_{E1}$, where:

$$\tau_{E1} = [(R_{E2} - R_{E1})^2 - h_{E1}^2]^{1/2}$$

Subroutine ARSSUB

Subroutine ARSSUB determines the chord length, L_{RS} , between the minimum point of a sector and a general point along the perimeter of a sector as shown in Figure 5.35. The required parameters are R_{A0} , X_{R0} , R_A , and X_R .

Subroutine ALRSUB

Subroutine ALRSUB determines the arc length of a sector, L_R , from the minimum point of a sector to a general point along the perimeter as shown in Figure 5.35. The required parameters are L_{RS} and R_T .

Subroutine XRSUB

Subroutine XRSUB determines the X-coordinate of a general point on the perimeter of a sector. A separate equation is used for each sector. The required parameters are R_A and τ .

Subroutine RASUB

Subroutine RASUB determines the length of a radius vector from the motor axis to a general point on the perimeter of a sector. A separate equation is used for each sector. The perimeter length along the sector and the distance burned τ are required.

Subroutine HESUB

Subroutine HESUB determines the length of the trapezoidal elements, h_E , used to determine the incremental volumes and areas, Figure 5.36.

5.2.3.2.1 Zone A Calculations

When $R_{A0} < R_{E1}$, the surface area is computed in Zone A. When $R_{A0} \geq R_{E1}$, the analysis proceeds to the next zone and R_{Amax} is set to the smaller value of R_{AX} and R_{E1} .

The following Zone A analysis applies to sectors 1 through 7 and 9 through 13. Figure 5.35 is used as an example to define calculation parameters. It illustrates sector 3.

The burning surface area in zone A is determined from an algebraic composition of simple geometric figures such as shown in Figure 5.35.

The value of γ_T , L_R , and L_{RS} are determined as follows:

$$\gamma_T = 2 \arccos \left(\frac{[(2R_T)^2 - L_{RS}^2]^{1/2}}{2R_T} \right)$$

$$L_R = \gamma_T |R_T|$$

$$L_{RS} = \left\{ \left[R_{Amax}^2 - x_{Rmax}^2 \right]^{1/2} - \left[R_{Amin}^2 - x_{Rmin}^2 \right]^{1/2} + \frac{(x_{Rmax} - x_{Rmin})^2}{2} \right\}^{1/2}$$

where $R_T = R_3 - T$ for sector 3

A_{T0} is the area between the chord L_{RS} and the circular arc L_R and is determined by subtracting the area of the inscribed triangle from the area of the circular sector, abg:

$$A_{T0} = |R_T| L_R - L_{RS} \left[R_T^2 - \frac{(L_{RS})^2}{2} \right]^{1/2}$$

A_{TT} is equal in magnitude to A_{T0} and is positive if R_T is positive, negative if R_T is negative, and zero if R_T is zero. A_{FF} is the area of the trapezoid, abcf:

$$A_{FF} = \left\{ [R_{Amax}^2 - x_{Rmax}^2]^{1/2} - [R_{Amin}^2 - x_{Rmin}^2]^{1/2} \right\} \frac{(x_{Rmax} - x_{Rmin})}{2}$$

5.2.3.2.1 Zone A Calculations (Continued)

A_R is the area bcd determined by subtracting the triangular area obd from the circular sector obc:

$$A_R = \frac{R_{Amax}^2 \gamma_R - X_{Rmax} [R_{Amax}^2 - X_{Rmax}^2]^{1/2}}{2}$$

where

$$\gamma_R = \arcsin \left(\frac{X_{Rmax}}{R_{Amax}} \right)$$

A_{RO} is the area aef determined by subtracting the triangular area oaf from the area of circular sector oae:

$$A_{RO} = \frac{R_{Amin}^2 \gamma_{RO} - X_{Rmin} [R_{Amin}^2 - X_{Rmin}^2]^{1/2}}{2}$$

where

$$\gamma_{RO} = \arcsin \left(\frac{X_{Rmin}}{R_{Amin}} \right)$$

The burning area along the side of the propellant tip is $h_E(L_R)$ and the total sector area A_{EE} is:

$$A_{EE} = 2 NO [L_R h_E + A_{TT} + A_{FF} + A_R - A_{RO}]$$

The sector volume is:

$$DV = (A_{FF} + A_R - A_{RO} + A_{TT}) h_E NO 2$$

If the maximum point of the sector, R_{Amax} is within zone A, then control is returned to subroutine AEPSUB; otherwise, computation will proceed to zone B.

5.2.3.2.2 Zone B Calculations

When R_{AO} for a sector is less than R_C , surface area is computed in zone B. When R_{AO} is greater than or equal to R_C , computation proceeds to Zone C.

Initially, R_{Amax} is set to the smallest value of R_{AX} and R_C from which L_{Rmax} is determined by subroutine ARSSUB and ALRSUB. L_{R1}

5.2.3.2.2 Zone B Calculations (Continued)

is determined in the same manner from R_{Amin} . The burning surface area is then computed in increments of ΔL where $\Delta L = R_f$ (DLRF) by integrating over the perimeter length, L_{Rmax} . DLRF is an input parameter. For each increment, R_{Amax} is determined from $L = L_{R1} + \Delta L$, and R_{Amin} is determined from $L = L_{R1}$. Figure 5.36, The X-coordinate, X_R , of the centroid, Figure 5.36, is obtained from subroutine XRSUB and the radius vector R_A is obtained from subroutine RASUB. The angle γ_R is:

$$\gamma_R = \arcsin \left(\frac{X_R}{R_A} \right)$$

The cross sectional area of the end face is equal to the product of the incremental arc length $(\lambda - \lambda_{min})\tau$, and the arc length, $\gamma_R R_A$, through which the centroid is rotated.

The surface area along the side of the propellant tips are approximated by trapezoidal increments and is added to the area of the end face. The burning surface areas and volumes of each increment are added to the sum of the previous increment values. They are determined for an increment as follows:

$$A_{EE} = 2 NO \left[(L - L_{R1}) \frac{h_E + h_E^i}{2} + R_A \gamma_R (\lambda - \lambda_{min})\tau \right]$$

where

$$h_E = |h_{ER} - [\gamma^2 - (R_{Amax} - R_{E1})^2]^{1/2}|$$

$$h_E^i = |h_{ER} - [\gamma^2 - (R_{Amin} - R_{E1})^2]^{1/2}|$$

$$DV = 2 NO (R_{Amax} - R_{Amin}) \frac{h_E + h_E^i}{2} \gamma_R R_A$$

The next increment in the sector is determined by setting $L_{R1} = L$, $h_E^i = h_E$, $R_{Amin} = R_{Amax}$, and $L_{R1} = L_{R1} + \Delta L = L$. L is set to L_{Rmax} for the last iteration for a sector.

5.2.3.2.2 Zone B Calculations (Continued)

The parameters R_A , R_{Amax} , L , and h_E are determined for each increment.

The toroidal and burning area is formed by revolving an arc about the motor axis, and is equal to the product of the length of the arc increment and the arc length through which the centroid of the arc increment is rotated (Theorem of Pappus). The area along the side of the propellant clip is determined from the trapezoids.

The radial vector, R_A , to the centroid of the arc increment, as shown in Figure 5.36, is:

$$R_A = \frac{2\tau}{\lambda - \lambda_{min}} \sin\left(\frac{\lambda - \lambda_{min}}{2}\right) \sin\left(\frac{\lambda + \lambda_{min}}{2}\right) + R_{E1}$$

where $\frac{2\tau}{\lambda - \lambda_{min}} \sin\left(\frac{\lambda - \lambda_{min}}{2}\right)$ is the distance from the centroid of the arc increment to the origin of the circle about which the arc increment is revolved.

The angles λ and λ_{min} are determined as follows:

$$\lambda = \arcsin\left(\frac{R_{Amax} - R_{E1}}{\tau}\right)$$

$$\lambda_{min} = \arcsin\left(\frac{R_{Amin} - R_{E1}}{\tau}\right)$$

If R_{AX} is less than R_C , computation will proceed to the next sector. If R_{AX} is greater than or equal to R_C , computation will proceed to zone C.

5.2.3.2.3 Zone C Calculations

The burning surface area in Zone C consists only of the surface along the side of the propellant tip, and is determined from trapezoidal elements. If a sector exists in zones B and C, R_A is set equal to R_{Amax} of zone B; otherwise, $R_A = R_{A0}$. With R_A , L_{A1} is determined from subroutines ARSSUB and ALRSUB. The length of the initial edge, h_{E1} , of the trapezoidal element is determined in subroutine HESUB as follows:

5.2.3.2.3 Zone C Calculations (Continued)

If $R_A \leq R_{E2}$,

$$h_E^i = h_{ER} - h_{E1} \left(\frac{R_A - R_{E1}}{R_{E2} - R_{E1}} \right)$$

Or if $R_A > R_{E2}$,

$$h_E^i = h_{ER} + \frac{(R_f^2 - R_A^2)^{1/2}}{\beta_E} - h_{E0}$$

An incremental length ΔL is added to L_{R1} and a corresponding R_A is determined from subroutine RASUB. The length of the top edge h_E of the trapezoidal element is determined from the above equations in subroutine NESUB and the elemental trapezoidal area and volume are added to the previous sectors as follows:

$$A_{EE} = 2 NO (L - L_{R1}) \left(\frac{h_E + h_E^i}{2} \right)$$

where

$$R_A = \frac{R_{Amax} + R_{Amin}}{2}$$

$$DV = 2 NO (R_{Amax} - R_{Amin}) \frac{(h_E + h_E^i)}{2} \gamma_R$$

5.2.3.2.4 Web Zone Calculations

Subroutine AWESUB determines burning surface area and initial volume of the web zone.

The burning surface area of sector 8 is determined first from the trapezoidal element of length h_E , which is determined from $R_{A0} = R_f - \tau_w + \tau$, as follows:

$$AWE = 2 NO h_E L_8$$

L_8 is the perimeter length of sector 8.

The volume of propellant in the web zone is determined as follows: (geometric symbols are given in Figures 5.33 and 5.36)

5.2.3.2.4 Web Zone Calculations (Continued)

If $R_{E2} > (R_f - \tau_w + \tau)$, calculate the parameter,

$$h_{EFC} = \frac{(R_{E2} - R_f + \tau_w - \tau)}{R_{E2} - R_{E1}} h_E^i$$

and the volume as:

$$DV = \left\{ \left[\left(\frac{R_f}{\beta_E} \right)^2 h_{E2} - \frac{h_{E2}^3}{3} \right] \beta_E^2 + (h_{ER} - h_{EO}) R_f^2 \right. \\ \left. + \left[(R_f - \tau_w + \tau)^2 + R_{E2} (R_f - \tau_w + \tau) + R_{E2}^2 \right] \frac{h_{EFC}}{3} \right. \\ \left. - (h_{EFC} + h_{ER} - h_{E1}) (R_f - \tau_w + \tau)^2 \right\} \pi$$

If $R_{E2} \leq (R_f - \tau_w)$, calculate the parameter,

$$Z_1 = \frac{[R_f^2 - (R_f - \tau_w + \tau)^2]^{1/2}}{\beta_E}$$

and the volume as:

$$DV = \left\{ \left[\left(\frac{R_f}{\beta_E} \right)^2 Z_1 - \frac{Z_1^3}{3} \right] \beta_E^2 + (h_{ER} - h_{EO}) R_f^2 \right. \\ \left. - (Z_1 + h_{ER} - h_{EO}) (R_f - \tau_w + \tau)^2 \right\} \pi$$

The additional end burning area and initial propellant volume, when $R_{E1} > R_f - \tau_w + \tau$, are determined as follows:

When $R_{E1} < R_C$

$$A_{WE} = 2 \pi \theta_1 (R_{E1}^2 - R_{AO}^2)$$

$$DV = \pi \beta_E (R_{E1}^2 - R_{AO}^2)$$

The toroidal end burning surface exists when $R_C > R_{E1}$. The re-

5.2.3.2.4 Web Zone Calculations (Continued)

volved area is a product of the arc length and the circumference of the circle described by the centroid of the arc length. The radial vector to the centroid of the arc increment, Figure 5.36, is:

$$R_A = \frac{2\tau}{\lambda - \lambda_{min}} \sin\left(\frac{\lambda - \lambda_{min}}{2}\right) \sin\left(\frac{\lambda + \lambda_{min}}{2}\right) + R_{E1}$$

The toroidal surface area is determined from the product of the arc length, $(\lambda - \lambda_{min})\tau$, and the circumference of the circle, $2\pi R_A$, described by the centroid of the curve:

$$A_{WE} = 2(\lambda - \lambda_{min}) \tau \pi R_A$$

5.3

Moments of Inertia and CG Location

Pitch and roll moments of inertia (MOI) and the center of gravity (CG) location during motor burning can be calculated. The roll moment (J-ROLL) is taken about the longitudinal axis of the motor. The pitch moment (J-X-Y) is taken about an axis passing through the motor CG and centerline. The center of gravity is measured from the aft tangent plane. The value is positive when the CG is forward of the aft tangent plane. The moments about the pitch and yaw axes are assumed to be equal. This assumption is valid for any configuration with an even multiple of 4 propellant tips.

The MOI and CG location of the motor are based on the combined values of each section; fore-head, cylinder, and aft-head.

The pitch MOI of the fore-head is initially determined about the forward tangent plane and then transferred to the aft tangent plane, the cylindrical and aft-head section MOI's are initially determined about the aft tangent plane. These values about the aft-tangent plane are then transferred to the motor CG. The transfer formula is:

$$J_{CG} = J_{\text{aft tangent plane}} + d^2 W / g_0$$

where d is the distance between the motor CG and aft tangent plane.

The MOI of a body with respect to a given axis is defined as the product of the mass and the square of the distance from the axis. If $dm = dW/g_0$ represents an elemental mass and Y its distance from an axis, the MOI, J , of the object about this axis will be equal to $\int Y^2 dW/g_0$, Reference 8.

The CG is that point at which the mass of an object is concentrated so that the moment of the concentrated mass about any axis or plane is the same as the sum of the moments of all the elements of the mass about the same axis or plane. The sum of the moments from a plane is $\int \frac{x dW}{g_0}$

and the CG is defined as: $\bar{x} = \frac{\int x dW}{W}$

where

\bar{x} = distance to the CG location from a plane.

The MOI and CG location for each section are determined from a summation of incremental volumes and areas about the desired axis. The incremental volumes are hollow circular cylinders for the cylindrical section and thin shells for the head-end sections. The radius of gyration for the cylindrical section is determined from the roll MOI of the grain cross-sectional area. The incremental rectangular MOI's are first taken about the CG of the incremental volume and then transferred to the desired axis. The transfer formula is $I = I_{CG} + d^2 m$, where I_{CG} is the MOI about the CG and d is the distance to the reference axis.

5.3.1

Roll Moment of Inertia

The roll MOI of an incremental thin shell for the head sections are determined from the fundamental equation; Figure 5.37:

$$J_p = \frac{W}{g_0} r^2, \text{ slug-in}^2$$

The thin shells are based on a subdivision of sector boundaries.

The roll MOI of the cross sectional area of an incremental hollow circular cylinder, Figure 5.38, is determined from the fundamental equation:

$$J_p = \frac{(\theta_{r_i} + \theta_{r_o})}{4} (r_o^4 - r_i^4) N_0, \text{ in}^4$$

where

r_o = outer incremental radius, in

r_i = inner incremental radius, in

The radius of gyration is determined from:

$$K = \frac{J_p}{AFP}^{1/2}, \text{ in}$$

where AFP is the cross sectional area of propellant, in².

5.3.1.1

Motor End Sections

The roll MOI's for the motor end sections are determined in sub-routines PT1AA and SD1D13 from a summation of thin shells of each sector and the web region as follows:

$$AJPP = \sum_{i=1}^{12} [J_{pX}] + (R_{AO}^2 + R_A^2) (R_A^2 - R_{AO}^2) \pi \frac{(h_E + h'_E)}{2} \frac{p_f}{2g_0}$$

$$\text{where, } J_{pX} = \frac{(R_A^2 + R_{AO}^2) W_i}{2g_0}$$

$$W_i = (\theta_{r_i} + \theta_{r_o}) N_0 p_f (R_A^2 - R_{AO}^2) \frac{(h_E + h'_E)}{4}$$

R_{AO} is the minimum radius of the increment

R_A is the maximum radius of the increment

5.3.1.2

Cylindrical Section

The roll MOI for the cylindrical section is determined in subroutine SEGSUB using the radius of gyration of the propellant cross section. The radius of gyration of the cross section is determined in subroutines PT1AA and SD1D13 from a summation of the roll MOI for the elementary hollow circular cylinders of each sector and the web region as follows:

$$J_{PP} = \sum_1^{13} \left[\frac{(\theta_{r1} + \theta_{ro})}{4} (R_A^4 - R_{AO}^4) NO \right] + \frac{\pi}{2} (R_A^4 - R_{AO}^4)$$

$$W_T = \sum_1^{13} \left[\frac{(\theta_{r1} + \theta_{ro})}{2} (R_A^2 - R_{AO}^2) NO \right] + \pi (R_A^2 - R_{AO}^2)$$

$$K_{GY} = \left[\frac{J_{PP}}{W_T} \right]^{1/2}$$

The radius of gyration is calculated only at the input reference planes and linearly interpolated at each increment dividing plane. The cylindrical section total roll MOI is determined from a summation of individual mass addition region roll MOI values as follows, Figure 4.3:

$$I_{PCYL} = \sum_1^{NI} \left[(\pi R_{fhi}^2 - A_{PHI}) K_{GYHI}^2 + (\pi R_f^2 - A_P) K_{GY}^2 \right] \frac{\Delta Z \rho_f}{2 g_0}$$

The subscripted HI parameters are the values at the adjacent upstream increment dividing plane. NI is the total number of increment dividing planes.

5.3.2

Pitch MOI

The pitch MOI's of the head sections are taken with reference to the adjacent tangent plane such that:

$$J_B = \frac{W}{g_0} \left(\frac{r^2}{2} + \frac{L^2}{12} \right) + \frac{W}{g_0} R_{CG}^2$$

where

r = radius to CG of cross section, in

L = incremental length of shell, in

R_{CG} = distance from reference axes (tangent plane) to the CG, in

5.3.2

Pitch MOI (Continued)

For the incremental hollow circular cylinders of the cylindrical section the calculations are taken with reference to the CG of the incremental cylinder and then transferred to the aft tangent plane such that:

$$J_B = \frac{W}{g_0} \left(\frac{K^2}{2} + \frac{L^2}{12} \right) + \frac{W}{g_0} d^2$$

where

K = radius of gyration of cross section, in²

d = distance from the CG to aft tangent plane, in

5.3.2.1

Motor End Sections

The pitch MOI for the motor end sections are determined in sub-routines PT1AA and SD1D13 from a summation of MOI's for elemental thin shells of each sector and the web region as follows:

$$A_{JBB} = \sum_1^{13} \left\{ \left[\frac{(h_E + h'_E)^2}{2} \right] \frac{W_1}{12g_0} + \frac{J_{PX}}{2} + \frac{W_1 R_{CG}^2}{g_0} \right\} \\ + \frac{R_{CG}^2 W_1}{g_0} + \left[\frac{(h_E + h'_E)^2}{12} + (R_A^2 + R_{A0}^2) \right] \frac{W_1}{4g_0}$$

where

$$R_{CG} = \begin{cases} h_{E0} + \frac{(h_E + h'_E)}{4} & \text{for the fore-head and} \\ \frac{h_E + h'_E}{4} & \text{for the aft-head} \end{cases}$$

$$J_{PX} = (R_A^2 + R_{A0}^2) \frac{W_1}{2g_0}$$

5.3.2.2

Cylindrical Section

The MOI is determined in subroutine SEGSUB from a summation of individual mass addition region values as follows:

$$I_{BCYL} = \sum_1^{NI} \left\{ \frac{(\pi R_{FHI}^2 - A_{PHI})}{2} \left[K_{GYHI}^2 + 2 \left(\frac{3}{4} (A_{INCW} - A_{INCHI}) + h_{CO} - A_{INCW} \right)^2 \right] \right\}$$

5.3.2.2 Cylindrical Section (Continued)

$$+ \frac{2(AINCW-AINCHI)^2}{12}] + [K_{GY}^2 + 2 \left(\frac{AINCW-AINCHI}{4} + h_{CO} - AINCW \right)^2]$$

$$\left. \frac{(\pi R_f^2 - A_p)}{2} \right\} \frac{\rho_f (AINCW-AINCHI)}{2 g_0}$$

5.3.3 CG of Sections

The CG for each section is determined from a summation of the moments of incremental volumes about the desired axis. The CG for the cylindrical section is determined from a summation of the moments of incremental hollow circular cylinders about the aft tangent plane, Figure 5.38, and the CG for the head sections are determined from a summation of the moments of thin shells about the adjacent tangent plane, Figure 5.37. Thus:

$$\overline{MX} = \frac{W}{g_0} \bar{X} = \sum X_i \frac{dW}{g_0}$$

therefore

$$\bar{X} = \sum X_i dW/W$$

where

X_i = moment arm of incremental volume, in

dW = incremental volume weight, lb

W = total weight, lb

5.3.3.1 Head Sections

The CG is determined in subroutines PTIAA and SD113 from a summation of moments for elemental thin shells of each sector and the web region as follows:

$$\bar{X}_i = \sum_1^{13} [(W_T \bar{X}_i \text{ previous} + (h_E + h'_E) \frac{W_i}{4}) / (W_i + W_T)]$$

$$\text{where } W_T = \sum_1^{13} W_i$$

subscript i is N for aft-head,

H for fore-head.

5.3.3.2 Cylindrical Section CG Location

The CG location is determined in subroutine SEGSUB from a summation of the individual mass addition region moments as follows, Figure 5.38:

$$AOMCYL = \sum_{i=1}^{NI} \left\{ \left[\left(\frac{3(AINCW-AINCHI)}{4} + h_{CO} - AINCW \right) (\pi R_{FH}^2 - A_{PH}) \right. \right. \\ \left. \left. + \left(\frac{AINCW-AINCHI}{4} + h_{CO} - AINCW \right) (\pi R_f^2 - A_p) \right] \frac{(AINCW-AINCHI)}{2} \rho_f \right\}$$

5.3.4 Motor MOI and CG

Motor Roll MOI:

$$J_{PP} = J_{PHed} + J_{PNoz} + I_{Pcyl}$$

The motor CG location and pitch MOI are determined by a transfer of axes of the MOI of each section as follows:

Motor CG:

$$\bar{X}_{IH} = \frac{(\bar{X}_H + h_{CO}) V_{FH} \rho_f + AOMCYL - \bar{X}_N V_{FN} \rho_f}{W_f}$$

Fore-Head Section Pitch MOI:

$$J_{BHed} = (J_{BHed})_{Aft} - \left[\bar{X}_H^2 - (\bar{X}_H + h_{CO} - \bar{X}_{IH})^2 \right] \frac{V_{FH} \rho_f}{g_0}$$

Aft-Head Section Pitch MOI:

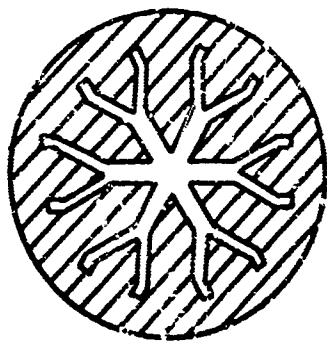
$$J_{BNoz} = (J_{BNoz})_{Aft} - \left[\bar{X}_N^2 - (\bar{X}_N + \bar{X}_{IH})^2 \right] \frac{V_{FN} \rho_f}{g_0}$$

Cylindrical Section Pitch MOI:

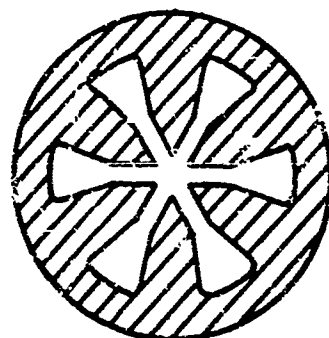
$$I_{Bcyl} = (I_{Bcyl})_{Aft} - \left\{ \left[\bar{X}_{IH} W_f - (\bar{X}_H + h_{CO}) V_{FH} \rho_f \right. \right. \\ \left. \left. + \bar{X}_N V_{FN} \rho_f \right] / \left[W_f - (V_{FH} + V_{FN}) \rho_f \right] \right\}^2 \\ \left[W_f - (V_{FH} + V_{FN}) \rho_f \right] / g_0$$

Motor Pitch MOI:

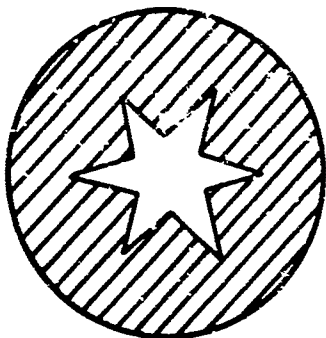
$$J_{BB} = J_{BHed} + J_{BNoz} + I_{Bcyl}$$



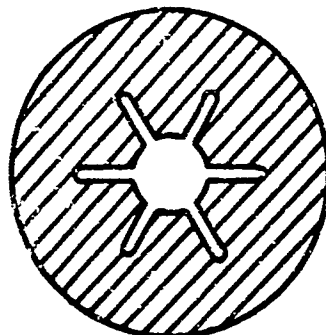
Forked Wagon Wheel



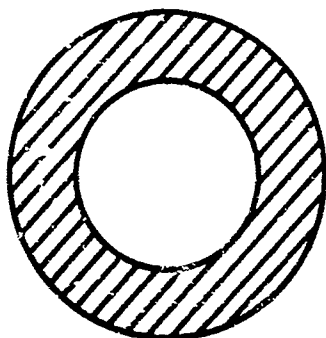
Conventional Wagon Wheel



Standard Star



Slotted-Cone



Circular Port

Figure 5.1. Grain Design Options

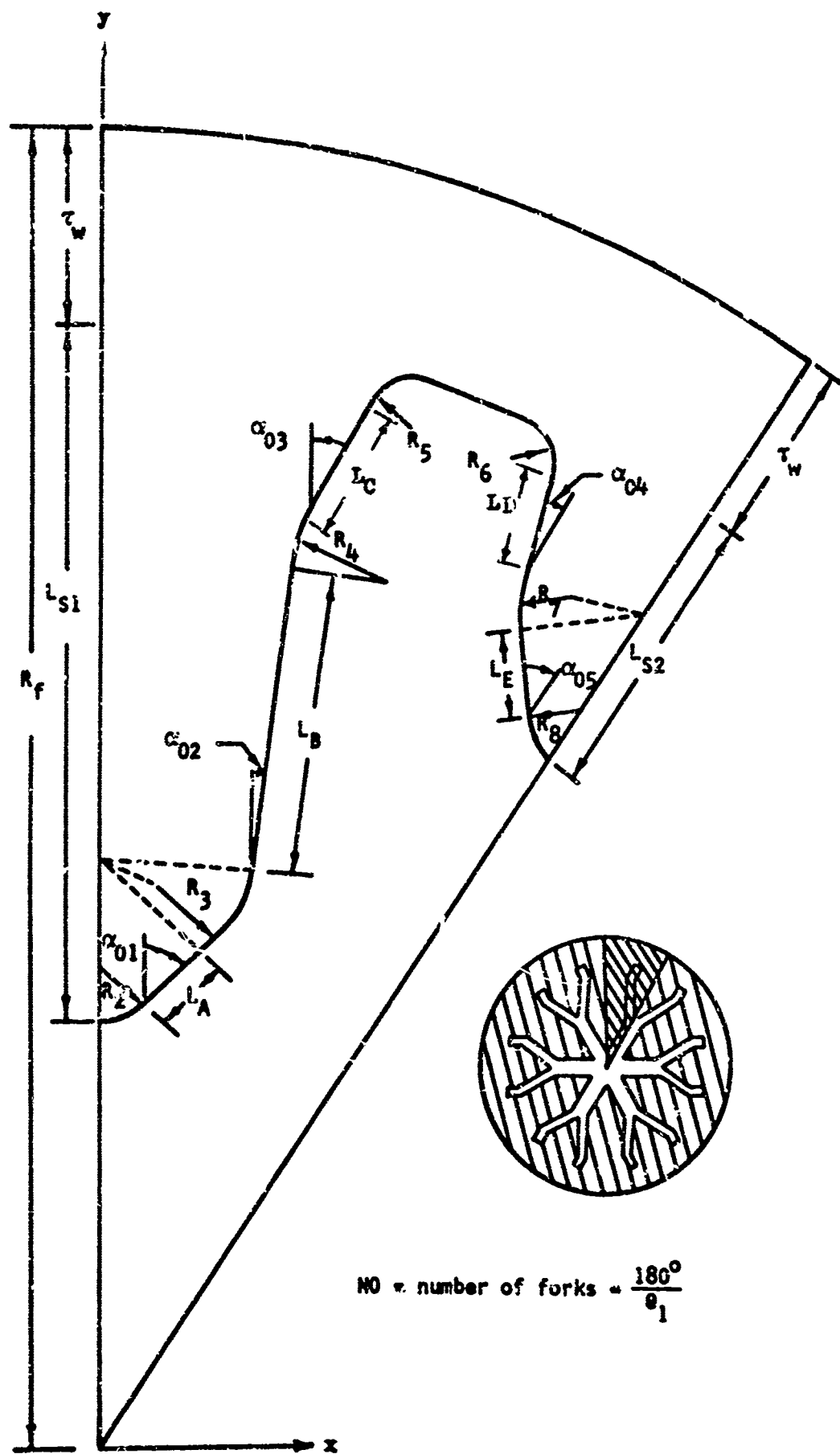
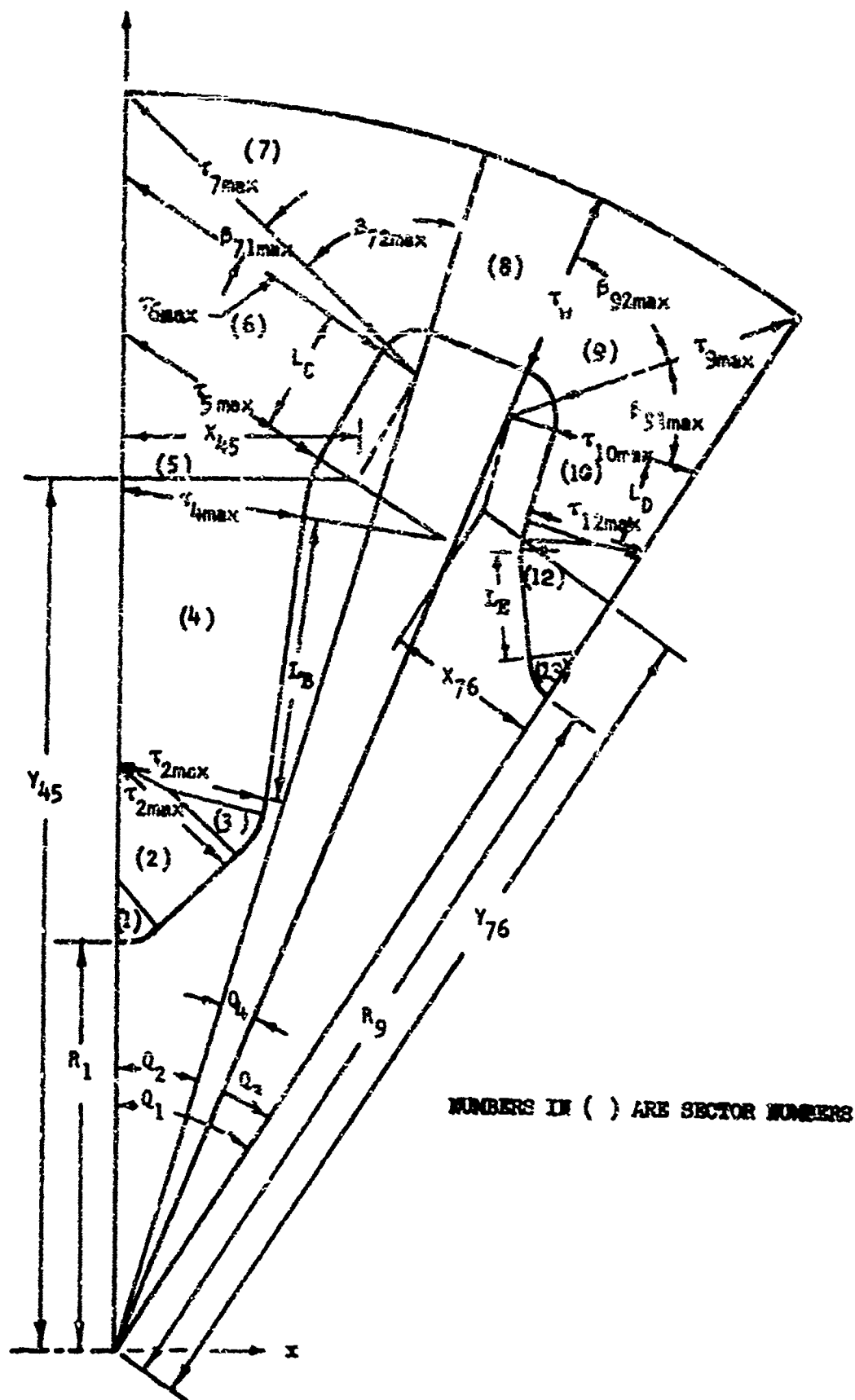


Figure 5.2 One-Half Fork of General Modified Wagon Wheel Configuration



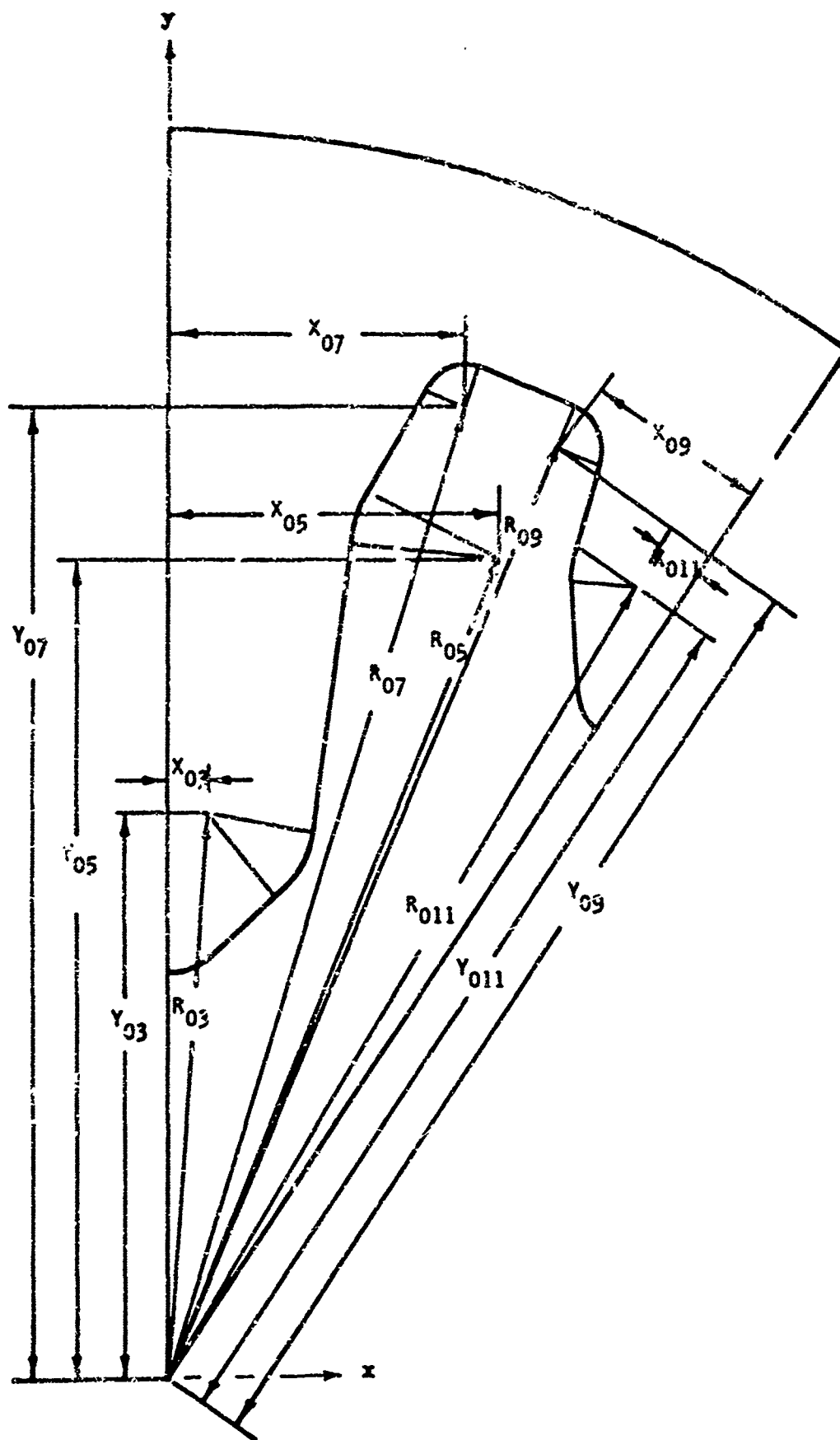


Figure 5.4 Part of Calculated Constants for One-Half Fork of General Modified Wagon Wheel Configuration Produced by FLNCNS Subroutine

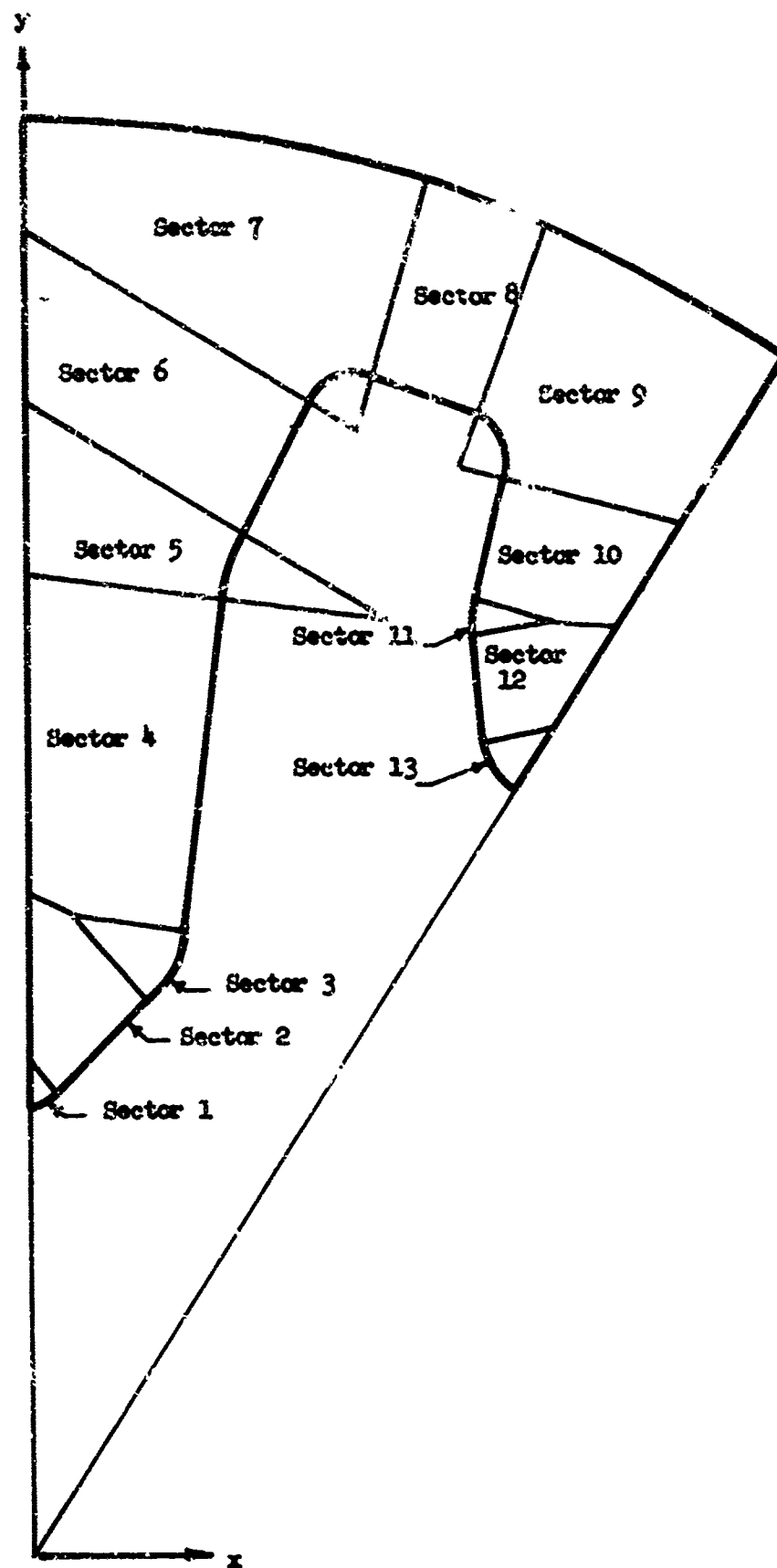


Figure 5.5 Sector Definition

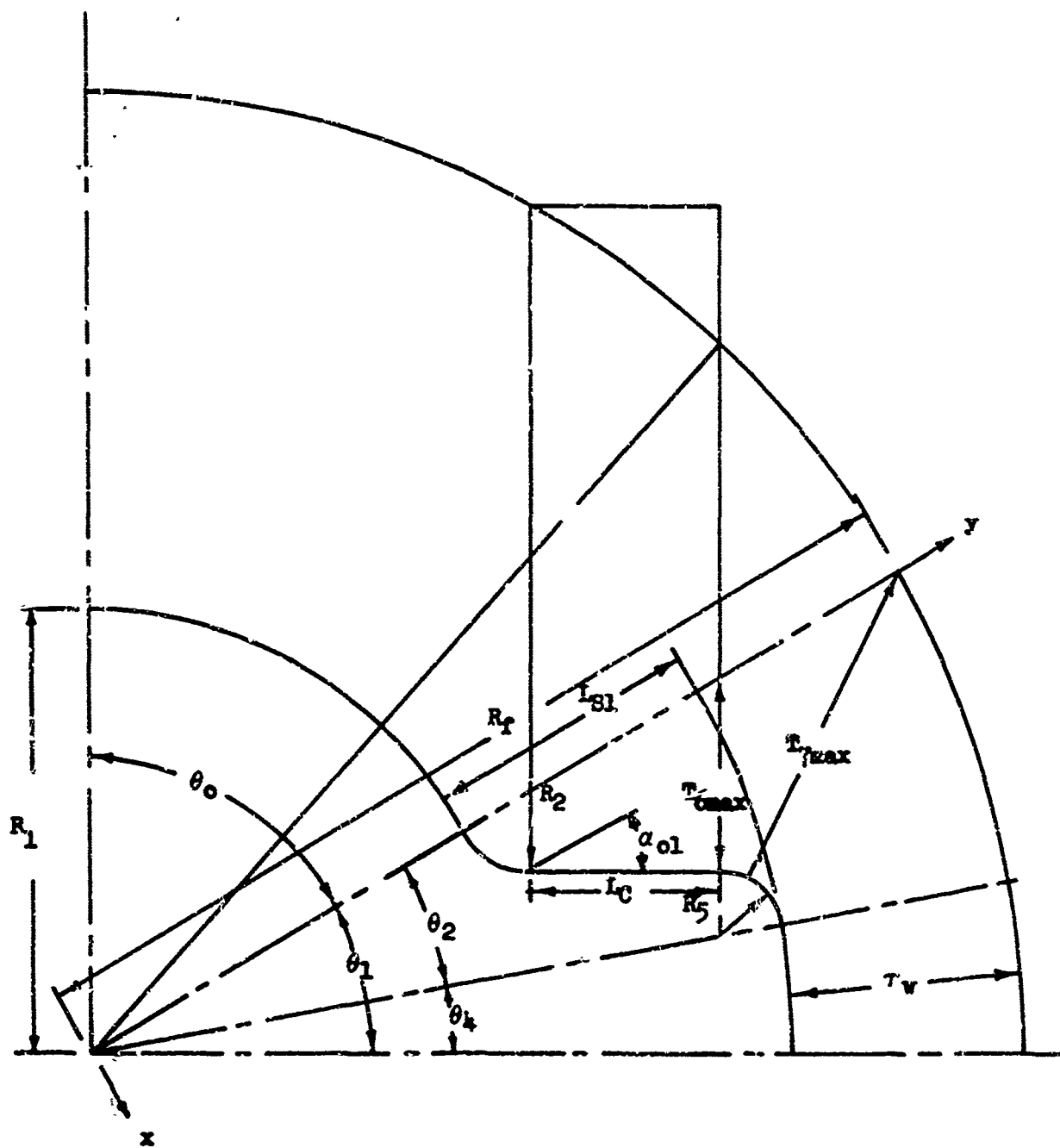
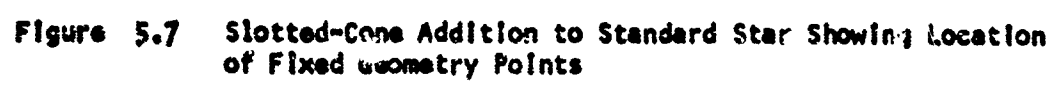
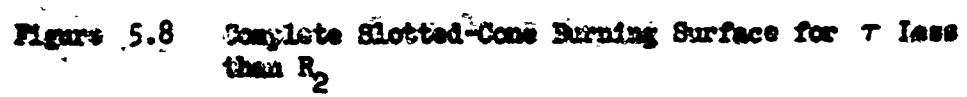
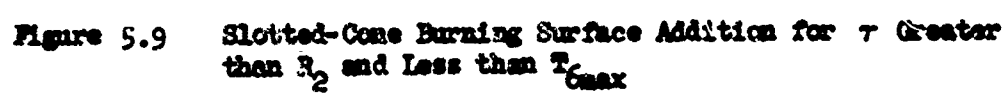
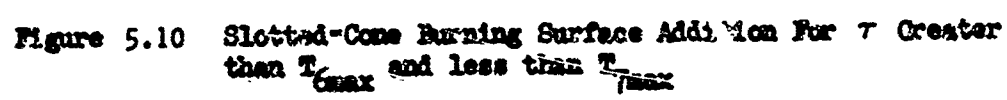


Figure 5.6 Slotted-Cone









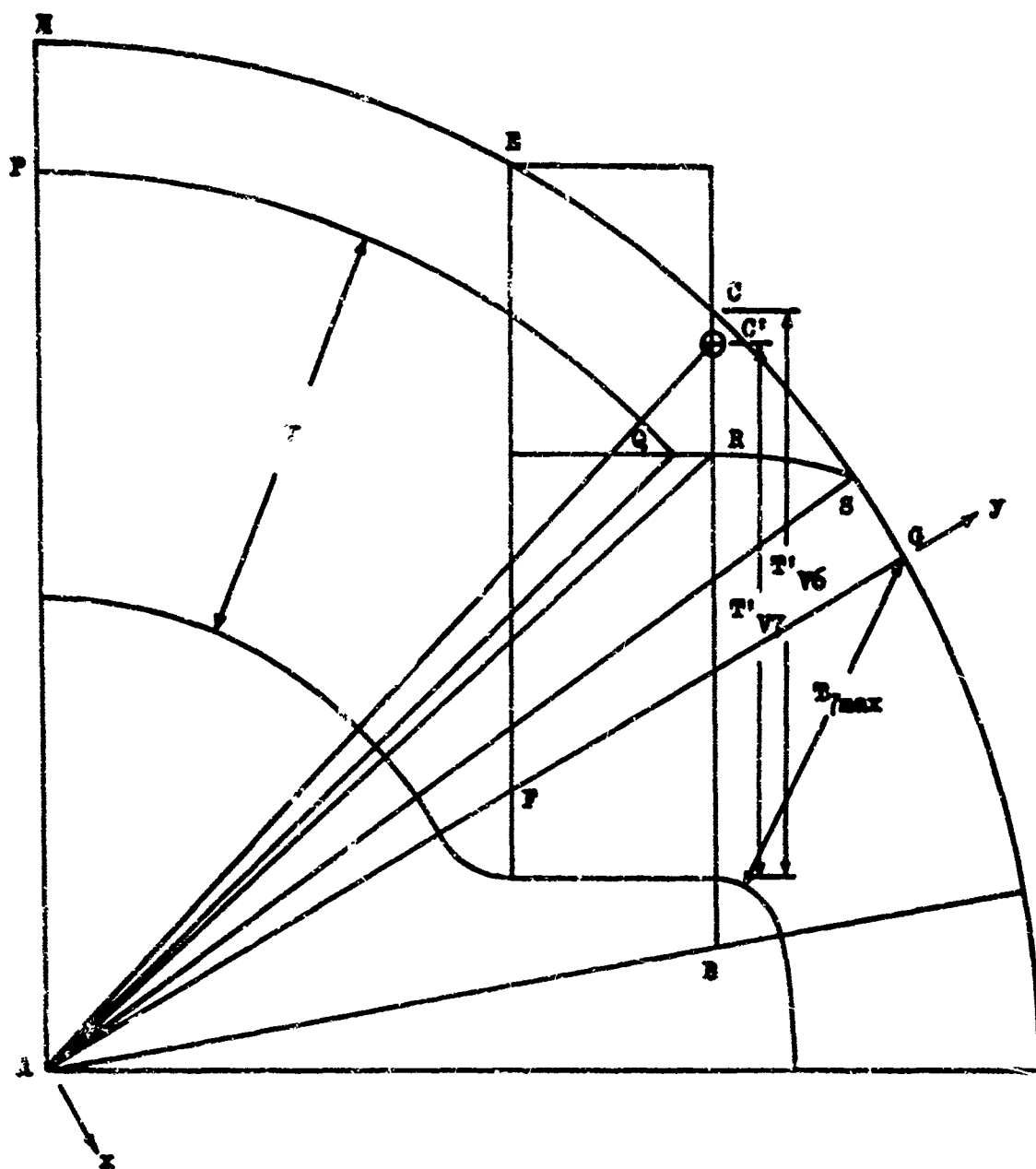


Figure 5.11 Slotted-Cone Burning Surface Addition for r Greater than r_{max} and Less than r_{v1} , with r_{v1} less than r_{v2}

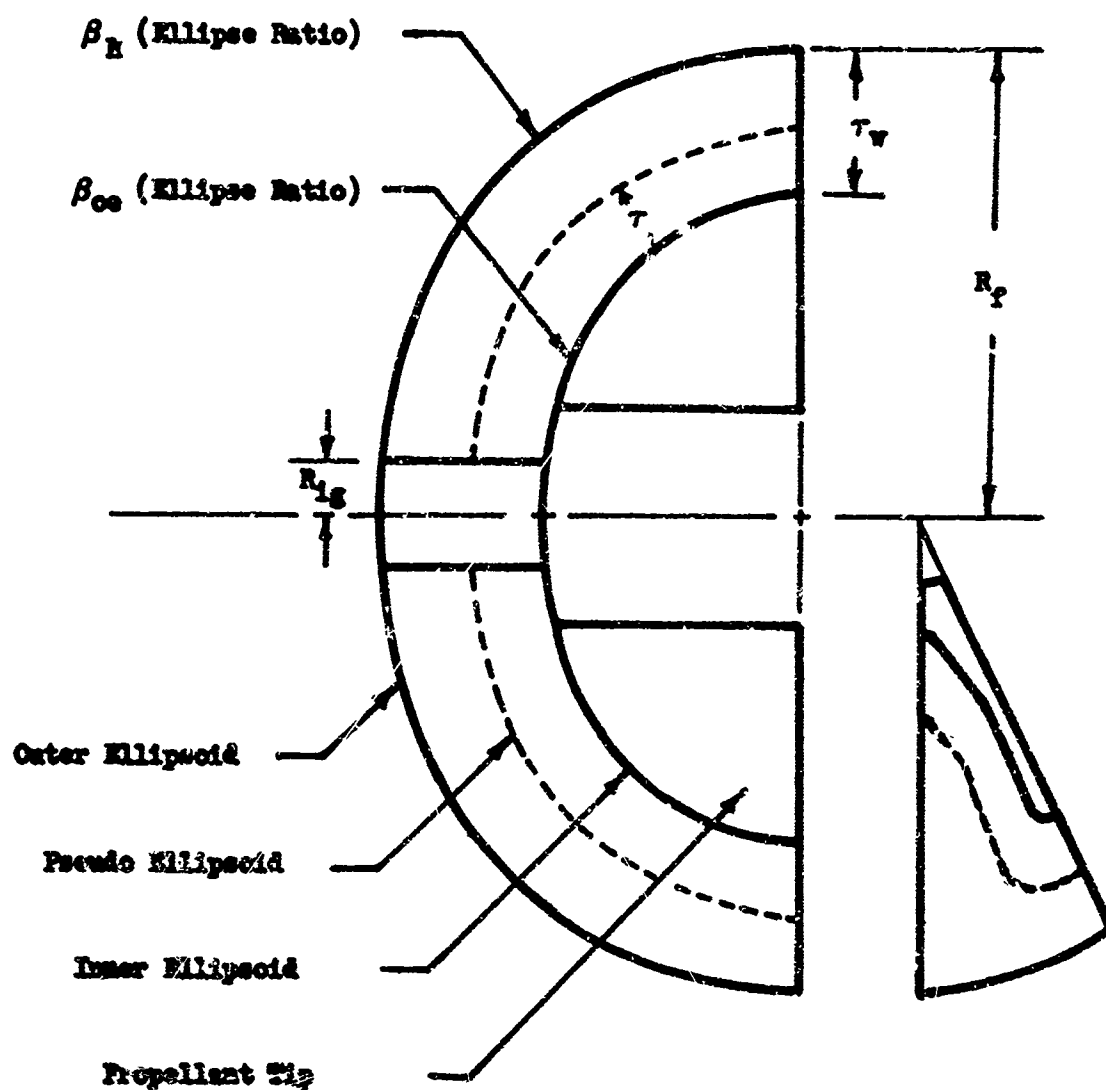


Figure 5.14 Head-End with Web, Motor Fore-Head

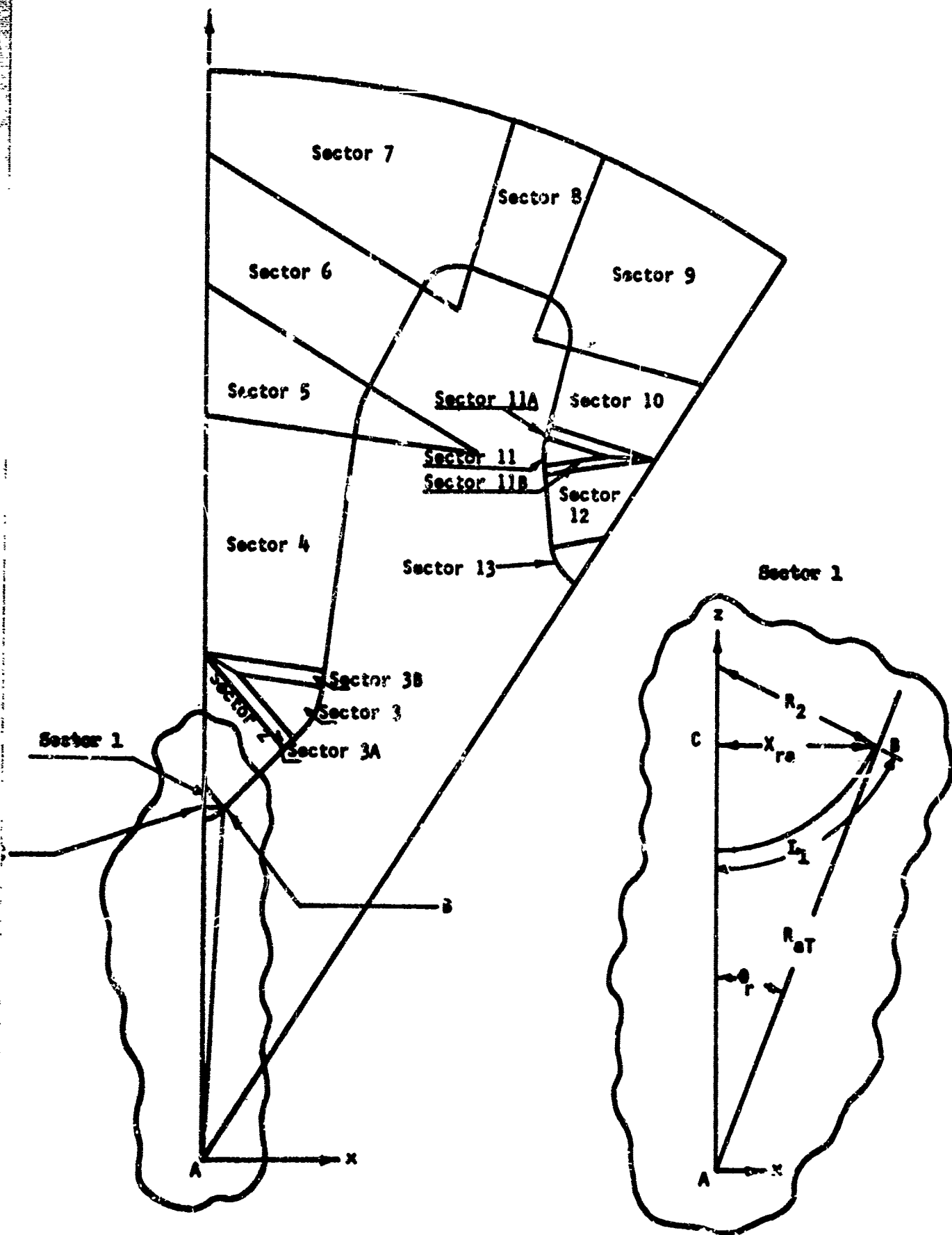


Figure 5.15 Sectors for Block No. 1

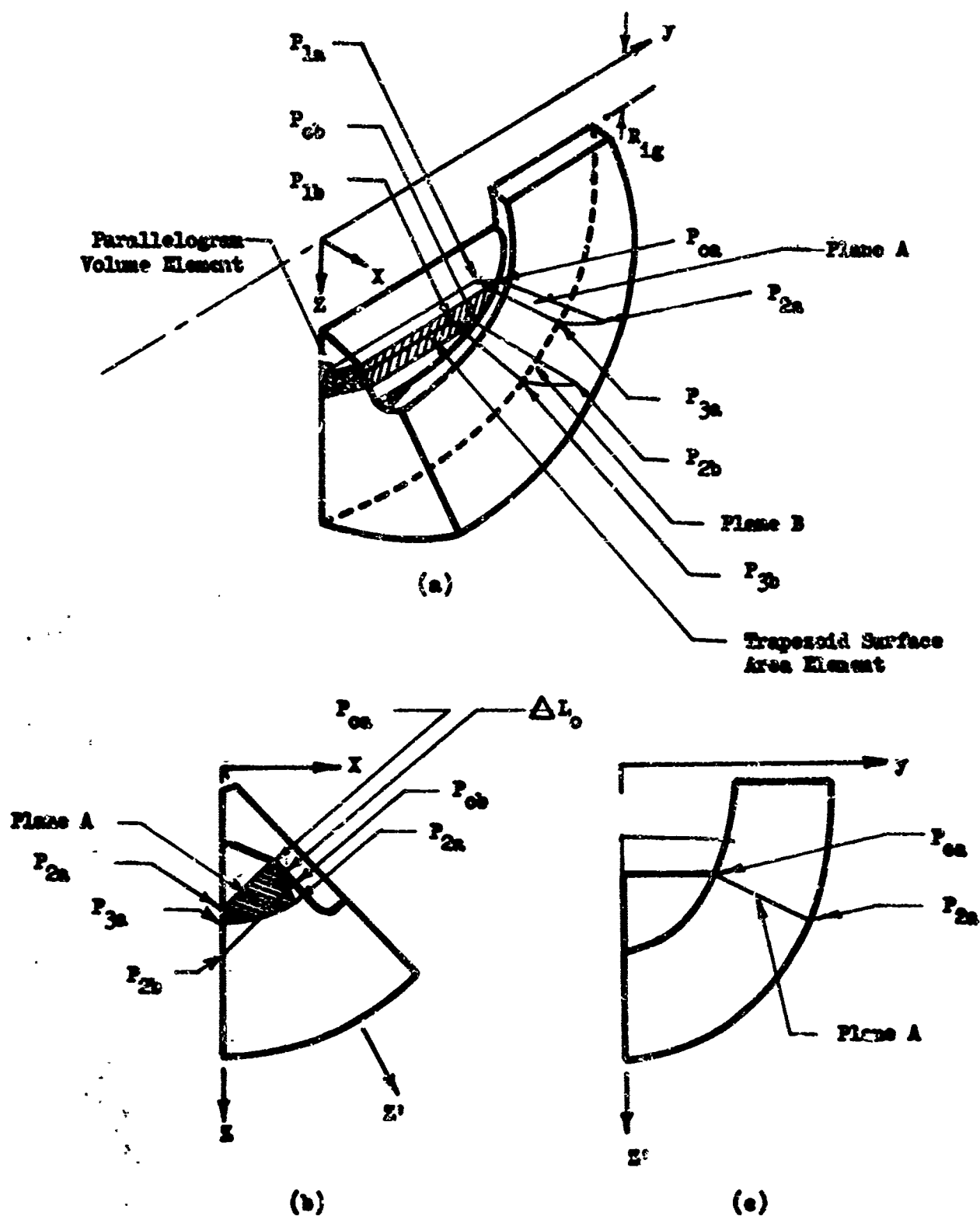


Figure 5.16 Head-End with Web Plane Definition

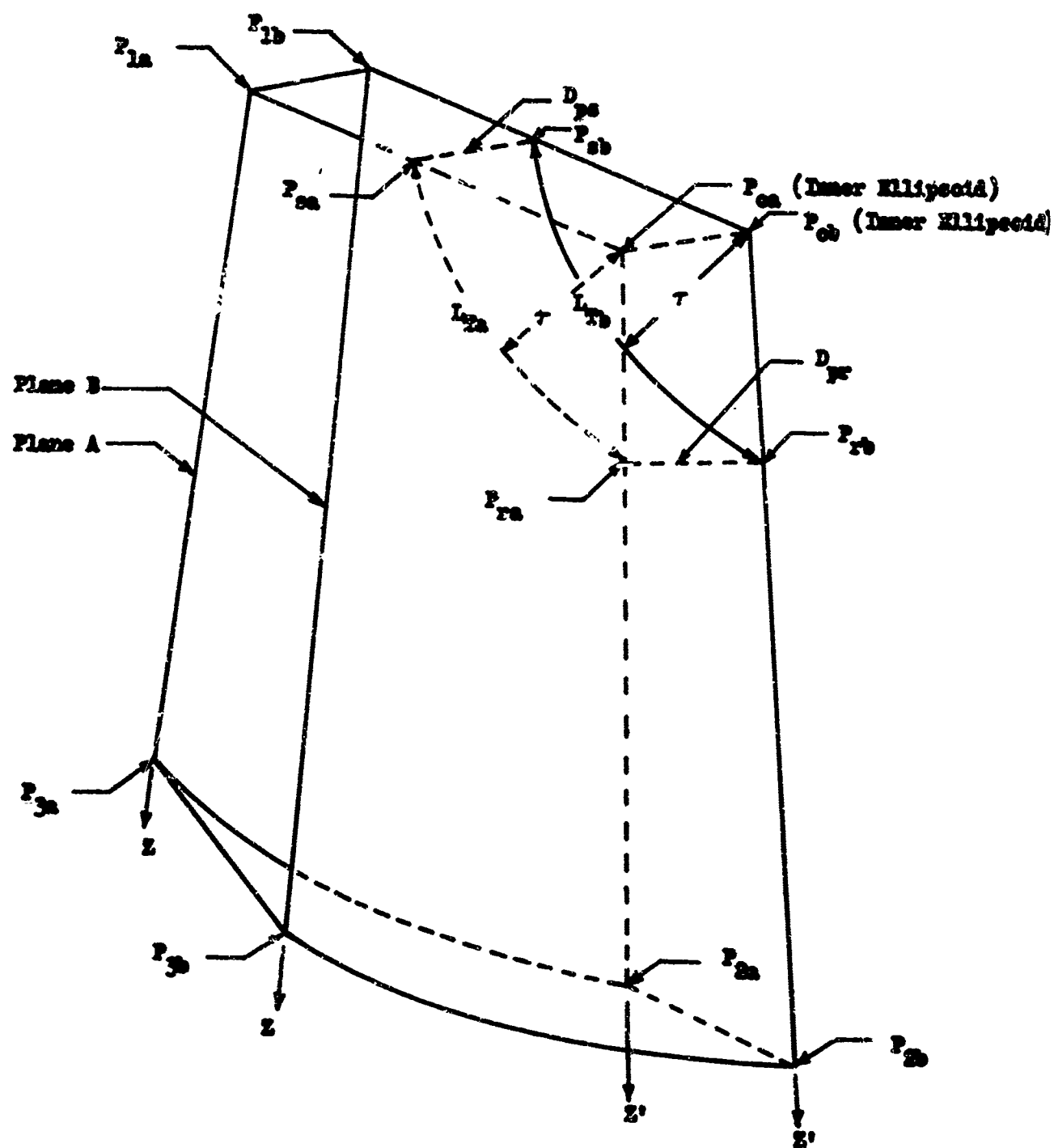


Figure 5.17 Head-Neck with Web, Block 1 Plane Definition

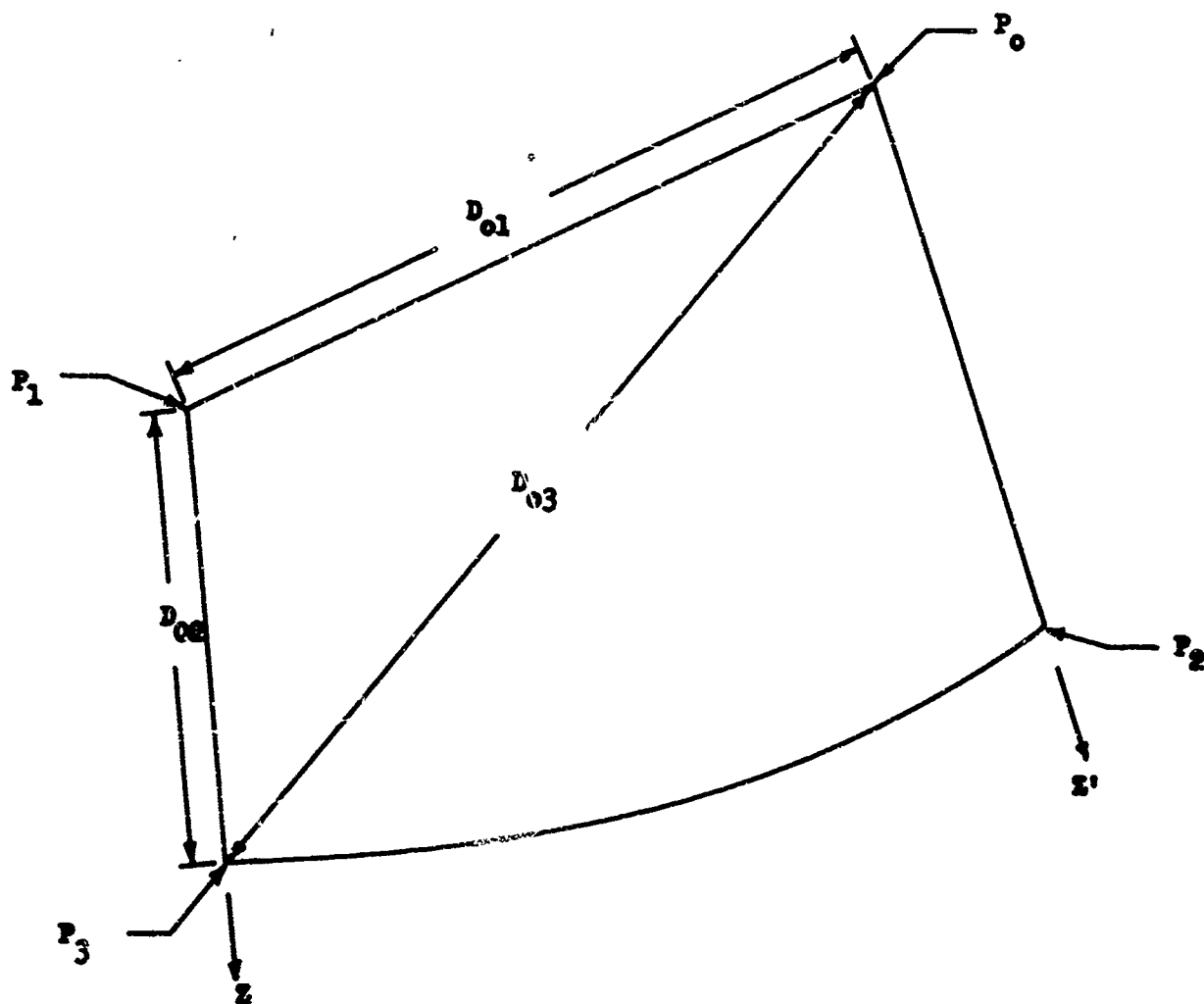


Figure 5.18 Plane for Block 1 Analysis

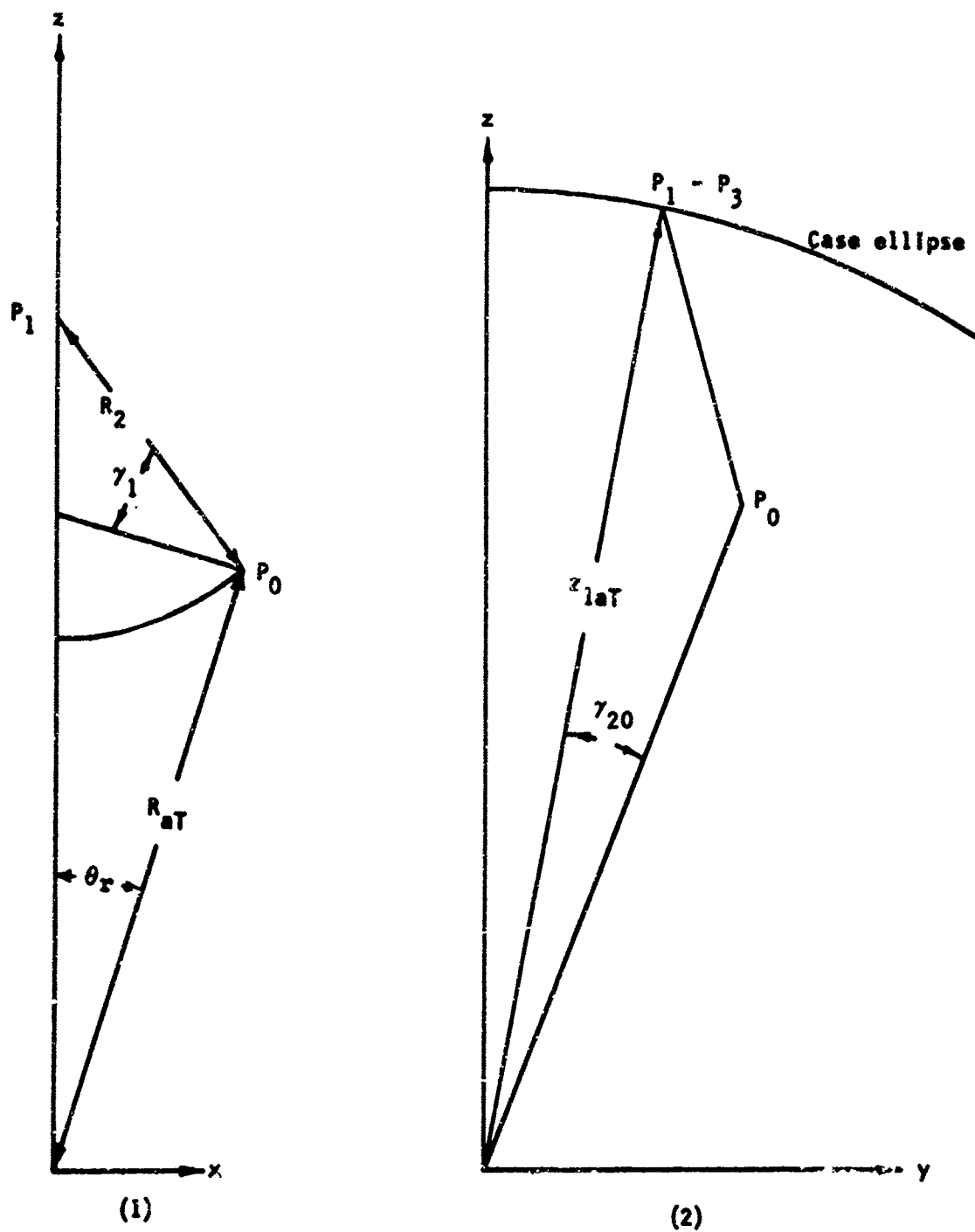


Figure 5.19 γ_1 for Subroutine GAMSUB

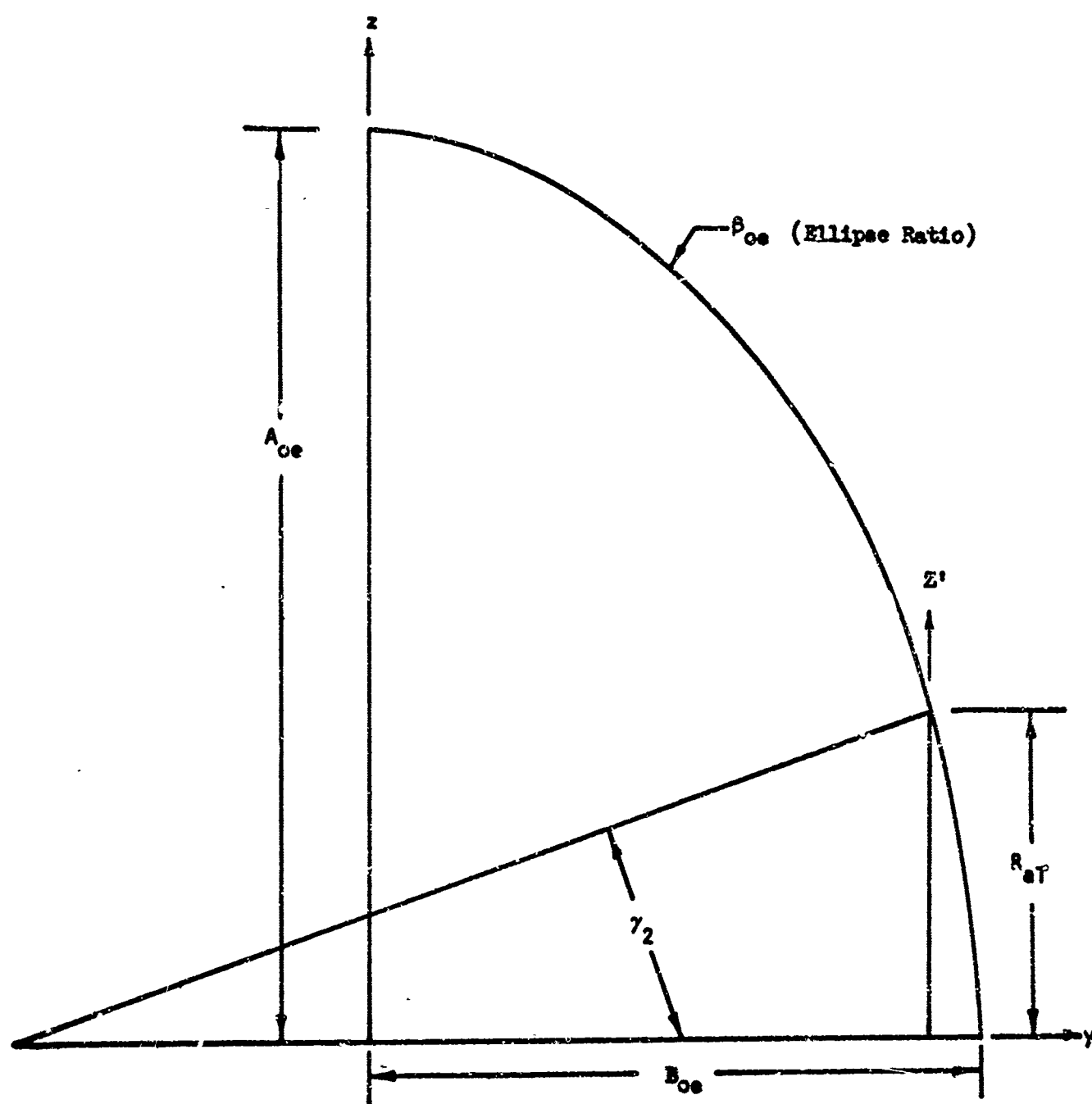


Figure 5.20 γ_2 for Subroutine GAM2S

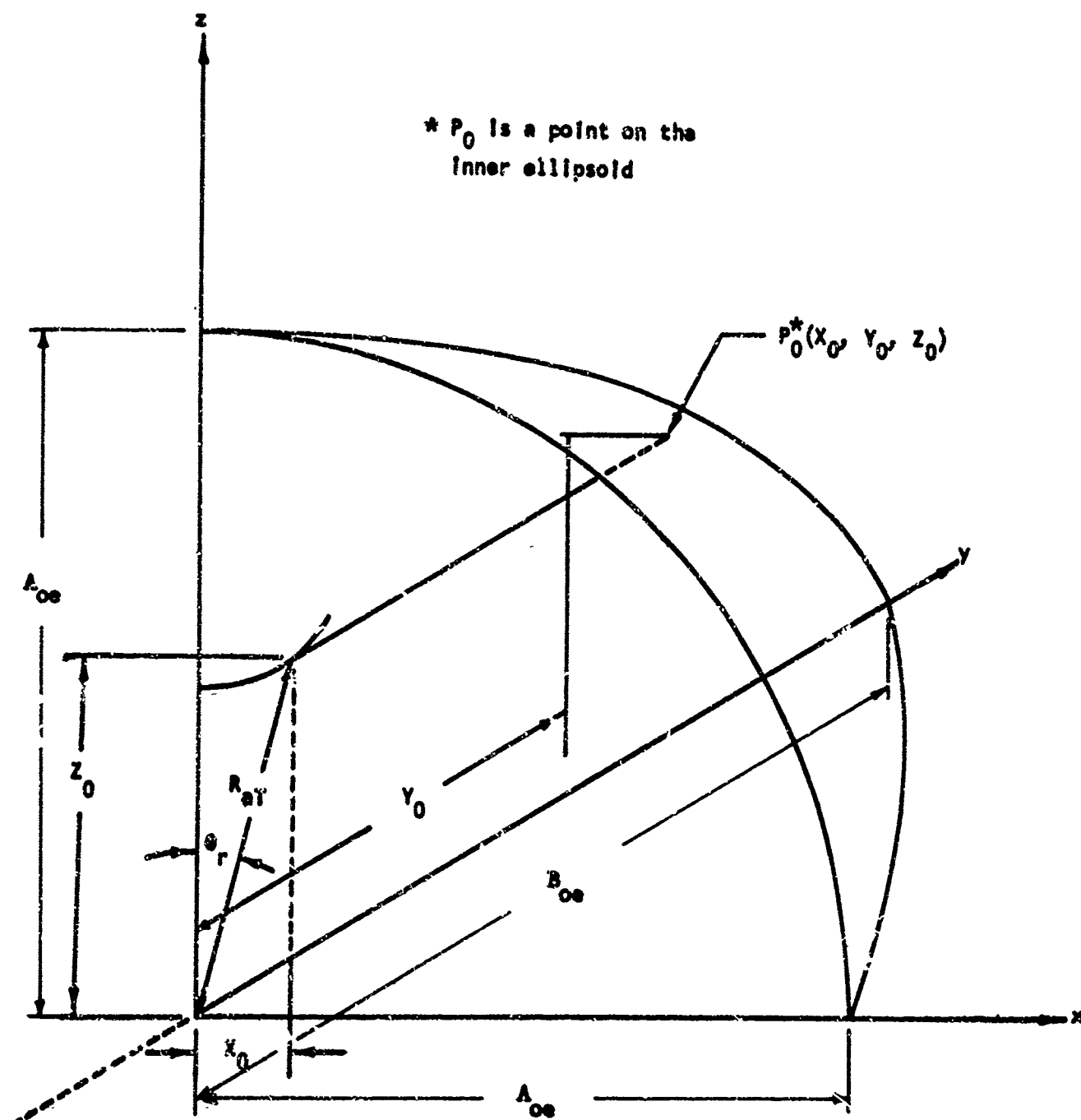


Figure 5.21 P_0 for Subroutine POSUB

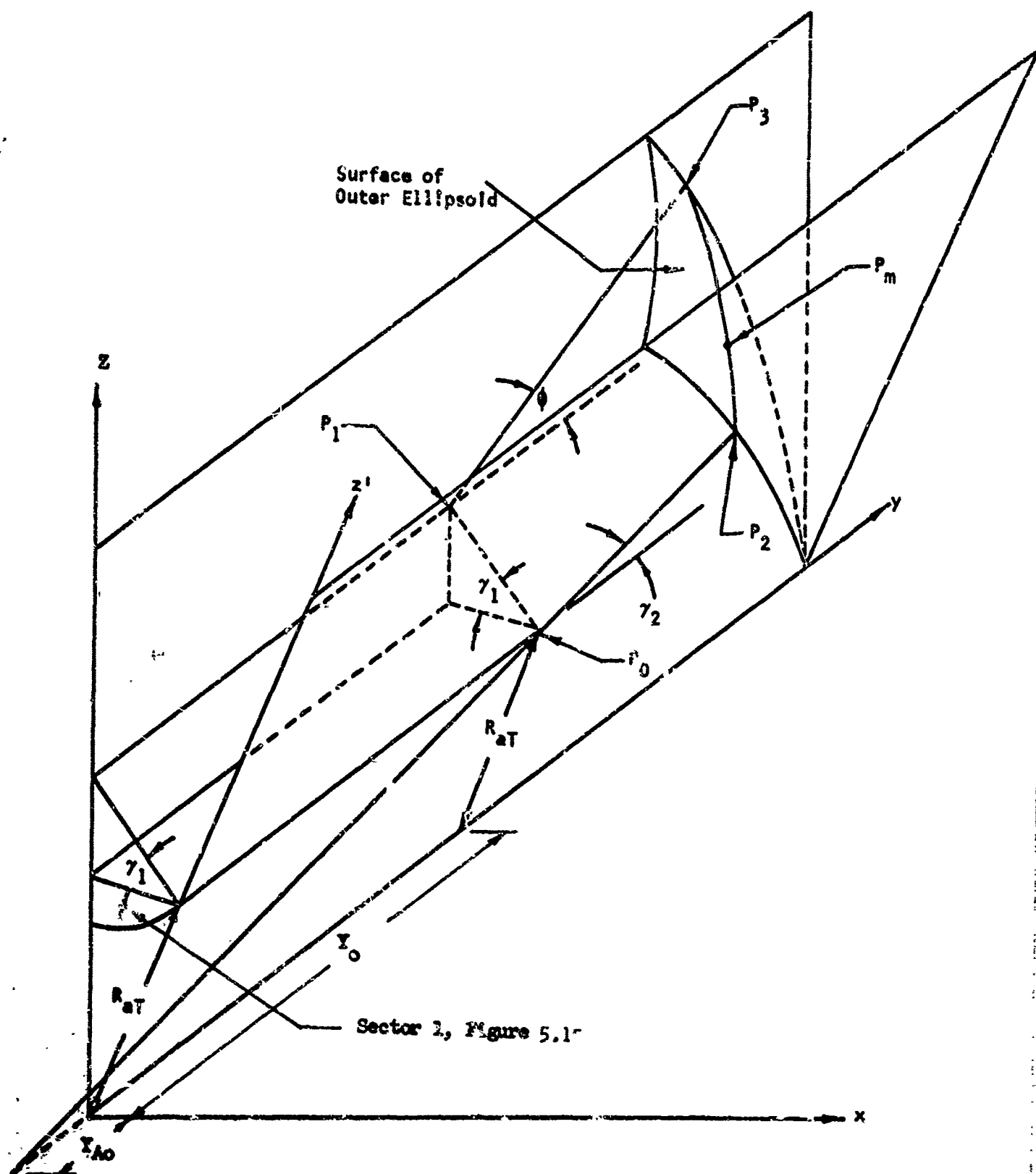


Figure 5.22 P_3 for Subroutine P3SUB

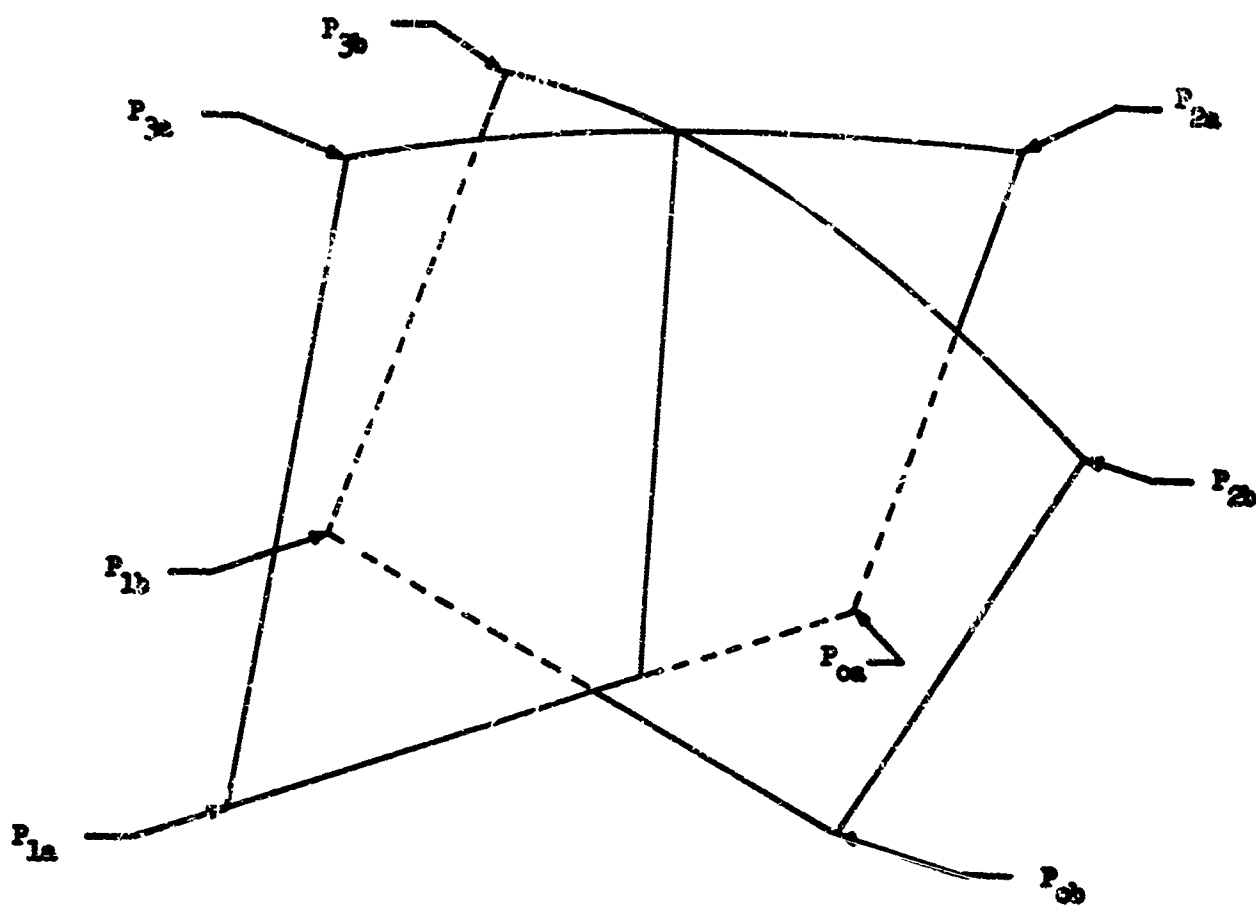


Figure 5.23 Planes for Block i Analysis

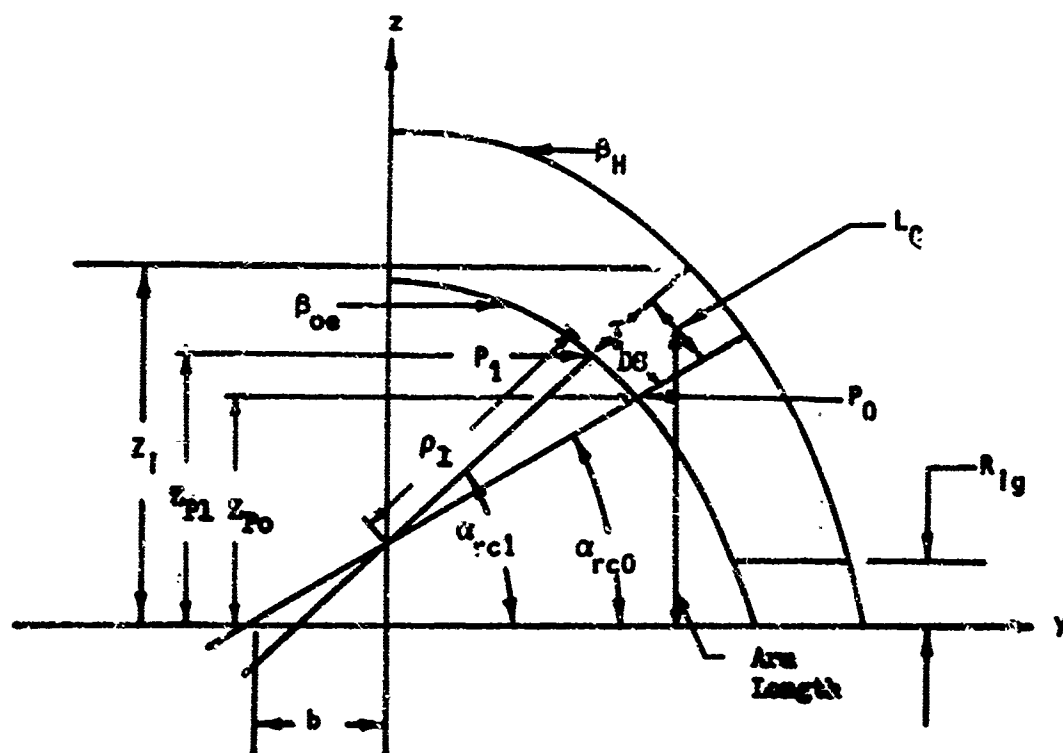
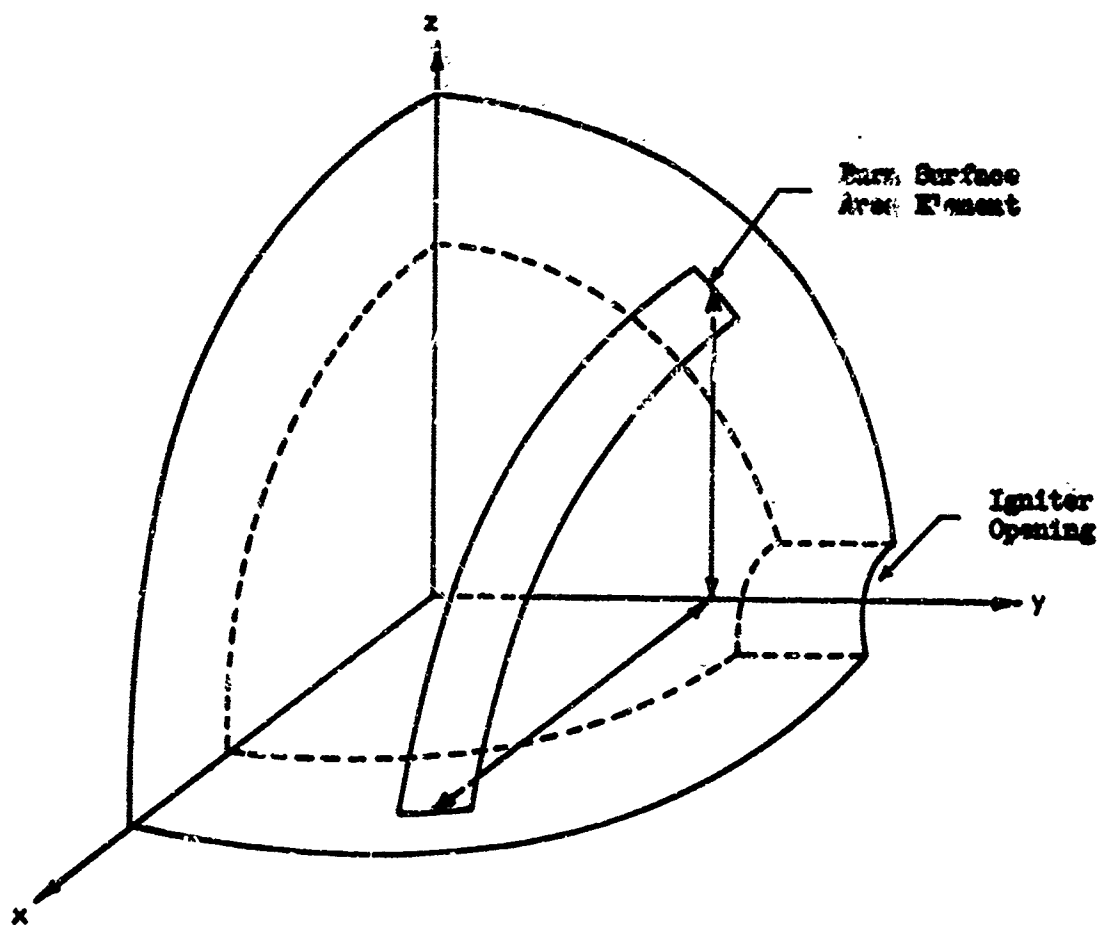


Figure 5.25 Area for Block No. 2A and 2B

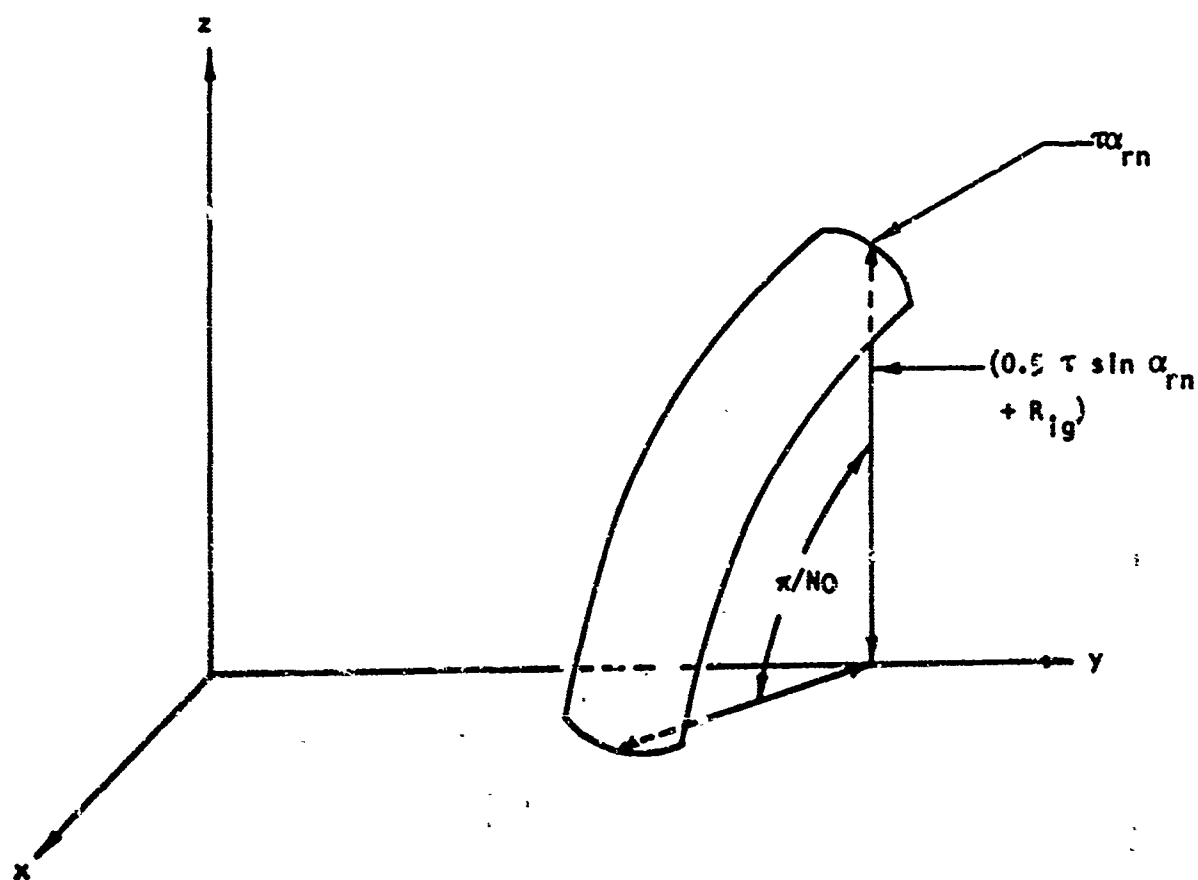
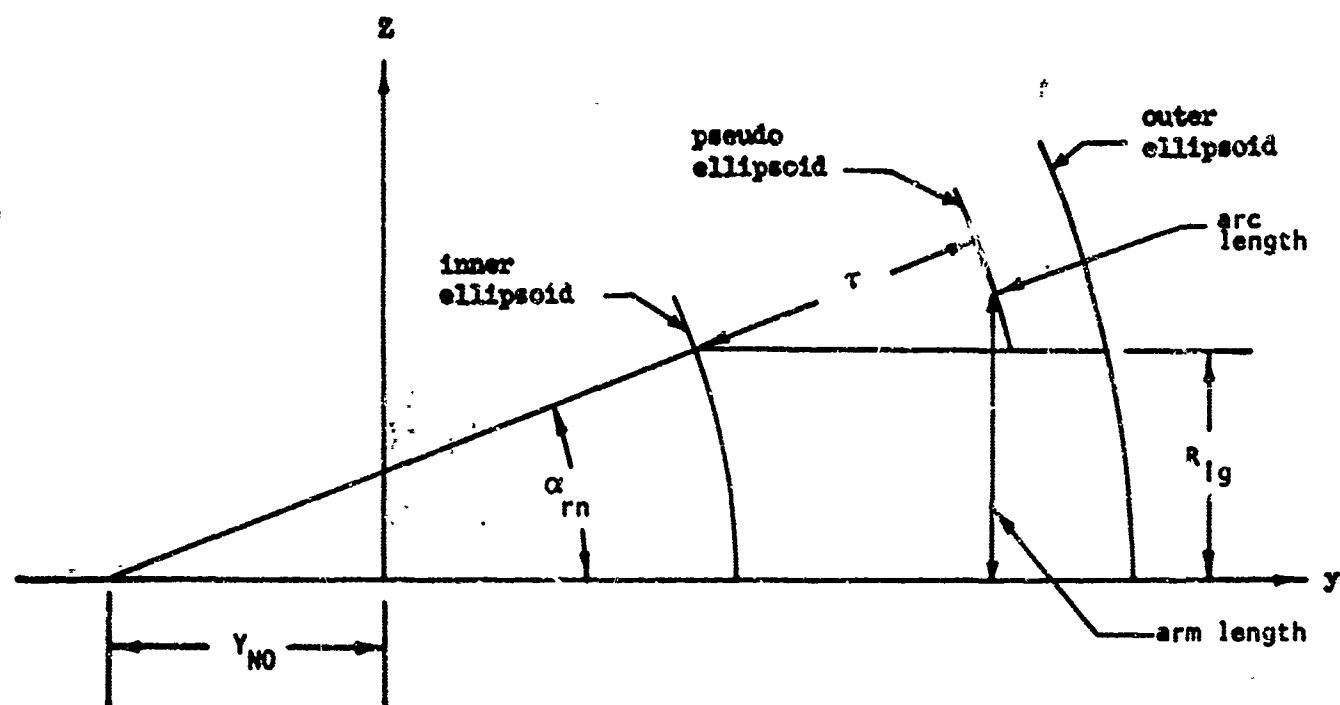


Figure 5.26 A_{1g} for Subroutine AIGSUB

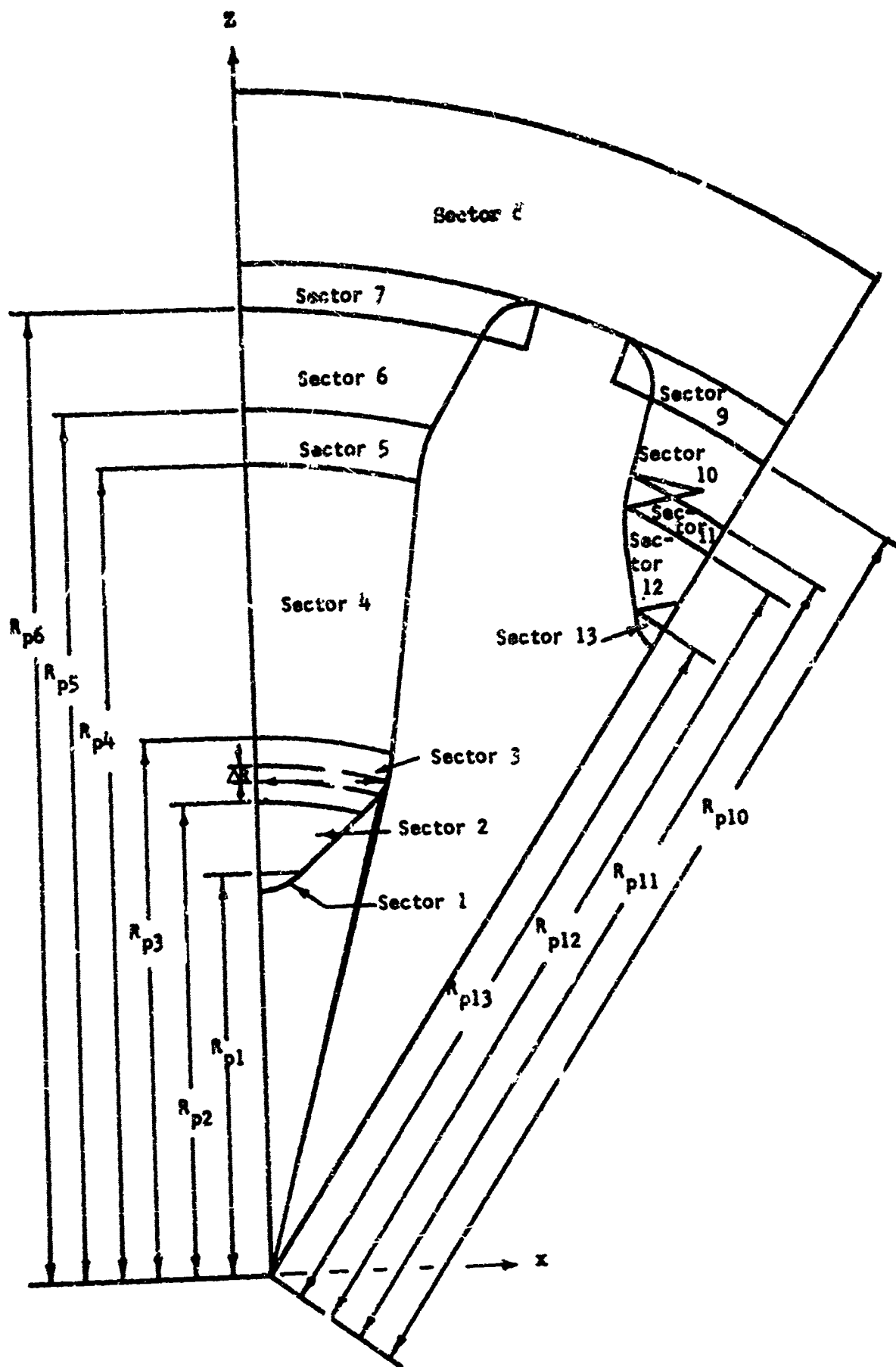


Figure 5.27 Sectors for Block 28 of Pre-Head Section

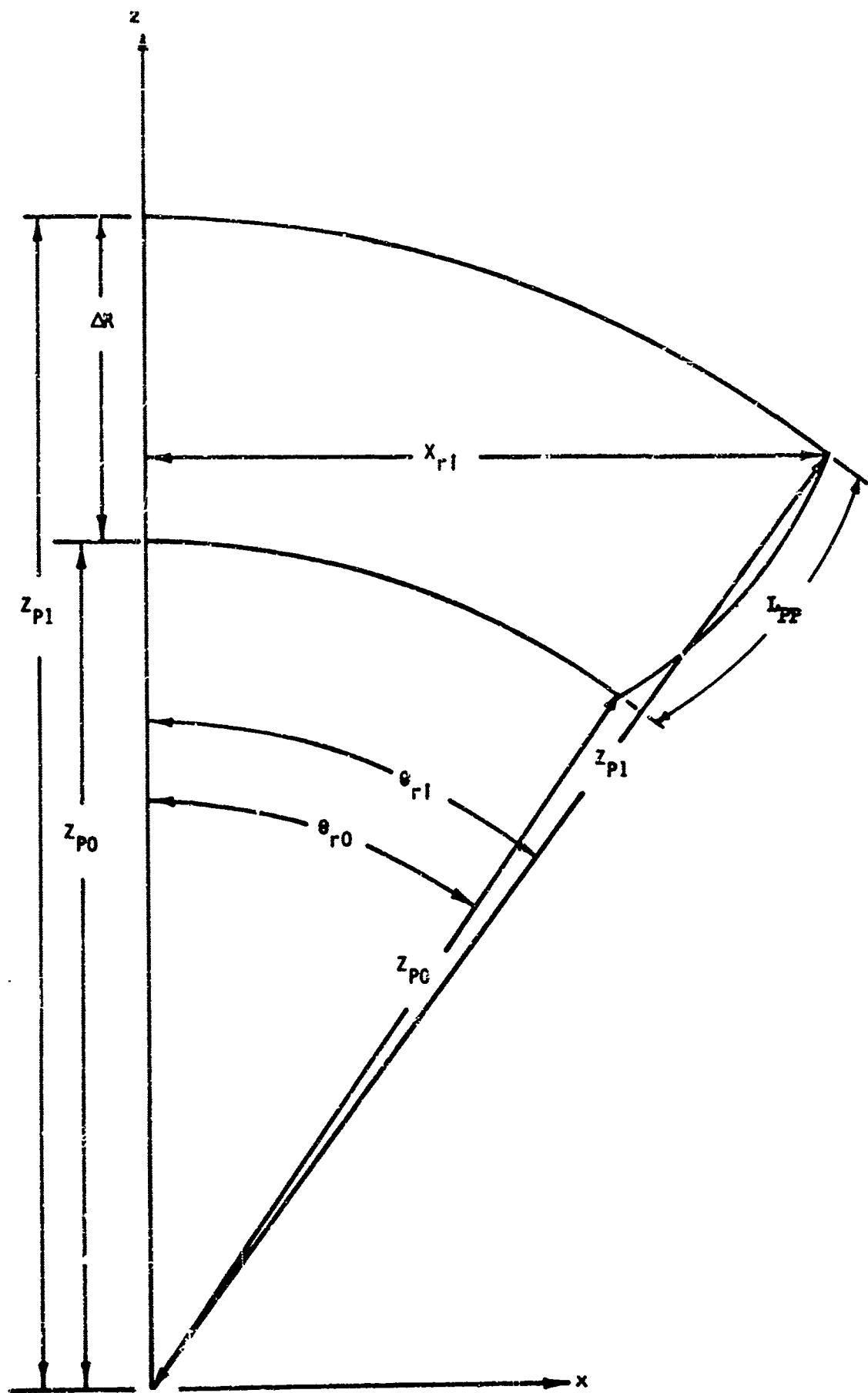


Figure 5.28 Sector for Block 2B

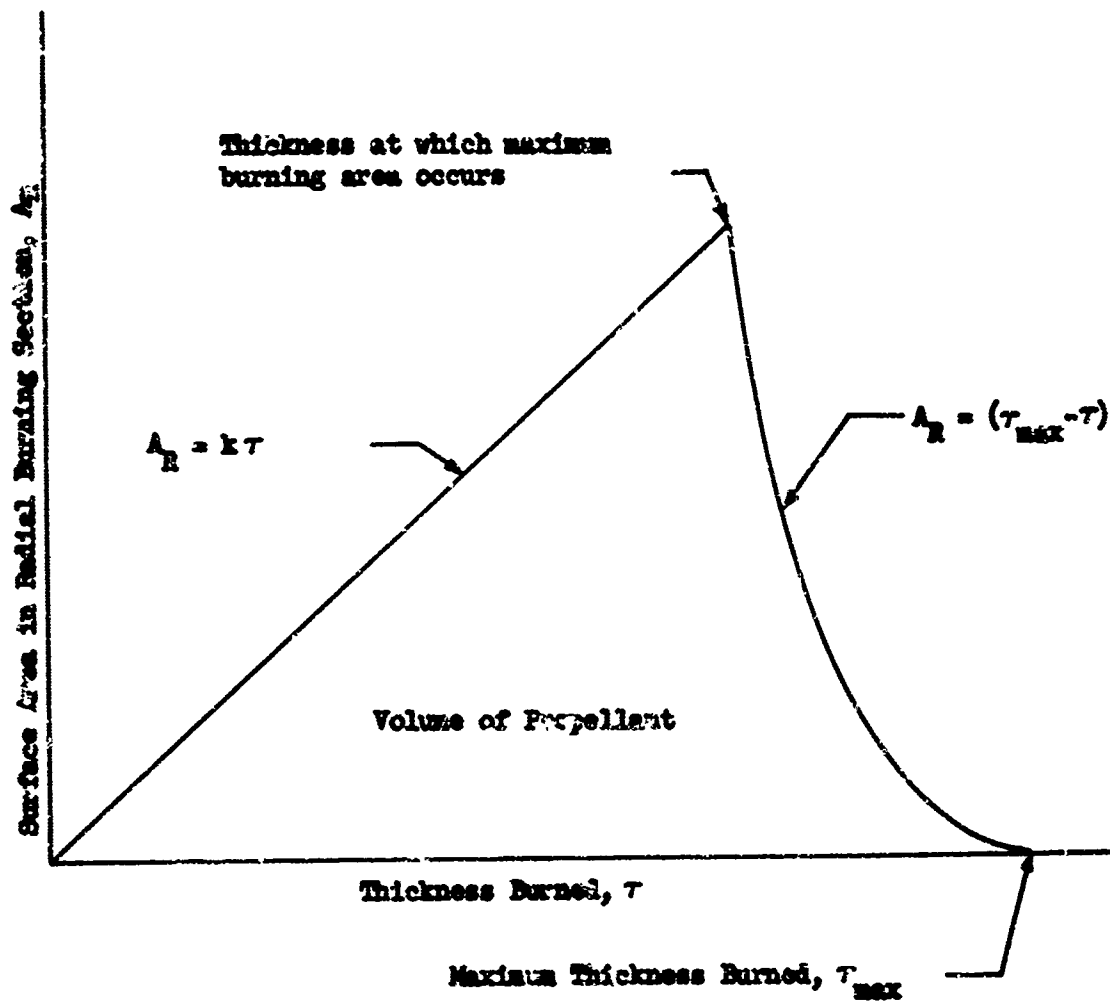


Figure 5.29 Distribution of Volume in Radial Burning Section

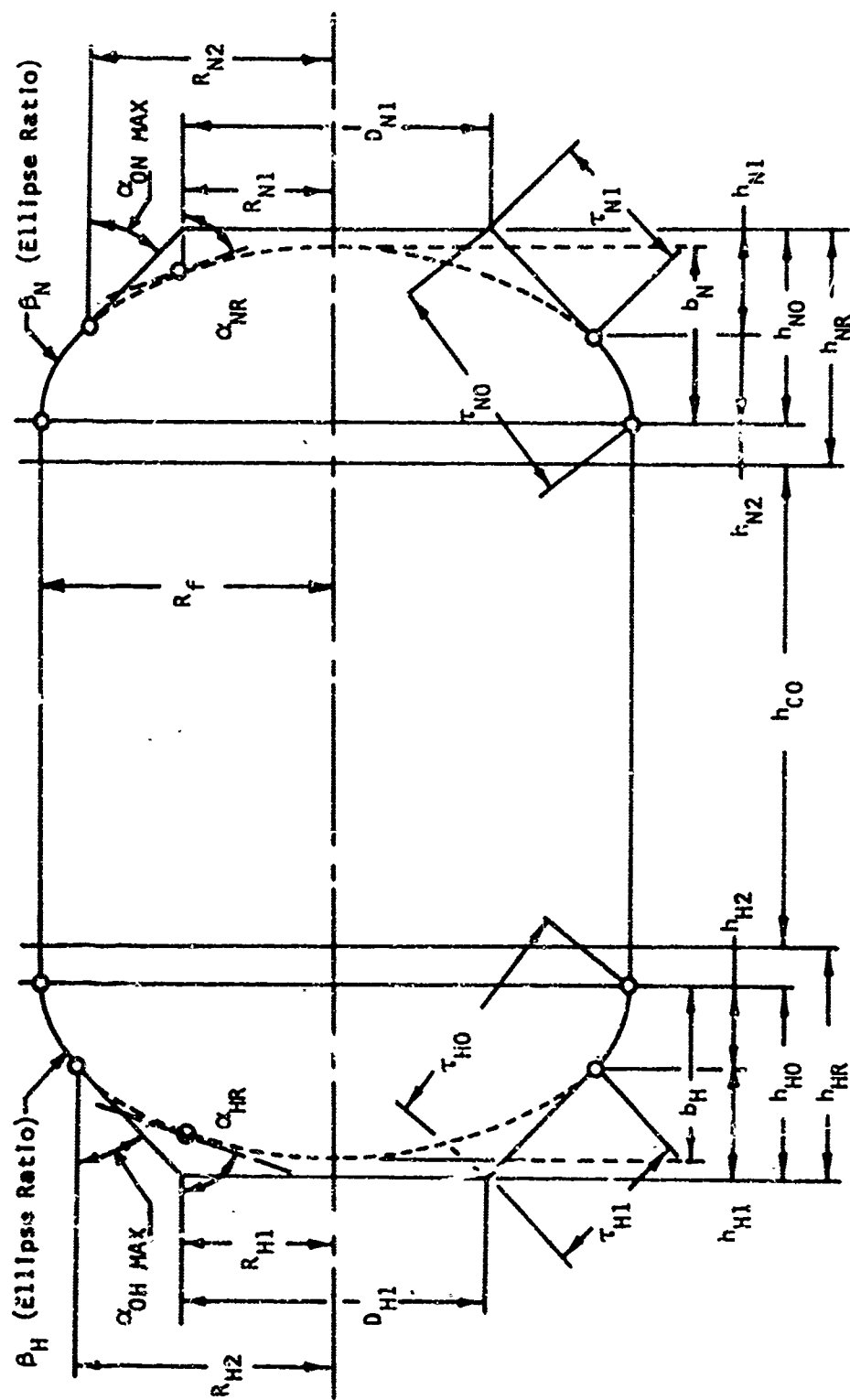


Figure 5.30 Motor Case Longitudinal Constants

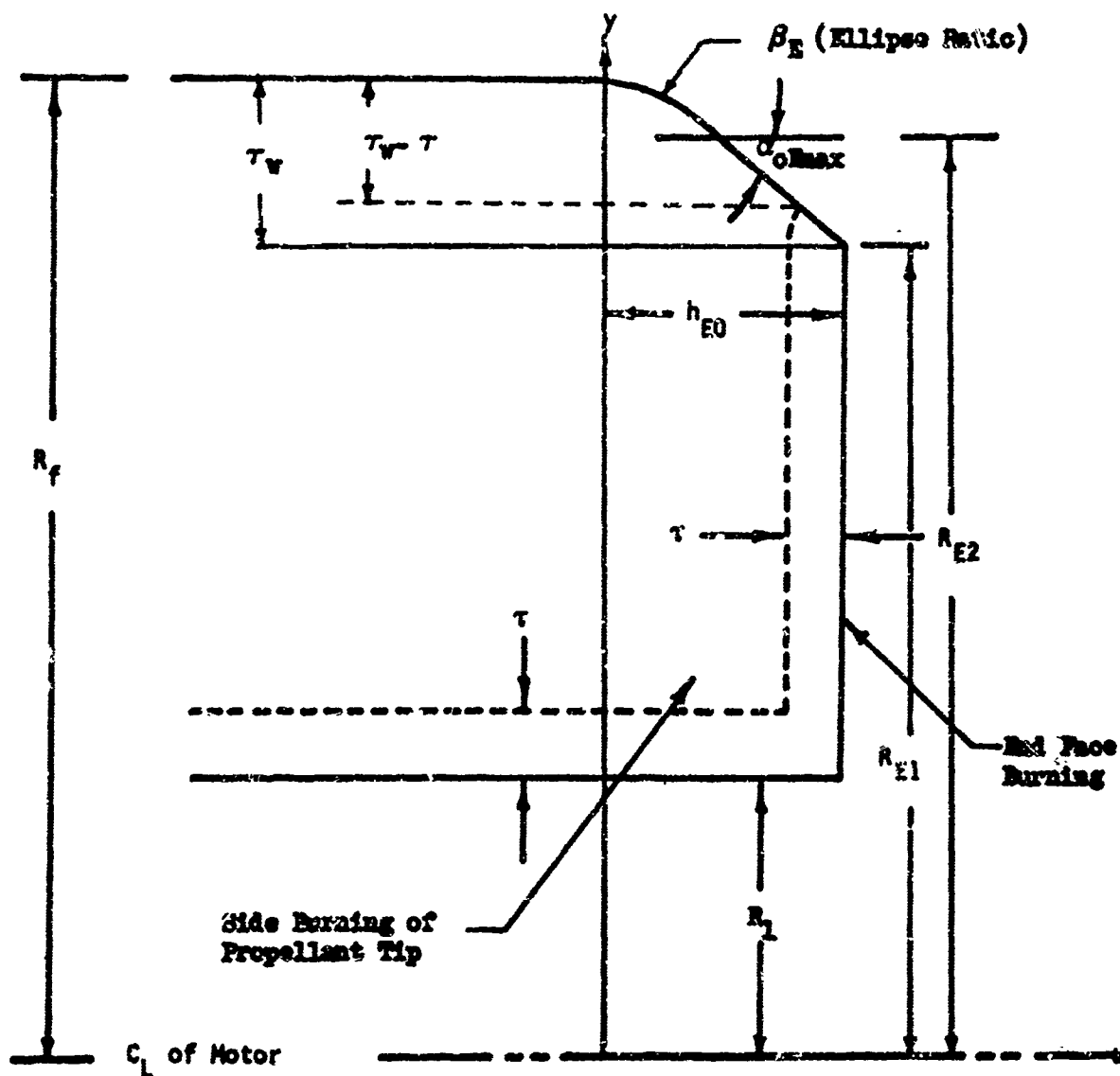


Figure 5.31 Straight Through Grain Configuration

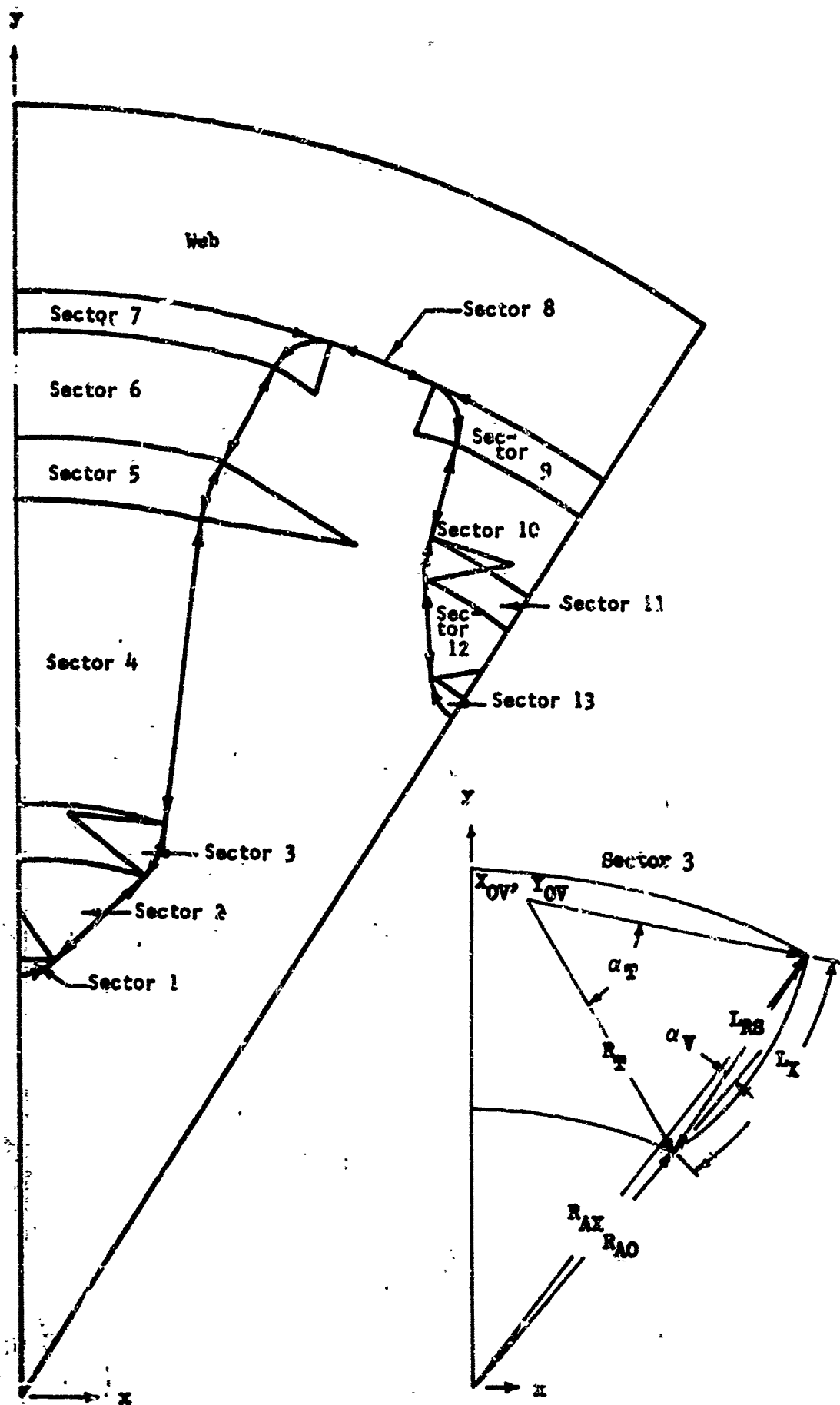


Figure 5.32 Sector Definition

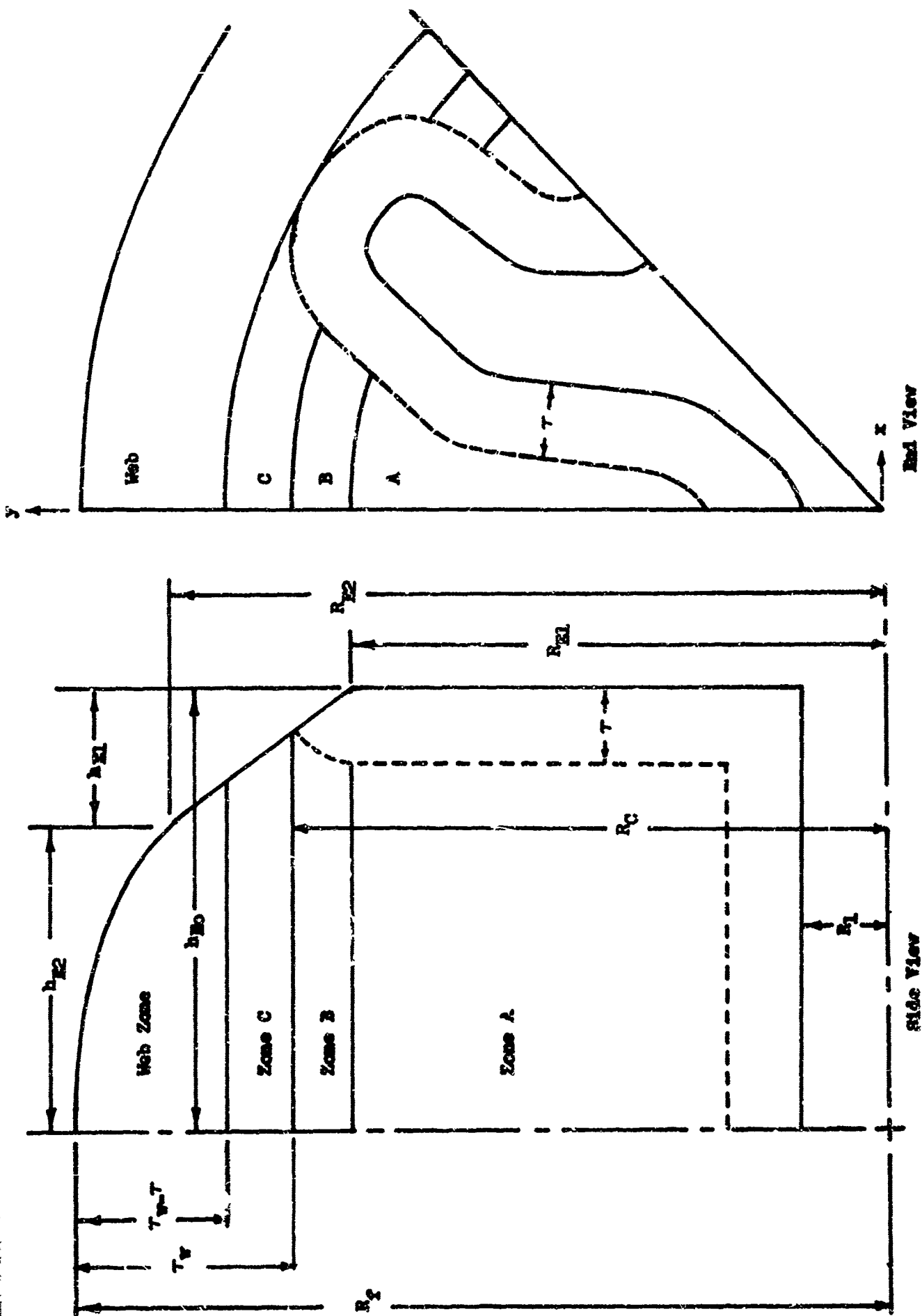
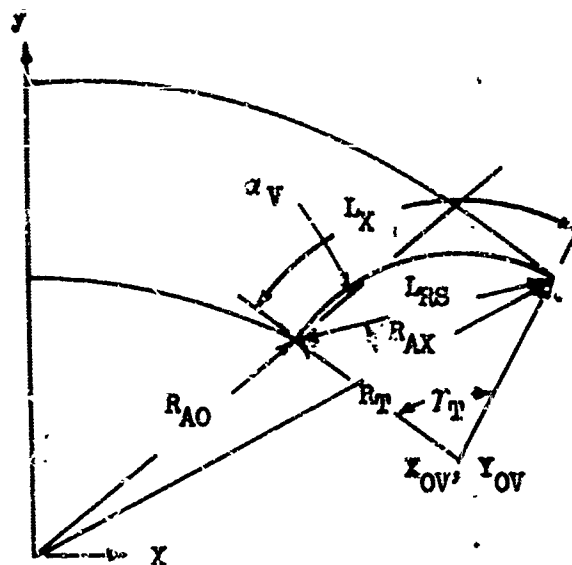
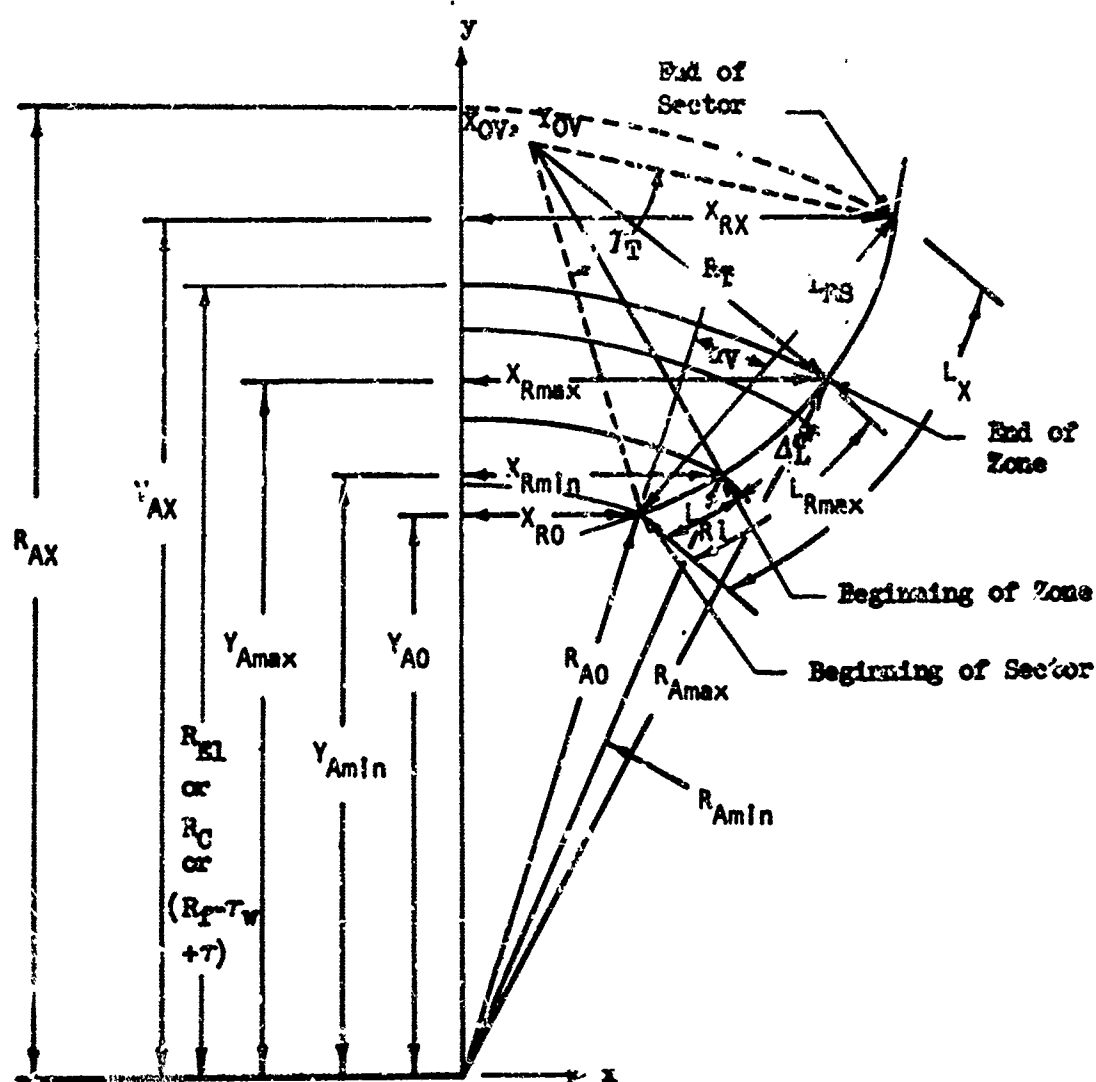


Figure 5.33 Zone Definition



Sectors 5, 7, 9



Sectors 1, 3, 11, 13

Figure 5.34 Sector Parameters, Zones B, C, and web

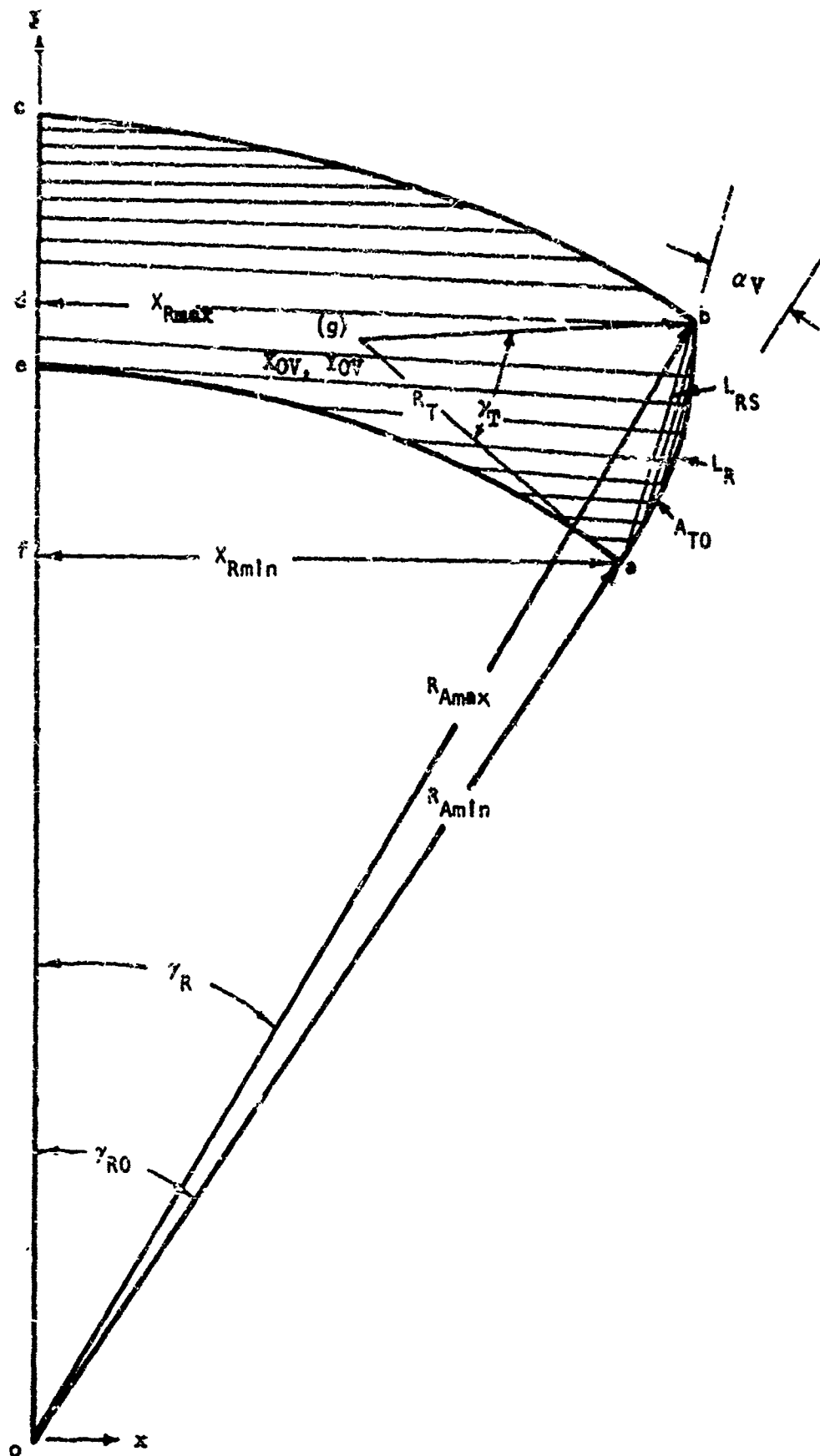


Figure 5.35 Circular Arc Sector 3 Zone A

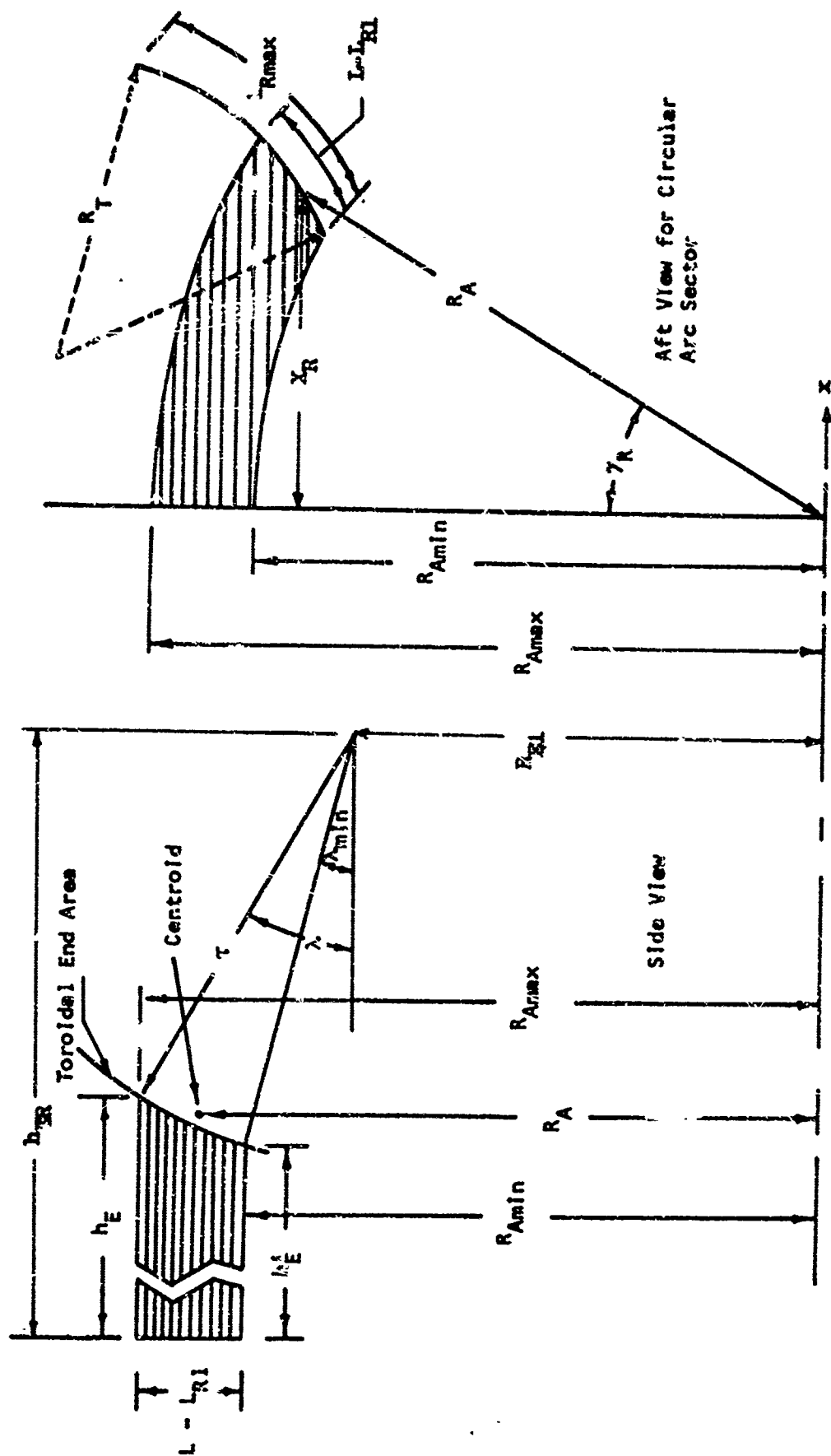


Figure 5.36 Element of Incremental Area for Zone B

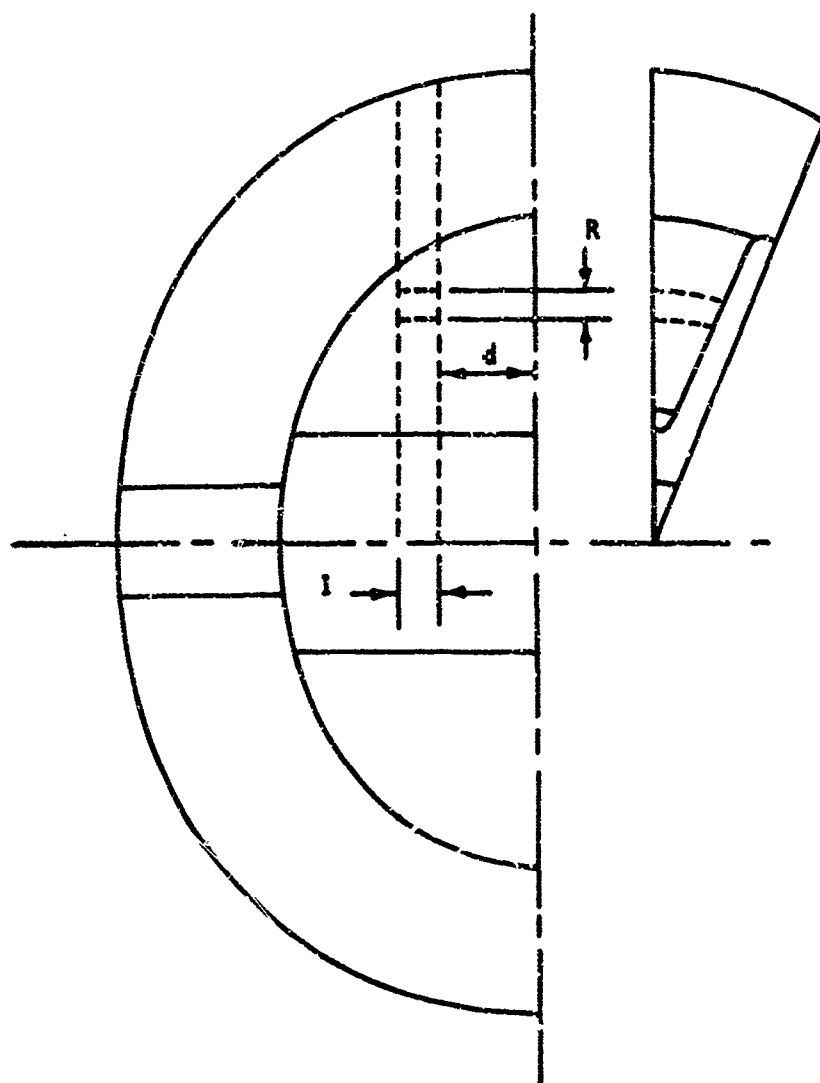


Figure 5.57 Head-End Section Elemental Volumes for MOI and CG Calculations

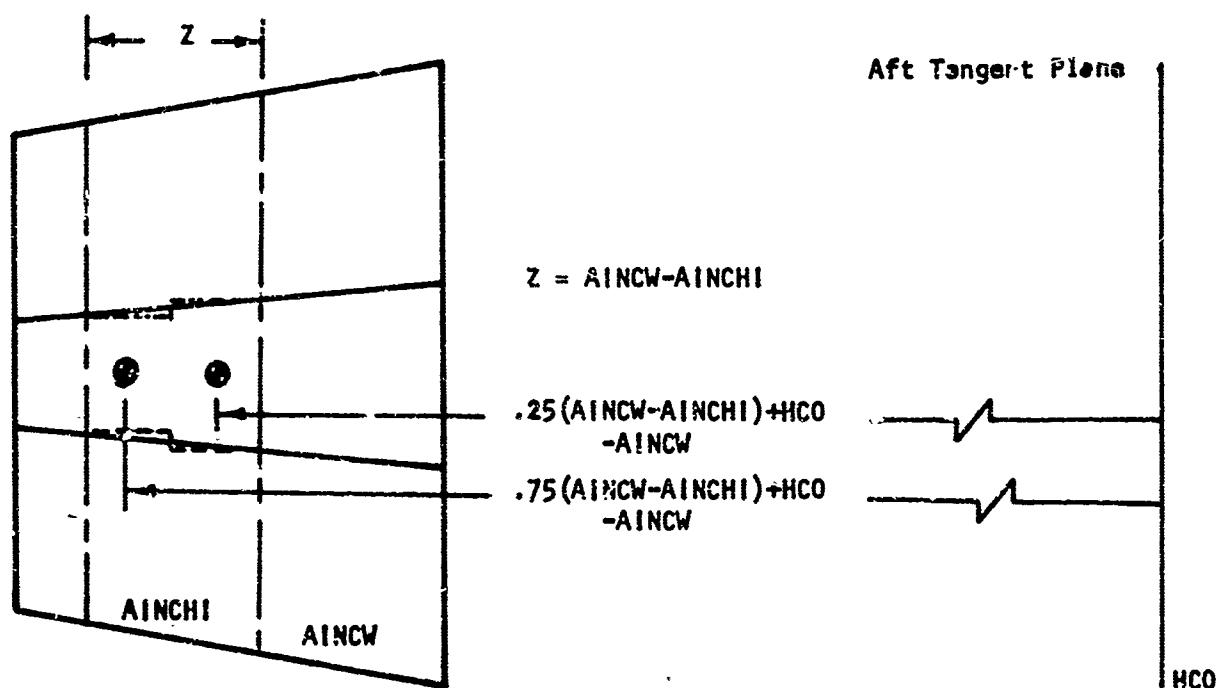
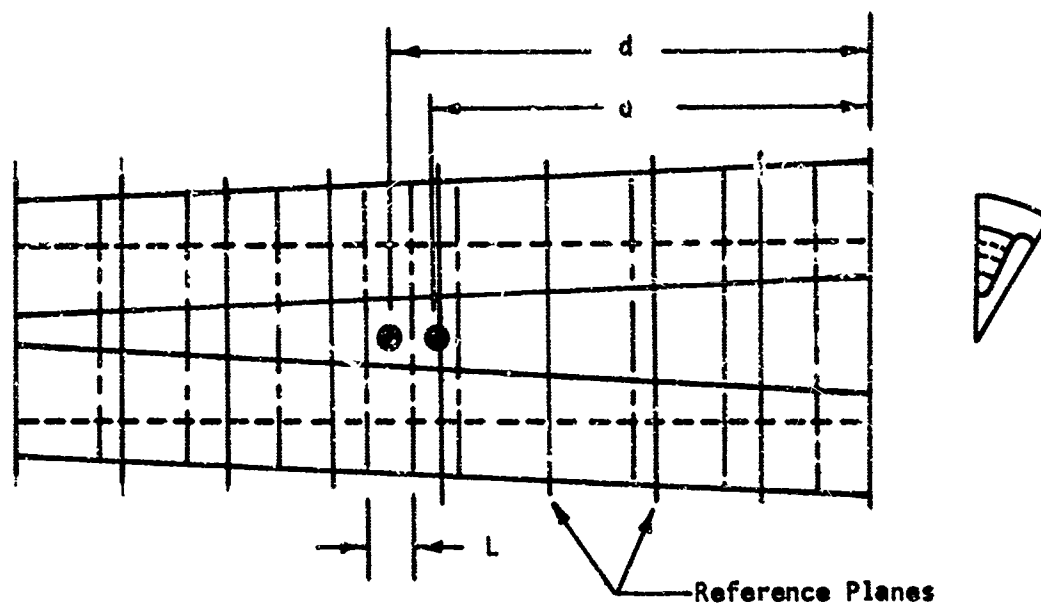


Figure 5.38 Cylindrical Section Element Volumes for MOI and CG Calculations

6.0

DETAILED PROGRAMMING INFORMATION

Information required to maintain and revise the program is presented in this section. A brief description of all program subroutines, macroscopic program logic flow charts, the program storage allocation, a description of the computing system, program diagnostic aids, and a list of the program nomenclature are included.

As stated in Section 3.0 on the method of solution, the primary purpose of this computer program is to obtain the performance characteristics of solid propellant rocket motors, which requires the solution of the internal ballistics. In order to obtain the performance characteristics, the computer solution is separated into two major sections. One section obtains the propellant burning surface area and volume (geometry calculations), and the other section obtains the solution of the gas dynamic equations (internal ballistic solution). The computer solution of the geometry equations requires three separate core loads and the computer solution of the gas dynamic equations requires a fourth core load. Each computer core load contains a control subroutine which calls the required subroutines and computes values of control parameters. A common data region named CDM and dimensioned 6600, which resides in the machine memory core at all times during program execution, contains all of the computed variables so that each core load may be linked to all other core loads. Another common section named TBLK and dimensioned 2580 is used to store the geometry tables which are calculated in core loads 1-3 and which are used in core load 4. The individual core load control subroutines are linked through the MAIN program by a control variable named ICHN. The control subroutine for the first computer core load is MNCHN1, for the second computer core load - MNCHN2, for the third computer core load - MNCHN3, and for the fourth computer core load - MNCHN4.

The first computer core load (ICHN = 1) contains the subroutines required to read the input data, initialize the data cells, compute the input reference plane constants, locate the increment dividing planes, check for input data errors, and print the program inputs and computed constants. The second computer core load (ICHN = 2) contains the geometry subroutines required to compute the initial propellant area, perimeter length, and radius of gyration for the cylindrical section reference planes; and to compute the initial propellant volume, burn area, center of gravity location, and moments of inertia for the aft-head and straight through grain fore-head section. The third computer core load (ICHN = 3) contains the geometry subroutines required to compute the initial propellant volume, burn area, center of gravity, and moments of inertia for the fore-head with web. The fourth computer core load (ICHN = 4) contains the subroutines required to obtain the internal ballistic solution.

6.1 Subroutine Description

This subsection is divided into two parts. Part one (6.1.1) contains a verbal description of the purpose of each subroutine and includes cross-references to other sections which give additional, detailed explanations of particularly complex or important subroutines. Part two (6.1.2) contains a tabular description of the subroutine linkage. The table identifies all lower level subroutines called by a particular routine plus all routines which call that particular subroutine.

6.1.1 Subroutine Descriptions

- ACOS - Subroutine ACOS determines the arc cosine for arguments between 0 and 2π radians.
- AEPSUB - Subroutine AEPSUB tests for the existence of a sector for the end sections. If a sector is burned out or does not exist, program control is returned to subroutine ASESUB, otherwise computation proceeds to subroutine AESUB. The sector areas are then summed and program control is returned to subroutine ASESUB (Section 5.2.3.2).
- AESUB - Subroutine AESUB determines the surface area and initial volume of a sector for the zones in the end sections (Section 5.2.3.2).
- AFPSUB - Subroutine AFPSUB determines the perimeter length and cross-sectional area of all sectors, except sector 8, in the cylindrical section (Section 5.1.1).
- AIBST - Subroutine AIBST determines the pressure loss and changes in the gas properties between increment dividing planes due to mass addition and area change for the non-steady flow solution of the internal ballistics (Section 4.1.2.1).
- AIBSUB - Subroutine AIBSUB determines the pressure loss and changes in the gas properties between increment dividing planes due to mass addition and area change for the solution of the internal ballistics neglecting transient effects (Section 4.1.1).
- AIGSUB - Subroutine AIGSUB determines the surface area around the igniter opening in the head end section (Section 5.2.1.2).
- ALRSUB - Subroutine ALRSUB determines the arc length of a sector in the end sections from the minimum point of a sector to a general point along the perimeter of the sector (Section 5.2.3.2).

6.1.1

Subroutine Descriptions (Continued)

- ARSSUB - Subroutine ARSSUB determines the chord length between the minimum point of a sector and a general point along the perimeter of the sector (Section 5.2.3.2).
- ASESUB - Subroutine ASESUB sets up the correct equations for subroutines XRSUB and RASUB and assigns for each sector the proper values for the coordinates of the origin of the circular arc (RA0, XA0), the radius of curvature of the sector (RT), and the perimeter length (AL) of the sector (Section 5.2.3.2).
- ASTSUB - Subroutine ASTSUB sets up the correct equations for subroutine PTIAA to determine the moments of Inertia for the block 1 analysis of the head end with web (AJSTP and AJSTB).
- ASUBC - Subroutine ASUBC sets up the correct variables and equations to determine the coordinates (X, Y, and Z) of the points POA, P1A, and P3A for the block 1 analysis in subroutine SC1 (Section 5.2.1.1).
- AWESUB - Subroutine AWESUB determines the total burning surface area of the web zone at thickness TAU and the burning surface area of sector 8 for the end sections (Section 5.2.3.2.4).
- BRAKSB - Subroutine BRAKSB determines the length of the diagonal of the parallelogram that is formed by the intersection of two planes in the block 1 analysis (See Figure 5.22).
- BSUBC - Subroutine BSUBC sets up the correct variables and equations to determine the coordinates (X, Y, and Z) of the points POB, P1B, and P3B on the pseudoellipsoid for the block 1 analysis in subroutine SC1 (Section 5.2.1.1.1).
- COMPSC - Subroutine COMPSC determines the sine and cosine for the reference plane geometry angles A(1) thru A(5).
- CONV - Subroutine CONV determines new iterations value for either AKRST or PCTAB during the start transient calculations for the internal ballistic solution.

6.1.1

Subroutine Descriptions (Continued)

CSTRSB - Subroutine CSTRSB determines the propellant gas properties, γ , STAR, molecular weight, specific heat ratio, gas constant, and combustion temperature as a function of the chamber pressure during the internal ballistic solution (Section 4.3.3).

DPRASB - Subroutine DPRASB determines the distance between the points P_{ra} and P'_{ra} ; P_{sa} and P'_{sa} ; P_{rb} and P'_{rb} ; and P_{sb} and P'_{sb} that lie on the planes produced in sectors 3A and 3B or 11A and 11B in the block 1 analysis of subroutine SCI (Section 5.2.1.1.2).

ENDCSB - Subroutine ENDCSB determines the coefficients of a fourth degree polynomial equation obtained by the intersection of an ellipse and a circle, CAE, CBE, CCCE, CCVE, CDCE, CDVE, CECE, and CEVE and determines the constants RE1, RE2, ALFE, ALFEM, HE1, HE2, and HE0 that define the geometry of the fore-head and aft-head sections (Section 5.2.3.1).

FDGRE - Subroutine FDGRE solves for the roots of a fourth degree polynomial equation by reducing to the form

$$X^4 + A X^2 + B X + C = 0$$

by the substitution

$$Y = (X - P/R)$$

and then solving the resultant cubic

$$T^3 + \frac{A}{2} T^2 + \frac{(A^2 - 4C)}{16} T - \frac{B^2}{64} = 0$$

GAMA2S - Subroutine GAMA2S determines the angle between the Y-axis and a line normal to the ellipse

$$\left(\frac{Y}{BOE}\right)^2 + \left(\frac{Z'}{AOE}\right)^2 = 1$$

(which is defined by the ellipse ratio β_{OE}) at the point $Z' = RAT$ (Section 5.2.1.1.1).

GAMSUB - Subroutine GAMSUB determines the angle γ_1 between a line normal to the perimeter in the X-Z plane, and a line normal to the line segment RAT which is a radial vector from the motor axis to a point on a sector perimeter (Section 5.2.1.1.1).

6.1.1

Subroutine Descriptions (Continued)

- HAPSBC - Subroutine HAPSBC sets up the correct equations to determine the coordinates (XOP, YOP, ZOP) of the points POA', P1A', and P3A' on the pseudoellipsoid for the block 1 analysis of the intersecting planes for sectors 3 and 11 in subroutine SCI (Section 5.2.1.1.2).
- HASUBC - Subroutine HASUBC sets up the correct variables to determine the coordinates (XO, YO, ZO) of the points POA, P1A, and P3A that lie on the pseudoellipsoid produced in the block 1 analysis of the intersecting plane for sectors 3 and 11 in subroutine SCI (Section 5.2.1.1.2).
- HBPSBC - Subroutine HBPSBC sets up the correct equations and variables to determine the coordinates (XOP, YOP, ZOP) of the points POB', P1B', and P3B' that lie on the pseudoellipsoid produced in the block 1 analysis of the intersecting planes for sectors 3 and 11 in subroutine SCI (Section 5.2.1.1.2).
- HDNSUB - Subroutine HDNSUB sets up the correct variables to perform the block 1, 2A, 2B, and 3 analysis of the head end with web (Section 5.2.1).
- HESUB - Subroutine HESUB determines the length of the zones in the end sections from which the incremental surface areas in subroutine AESUB are determined (Section 5.2.3.2).
- LBSUB - Subroutine LBSUB determines the length (b) of the Y intercept produced by the intersection of the line $Y = 0$ and the line normal to the ellipse at P0 (Section 5.2.1.2).
- LPDAPS - Subroutine LPDAPS sets up the correct variables to determine the perimeter length, ALP, and the cross-sectional fuel area, AFP, of the propellant tips in subroutine AFPSUB for the cylindrical section reference planes (Section 5.1.1).
- LPTO - Subroutine LPTO determines the perimeter length AL7 and AL8 of the anisotropic propellant in sectors 7 and 8 during the motor tail-off interval (Section 4.3.3).

6.1.1

Subroutine Descriptions (Continued)

- MNCHN1 - Subroutine MNCHN1 is the control routine for the first core load which reads the input data, computes the constants that define the geometry of the grain cross-section and longitudinal configuration for use by the second and third core loads, checks for data errors, and prints the program inputs and geometry constants.

- MNCHN2 - Subroutine MNCHN2 is the control routine for the second core load which determines the initial fuel area (AFF) and port area (A_p) for the cylindrical section reference planes and determines the burn area and initial fuel volume of the straight through grain fore-head and aft-head sections as a function of distance burned.

- MNCHN3 - Subroutine MNCHN3 is the control routine for the third computer core load which determines the initial fuel volume and burn area as a function of time for the head end with web.

- MNCHN4 - Subroutine MNCHN4 is the control routine for the fourth computer core load which obtains the internal ballistic solution (Section 5.2.2).

- MODTSB - Subroutine MODTSB modifies the value of TIME and the value of the nozzle throat diameter after convergence of the ballistic solution iteration and initializes X and Y reference planes for interpolation of the increment dividing planes in subroutine TISUB.

- MSISUB - Subroutine MSISUB determines the location of the center of gravity and the polar and rectangular moment of inertia for the block 2A analysis of the head-end with web.

- MTISUB - Subroutine MTISUB determines the location of the center of gravity and the polar and rectangular moment of inertia for the block 2B analysis of the head end with web.

- PCHGIS - Subroutine PCHGIS prints the program inputs for the propellant properties and the burning rate equation constants.

- PCHPLI - Subroutine PCHPLI prints the geometry constants calculated for each reference plane.

6.1.1

Subroutine Descriptions (Continued)

- PLNCNS - Subroutine PLNCNS calculates the geometry constants of each cylindrical section reference plane (Section 5.1.1).
- PLNLCS - Subroutine PLNLCS checks for reference plane input data errors, prints appropriate diagnostic comments, and flags the program for case termination if an error exists.
- POSUB - Subroutine POSUB determines the coordinates (X0, Y0, Z0) of the point P0 that is located on the inner section of the inner ellipsoid with the core (Section 5.2.1.1.1).
- PT1AA - Subroutine PT1AA determines the polar and rectangular moment of inertia for the cylindrical section, straight through grain end sections, and the block 1 analysis of the head end with web (Section 5.3).
- P1SUB - Subroutine P1SUB determines the coordinates (X1, Y1, and Z1) of the point P1 that is located on the Z axis along a line through point P0 and normal to the sector perimeter (Section 5.2.1.1.1).
- P3SUB - Subroutine P3SUB determines the coordinates (X3, Y3, and Z3) of the point P3 that is located in the Y-Z plane and on the outer ellipse (Section 5.2.1.1.1).
- RASUB - Subroutine RASUB determines the length of a radius vector from the motor axis to a point on the perimeter for each sector in the end sections with a straight through web (Section 5.2.3.2).
- RASUBB - Subroutine RASUBB determines the length of a radius vector from the motor axis to a general point in a sector for the block 1 analysis of the head end with web (Section 5.2.1.1.1).
- RBSTSB - Subroutine RBSTSB determines the initial estimate of the burn rate coefficient, AKRST, for each time increment during the start transient interval and performs the table look-ups for PH and AKRST (Section 4.3.3).
- RBSUB - Subroutine RBSUB determines the propellant burning rate at each increment dividing plane (Section 4.3.2).
- RBVSUB - Subroutine RBVSUB checks the validity of the burning rate equation constants and prints appropriate diagnostic comments.

6.1.1

Subroutine Descriptions (Continued)

- RCSUB - Subroutine RCSUB determines the value of the radial distance from the motor axis to the intersection of the aft-end burning surface and the motor case for any configuration (Section 5.2.3.2).
- RGISUB - Subroutine RGISUB determines the radius of gyration for the incremental thin shells of the head end with web.
- ROE1SB - Subroutine ROE1SB determines the radius of curvature, ρ_1 , at the point P_1 on the pseudoellipsoid for the block 2A analysis in subroutine SCI (Section 5.2.1.2).
- ROPSB - Subroutine ROPSB sums the values of the Y coordinates PO (YOA and YOB) or PO' (YOA' and YOB') for the A and B planes from which the block 1 surface area is obtained in subroutine SCI (Section 5.2.1.1.1).
- RSSPLN - Subroutine RSSPLN determines the coefficients of the piecewise cubics that are used for the spline interpolation procedure.
- SCI - Subroutine SCI is the control routine to determine the surface area and initial volume of the propellant tip for the block 1 analysis of the head end with web (Section 5.2.1.1).
- SCTOR1 - Subroutine SCTOR1 is the control routine to determine the surface of the pseudoellipsoid for the block 2A analysis of the head end with web (Section 5.2.1.2).
- SCTOR2 - Subroutine SCTOR2 is the control routine to determine the surface area on the pseudoellipsoid of the projected propellant core in the block 2B analysis of the head-end with web (Section 5.2.1.3).
- SD1D13 - Subroutine SD1D13 determines the center of gravity and moments of inertia of the straight through grain end sections (Section 5.3).
- SEGSUB - Subroutine SEGSUB is the cylindrical section control routine to determine the mass generation rate, port area, perimeter length, and cross-sectional fuel area for each increment dividing plane and mass addition region during the internal ballistic solution (Section 5.2.2).

6.1.1

Subroutine Descriptions (Continued)

- SETPH - Subroutine SETPH is the internal ballistic solution control routine to obtain convergence on the fore head pressure by matching the grain discharge flow with the nozzle flow determined from the nozzle pressure. The performance calculations for thrust, total impulse, thrust coefficient, etc., are included in subroutine SETPH (Section 4.2).
- SLOT - Subroutine SLOT determines the gas properties at the discharge section of a slot between grain segments for the non-steady flow solution of the internal ballistics (Section 4.1.2.2).
- SPLN1A - Subroutine SPLN1A sets up subroutine RSSPLN to perform the initialization for the spline interpolation procedure.
- SPLN2A - Subroutine SPLN2A sets up subroutine RSSPLN to determine the functional values and derivatives for the arguments of the spline interpolation functions after SPLN1A has been executed.
- SPLN3A - Subroutine SPLN3A sets up subroutine RSSPLN to determine the coefficients of the interpolating function for the spline interpolation procedure.
- SQRT - Subroutine SQRT is a modification of the IBSYS-13 monitor library routine to determine the square root of negative numbers. Only the positive value of the argument is transferred to the designated register.
- STUPPS - Subroutine STUPPS stores the variables defining the plane A produced in sectors 3A or 11A for the block 1 analysis in subroutine SCI of the head end with web (Section 5.2.1.1.2).
- STUPKS - Subroutine STUPKS stores the variables defining plane B produced in sectors 3A or 11A for the block 1 analysis in subroutine SCI of the head end with web (Section 5.2.1.1.2).
- S2SK - Subroutine S2SK determines the sector surface area on the pseudoellipsoid of the projected grain cross-section for the block 2B analysis in subroutine SCTOR2 of the head end with web (Section 5.2.1.3).
- TDGRE - Subroutine TDGRE determines the largest real root of a third degree polynomial for the argument X.

6.1.1

Subroutine Descriptions (Continued)

- THETAR - Subroutine THETAR determines the angle between the Z-axis and the line segment RAT for the block 1 analysis in subroutine SCI of the head end with web (Section 5.2.1.1.1).
- TISUB - Subroutine TISUB determines the value of DELT for the steady state internal ballistic solution neglecting transient effects and modifies the values of thickness burned in each increment dividing plane after the ballistic solution is converged for each time point.
- TRAN - Subroutine TRAN transfers the geometry constants from the permanent common storage location to the working array common storage location.
- VFPPSB - Subroutine VFPPSB determines the port volume of each cylindrical section segment and sums the segment port volumes to obtain the total cylindrical section port volume.
- VOLSUB - Subroutine VOLSUB is the control routine which determines the initial volume for the block 3 analysis of the head-end with web (Section 5.2.1.4).
- VSEC - Subroutine VSEC determines the volume produced by the difference of volumes of two oblate spheroids, minus the volume of the igniter hole in the block 3 analysis of the head end with web (Section 5.2.1.4).
- VSTRSB - Subroutine VSTRSB determines the initial core volume that is present in the head end with web for the block 3 analysis (Section 5.2.1.4).
- XRSUB - Subroutine XRSUB determines the X-coordinate of a general point on the perimeter of a sector in the end sections (Section 5.2.3.2).
- XRSUBB - Subroutine XRSUBB determines the X-coordinate of the RAT line segment which is a radial vector from the motor axis to a point on a sector perimeter for the analysis of the head end with web (Section 5.2.1.1.1).
- XRTHR - Subroutine XRTHR is a set up subroutine that uses subroutine XRSUBB to obtain the X-coordinate of a point located on the perimeter of a sector in the block 2B analysis of the head end with web. The angle θ_1 between the Z axis and a line from the motor axis to a general point in a sector is also determined (Section 5.2.1.3).

6.1.1

Subroutine Descriptions (Continued)

- YPSUB - Subroutine YPSUB determines the Y-coordinate of the points P0 and P3 which are located on the surface of the inner and outer ellipsoids respectively for the block 2 analysis of the head end with web (Section 5.2.1.2).
- ZISUB - Subroutine ZISUB determines the Z-coordinate produced by the intersection of the outer ellipse and the line normal to the ellipse at P1 (Section 5.2.1.2).

6.1.2

Subroutine Linkage Table

<u>NAME</u>	<u>LOWER-LEVEL CALLS</u>	<u>CALLED BY</u>
ACØS	SQRT	AESUB GAMA2A RASUBB AFPSUB LPTØ SD1D13 AIGSUB MNCHN2 THETAR ALRSUB PLNCNS XRTHR AWESUB P1SUB YPSUB ENDCSB P3SUB FDGRE RASUB
AEPSUB	AESUB	ASESUB
AESUB	ACØS ALRSUB ARSSUB HESUB RASUB SQRT XRSUB	AEPSUB
AFPSUB	ACØS SQRT	LPDAPS
AIBST	AIBSUB SQRT	AIBSUB MNCHN4
AIBSUB	AIBST SQRT	AIBST MNCHN4 SEGSUB
AIGSUB	ACØS SQRT	SCTØR1
ALRSUB	ACØS SQRT	AESUB
ARSSUB	SQRT	AESUB
ASESUB	AEPSUB AWESUB RCSUB	ENDCSB MNCHN2

6.1.2

Subroutine Linkage Table (Continued)

<u>NAME</u>	<u>LOWER LEVEL CALLS</u>	<u>CALLED BY</u>
ASTSUB	PT1AA	MNCHN3
ASUBC	GAMA2S GAMSUB P0SUB P1SUB P3SUB RASUBB	SC1
AWESUB	AC0S HESUB SQRT	ASESUB
BRKSB	SQRT	SC1
BSUBC	GAMA2S GAMSUB P0SUB P1SUB P3SUB RASUBB	SC1
COMPSC		LPT0 MNCHN1 MNCHN2 MNCHN3
CONV		SETPH
CSTRSB	SPLN1A SPLN2A	MNCHN4 RBSTSB
DPRASB	SQRT	SC1
ENDCSB	AC0S ASESUB LPDAPS SQRT	MNCHN1

6.1.2

Subroutine Linkage Table (Continued)

<u>NAME</u>	<u>LOWER-LEVEL CALLS</u>	<u>CALLED BY</u>
FDGRE	ACØS SQRT	RCSUB
GAMA2S	ACØS SQRT	ASUBC BSUBC HAPSBC HASUBC HBPSBC HBSUBC
GAMSUB		ASUBC BSUBC HABSBC HASUBC HBPSBC HBSUBC
HAPSBC	GAMA2S GAMSUB PØSUB P1SUB P3SUB RASUBB	THETAR TRAN XRSUBB SCI
HASUBC	GAMA2S GAMSUB PØSUB P1SUB P3SUB RASUBB	THETAR TRAN XRSUBB SCI
HBPSBC	GAMA2S GAMSUB PØSUB P1SUB P3SUB RASUBB	THETAR TRAN XRSUBB SCI
HBSUBC	GAMA2S GAMSUB PØSUB P1SUB P3SUB RASUBB	THETAR TRAN XRSUBB SCI

6.1.2

Subroutine Linkage Table (Continued)

<u>NAME</u>	<u>LOWER-LEVEL CALLS</u>	<u>CALLED BY</u>
HDNSUB	SCI SCTØR1 SCTØR2 VØLSUB	MNCHN3
HESUB	SQRT	AESUB AWESUB PT1AA SD1Ø13
INPT		MAIN
LBSUB		SCTØR1 S2ØK
LPDAPS	AFPSUB PT1AA	ENDCSB MNCHN2 MNCHN3
LPTØ	ACØS ØØMPSC SQRT TRAN	SEGSUB
MAIN	INPT MNCHN1 MNCHN2 MNCHN3 MNCHN4	
MNCHN1	ØØMPSC ENDCSB PØHG1S PØHPL1 PLNØKS PLNLCS	RBVSUB MAIN

6.1.2

Subroutine Linkage Table (Continued)

<u>NAME</u>	<u>LOWER-LEVEL CALLS</u>	<u>CALLED BY</u>
MNCHN2	ACOS ASESUB COMPSC LPDAPS PTIAA RCSUB TRAN	MAIN
MNCHN3	ASTSUB COMPSC HDNSUB LPDAPS RCSUB RGISUB SQRT TRAN	MAIN
MNCHN4	AIBST AIBSUB CSTRSB OUTPUT RBSTSB RBSUB STGSUB	SETPH SQRT TRAN MAIN
M0DTSB	TISUB	OUTPUT
MSISUB	SQRT	SCT0R1
MTISUB	SQRT	S2SK
OUTPUT	M0DTSB	MNCNN4
PCHGIS		MNCHN1
PCHPL1		MNCHN1
PLNCNS	ACOS SQRT	MNCHN1

6.1.2

Subroutine Linkage Table (Continued)

<u>NAME</u>	<u>LOWER-LEVEL CALLS</u>	<u>CALLED BY</u>
PLNLCS		MNCHN1
P0SUB	SQRT	ASUBC BSUBC HAPSBC HASUBC HBPSBC HBSUBC SCT001
PT1AA	HESUB SD1D13 SQRT	ASTSUB LPDAPS MNCHN2 RGISUB
P1SUB	AC0S SQRT	ASURC BSUBC HAPSBC HASUBC HBPSBC HBSUBC
P3SUB	AC0S SQRT TD0RE	ASUBC BSIBC HAPSBC HASUBC HBPSBC HBSUBC
RASIJB	AC0S SQRT	AESUB SD1D13
RASUBB	AC0S SQRT	ASUBC BSUBC HAPSBC HASUBC HBPSBC HBSURC SCT001
RBSTSB	CSTRSB	RBSUB

6.1.2

Subroutine Linkage Table (Continued)

<u>NAME</u>	<u>LOWER-LEVEL CALLS</u>	<u>CALLED BY</u>
R5SUB	RBCTSB	MNCHN4 SEGSUB SLDT
RBV5UB		MNCHN1
RCSUB	FDGRE TDGRE	ASESUB MNCHN2 MNCHN3
RG1SUB	PT1AA SQRT	MNCHN3
RØE1SB		SCTØR1 S2SK
RØPSB		SCI
RSSPLN		SPLN1A SPLN2A SPLN3A
SCI	ASUBC BRX3B BSUBC DPRASB HAPSBC HASUBC HBPSBC	HBSUBC RØPSB SQRT STUPPS STUPRS TRAN VSTRSB
SCTØR1	A1GSUB LBSUB MS1SUB PØSUB RASUBB	RØE1SB SQRT YPSUB Z1SUB
SCTØR2	S2SK	HDNSUB

6.1.2

Subroutine Linkage Table (Continued)

<u>NAME</u>	<u>LOWER-LEVEL CALLS</u>	<u>CALLED BY</u>
SD1D13	ACBS HESUB RASUB SQRT XRSUB	PT1AA
SEGSUB	AIBSUB LPT0 RBSUB SL0T SQRT	MNCHN4
SETPH	C0N7 SQRT VFPPSB	MNCHN4
SL0T	RBSUB SQRT	SEGSUB
SPLN1A	RSSPLN	C0TRSB
SPLN2A	RSSPLN	C0TRSB
SPLN3A	RSSPLN	(For Diagnostic Use)
SQRT		ACBS LPT0 SD1D13 AESUB MNCHN3 SEGSUB AFPSUB MNCHN4 SETPH AIBST MSISUB SL0T AIBSUB MTISUB S2SK AIGSUB PLNCNS TDGRE ALRSUB P0SUB THETAR ARSSUB PT1AA V0LSUB AWESUB P1SUB VSEC BRAKSB P3SUB VSTRSB DPRASB RASUB XRSUB ENJCSX RASUBB XRSUBB FDGRE RGISUB XETHP GAMA2S SCI YPSUB HESUB SCT0R1

6.1.2

Subroutine Linkage Table (Continued)

<u>NAME</u>	<u>LOWER-LEVEL CALLS</u>	<u>CALLED BY</u>
STUPPS		SCI
STUPRS		SCI
SZSK	LBSUB MTISUB RØEISB SQRT XRTHR YPSUB ZISUB	SCTØR2
TDGRE	SQRT	P3SUB RCSUB ZISUB
THETAR	ACØS SQRT	ASUBC BSUBC HAPSBC HASUBC HBPSBC HBSUBC
TISUB		MØSTSB
TRAN		ASUBC BSUBC HAPSBC HASUBC HBPSBC HBSUBC LPTØ MNCHN2 MNCHN3 MNCHN4 SCI
VFPPSB		SETPH
VØLSVB	SQRT VSEC	HDNSUB
VSEC	SQRT XRTHR YPSUB	VØLSUB

6.1.2

Subroutine Linkage Table (Continued)

<u>NAME</u>	<u>LOWER-LEVEL CALLS</u>	<u>CALLED BY</u>
VSTRSB	SQRT	SCI
XRSUB	SQRT	AESUB SD1D13
XRSUBB	SQRT	ASUBC LJUBC H4PSBC FASUBC HBPSC HBSUBC XRTHR
XTHR	ACOS SQRT XRSUBB	S2SK VSEC
YPSUB	ACOS SQRT	SCTØR1 S2SK VSEC
ZISUB	TØGRE	SCTØR1 S2SK

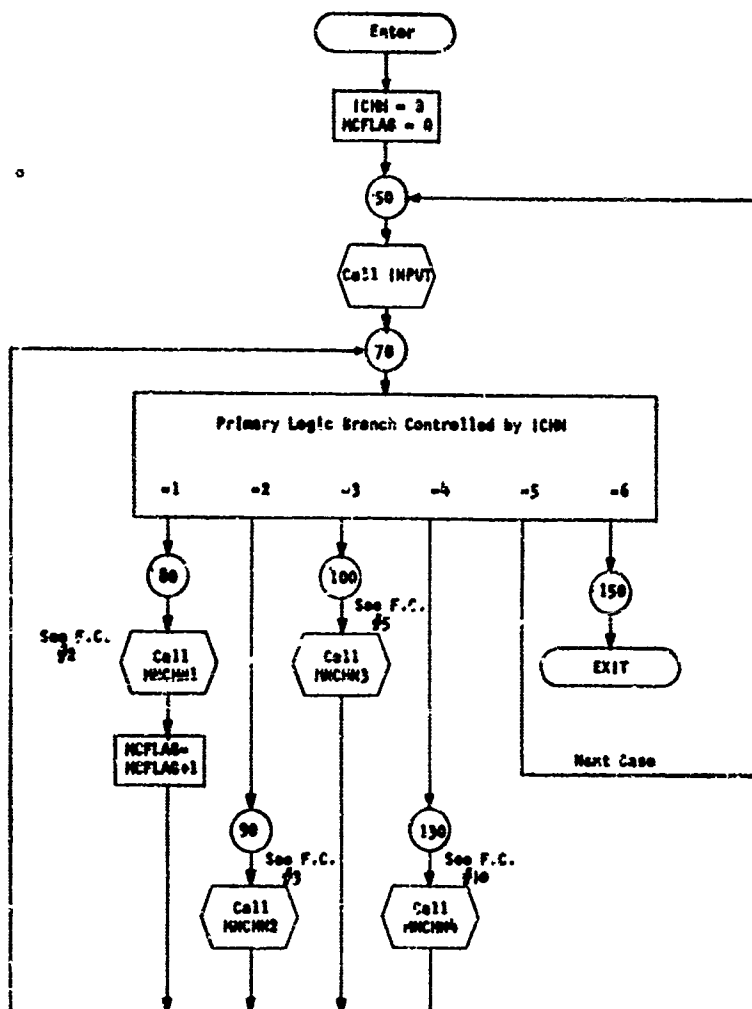
6.2

Flow Charts

This section contains macro-scopic flow charts in schematic form of the first, second and third level subroutines. The Fortran listings themselves are considered to be the flow charts for the lower level subroutines. In order to facilitate their use each routine has been processed by a special program which re-numbers all statement numbers in steps of ten. These routines are also annotated by comment cards which define the computational blocks and locate important logic branches.

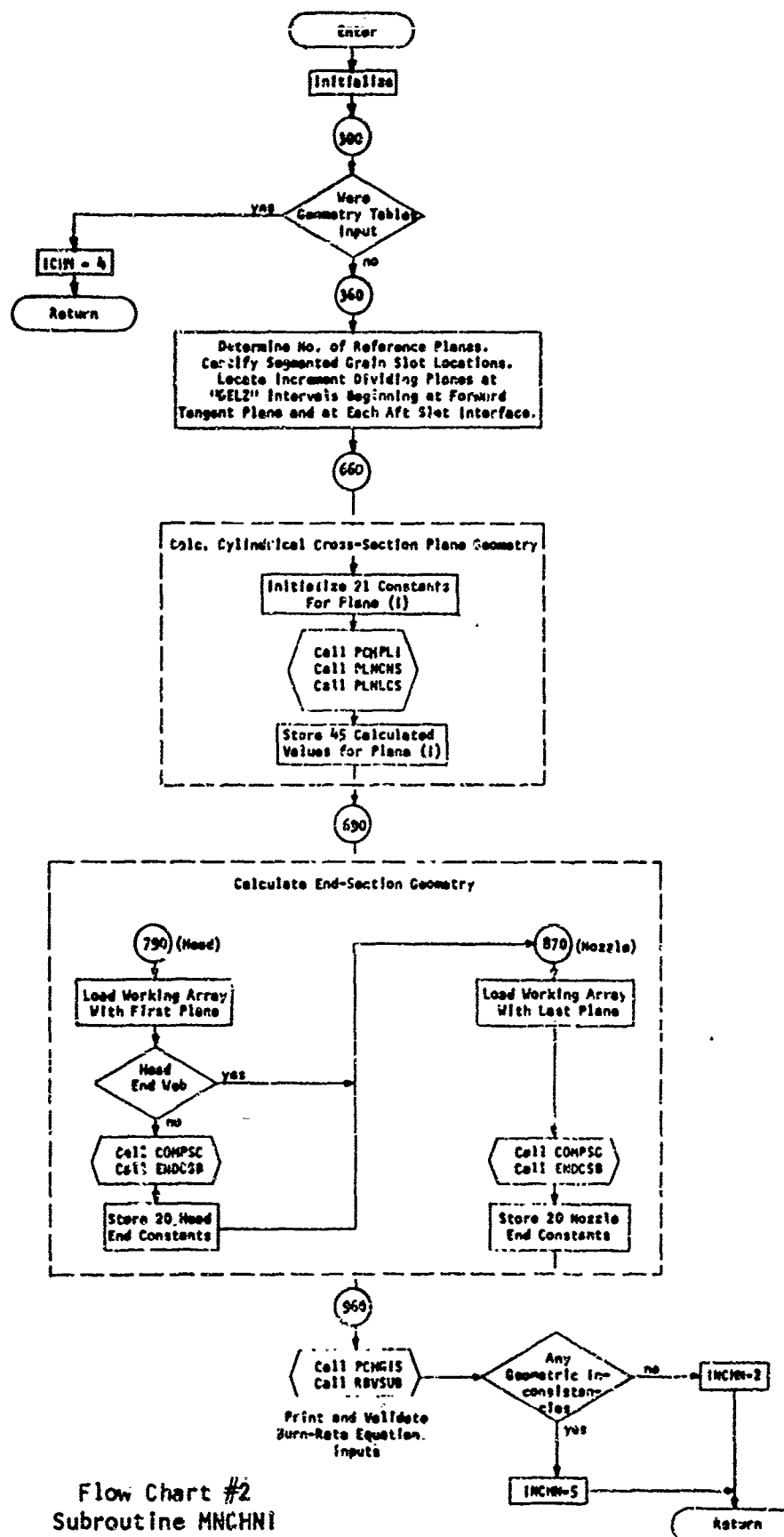
The following schematic flow charts are included:

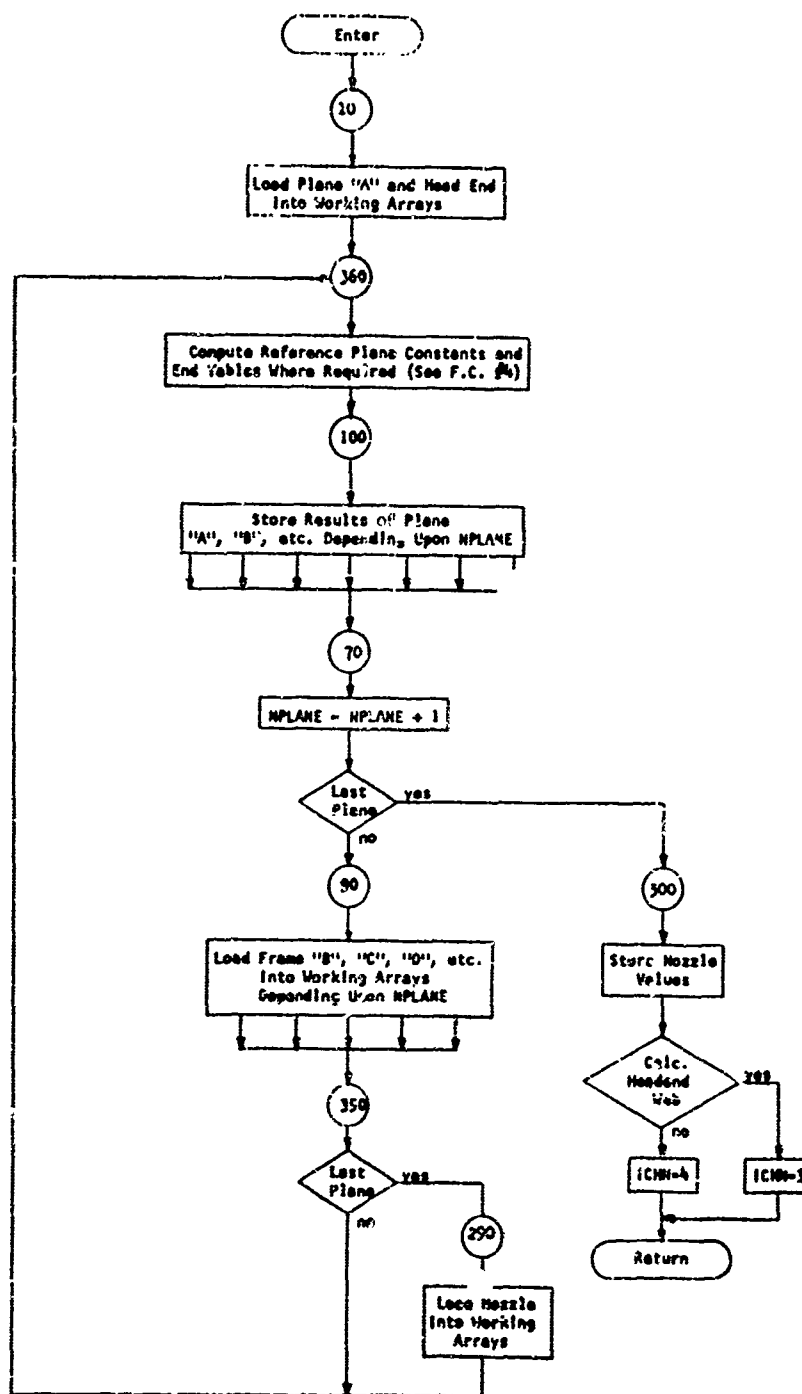
<u>Name</u>	<u>Flow Chart No.</u>
MAIN Program	1
Subroutine MNCHN1	2
Subroutine MNCHN2	3
Compute Plane Constants	4
Subroutine AESUB	5
Subroutine MNCHN3	6
Subroutine SCI	7
Subroutine SCTOR1	8
Subroutine SCTOR2	9
Subroutine MNCHN4	10
Subroutine SEGSUB	11
Subroutine SETPH	12
Subroutine TISUB	13
Check For Case Termination	14



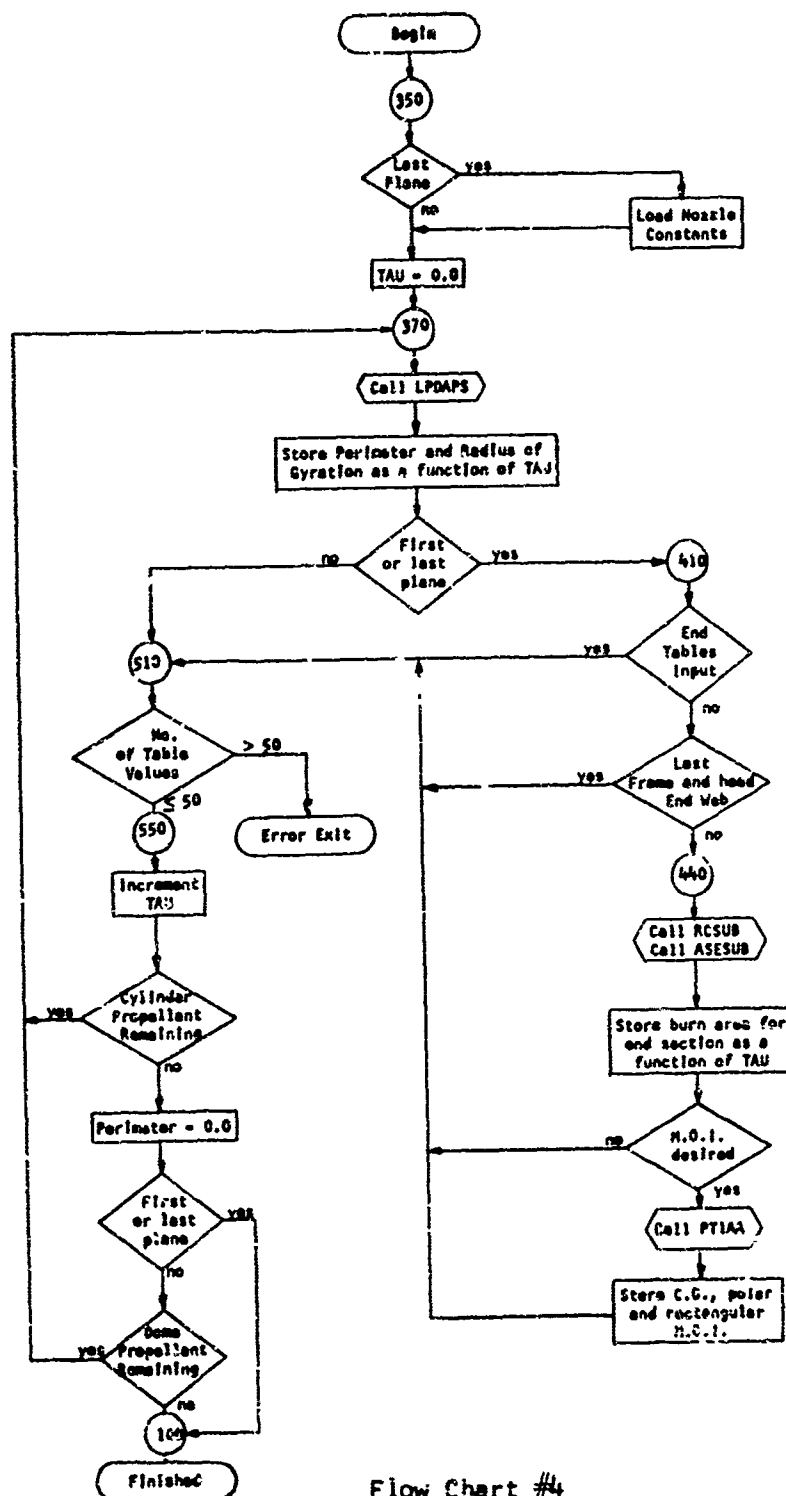
Flow Chart #1
MAIN Program

A

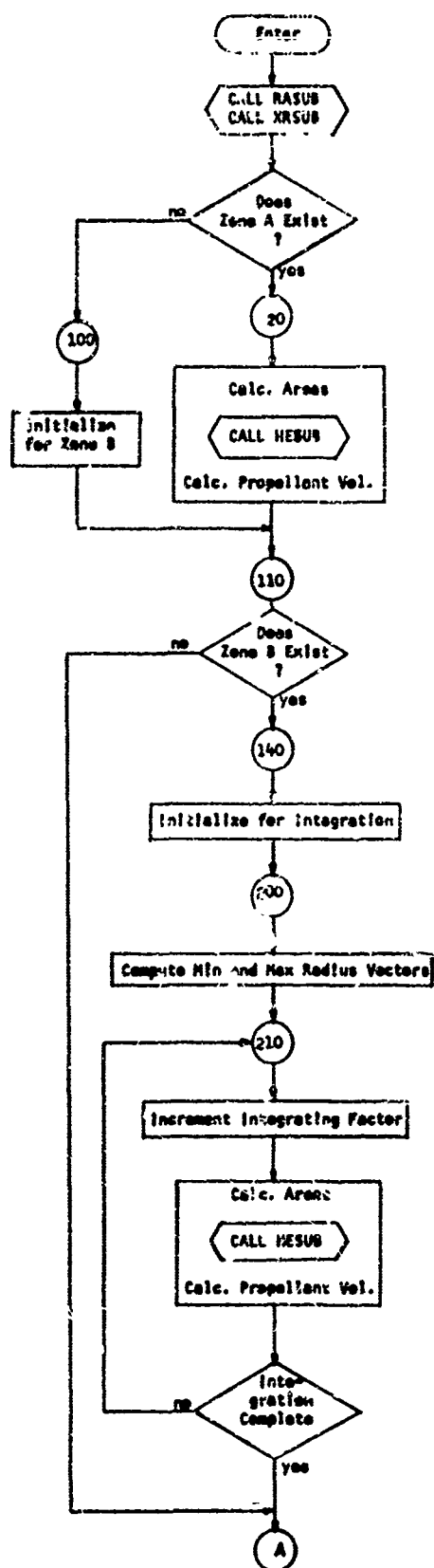




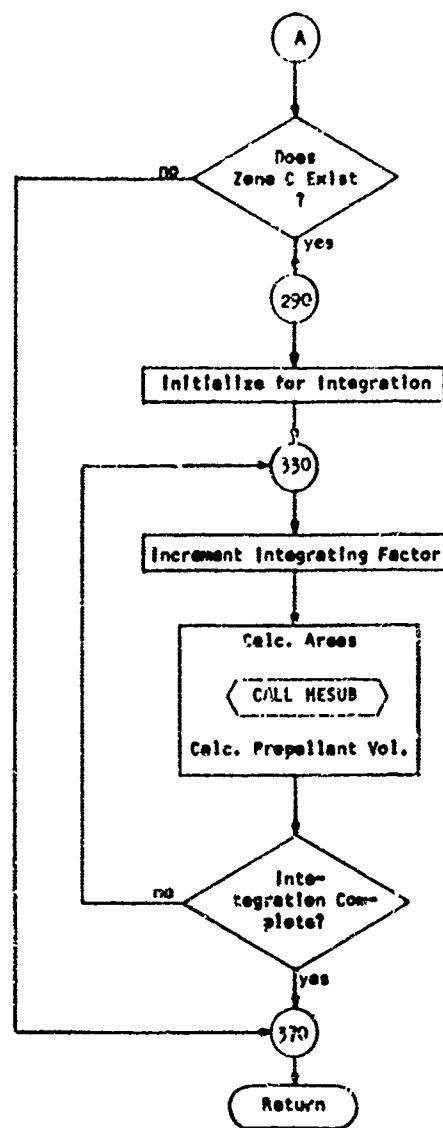
Flow Chart #3
Subroutine MNCHN2



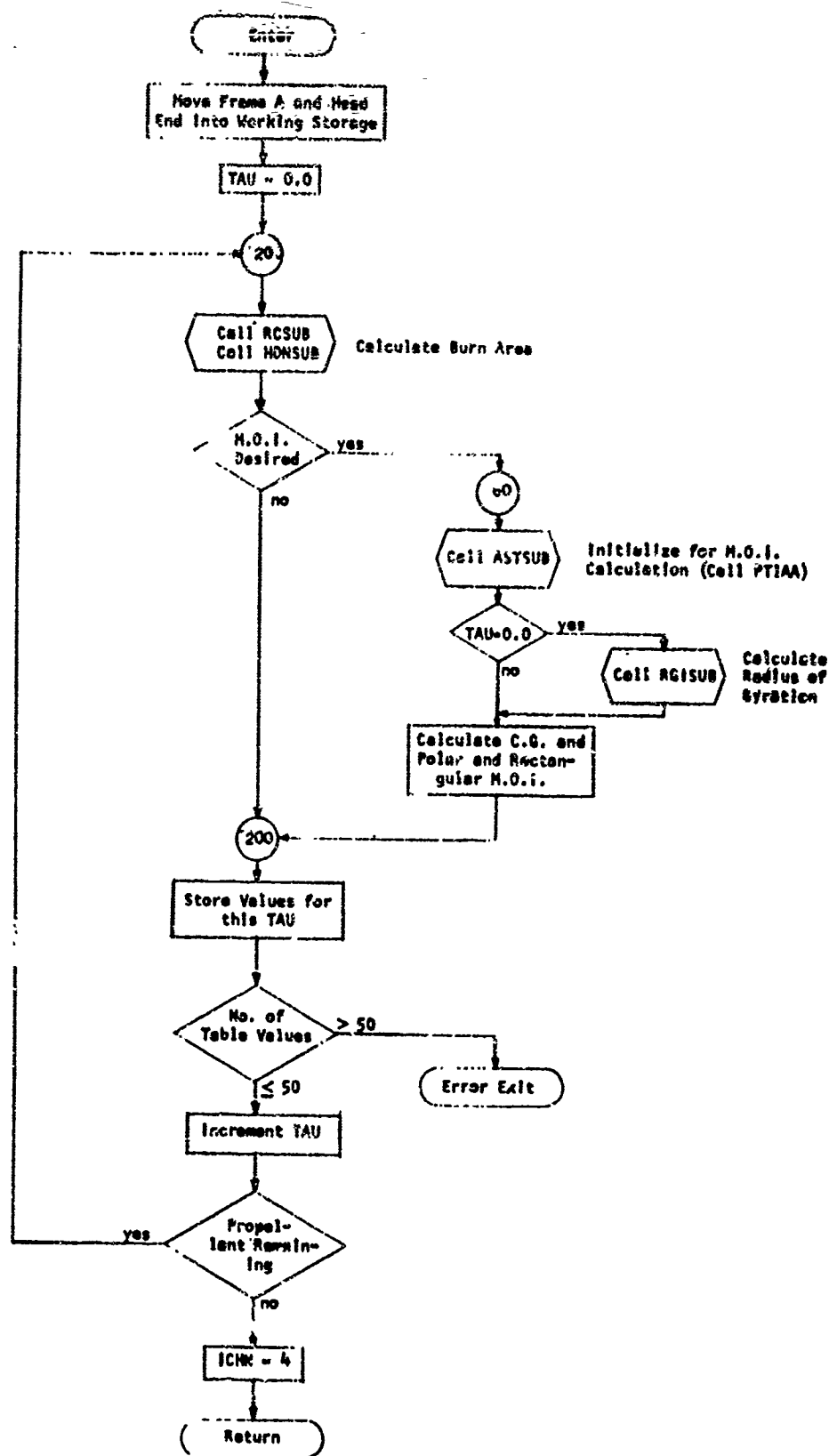
Flow Chart #4
Compute Plane Constants



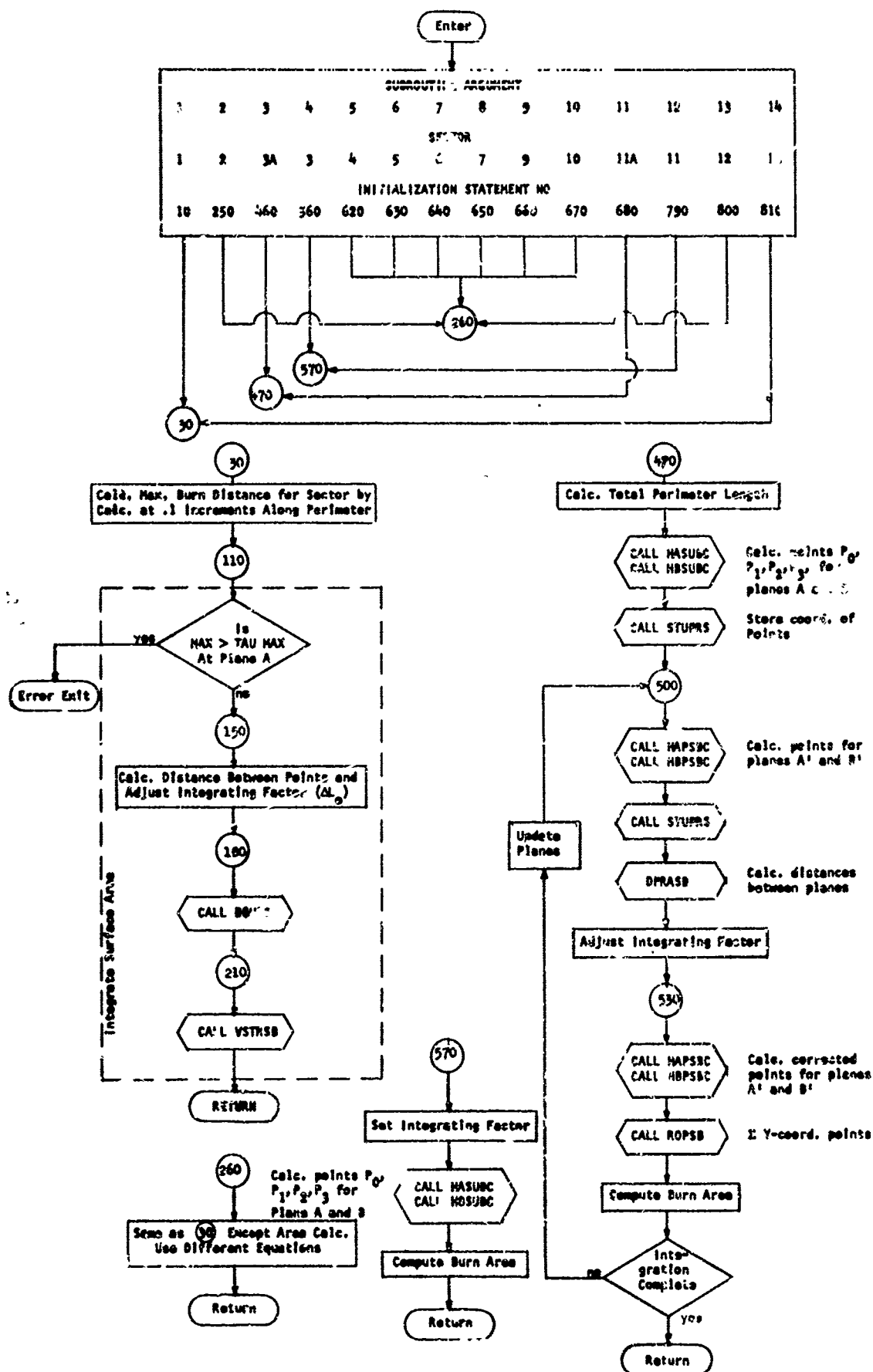
Flow Chart #5
Subroutine AESUB (1 of 2)



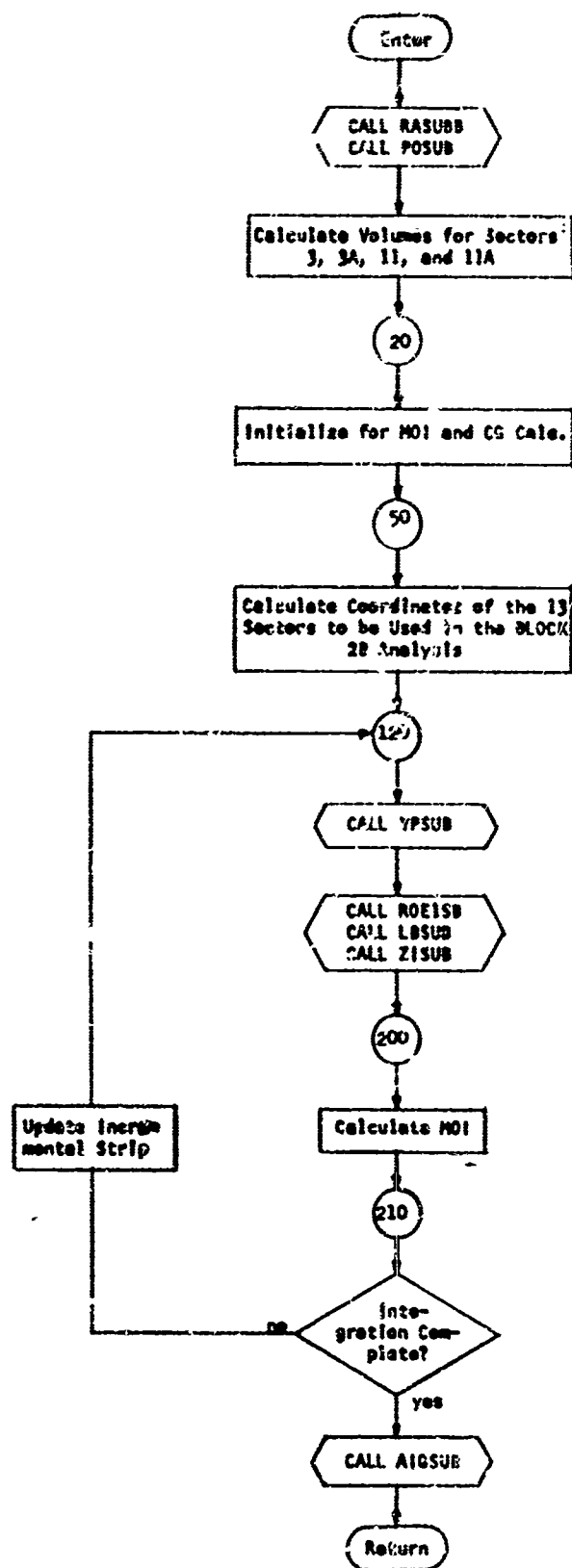
Flow Chart #5
Subroutine AESUB (2 of 2)



Flow Chart #6
Subroutine MRCHN3



Flow Chart #/
Subroutine SC1



Calculate Coordinates of
Points A and B for Sectors
3, 3A, 11 and 11A

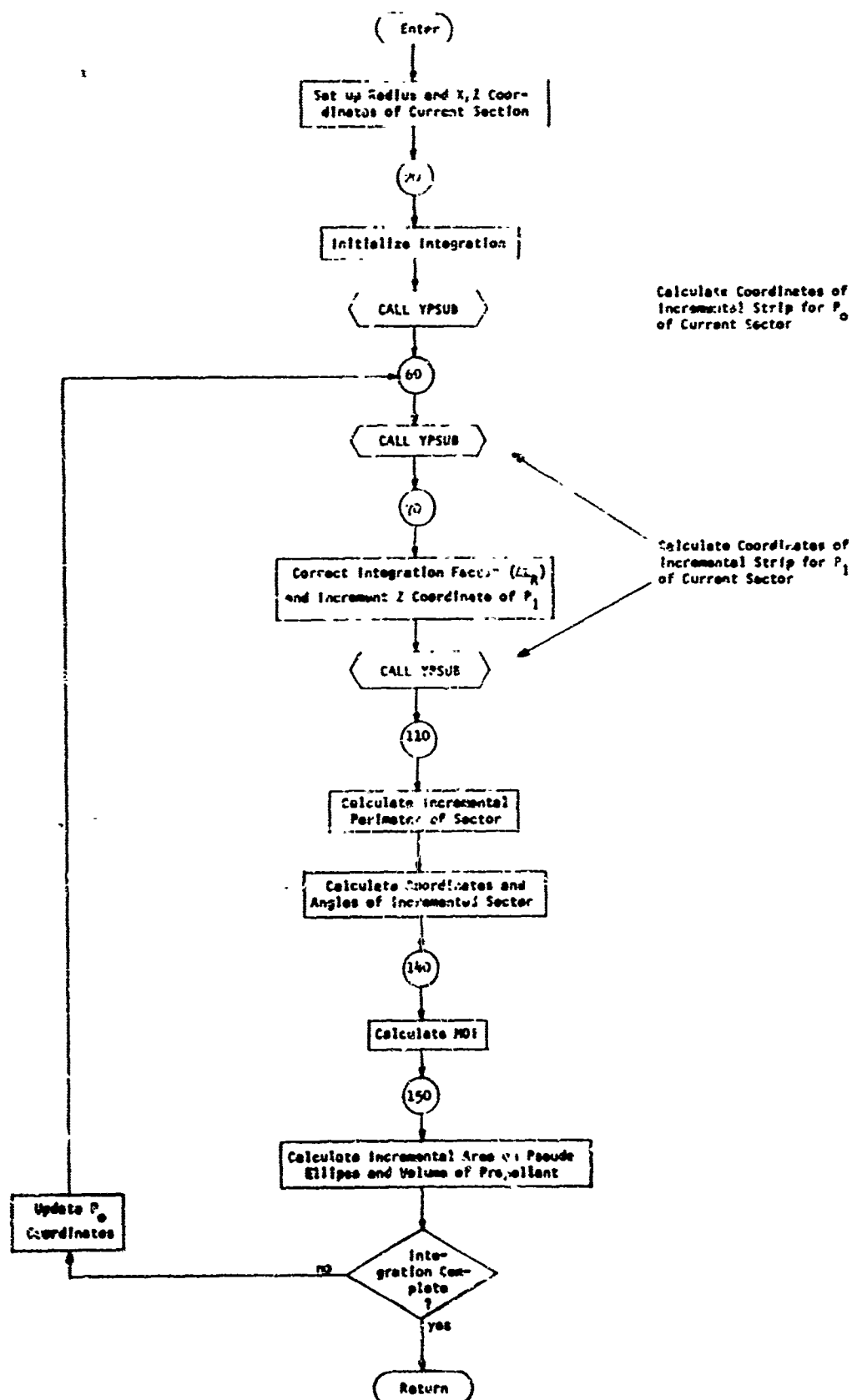
(Remaining Volumes are
Calc. in Subroutine SCT0R1)

Calculate Coordinates of the
Incremental Strip to be Used
in Integrating for Area

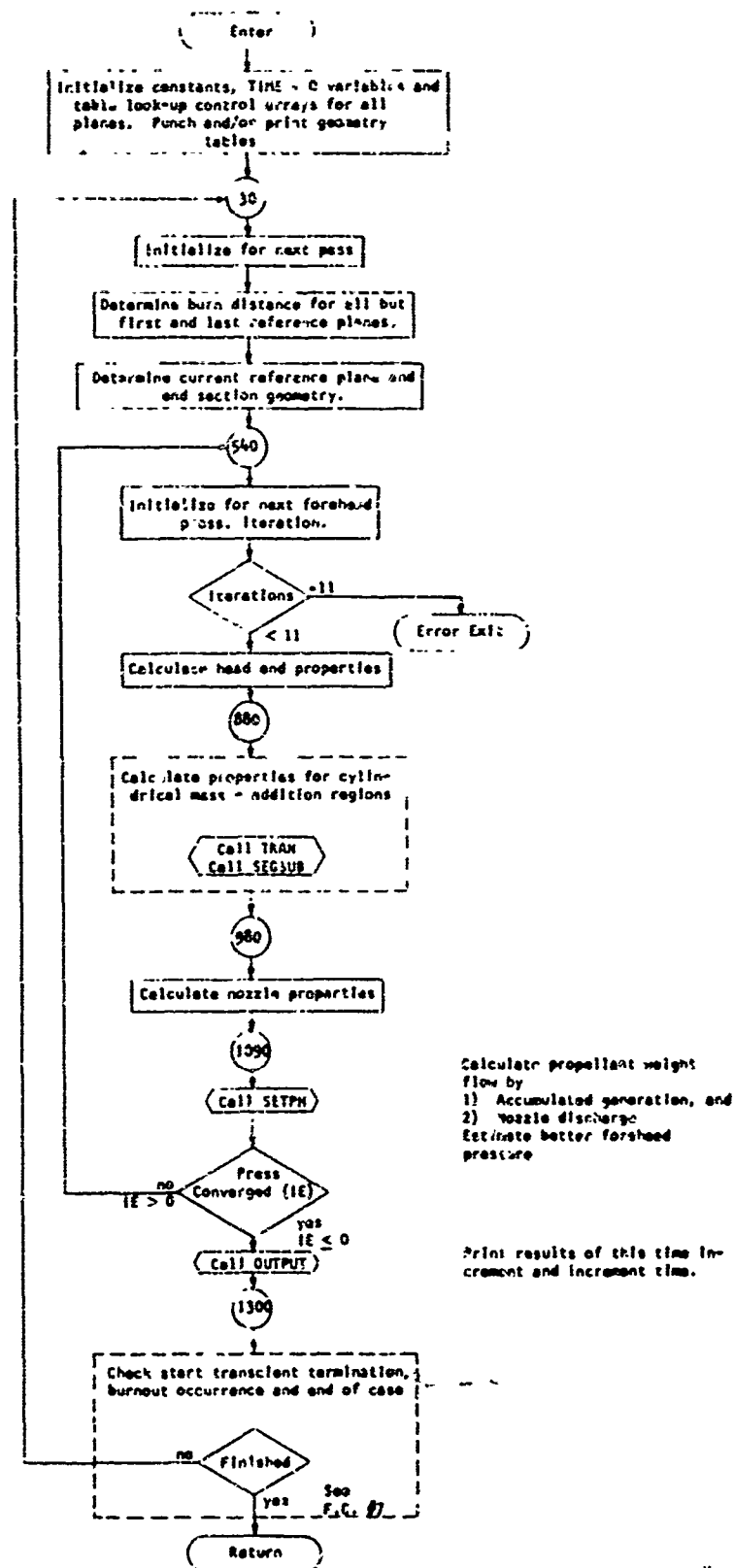
Calculate Radius of Curvature
of the Incremental arc.
Calculate Y-Axis Intercepts
of Lines Normal to the Ellipse.
Calculate Z Coordinates of P₁
Normal Line on Outer Ellipse.

Calc. Surface Area of the
Igniter Hole.

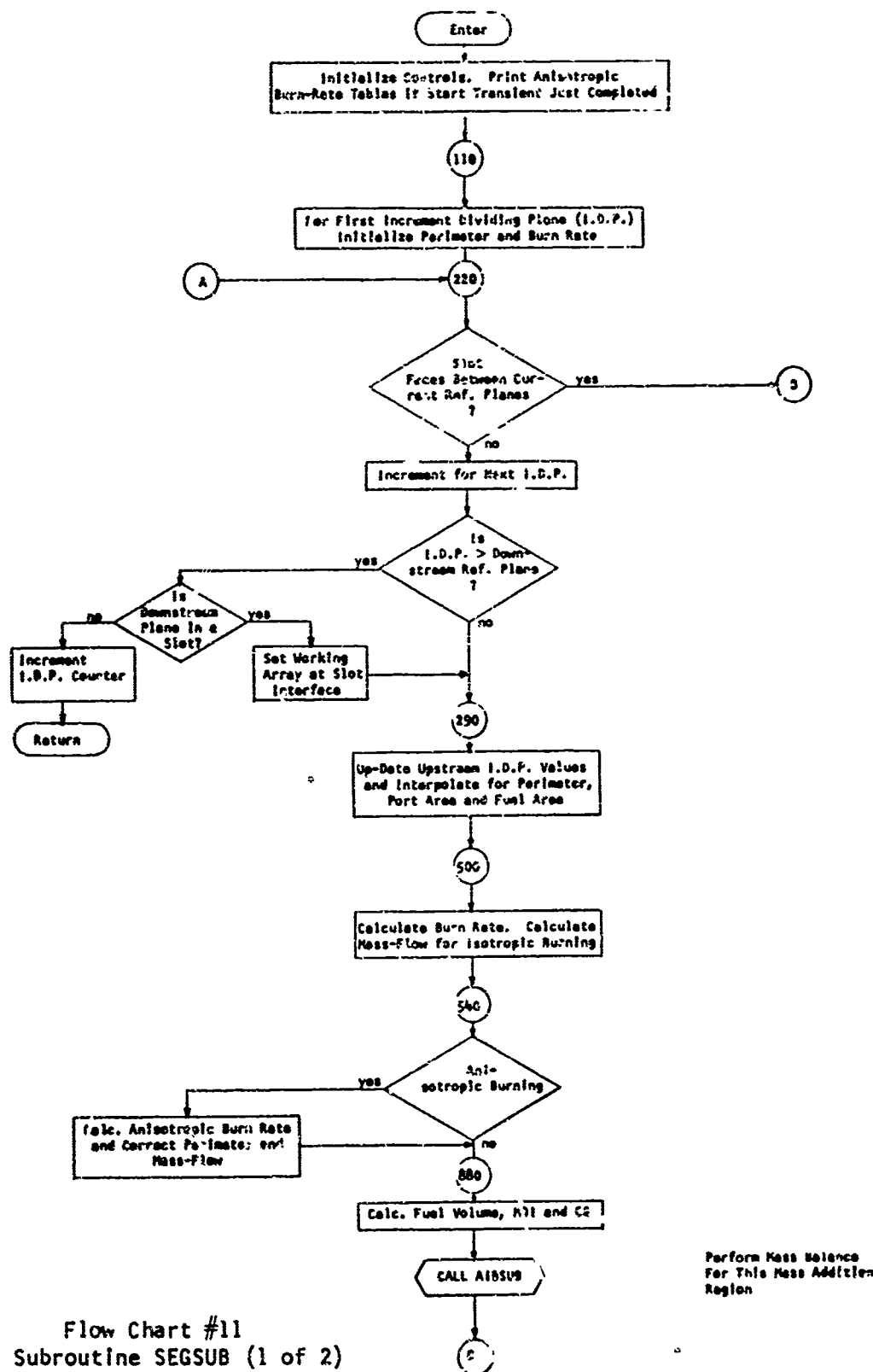
Flow Chart #8
Subroutine SCT0R1

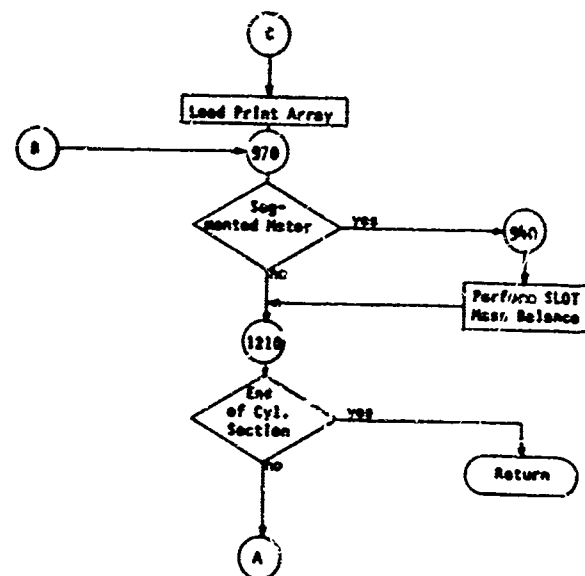


Flow Chart #9
Subroutine SCTDR2

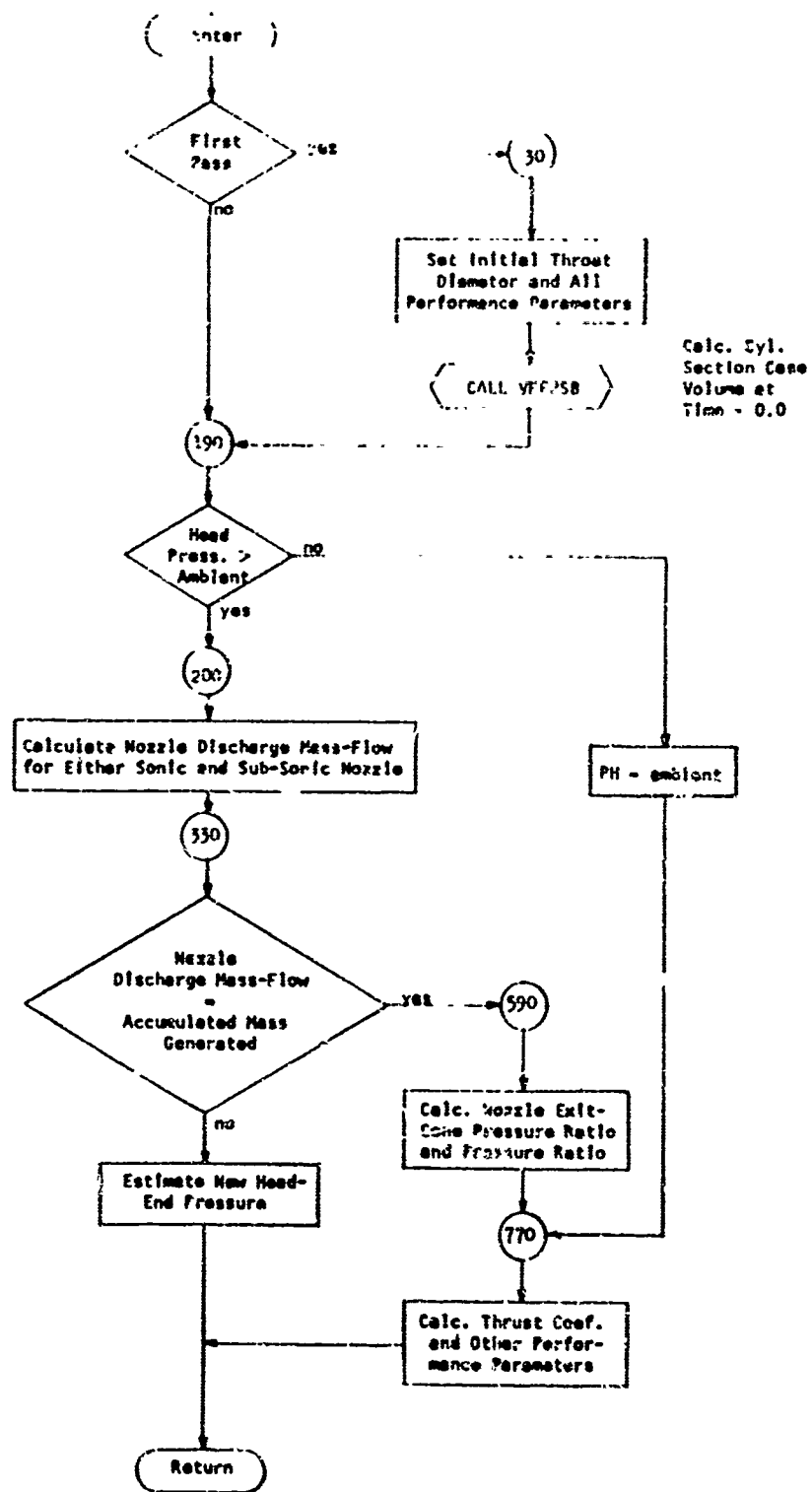


Flow Chart #10
Subroutine MNCHN4

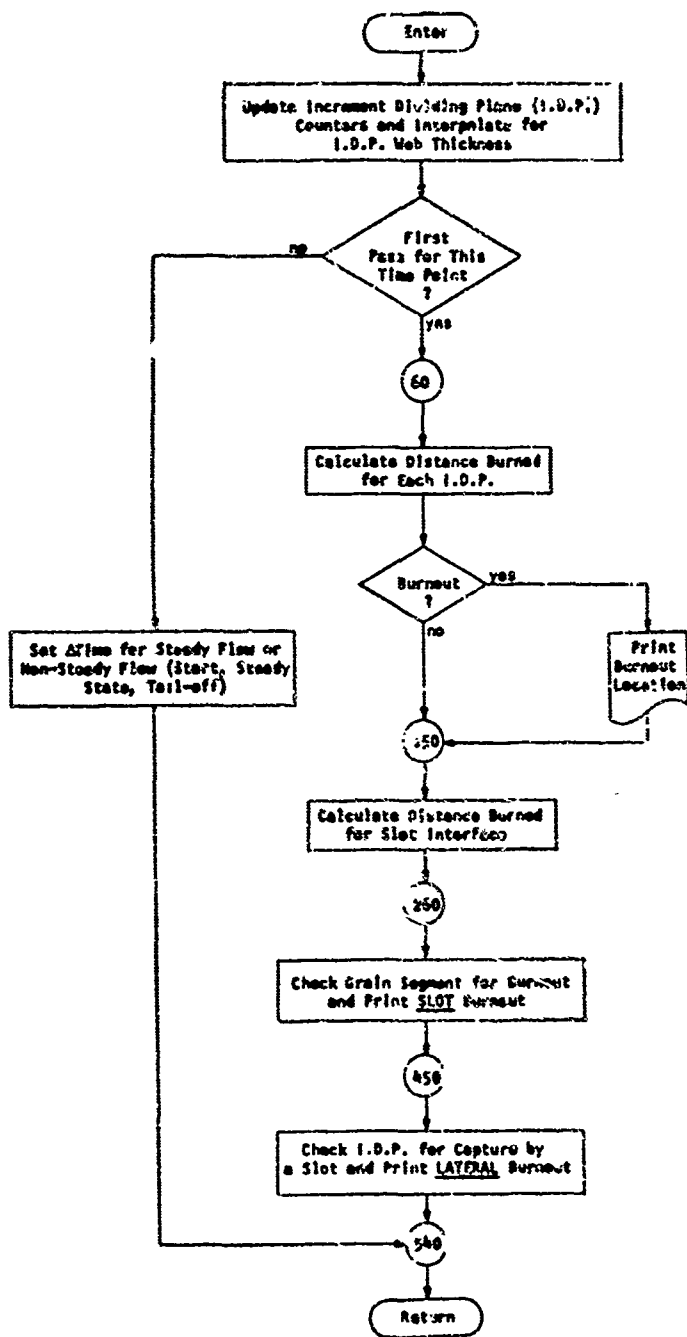




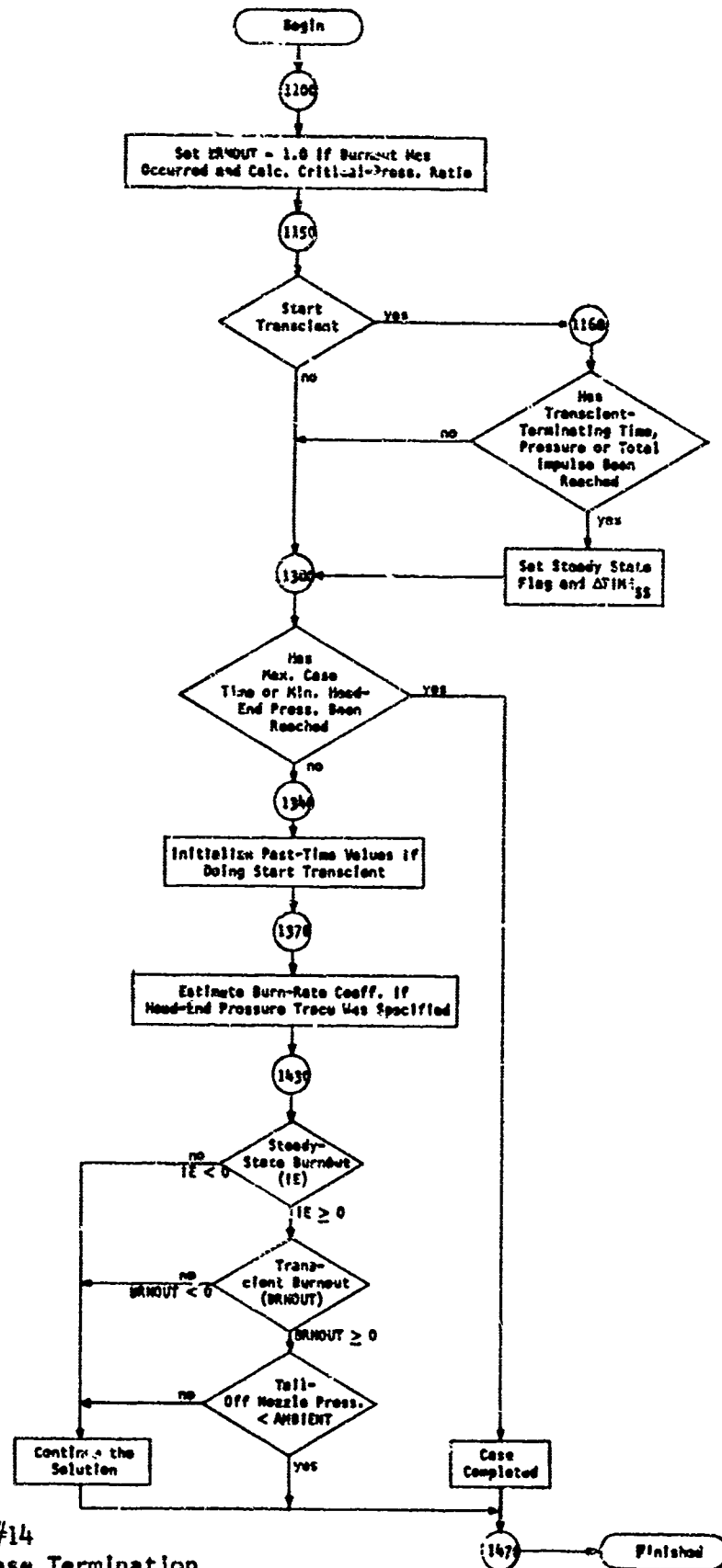
Flow Chart #11
Subroutine SEG4UB (2 of 2)



Flow Chart #12
Subroutine SETPH



Flow Chart #13
Subroutine TISUB



6.3 Storage Allocation and Computer System

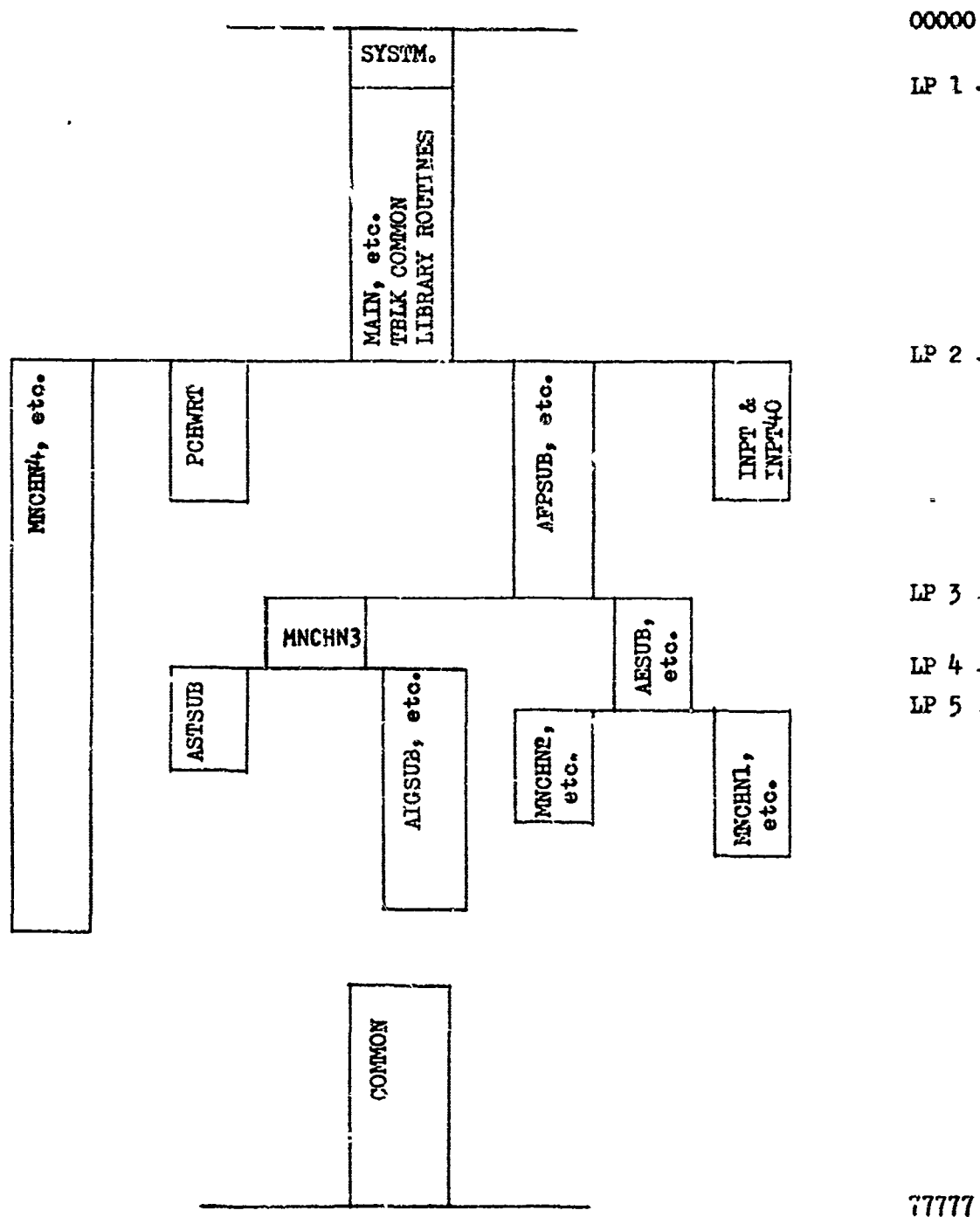
6.3.1 Storage Allocation

The program is divided into four core loads. Subsection 6.3.1.1 consists of a table showing which routines are required in each core load. Subsection 6.3.1.2 contains a diagram explaining the computer allocation of the program code and geometry tables. Subsection 6.3.1.3 contains both an alphabetical and a numerical listing of COMMON allocation. Subsection 6.3.1.4 contains a table which defines the labeled COMMON allocation of the geometry tables. Subsection 6.3.1.5 consists of the allocation map printed out by the computer system.

6.3.1.1 Subroutine Requirements for Each Core Load

Core Load					Core Load					Core Load				
Name	1	2	3	4	Name	1	2	3	4	Name	1	2	3	4
ACOS	X	X	X	X	LBSUB			X		SCI			X	
AEPSUB	X	X			LPDAPS	X	X	X		SCTOR1			X	
AESUB	X	X			LPTO			X		SCTOR2			X	
AFPSUB	X	X	X		MAIN	X	X	X	X	SD1D13	X	X	X	
AIBST				X	MNCHN1	X				SEGSUB				X
AIBSUB				X	MNCHN2		X			SETPH				X
AIGSUB			X		MNCHN3			X		SLOT				X
ALRSUB	X	X			MNCHN4				X	SPLN1A				X
ARSSUB	X	X			MODTSB				X	SPLN2A				X
ASESUB	X	X			MSISUB			X		SPLN3A				X
ASTSUB			X		MTISUB			X		SORT	X	X	X	X
ASUBC			X		OUTPUT				X	STUPPS			X	
AWESUB	X	X			PCHGIS	X				STUPRS			X	
BRKASB			X		PCHPL1	X				S2SK			X	
BSUBC			X		PLNCNS	X				TDGRE	X	X	X	
COMPSC	X	X	X	X	PLNLCS	X				THETAR			X	
CONV				X	POSUB			X		TISUB				X
CSTRSB				X	PTIAA	X	X	X		TRAN		X	X	X
DPRASB			X		PISUB			X		VFPPSB				X
ENDCSB	X				P3SUB			X		VOLSUB			X	
FDGRE	X	X	X		RASUB	X	X	X		VSEC			X	
GAMA2S			X		RASUBB			X		VSTRSB			X	
GAMSUB			X		RBSTSB				X	XRSUB	X	X	X	
HAPSBC			X		RBSUB				X	XRSUBB			X	
HASUBC			X		RBVSUB		X	X		XRTHR			X	
HBPSC			X		RCSUB	X	X	X		YPSUB			X	
HBSUBC			X		RGISUB			X		ZISUB			X	
HDNSUB			X		ROE1SB			X						
HESUB	X	X	X		ROPSB			X						
INPT	X				RSSPLN				X					

6.3.1.2 Schematic Diagram of Computer Storage Allocation



Notes:

1. Storage locations are in octal numbers.
2. Load points are located as follows:

LP 1 - 4252	LP 4 - 37625
LP 2 - 23672	LP 5 - 41563
LP 3 - 36743	

6.3.1.3

COMMON Allocation

The following pages contain output from a special Boeing Company pre-compiler which lists numerically and alphabetically those variables which are assigned to unlabeled COMMON through equivalence statements.

There are, in addition, two blocks of labeled common.

- 1) "TBIA" contains the geometry tables and is explained on page 199.
- 2) "CRITER" contains the three convergence criteria CRP, CRT and CRW in cells 1-3 respectively.



NUMERIC LISTING OF PROGRAM VARIABLES IN C04 ARRAY

1	AINC	2	ANO	3	RF	4	TAUM	5	R2	6	43
7	R4	8	R5	9	R6	10	R7	11	R8	12	ALSI
13	ALS2	14	ALA	15	ALB	16	ALE	17	AO	22	AINCA
24	RFA	25	TAUWA	43	AINCB	45	RFB	46	TAUWB	64	AINCC
66	RFC	67	TAUWC	85	AINCO	87	RFO	88	TAUWD	106	AINCE
102	RFE	109	TAUWE	122	AOE	127	AINCF	129	RFF	130	TAUWF
188	AINCG	150	RFG	151	TAUWG	169	AINCH	171	RFH	172	TAUWH
190	AINCI	192	RFI	193	TAUWI	211	AINCJ	213	RFJ	214	TAUWJ
232	AINCK	234	RFK	235	TAUWK	253	AINCN	254	REL	275	ALFEM
276	ALFE	277	RE2	278	HE1	279	HE2	280	HEO	281	HER
282	VFE0	283	VCE	284	TAUE0	285	TAUE1	286	CAE	287	CBE
288	CCCE	289	CCVF	290	CDCE	291	CDVE	292	CECE	293	CEVE
294	PH1	299	HH2	301	HRH	302	VFOH	303	VGH	314	RNI
320	MIR	323	VCH	334	A	339	R1	340	R9	341	TH1
342	T2	343	TAM	344	T5A	345	X45	346	Y45	347	ALC
348	X03	349	Y03	350	R03	351	X05	352	Y05	353	R05
354	X07	355	Y07	356	R07	357	T6M	358	T7M	359	T12M
360	X76	361	Y76	362	ALD	363	X09	364	Y09	365	R09
368	X011	367	Y011	368	X011	369	T10M	370	T9M	371	TAUM
372	TH2	373	TH3	374	TH4	375	T71M	376	B72M	377	B91M
378	B92M	379	AC	424	A3	469	AC	514	AD	559	AE
604	AF	649	AG	694	AH	739	AI	794	AJ	829	AK
874	AI	919	DE1	920	BE	921	AUEH	922	OH1	923	OH
925	DM1	928	BIADE	929	RIG	930	ANJ	931	HCO	932	GAMA
933	R	934	TO	935	AKK	936	DLRF	937	DLRF	938	DRRF
939	DRVRF	940	DELT	941	DELF	942	AKG	947	AKU	952	AKR
991	PA	992	DT	993	DE	994	UELLA	995	DELLM	996	AN2
997	CELIS	998	CM	999	AAK	1029	SPOP	1030	SYOT	1031	ANSIG
1032	PYPHY	1033	SC	1034	SCULT	1035	WP	1036	DELC	1037	DELLL
1038	DELIN	1039	PL	1040	SIGK	1041	TH1	1042	TLO	1043	TREF
1044	ANN	1045	SPE	1046	SN	1047	AN1	1048	BETA	1049	DELN
1050	DELME	1051	DELI	1052	PHI	1053	AMTJ	1054	AMTJ	1056	ANSJ
1051	ALPHO	1052	ALPHO	1053	WBE	1060	WLE	1061	WIG	1062	XRARIE
1063	WTE	1064	RHOLD	1065	TAUHD	1066	RHOLD	1067	RGF	1068	RGI
1069	YBARST	1070	AJSTP	1071	AJSTB	1072	WTST	1073	RGFB	1074	RGFB
1075	XBARBI	1076	XBARBF	1077	YV7	1078	TAUNEI	1079	XCGA	1080	XGCB
1081	ZRO	1082	ACGA	1083	ACGR	1084	RCGO	1085	ZCC	1086	YCG
1087	WISI	1088	TAUZ	1089	RPZ	1090	TAUZTO	1091	RBZTG	1092	TAUWOP
1093	PD	1094	PDPR	1095	V	1096	VPR	1097	AKRTAU	1098	TAUAKR
1197	CMPTHE	1199	MACCEL	1200	ACCELT	1201	TIMEA	1202	TIMEPS	1203	EPKA
1200	EPCU	1201	PPRESS	1202	TCOPB	1203	AWG	1204	CSTR	1205	GAMAG
1250	TIMEPH	1251	PHST	1252	SIA	1253	S2A	1254	S3A	1255	S4A
1295	S5A	1296	S6A	1297	S7A	1298	S8A	1299	S9A	1300	S10A
1301	S11A	1302	S12	1303	S2R	1304	S3B	1305	S4B	1306	S5B
1307	S6B	1308	S7B	1309	S8B	1310	S9B	1311	S10B	1312	S11B
1313	ABSLTA	1314	ARSLTF	1315	APA	1316	TABHA	1317	APF	1318	OWSLTA
1319	OWDTS	1320	TABHV	1321	OWSLTF	1322	PSA	1323	PSF	1324	TABNW
1325	POA	1326	POF	1327	RBSLTA	1328	RBSLTF	1329	RBRPL	1330	TABIV
1331	TSA	1332	TSF	1333	APORTX	1334	AFHI	1335	AKPH	1336	AKRN
1337	DELZ	1338	TITL	1339	CKNOMP	1340	KOUHP	1341	1SLVRN	1342	APORTA
1343	DIARST	1344	PCTAB	1345	TAUTOZ	1346	RSLVRN	1347	APORTF	1348	APORTG
1349	APORTS	1350	APORTC	1351	APORTD	1352	APORTE	1353	1SLVRB	1354	1SLVRB
1355	APORTH	1356	APORTJ	1357	APORTK	1358	APORTL	1359	1SLVRG	1360	1SLVRM
1361	1SLVRC	1362	1SLVRD	1363	1SLVRE	1364	1SLVRF	1365	1SLVRG	1366	1SLVRM
1367	1SLVRI	1368	1SLVRJ	1369	1SLVRK	1370	1SLVLA	1371	1SLVLY	1372	1SLVRX
1373	1SLVRX	1374	1SLVRX	1375	1SLVRX	1376	1SLVRX	1377	1SLVRX	1378	1SLVRX

NUMERIC LISTING

3083	TSLVR	3084	TSLVV	3085	TSLVRV	3086	ASLVR	3087	VFHPR	3088	STFLAG
3089	TRAX	3102	DELL	3103	DELO	3104	DELL	3106	ALITBE	3107	TAU
3108	VXK	3105	ALYD	3110	COUHT	3111	VFREWI	3112	VSTR	3113	VSTO
3114	VEX	3115	VR	3116	ASTO	3117	ASCMEK	3118	APD	3121	MEFC
3124	RC	3125	SUMOV	3126	XR	3131	DV	3132	HE	3133	SINA
3138	COSA	3143	KV2	3144	AV2	3145	AV3	3146	BV14	3147	BV2M
3148	TMV	3149	TV2	3150	TV4	3151	TV5	3152	TV6	3153	TV7
3154	ALVA	3155	ALV8	3156	ALVC	3157	RV2	3158	RV3	3159	RV4
3160	RV5	3161	RV7	3162	XV7	3163	APF	3165	AL	3177	AP
3178	DELL3	3179	DEL3	3180	DEL7	3181	871	3182	891	3183	AFD
3184	TAUSQ	3185	AER	3186	DELRV	3187	8V1	3188	BV2	3189	KRASUB
3190	KXRSUB	3215	AJUB	3216	KCG	3217	DELL	3219	RVI	3220	XEARIH
3241	XHAREN	3242	MCR	3243	KW11	3244	KW12	3245	LSW11	3246	LSW12
3247	AY	3248	TAUMX	3249	AY	3250	TAUMY	3251	AINCX	3252	RFX
3340	TAUMX	3356	AINCY	3360	RFV	3361	YAUDY	3362	PHYN	3363	PHAX
3381	RB	3383	PH	3384	TAUMT	3385	TAUNT	3386	AHO	3387	TIME
3389	ASE	3390	AHH	3391	VFN	3392	VF	3393	APHI	3394	AINCM
3395	T	3396	P	3397	DELTA	3398	CHDOT	3400	U	3401	AAN
3402	VFN	3403	ALPHI	3404	RHHT	3405	RFHI	3406	THOLD	3407	TAUMW
3409	ALPX	3410	APX	3411	ALPY	3412	APY	3413	MGOTI	3414	WDOT
3414	CAA	3415	CRB	3416	CC	3417	RAD	3418	Q190	3419	ANIBW
3420	TIMEW	3421	GCR	3422	UCR	3423	G	3424	THE	3425	MPB
3426	RT	3427	XRO	3428	RAX	3429	RAMAX	3430	AR	3431	AAR
3432	ATT	3433	ATO	3434	AF	3435	GAMAR	3436	AR	3437	GAMARO
3438	ARO	3439	APE	3440	RAVIN	3441	ALRI	3442	HEI	3443	ALAMIN
3444	XFC	3445	GAMAT	3446	AF	3447	AFY	3448	PLIT	3449	GLIT
3450	PLIT	3451	SLIT	3452	RIE	3453	BOE	3454	ALRIAX	3455	UY
3458	TAINLST	3462	ARIGR	3463	ASHOLD	3467	PHOLD	3469	DLTHP	3469	PIMP
3470	TT-P	3471	ITNP	3472	AJRH	3473	AJRH	3474	XBARI	3475	WI
3476	WT	3477	PA	3478	RAO	3479	THRI	3480	ALL	3481	ALSX
3482	AKGY	3483	AJPP	3484	XJH	3485	ADNCYL	3486	AIGCYL	3487	AIPCYL
3488	AKGYH	3489	AKGYX	3490	AKGY	3491	WTH	3492	WTN	3493	AKRIP
3494	AKRFP	3495	AKRIB	3496	AKRFB	3497	AJPH	3498	AJPH	3499	TAUZO
3500	AJPHI	3501	AJBHN	3502	AJBHD	3503	AJBHD	3504	AJBNOZ	3505	AJBNOZ
3506	AJBHEH	3507	AJBHEH	3508	XRH	3509	XBN	3510	XBHEW	3511	APX
3512	FHOF	3513	OTINT	3514	ALAPN	3516	CEMPC	3517	TSS	3518	AMBSS
3519	CFC	3520	A-BSU	3521	EXP1	3522	PSOPO	3523	GPI	3524	GMI
3525	CODET	3526	WIS	3527	VTS	3528	CODEB	3529	AIT	3530	PHMAX
3531	SPHOT	3532	SPHODT	3533	WR	3534	VFINT	3535	VPINT	3536	VFPF
3537	POI	3538	OTS	3539	AMQSE	3540	OTS	3541	OELF	3544	AMPN
3545	AT	3546	F	3547	EPG	3548	EPS	3549	EPI	3550	PEPO
3551	PEPO2	3552	CFOL	3553	VE	3554	FVAG	3555	FAVGB	3556	VFEB
3557	YAREH	3558	PHAVMB	3559	POHAW	3560	ATAVG	3561	AISPWB	3562	CFVL
3563	FX	3564	PHR	3565	POH	3566	TX	3567	ATHAX	3568	GNOY
3570	HD	3571	DEED	3572	OTSR	3574	DTSC	3576	WOR	3588	CLOPS
3589	RSSTOR	3590	OTMAX	3591	OTTHN	3592	ANITW	3593	COOTI	3594	CSTAR
3595	TIMEW	3596	DTWR	3597	OTTOR	3598	ANNN	3599	TOMAX	3600	OOIA
3601	OOIB	3602	XMAX	3603	ZMAX	3604	YMAX	3605	DWB	3606	DSI
3607	PS2	3608	XWB	3609	ZG	3610	ALHO	3613	TNH	3614	X11A
3615	X11B	3616	Y11A	3617	Y11B	3618	PK	3619	RXX	3620	AS11
3644	HOLDR	3645	DELLY	3646	ALYX	3648	GMAZO	3655	THRX	3656	SI
3657	O2	3658	RFZ	3659	XP	3660	AZ	3662	DELLOI	3664	ASI
3665	ALSURX	3669	VFH	3674	ALL2	3675	RAT	3676	XRT	3677	THR
3677	GAVAL	3678	GMAZ	3679	DPR	3680	UPS	3681	DPRR	3682	OPSA
3683	DPRB	3684	DPSR	3685	ROPE1	3686	ROPE2	3687	ROPE3	3688	ROPE4
3689	AL3A	3690	BRAX	3691	AL11A	3692	AS	3694	RPX	3697	AIE
3700	ZINT	3702	PHYI	3703	YAI	3712	CO3	3789	ALIP	3792	YPO
3798	AAA	3799	528	3800	CCC	3814	YI	3838	ZPO	3839	YPO

3840	ZP1	3841	YPI	3842	DS	3843	ARCO	3844	ARC1	3845	ROE1
3846	ALITL	3847	ZI	3848	ALO	3849	AIG	3850	THRI	3851	ALP
3852	THRO	3853	THRZ	3854	YNO	3855	ARN	3856	XP1	3857	YPI
3858	RP1	3859	XP2	3860	YP3	3861	RP2	3862	XP3	3863	YP3
3864	RP3	3865	XP4	3866	YP4	3867	RP4	3868	XP5	3869	YP5
3870	RP5	3871	XP6	3872	YP6	3873	RP6	3874	XP13	3875	YP13
3876	RP13	3877	XP12	3878	YP12	3879	RP12	3880	XP11	3881	YP11
3882	RP11	3883	XP10	3884	YP10	3885	RP10	3886	XP10	3887	YP10
3889	KGAM	3890	KBRK	3891	ANRA	3892	ANYOB	3893	KRASBB	3894	KRESBB
3895	ANZ1A	3896	ANRAB	3897	ANX2A	3898	ANXOB	3899	ANY1B	3900	ANZOB
3902	ANX1B	3903	ANZ1B	3904	ANX2B	3905	ANXOB	3906	ANZ1B	3907	ANZOB
3908	ANZOA	3909	ANX1A	3910	ANX2A	3911	ANXOB	3912	ANZ1A	3913	ANZOB
3914	ANZOB	3915	ANX1B	3916	ANX2B	3917	ANXOB	3918	ANZ1B	3919	ANZOB
3920	ANZOA	3921	ANX1A	3922	ANX2A	3923	ANXOB	3924	ANZ1A	3925	ANZOB
3926	ANZOB	3927	ANX1B	3928	ANX2B	3929	ANXOB	3930	ANZ1B	3931	ANZOB
3932	ANZOA	3933	ANX1A	3934	ANX2A	3935	ANXOB	3936	ANZ1A	3937	ANZOB
3938	ANZOB	3939	ANX1B	3940	ANX2B	3941	ANXOB	3942	ANZ1B	3943	ANZOB
3944	ANZOA	3945	ANX1A	3946	ANX2A	3947	ANXOB	3948	ANZ1A	3949	ANZOB
3950	ANZOB	3951	ANX1B	3952	ANX2B	3953	ANXOB	3954	ANZ1B	3955	ANZOB
3956	ANZOA	3957	ANX1A	3958	ANX2A	3959	ANXOB	3960	ANZ1A	3961	ANZOB
3962	ANZOB	3963	ANX1B	3964	ANX2B	3965	ANXOB	3966	ANZ1B	3967	ANZOB
3968	ANZOA	3969	ANX1A	3970	ANX2A	3971	ANXOB	3972	ANZ1A	3973	ANZOB
3974	ANZOB	3975	ANX1B	3976	ANX2B	3977	ANXOB	3978	ANZ1B	3979	ANZOB
3980	ANZOA	3981	ANX1A	3982	ANX2A	3983	ANXOB	3984	ANZ1A	3985	ANZOB
3986	ANZOB	3987	ANX1B	3988	ANX2B	3989	ANXOB	3990	ANZ1B	3991	ANZOB
3992	ANZOA	3993	ANX1A	3994	ANX2A	3995	ANXOB	3996	ANZ1A	3997	ANZOB
3998	ANZOB	3999	ANX1B	4000	ANX2B	4001	ANXOB	4002	ANZ1B	4003	ANZOB
4004	ANZOA	4005	ANX1A	4006	ANX2A	4007	ANXOB	4008	ANZ1A	4009	ANZOB
4010	ANZOB	4011	ANX1B	4012	ANX2B	4013	ANXOB	4014	ANZ1B	4015	ANZOB
4016	ANZOA	4017	ANX1A	4018	ANX2A	4019	ANXOB	4020	ANZ1A	4021	ANZOB
4022	ANZOB	4023	ANX1B	4024	ANX2B	4025	ANXOB	4026	ANZ1B	4027	ANZOB
4028	ANZOA	4029	ANX1A	4030	ANX2A	4031	ANXOB	4032	ANZ1A	4033	ANZOB
4034	ANZOB	4035	ANX1B	4036	ANX2B	4037	ANXOB	4038	ANZ1B	4039	ANZOB
4040	ANZOA	4041	ANX1A	4042	ANX2A	4043	ANXOB	4044	ANZ1A	4045	ANZOB
4046	ANZOB	4047	ANX1B	4048	ANX2B	4049	ANXOB	4050	ANZ1B	4051	ANZOB
4052	ANZOA	4053	ANX1A	4054	ANX2A	4055	ANXOB	4056	ANZ1A	4057	ANZOB
4058	ANZOB	4059	ANX1B	4060	ANX2B	4061	ANXOB	4062	ANZ1B	4063	ANZOB
4064	ANZOA	4065	ANX1A	4066	ANX2A	4067	ANXOB	4068	ANZ1A	4069	ANZOB
4070	ANZOB	4071	ANX1B	4072	ANX2B	4073	ANXOB	4074	ANZ1B	4075	ANZOB
4076	ANZOA	4077	ANX1A	4078	ANX2A	4079	ANXOB	4080	ANZ1A	4081	ANZOB
4082	ANZOB	4083	ANX1B	4084	ANX2B	4085	ANXOB	4086	ANZ1B	4087	ANZOB
4088	ANZOA	4089	ANX1A	4090	ANX2A	4091	ANXOB	4092	ANZ1A	4093	ANZOB
4094	ANZOB	4095	ANX1B	4096	ANX2B	4097	ANXOB	4098	ANZ1B	4099	ANZOB
4100	ANZOA	4101	ANX1A	4102	ANX2A	4103	ANXOB	4104	ANZ1A	4105	ANZOB
4106	ANZOB	4107	ANX1B	4108	ANX2B	4109	ANXOB	4110	ANZ1B	4111	ANZOB
4112	ANZOA	4113	ANX1A	4114	ANX2A	4115	ANXOB	4116	ANZ1A	4117	ANZOB
4118	ANZOB	4119	ANX1B	4120	ANX2B	4121	ANXOB	4122	ANZ1B	4123	ANZOB
4124	ANZOA	4125	ANX1A	4126	ANX2A	4127	ANXOB	4128	ANZ1A	4129	ANZOB
4130	ANZOB	4131	ANX1B	4132	ANX2B	4133	ANXOB	4134	ANZ1B	4135	ANZOB
4136	ANZOA	4137	ANX1A	4138	ANX2A	4139	ANXOB	4140	ANZ1A	4141	ANZOB
4142	ANZOB	4143	ANX1B	4144	ANX2B	4145	ANXOB	4146	ANZ1B	4147	ANZOB
4148	ANZOA	4149	ANX1A	4150	ANX2A	4151	ANXOB	4152	ANZ1A	4153	ANZOB
4154	ANZOB	4155	ANX1B	4156	ANX2B	4157	ANXOB	4158	ANZ1B	4159	ANZOB
4160	ANZOA	4161	ANX1A	4162	ANX2A	4163	ANXOB	4164	ANZ1A	4165	ANZOB
4166	ANZOB	4167	ANX1B	4168	ANX2B	4169	ANXOB	4170	ANZ1B	4171	ANZOB
4172	ANZOA	4173	ANX1A	4174	ANX2A	4175	ANXOB	4176	ANZ1A	4177	ANZOB
4178	ANZOB	4179	ANX1B	4180	ANX2B	4181	ANXOB	4182	ANZ1B	4183	ANZOB
4184	ANZOA	4185	ANX1A	4186	ANX2A	4187	ANXOB	4188	ANZ1A	4189	ANZOB
4190	ANZOB	4191	ANX1B	4192	ANX2B	4193	ANXOB	4194	ANZ1B	4195	ANZOB
4196	ANZOA	4197	ANX1A	4198	ANX2A	4199	ANXOB	4200	ANZ1A	4201	ANZOB
4202	ANZOB	4203	ANX1B	4204	ANX2B	4205	ANXOB	4206	ANZ1B	4207	ANZOB
4208	ANZOA	4209	ANX1A	4210	ANX2A	4211	ANXOB	4212	ANZ1A	4213	ANZOB
4214	ANZOB	4215	ANX1B	4216	ANX2B	4217	ANXOB	4218	ANZ1B	4219	ANZOB
4220	ANZOA	4221	ANX1A	4222	ANX2A	4223	ANXOB	4224	ANZ1A	4225	ANZOB
4226	ANZOB	4227	ANX1B	4228	ANX2B	4229	ANXOB	4230	ANZ1B	4231	ANZOB
4232	ANZOA	4233	ANX1A	4234	ANX2A	4235	ANXOB	4236	ANZ1A	4237	ANZOB
4238	ANZOB	4239	ANX1B	4240	ANX2B	4241	ANXOB	4242	ANZ1B	4243	ANZOB
4244	ANZOA	4245	ANX1A	4246	ANX2A	4247	ANXOB	4248	ANZ1A	4249	ANZOB
4250	ANZOB	4251	ANX1B	4252	ANX2B	4253	ANXOB	4254	ANZ1B	4255	ANZOB
4256	ANZOA	4257	ANX1A	4258	ANX2A	4259	ANXOB	4260	ANZ1A	4261	ANZOB
4262	ANZOB	4263	ANX1B	4264	ANX2B	4265	ANXOB	4266	ANZ1B	4267	ANZOB
4268	ANZOA	4269	ANX1A	4270	ANX2A	4271	ANXOB	4272	ANZ1A	4273	ANZOB
4274	ANZOB	4275	ANX1B	4276	ANX2B	4277	ANXOB	4278	ANZ1B	4279	ANZOB
4280	ANZOA	4281	ANX1A	4282	ANX2A	4283	ANXOB	4284	ANZ1A	4285	ANZOB
4286	ANZOB	4287	ANX1B	4288	ANX2B	4289	ANXOB	4290	ANZ1B	4291	ANZOB
4292	ANZOA	4293	ANX1A	4294	ANX2A	4295	ANXOB	4296	ANZ1A	4297	ANZOB
4298	ANZOB	4299	ANX1B	4300	ANX2B	4301	ANXOB	4302	ANZ1B	4303	ANZOB
4304	ANZOA	4305	ANX1A	4306	ANX2A	4307	ANXOB	4308	ANZ1A	4309	ANZOB
4310	ANZOB	4311	ANX1B	4312	ANX2B	4313	ANXOB	4314	ANZ1B	4315	ANZOB
4316	ANZOA	4317	ANX1A	4318	ANX2A	4319	ANXOB	4320	ANZ1A	4321	ANZOB
4322	ANZOB	4323	ANX1B	4324	ANX2B	4325	ANXOB	4326	ANZ1B	4327	ANZOB
4328	ANZOA	4329	ANX1A	4330	ANX2A	4331	ANXOB	4332	ANZ1A	4333	ANZOB
4334	ANZOB	4335	ANX1B	4336	ANX2B	4337	ANXOB	4338	ANZ1B	4339	ANZOB
4340	ANZOA	4341	ANX1A	4342	ANX2A	4343	ANXOB	4344	ANZ1A	4345	ANZOB
4346	ANZOB	4347	ANX1B	4348	ANX2B	4349	ANXOB	4350	ANZ1B	4351	ANZOB
4352	ANZOA	4353	ANX1A	4354	ANX2A	4355	ANXOB	4356	ANZ1A	4357	ANZOB
4358	ANZOB	4359	ANX1B	4360	ANX2B	4361	ANXOB	4362	ANZ1B	4363	ANZOB
4364	ANZOA	4365	ANX1A	4366	ANX2A	4367	ANXOB	4368	ANZ1A	4369	ANZOB
4370	ANZOB	4371	ANX1B	4372	ANX2B	4373	ANXOB	4374	ANZ1B	4375	ANZOB
4376	ANZOA	4377	ANX1A	4378	ANX2A	4379	ANXOB	4380	ANZ1A	4381	ANZOB
4382	ANZOB	4383	ANX1B	4384	ANX2B	4385	ANXOB	4386	ANZ1B	4387	ANZOB
4388	ANZOA	4389	ANX1A	4390	ANX2A	4391	ANXOB	4392	ANZ1A	4393	ANZOB
4394	ANZOB	4395	ANX1B	4396	ANX2B	4397	ANXOB	4398	ANZ1B	4399	ANZOB
4400	ANZOA	4401	ANX1A	4402	ANX2A	4403	ANXOB	4404	ANZ1A	4405	ANZOB
4406	ANZOB	4407	ANX1B	4408	ANX2B	4409	ANXOB	4410	ANZ1B	4411	ANZOB
4412	ANZOA	4413	ANX1A	4414	ANX2A	4415	ANXOB	4416	ANZ1A	4417	ANZOB
4418	ANZOB	4419	ANX1B	4420	ANX2B	4421	ANXOB	4422	ANZ1B	4423	ANZOB
4424	ANZOA	4425	ANX1A	4426	ANX2A	4427	ANXOB	4428	ANZ1A	4429	ANZOB
4430	ANZOB	4431	ANX1B	4432	ANX2B	4433	ANXOB	4434	ANZ1B	4435	ANZOB
4436	ANZOA	4437	ANX1A	4438	ANX2A	4439	ANXOB	4440	ANZ1A	4441	ANZOB
4442	ANZOB	4443	ANX1B	4444	ANX2B	4445	ANXOB	4446	ANZ1B	4447	ANZOB
4448	ANZOA	4449	ANX1A	4450	ANX2A	4451	ANXOB	4452	ANZ1A	4453	ANZOB
4454	ANZOB	4455	ANX1B	4456	ANX2B	4457	ANXOB	4458	ANZ1B	4459	ANZOB
4460	ANZOA	4461	ANX1A	4462	ANX2A	4463	ANXOB	4464	ANZ1A	4465	ANZOB
4466	ANZOB	4467	ANX1B	4468	ANX2B	4469	ANXOB	4470	ANZ1B	4471	ANZOB
4472	ANZOA	4473	ANX1A	4474	ANX2A	4475	ANXOB	4476	ANZ1A	4477	ANZOB
4478	ANZOB	4479	ANX1B	4480	ANX2B	4481	ANXOB	4482	ANZ1B	4483	ANZOB
4484	ANZOA	4485	ANX1A	4486	ANX2A	4487	ANXOB	4488	ANZ1A	4489	ANZOB
4490	ANZOB	4491	ANX1B	4492	ANX2B	4493	ANXOB	4494	ANZ1B	4495	ANZOB
4496	ANZOA	4497	ANX1A	4498	ANX2A	4499	ANXOB	4500	ANZ1A	4501	ANZOB
4502	ANZOB	4503	ANX1B	4504	ANX2B	4505	ANXOB	4506	ANZ1B	4507	ANZOB
4508	ANZOA	4509	ANX1A	4510	ANX2A	4511	ANXOB	4512	ANZ1A	4513	ANZOB
4514	ANZOB	4515	ANX1B	4516	ANX2B	4517	ANXOB	4518	ANZ1B	4519	ANZOB

4539	ISI	4540	152	4541	KPLANE	4542	TAURPL	4555	NPLANE	4556	PI
4557	PI02	4558	TH0	4559	TH0A	4560	TH0B	4561	TH0C	4562	TH0D
4563	TH0E	4564	TH0F	4565	TH0G	4566	TH0H	4567	TH0I	4568	TH0J
4569	TH0K	4570	TH0W	4571	TSLOTA	4582	TSLOTF	4593	WDSLOT	4594	WISLOT
4595	NT	4596	NABRNH	4604	NABRNH	4612	NKGYPG	4620	NKGYPB	4628	NKGYPG
4636	NKGYPD	4644	NKGYPE	4652	NKGYPF	4660	NKGYPG	4668	NKGYPH	4676	NKGYPJ
4684	NKGYPK	4692	NKGYPK	4708	NKGYPK	4716	NKGYPK	4724	NKGYPK	4732	NKGYPK
4740	NKGYPK	4744	ANUG	4748	NKGYPK	4756	NKGYPK	4764	NKGYPK	4772	NKGYPK
4760	NKGYPK	4768	NKGYPK	4776	NKGYPK	4784	NKGYPK	4792	NKGYPK	4800	NKGYPK
4845	PHIT	6360	MCFLAG	6361	ISET	6371	TH0W	6441	GEOM	6442	AKRFLG
6443	PPTAIR	6444	WGPORT	6445	NGTOT	6446	SWDOTN	6447	AICHMI	6448	AMACH
6449	ANACHO	6450	PSAPR	6460	PSFPR	6470	SCUR	6498	PRCRIT	6499	ZCALC

NUMBER OF VARIABLES = 1104

NUMERIC LISTING (CONTINUED)

ALPHABETIC LISTING OF PROGRAM VARIABLES IN COM ARRAY

A	334	AA	379	AAA	796	AAAA	4005	AAV	999	AAW	3461
AANN	3558	AAP	4097	AB	424	ABB	4051	ABGR	4430	ABIGR	3462
ABF	4113	ABSLTA	2760	ABSLIF	2771	ABTOT	2771	AC	4429	AC	469
ACCEL	4415	ACCEL	2200	ACDA	1082	ACGE	1083	AD	3953	AD	519
AE	559	AEE	3439	AER	3185	AF	604	AFF	3183	AFF	3434
AFHI	2937	AF	3163	AFRPLA	4485	AFRPLB	4486	AFRPLC	4487	AFRPLD	4488
AFRPLE	4489	AFRPLF	4490	AFRPLG	4491	AFRPLH	4492	AFRPLI	4493	AFRPLJ	4494
AFRPLK	4495	AFRPLX	4496	AFX	3446	AFY	3447	AG	649	AG	694
AHI	3390	AHO	3386	AI	739	AIBCYL	3486	AIG	3849	AINC	1
AIRCA	22	AICB	43	AICCC	64	AICCD	65	AINCE	106	AINCF	127
AIRCG	148	AICCH	169	AICCHI	647	AINCI	190	AINCK	211	AINCK	232
AIRCN	253	AINCPL	4497	AINCW	3394	AINCX	3337	AINCY	3358	AIPCYL	3407
AISPNS	3561	AIT	3529	AITST	4436	AJ	194	AJBB	3215	AJBN	3473
AJBHED	3503	AJBHEW	3577	AJBHPI	3501	AJBHO	1758	AJBHJ	3472	AJBHOZ	3505
AJBH	3498	AJBHEO	3502	AJBHEW	3506	AJBHN	3506	AJBHJ	1057	AJBPN	3497
AJPNZ	3504	AJPP	3483	AJPH	3512	AJSTB	1071	AJSTP	1070	AK	829
AKG	942	AKGY	3482	AKGYHI	3488	AKGYX	3489	AKK	3490	AKK	935
AKR	952	AKRFB	3496	AKRELG	6442	AKREP	3494	AKRIB	3050	AKRIB	3495
AKRIP	3493	AKRN	3031	AKRST	4437	AKRTAU	1997	AKU	4498	AKU	947
AL	3164	ALA	14	ALAMDA	4266	ALAMIN	3443	ALB	3514	ALB	15
ALC	347	ALO	762	ALOP	3789	ALE	16	ALFE	276	ALFEM	275
ALMO	3610	ALITBE	3106	ALITO	3109	ALITTL	3846	ALL	3480	ALLQ	3670
ALP	351	ALPHI	3403	ALPPA	4500	ALPRB	4501	ALRPC	4502	ALPRPD	4503
ALPPE	4504	ALPRPF	4505	ALPRPG	4506	ALPRPH	4507	ALPRPI	4508	ALPRPJ	4509
ALPRPK	4510	ALPRPO	4511	ALPX	3408	ALPY	3410	ALQ	3846	ALR	3431
ALRI	3454	ALRWAX	4514	ALRS	3430	ALSI	12	ALSUEY	3665	ALSX	3461
ALS2	13	ALTA	4014	ALTAP	4106	ALTA	4060	ALIBP	4152	ALVA	3154
ALV5	3155	ALVC	3156	ALX	4255	ALXX	3648	ALIA	3691	ALJA	3569
AL7	4400	ALB	4401	AMACH	6444	AMACHD	6449	AMBSE	3539	AMBSS	3518
AMBSU	3520	AMEN	3544	AMSI	1087	AMSV	1056	AMTI	1054	AMTU	1053
AMUG	4744	AMW	4407	AMWG	2490	AN	874	ANAB	3959	ANAB	3960
AMBA	3961	AMRR	3962	AMTAO	3967	ANCA	3963	ANCB	3964	ANCA	3965
AMDR	3966	ANI	930	ANIBO	3418	ANIGW	3419	ANITW	3592	ANLOPS	4363
ANI	1044	ANO	2	ANRAA	3931	ANRAB	3936	ANSIG	1031	ANXOA	3947
ANXOB	3939	ANX1A	3949	ANX1B	3942	ANX2A	3937	ANX2B	1031	ANXOA	3947
ANYOB	3932	ANY1A	3950	ANY1B	3940	ANY2A	3934	ANY2B	1031	ANYOA	3948
ANZOB	3941	ANZ1A	3935	ANZ1B	3943	ANZ2B	3945	ANL	1047	AN2	396
AO	17	AOE	122	AOEM	921	AOMCYL	3485	AP	3177	APA	2782
APF	2793	APHI	3393	APD	3116	APORTA	3054	APORTB	3057	APORTC	3058
APORTD	3059	APORTE	3060	APORTF	3061	APORTG	3062	APORTH	3063	APORTI	3064
APORTJ	3065	APORTK	3066	APORTX	2936	APX	3409	APY	3411	AR	3436
ARCO	3863	ARC1	3844	AR	3855	ARO	3438	AS	3692	ASCHEK	3117
ASE	3369	ASHOLD	3463	ASI	3664	ASINTR	3952	AST	3620	ASLVR	3086
ASTO	3116	AT	3545	ATANG2	3951	ATANP1	3957	ATAVG	3560	ATMAX	3557
ATO	3433	ATISLOT	2938	ATT	3432	AV1	3143	AV2	3144	AV3	3147
AWE	3444	AX	3247	AY	3292	AZ	3660	AIE	3697	BA	4006
BAP	4098	FR	4052	BBB	3799	BBP	4144	BCOSTR	3955	BE	920
BETA	1048	BH	923	BHOLD	1064	BHNTAO	3968	BOE	3453	BRAB	3690
BRNOJY	4421	BSINTR	3954	BTANG2	3956	BTANP1	3958	BTAOA	4009	BTACAP	4101
BTACON	4055	BTACBP	4147	BTACOE	928	BVAX	4412	BV1	4413	BV1	3187
BVIM	3146	BV2	3188	BV2M	3147	BX	3618	BIE	3452	B71	3181
B7IM	375	B72M	376	B91	3182	B914	377	B92M	378	CA	4007
CAA	3414	CAE	284	CAP	4099	CR	4053	CBE	3415	CBE	287
CCP	4145	CC	3416	CCC	3800	CCCE	288	CCVE	289	CDCE	290
COVE	291	CECE	292	CEMPC	3516	CEVE	293	CFC	3519	CF1Y	3417
CFO	4406	CFOL	3552	CFVL	3562	CKDAMP	2952	CLOPS	1548	CV	398

ALPHABETIC LISTING

X76	360	YA1	3703	YCG	1086	YI	3813	YMAX	3604	YUJ	3854
Y0	4157	Y0A	3978	Y0AP	4070	Y0B	4024	Y0EP	4126	Y011	367
Y03	349	Y05	352	Y07	355	Y09	364	Y01	3851	Y00	3839
Y01	3857	Y010	3884	Y011	3881	Y012	3878	Y013	3875	Y02	3860
Y03	3863	Y04	3866	Y05	3869	Y06	3872	Y00	3742	Y07	1077
Y1	4163	Y1A	3984	Y1AP	4076	Y1B	4030	Y1BP	4122	Y11A	3616
Y118	3617	Y2A	3981	Y2AP	4073	Y2B	4027	Y2BP	4119	Y3	4166
Y3A	3987	Y3D	4033	Y45	346	Y76	361	ZCALC	6499	ZCG	1085
Z6	3609	Z1	3847	ZMAX	3603	Z0	4158	Z0A	3479	Z0AP	4071
Z08	4025	Z0RP	4117	ZP0	3838	ZP1	3840	ZR0	1051	Z1	4164
Z1A	3985	Z1AP	4077	Z1AT	3761	Z13	4031	Z1BP	4123	Z2A	3982
Z2AP	4074	Z2B	4028	Z2BP	4120	Z3	4167	Z3A	3488	Z3B	4034

NUMBER OF VARIABLES = 1104

ALPHABETIC LISTING (CONTINUED)

6.3.1.4

Geometry Table Storage
(Labeled COMMON Block "TRLK")

Plane	NGEOM_	TAUPL_	ALPPL_	AKGYP_		
X	1	2	52	102		
A	152	153	203	253		
B	303	304	354	404		
C	454	455	505	555		
D	605	606	656	706		
E	756	757	807	857		
F	907	908	958	1008		
G	1058	1059	1109	1159		
H	1209	1210	1260	1310		
I	1360	1361	1411	1461		
J	1511	1512	1562	1612		
K	1662	1663	1713	1763		
End	NGEOM_	TAU_	AB_	PMOI_	RMOI_	XCG_
E	1813	1814	1864	1914	1964	2014
H	2064	2065	2115	2165	2215	2265
N	2315	2316	2366	2416	2466	2516

End Table Variable Names

NGEOM	PMOI
NGEOMD	PMOID
NGEOMN	PMOIN
TAUEND	RMOI
TAUHD	RMOID
TAUN	RMOIN
ABEND	XCGE
ABHD	XCGHD
ABN	XCGN

Table Control Variables

Name	Location
NWRTAB	2566
NPOTAB	2567
GEOM	2568
IDTAB(1)	2569

6.3.1.5

Monitor System Allocation Map

ISLDP

02/21/87

PAGE 2

OVERLAY CRIGIN CPODS AND ASSIGNED LINK NUMBERS

ORIGIN	LOPT2	IS LINK	1, PARENT LINK IS	0
ORIGIN	LOPT2	IS LINK	2, PARENT LINK IS	0
ORIGIN	LOPT2	IS LINK	3, PARENT LINK IS	0
ORIGIN	LOPT3	IS LINK	4, PARENT LINK IS	3
ORIGIN	LOPT4	IS LINK	5, PARENT LINK IS	4
ORIGIN	LOPT4	IS LINK	6, PARENT LINK IS	4
ORIGIN	LOPT3	IS LINK	7, PARENT LINK IS	4
ORIGIN	LOPT5	IS LINK	8, PARENT LINK IS	7
ORIGIN	LOPT5	IS LINK	9, PARENT LINK IS	7
ORIGIN	LOPT2	IS LINK	10, PARENT LINK IS	0

31

02/21/67

10100

ALR	37550	EVEN	37551	ALRSUB	37630				
ARS	37660	EVEN	37661	ARSSUB	37746				
ASE	40000	///	/(63016)	EVEN	40001	ASESUB	40345		
AHE	40363	///	/(63016)	AMESUM	41175				
<hr/>									
5									
MCH1	41207	///	/(63016)	7TBLK	/(104254)	MCHM1	43053		
ENOC	43071	///	/(63016)	EMOCSB	44167				
PCMG1	44204	///	/(63016)	EVEN	44707	PCMG15	44719		
PCMPL	44731	///	/(63016)	PCMPL1	45124				
PLMCH	49140	///	/(63016)	EVEN	45141	PLMCH5	47030		
PLMCL	47644	///	/(63016)	EVEN	47645	PLMCL5	47651		
<hr/>									
6									
MCH2	41207	///	/(63016)	7TBLK	/(104254)	MCHM2	43167		
<hr/>									
7									
MCH3	36367	///	/(63016)	7TBLK	/(104254)	MCHM3	37232		
<hr/>									
8									
ATR	37546	///	/(63016)	EVEN	37247	ATGSUB	37411		
ASUMC1	37423	///	/(63016)	ASUMC	37514				
BRAS	37424	///	/(63016)	EVEN	37527	BRASB	37627		
BSUMC1	37441	///	/(63016)	BSUMC	37732				
DPR4	37744	///	/(63016)	EVEN	37745	DPRASB	40017		
GAR	40031	///	/(63016)	GAMSUB	40210				
GAR2	40225	///	/(63016)	EVEN	40223	GAMA25	40934		
HAP	40340	///	/(63016)	EVEN	40347	HAPSOC	40447		
MA	40461	///	/(63016)	HASUMC	40561				
MAS	40573	///	/(63016)	HAPSAC	40673				
MA	40705	///	/(63016)	HBSUMC	41005				
MDM	41017	///	/(63016)	HONSUB	41243				
LA	41261	///	/(63016)	LSUB	41311				
MS1	41324	///	/(63016)	MS1SUB	41666				
MT1	41740	///	/(63016)	EVEN	41701	MT1SUB	42260		
PO	42272	///	/(63016)	EVEN	42273	POSUB	42401		
P1	42413	///	/(63016)	P1SUB	42671				
P1	42703	///	/(63016)	P3SUB	43114				
R44	43140	///	/(63016)	EVEN	43131	RASUB	44241		
RNP1	44253	///	/(63016)	ROELSA	44352				
RNP	44364	///	/(63016)	EVEN	44365	RNP18	44442		
SC11	44456	///	/(63016)	EVEN	44457	SCI	47314		
SC1MPA	47331	///	/(63016)	SC1OR1	50650				
SC1MPR	50652	///	/(63016)	EVEN	50653	SC1OR2	50734		
STUPR	50750	///	/(63016)	EVEN	50751	STUPPS	51077		
STUPR	51111	///	/(63016)	STUPRS	51230				
S2R1	51250	///	/(63016)	EVEN	51251	S2SK	52371		
TMFTR	52405	///	THFTAB	52445					
VOL	52472	///	/(63016)	EVFN	52473	VOLSUR	53231		
VSECL	53245	///	/(63016)	VSEC	54110				
V570	53246	///	/(63016)	EVFN	54125	V57R5K	54505		
XRA	54517	///	/(63016)	XRSUB	54545				
XATHM1	54657	///	/(63016)	XRTMR	55540				
VP	54954	///	EVFN	55554	VP5UR	55675			
Z1	55737	///	/(63016)	Z1SUB	56037				
<hr/>									
9									
AS1	37746	///	/(63016)	EVFN	37257	AS1SUB	37401		
RC1	37417	///	/(63016)	RC1SUB	40034				

02/21/67

18108

10	MCM4	23550	///	/1630161	/TRK /1042541	EVEN	23551	MNCM4	31067
	ATSTA	31105	///	/1630161	ATST 33403				
	ALR	33430	///	/1630161	EVEN 33431	ATSUB	34160		
	CONVI	34700	///	/1630161	EVEN 34701	CONV	34560		
	CSTR	34572	///	/1630161	EVEN 34573	CSTRSB	35514		
	LNOM	35526	///	/1630161	/TRK /1042541	EVEN	35527	LORUP	36474
	LPTOSR	36525	///	/1630161	LPTO 40430				
	MOOTSF	40444	///	/1630161	EVEN 40445	MOOTSB	41152		
	RBST	41213	///	/1042541	/// /1630161	OUTPUT	44344		
	RBST	44375	///	/1630161	RBSTSB 45113				
	RMSUM4	45127	///	/1630161	RBSTSB 46216				
	SFC	46274	///	/1630161	EVEN 46295	SEGSUB	51753		
	SETPH1	52002	///	/1630161	EVEN 52003	SETPH	54403		
	SLOTSA	54423	///	/1630161	SLOT 56653				
	RSPLB	56701	///	RSPLM 60022					
	SPLNA	60731	///	SPLN1A 60256					
	SPLNA	60712	///	EVEN 60713	SPLN2A 60342				
	SPLM	60766	///	EVEN 60767	SPLN3A 60416				
	TISUB	60434	///	/1630161	EVEN 60435	TISUB	61727		
	VFPB	61755	///	/1630161	VFPB 67037				

UNUSED CNF

02054 THRU 63015

6.3.2 Computer System

The program is written in the FORTRAN IV computer language; however, one subroutine (SQRT) is a modified FAP version of the standard library routine which permits a negative argument. The program is designed for use on an IBM 7094 computer using an IBSYS, version 13, monitor system. In order to conserve core space the abridged output package is used by exercising the 'ALTIO' system option.

6.4 Diagnostic Tools

Several intermediate, diagnostic print statements have been permanently built into the program to aid in program and data-error analysis. The complete COMMON regions are printed before program termination in the event of any convergence failure. In addition, several user-controlled dumps are available through the use of input card sets 48 and 49 as explained below.

Card Set 48 (Format (I2,IX,11E7.0))

<u>Column</u>	<u>Name</u>	<u>Location</u>	<u>Definition</u>
1-2	N		Card Set 48
4-10	CKDUMP(1)	MNCHN4	Time at which KDUMP(71) will start printing dumps 1, 2 and 3 (seconds)
11-17	CKDUMP(2)	MNCHN4	Time at which KDUMP(71) will stop printing dumps 1, 2 and 3 (seconds)
18-24	CKDUMP(3)	MNCHN4	Time at which KDUMP(72) will start printing dump 5 (seconds)
25-31	CKDUMP(4)	MNCHN4	Time at which KDUMP(72) will stop printing dump 5 (seconds)

Card Set 49 (Format (E011))

<u>Column</u>	<u>Name</u>	<u>Location</u>	<u>Definition</u>
1	KDUMP(1)	MNCHN4	Fore-head and Aft-head calculations of TAUZ, RBZ, P, AP, ALP, WDOT and DW DOT
2	KDUMP(2)	SEGSUB	Cylindrical section reference plane calculations of TAUZ, RBZ, P, AP, ALP, W DOT and DW DOT
3	KDUMP(3)	AIBST	Start transient calculations of PD (III), DW DOT, WDOTD, AMACHD in cylindrical section

6.4

Diagnostic Tools (Continued)

<u>Column</u>	<u>Name</u>	<u>Location</u>	<u>Definition</u>
4	KDUMP(4)	SEGSUB	Anisotropic burn perimeters and burn rates.
5	KDUMP(5)	MNCHN4	COMMON and TBLK Data regions. This particular dump is turned off after printing unless it is being controlled by KDUMP(72).
6	KDUMP(6)	SEGSUB	Fuel area, port area and port perimeter for interpolation of each increment dividing plane
71	KDUMP(71)	MNCHN4 SEGSUB AIBST	This flag overrides KDUMP(1), KDUMP(2) and KDUMP(3) settings and prints these dumps according to the simulated burning times specified in CKDUMP(1) and CKDUMP(2).
72	KDUMP(72)	MNCHN4	This flag overrides KDUMP(5) and prints this dump according to the simulated burning times specified in CKDUMP(3) and CKDUMP(4).

The subroutine SPLN3A has also been included in the program to permit printing out the coefficients of the spline-fit curves used in subroutine CSTR5B. If these coefficients are desired the appropriate coding must be inserted following calls to SPLN1A which perform the curve fits.

6.5

Nomenclature

The following pages contain the nomenclature list which contains all input and output variables, all variables used in the document text and a significant number of important, internal program variables. In order to facilitate inclusion of additional variables in this third category the nomenclature lists have been punched on data cards. A copy of this nomenclature "deck" is provided with the program decks.

MATH SYMBOL	PROGRAM SYMBOL	UNIT	DESCRIPTION
A	A		GENERAL FLOW AREA OF A CROSS SECTION.
	A(I)	RADIANS	WORKING ARRAY STORAGE LOCATION OF GRAIN DESIGN GEOMETRY ANGLES.
$\alpha_{01...05}$	AA(I) THRU AK(I)	RADIANS	REFERENCE PLANE GRAIN DESIGN GEOMETRY ANGLES.
	AAA	- - -	COEFFICIENT OF FIRST ORDER TERM IN THIRD DEGREE EQUATION IN SUBROUTINE P3SUB WHICH LOCATES THE POINT P3 ON THE OUTER ELLIPSE OF HEAD-END WITH WEB.
	AAAA	- - -	COEFFICIENT OF FIRST ORDER TERM IN THIRD DEGREE EQUATION IN SUBROUTINE STUPRS FOR THE INTERSECTING PLANES IN SUBROUTINE SCI.
	AAK(I)	- - -	STORAGE ARRAY OF PRELIMINARY DESIGN CONSTANTS NO LONGER USED IN PROGRAM.
A_N	AAN	SG IN	NOZZLE-AND SECTION BURN AREA.
NO	AANN	- - -	TEMPORARY VALUE OF NUMBER OF GRAIN CROSS SECTION SYMMETRICAL PARTS USED IN SUBROUTINE PT1AA.
	AAP	- - -	COEFFICIENT OF FIRST ORDER TERM IN SECOND DEGREE EQUATION $X^{*2} + Y^{*2} + A*X + B*Y + D=0$ USED TO APPROXIMATE ELLIPSE BETWEEN POINTS P2 AND P3 IN THE A PRIME PLANE FOR THE BLOCK 2A ANALYSIS OF THE HEAD-END WITH WEB IN SUBROUTINE SCI.

MATH SYMBOL	PROGRAM SYMBOL	UNIT	DESCRIPTION
	ABB	--	COEFFICIENT OF FIRST ORDER TERM IN SECOND DEGREE EQUATION $X^2 + Y^2 + A^2X + B^2Y + D = 0$ USED TO APPROXIMATE ELLIPSE BETWEEN POINTS P2 AND P3 IN THE B PLANE FOR THE BLOCK 2A ANALYSIS OF THE HEAD-END WITH WEB IN SUBROUTINE SCI.
A_{cyl}	ABCYL	SQ IN	CYLINDRICAL SECTION TOTAL BURN AREA.
	ABHD	SQ IN	FORE-HEAD GEOMETRY TABLE BURN AREA. (DEPENDENT VARIABLE) INPUT ON SUBSET CARD NUMBER 40-5.
A_R	ABIGR	SQ IN	CROSS-SECTIONAL AREA OF WEB ZONE IN BLOCK 3 ANALYSIS OF HEAD-END WITH WEB. USED IN SUBROUTINE VOLSUB.
	ARN	SQ IN	AFT-HEAD GEOMETRY TABLE BURN AREA. (DEPENDENT VARIABLE). INPUT ON SUBSET CARD NUMBER 40-6.
	ABP		COEFFICIENT OF FIRST ORDER TERM IN SECOND DEGREE EQUATION $X^2 + Y^2 + A^2X + B^2Y + D = 0$ USED TO APPROXIMATE ELLIPSE BETWEEN POINTS P1 AND P3 IN THE B PRIME PLANE FOR THE BLOCK 2A ANALYSIS OF THE HEAD-END WITH WEB IN SUBROUTINE SCI.
A_{slot}	ABSLT	SQ IN	TOTAL BURN AREA ON GRAIN SEGMENT FACES FOR SEGMENTED MOTORS.
	ABSLTA	SQ IN	BURN AREA ON SLOT AFT INTERFACE.
	ABSLTF	SQ IN	BURN AREA ON SLOT FORWARD INTERFACE.

MATH SYMBOL	PROGRAM SYMBOL	UNIT	DESCRIPTION
A_{BTot}	ABTOT	SQ IN	TOTAL MOTOR BURN AREA.
	ACC	SQ IN	INCREMENTAL AREA ON THE AFT FACE OF THE AFT END BURNING SURFACE. (FIGURE 5.20)
$\frac{a}{g_0}$	ACCEL	- G-S -	CURRENT TIME VALUE OF VEHICLE ACCELERATION OBTAINED FROM ACCELERATION-TIME CURVE IN SUBROUTINE AIBST.
	ACCELT	- G-S -	VEHICLE ACCELERATION-TIME CURVE DEPENDENT VARIABLE.
	ACGA	SQ IN	SECTOR AREA USED IN SUBROUTINE MSISUB TO OBTAIN POLAR MOMENT OF CROSS SECTION FOR HEAD-END WITH WEB.
	ACGB	SQ IN	SECTOR AREA USED IN SUBROUTINE MSISUR TO OBTAIN POLAR MOMENT OF CROSS SECTION FOR HEAD-END WITH WEB.
	ACOSTR	- - -	TEMPORARY STORAGE LOCATION OF COSINE THETA-R FOR PLANE A IN SUBROUTINES STUPRS AND STUPPS IN THE BLOCK 1 ANALYSIS OF THE HEAD-END WITH WEB.
A_{EE}	AEE	SQ IN	AREA OF SECTOR IN SUBROUTINE AESUB FOR END SECTION ANALYSIS.
α_{ER}	AER	RADIANS	ANGLE BETWEEN MOTOR CENTER LINE AND TANGENT TO END SECTION ELLIPSE. DETERMINED IN SUBROUTINE ENDC58.
	AFD	SQ IN	AREA OF SECTOR 3A OR 11A IN SUBROUTINE AFPSUB

MATH SYMBOL	PROGRAM SYMBOL	UNIT	DESCRIPTION
	AF	SQ IN	CROSS SECTIONAL AREA OF INCREMENT DIVIDING PLANE IN SUBROUTINE SEGSUB.
	AFHI	SQ IN	CROSS SECTIONAL AREA OF UPSTREAM INCREMENT DIVIDING PLANE IN SUBROUTINE SEGSUB.
	AFP	SQ IN	CROSS SECTIONAL AREA OF REFERENCE PLANE IN SUBROUTINE AFPSUB.
	AFRPLA THRU AFRPLK	SQ IN	REFERENCE PLANE CROSS SECTIONAL PROPELLANT AREA IN SUBROUTINE MNCHN4. DETERMINED FROM INTEGRATION OF PERIMETER LENGTH AT EACH TIME INCREMENT.
	AFRPLX	SQ IN	REFERENCE PLANE X CROSS SECTIONAL PROPELLANT AREA IN SUBROUTINE MNCHN4.
	AFRPLY	SQ IN	REFERENCE PLANE Y CROSS SECTIONAL PROPELLANT AREA IN SUBROUTINE MNCHN4.
	AFX	SQ IN	REFERENCE PLANE X CROSS SECTIONAL PROPELLANT AREA IN SUBROUTINE SEGSUB.
	AFY	SQ IN	REFERENCE PLANE Y CROSS SECTIONAL PROPELLANT AREA IN SUBROUTINE SEGSUB.
A _H	AHH	SQ IN	HEAD-END SECTION BURN AREA.
A _{HO}	AHO	SQ IN	INITIAL AND PAST TIME VALUE OF HEAD-END SECTION BURN AREA.
I _{Bcy1}	AIBCYL	SLUG-SQ IN	CYLINDRICAL SECTION RECTANGULAR MOMENT OF INERTIA DETERMINED IN SUBROUTINE SEGSUB.

MATH SYMBOL	PROGRAM SYMBOL	UNIT	DESCRIPTION
A _{ig}	AIG	SQ IN	IGNITER OPENING SURFACE AREA DETERMINED IN SUBROUTINE AIGSUB.
	AINC	IN	TEMPORARY STORAGE LOCATION OF CURRENT INCREMENT DIVIDING PLANE LOCATION MEASURED FROM FORWARD TANGENT PLANE.
INCA INCK	AINCA THRU AINCK	IN	REFERENCE PLANE LOCATION MEASURED FROM FORWARD TANGENT PLANE. INPUT ON CARD SET NUMBER 2.
	AINCN	IN	NOZZLE SECTION REFERENCE PLANE OR AFT TANGENT PLAN LOCATION MEASURED FROM FORWARD TANGENT PLANE.
NINCPL	AINCPL	IN	INCREMENT PLANE LOCATION MEASURED FROM FORWARD TANGENT PLANE WHERE ANISOTROPIC BURN RATE COEFFICIENT IS TO BE EVALUATED DURING START TRANSIENT INTERVAL. INPUT ON CARD SET NUMBER 44.
	AINCW	IN	WORKING INCREMENT DIVIDING PLANE LOCATION IN SUBROUTINE SEGSUB.
	AINCX	IN	REFERENCE PLANE X LOCATION IN SUBROUTINE SEGSUB.
	AINCY	IN	REFERENCE PLANE Y LOCATION IN SUBROUTINE SEGSUB.
I _{pcyl}	AIPCYL	IN**4	CYLINDRICAL SECTION POLAR MOMENT OF INERTIA OF CROSS SECTION IN SUBROUTINE SEGSUB.
I _{spwb}	AISPPWR	SEC	WEB-TIME SPECIFIC IMPULSE.
I _T	AIT	SEC	TOTAL IMPULSE

NAME SYMBOL	PROGRAM SYMBOL	UNIT	DESCRIPTION
i_{Tst}	AITST	SEC	START TRANSIENT INTERVAL TOTAL IMPULSE. WHEN THIS VALUE IS INPUT ON CARD SET NUMBER 44, THE START TRANSIENT INTERVAL WILL BE TERMINATED WHEN THE TOTAL IMPULSE, AIT, IS GREATER THAN OR EQUAL TO AITST IN SUBROUTINE MNCHN4.
J_B	AJSB	SLUG-SQ IN	MOTOR PITCH AXIS MOMENT OF INERTIA ABOUT CG GRAIN.
J_{BH}	AJRH	IN**4	HEAD-END SECTION RECTANGULAR MOMENT OF INERTIA ABOUT FORWARD TANGENT PLANE FOR INCREMENTAL VOLUMES. DETERMINED IN SUBROUTINE PTIAA.
J_{BHed}	AJBHED	SLUG-SQ IN	HEAD-END SECTION TOTAL RECTANGULAR MOMENT OF INERTIA ABOUT FORWARD TANGENT PLANE.
J_{BHew}	AJBHEW	SLUG-SQ IN	RECTANGULAR MOMENT OF INERTIA OF HEAD-END WITH WEB ABOUT FORWARD TANGENT PLANE. DETERMINED IN SUBROUTINE MNCHN4
J_{OH}	AJBHN	SLUG-SQ IN	INTERMEDIATE VALUE OF HEAD-END WITH WEB RECTANGULAR MOMENT OF INERTIA DETERMINED IN THE BLOCK 2A ANALYSIS IN SUBROUTINE SCTORI.
J_{OH}	AJBHO	SLUG-SQ IN	HEAD-END SECTION INITIAL RECTANGULAR MOMENT OF INERTIA.
J_{BH}	AJBN	IN**4	NOZZLE-END SECTION RECTANGULAR MOMENT OF INERTIA ABOUT AFT TANGENT PLANE FOR INCREMENTAL VOLUMES. DETERMINED IN SUBROUTINE PTIAA.
J_{BNoz}	AJBNOZ	SLUG-SQ IN	NOZZLE-END SECTION RECTANGULAR MOMENT OF INERTIA ABOUT AFT TANGENT PLANE.

MATH SYMBOL	PROGRAM SYMBOL	UNIT	DESCRIPTION
J _{PH}	AJPH	IN**4	HEAD-END SECTION POLAR MOMENT OF INERTIA ABOUT ROLL AXIS FOR INCREMENTAL THIN SHELLS. DETERMINED IN SUBROUTINE PTIAA.
J _{PHad}	AJPHED	SLUG-SQ IN	HEAD-END SECTION TOTAL POLAR MOMENT OF INERTIA ABOUT ROLL AXIS.
J _{PHew}	AJPHEW	SLUG-SQ IN	POLAR MOMENT OF INERTIA OF HEAD-END WITH WEB ABOUT ROLL AXIS. DETERMINED IN SUBROUTINE MNCHN4.
	AJPHN	IN**4	INTERMEDIATE VALUE OF HEAD-END WITH WEB POLAR MOMENT OF INERTIA DETERMINED IN THE BLOCK 2A ANALYSIS IN SUBROUTINE SCTORI.
J _{PHO}	AJPHO	SLUG-SQ IN	HEAD-END SECTION INITIAL POLAR MOMENT OF INERTIA.
J _{PN}	AJPN	IN**4	NOZZLE-END SECTION POLAR MOMENT OF INERTIA ABOUT ROLL AXIS FOR INCREMENTAL THIN SHELLS. DETERMINED IN SUBROUTINE PTIAA.
J _{PNoz}	AJPN0Z	SLUG-SQ IN	NOZZLE-END SECTION TOTAL POLAR MOMENT OF INERTIA ABOUT ROLL AXIS.
	AJPP	IN**4	INTERMEDIATE VALUE OF POLAR MOMENT OF INERTIA OF CROSS SECTION OF INCREMENTAL AREAS IN SUBROUTINE PTIAA.
	AJPX	SLUG-SQ IN	INTERMEDIATE VALUE OF POLAR MOMENT OF INERTIA OF CROSS SECTION OF INCREMENTAL AREAS IN SUBROUTINE PTIAA.
	AJSTB	SLUG-SQ IN	INITIAL VALUE OF HEAD-END WITH WEB RECTANGULAR MOMENT OF INERTIA. DETERMINED IN SUBROUTINE ASTSUB.

MATH SYMBOL	PROGRAM SYMBOL	UNIT	DESCRIPTION
	AJSTP	SLUG-SQ IN	INITIAL VALUE OF HEAD-END WITH WEB POLAR MOMENT OF INERTIA. DETERMINED IN SUBROUTINE ASTSUB.
K	AK	- - -	INPUT VALUE WHICH DETERMINES DISTANCE BETWEEN PLANES FOR THE HEAD-END WEB ANALYSIS AND FOR THE END SECTION ANALYSIS. INPUT ON CARD SET NUMBER 29.
KEROS	AKEROS	IN/SEC	NOZZLE THROAT EROSION RATE. INPUT ON CARD SET NUMBER 31.
KG1 THRU KG5	AKG1 THRU AKG5	- - -	CRITICAL MASS VELOCITY (G C R) PER UNIT AREA EQUATION CONSTANTS. INPUT ON CARD SET NUMBER 32.
K _{cy}	AKGY	SQ IN	RADIUS OF GYRATION OF CYLINDRICAL SECTION INCREMENTAL CROSS SECTIONS. DETERMINED IN SUBROUTINE PTIAA.
	AKGYM	SQ IN	RADIUS OF GYRATION OF UPSTREAM CYLINDRICAL SECTION INCREMENTAL CROSS SECTIONS. INITIALIZED IN SUBROUTINE SEGSUB.
	AKGYPA THRU AKGYPK	IN**4	REFERENCE PLANE GEOMETRY TABLE RADIUS OF GYRATION OF CROSS SECTION (DEPENDENT VARIABLE). THIS VARIABLE APPEARS ON SUBSET CARD NUMBER 40-7 ONLY IF THE MOMENT OF INERTIA OPTION (KMOICG ON CARD SET NUMBER 41) HAS NOT BEEN SUPPRESSED FROM A PRIOR CASE IN WHICH THE PUNCH OPTION (PUNTAB ON CARD SET NUMBER 40) HAS BEEN SELECTED.
	AKGYX	SQ IN	RADIUS OF GYRATION OF REFERENCE PLANE X IN SUBROUTINE SEGSUB.

MATH SYMBOL	PROGRAM SYMBOL	UNIT	DESCRIPTION
	AKGY	SQ IN	RADIUS OF GYRATION OF REFERENCE PLANE Y IN SUBROUTINE SEGSUB.
	AKINS	- - -	FRACTION OF SLIVER THAT IS INERT. INPUT ON CARD SET NUMBER 43.
KK	AKK		ADJUSTING FACTOR USED IN THE HEAD-END WEB BLOCK 2 ANALYSIS TO DETERMINE DISTANCE BETWEEN PLANES.
KR1 THRU KR39	AKR1 THRU AKR39		BURNING RATE EQUATION CONSTANTS. INPUT ON CARD SET NUMBERS 34, 35, 36 AND 37.
	AKRFB	SQ IN	INTERMEDIATE RADIUS OF GYRATION VALUE IN SUBROUTINE MNCHN4 FOR HEAD-END WITH WEB.
KRH	AKRH	- - -	HEAD-END SECTION BURN RATE COEFFICIENT. USUAL VALUE IS THE SAME AS THE CYLINDRICAL SECTION STEADY STATE BURN RATE COEFFICIENT. INPUT ON CARD SET NUMBER 44.
KRN	AKRN	- - -	NOZZLE END SECTION BURN RATE COEFFICIENT. USUAL VALUE IS THE SAME AS THE CYLINDRICAL SECTION STEADY STATE BURN RATE COEFFICIENT. INPUT ON CARD SET NUMBER 44.
	AKRTAU	- - -	START TRANSIENT BURN RATE COEFFICIENT TABLE DEPENDENT VARIABLE. INPUT FOLLOWING CARD SET NUMBER 45.
KSLOT	AKSLOT(I)	- - -	SLOT BURNING RATE EQUATION COEFFICIENT. INPUT ON CARD SET NUMBER 37.

MATH SYMBOL	PROGRAM SYMBOL	UNIT	DESCRIPTION
	AKRST	- - -	ANISOTROPIC PROPELLANT BURNING RATE EQUATION COEFFICIENT DURING THE START TRANSIENT AND TAIL-OFF INTERVALS.
KU1 THRU KU5	AKU1 THRU AKU5	- - -	CRITICAL GAS VELOCITY (U C R) EQUATION CONSTANTS. INPUT ON CARD SET NUMBER 33.
L _A	ALA	IN	INITIAL LENGTH OF SECTOR 2. DETERMINED IN SUBROUTINE PLNCNS (FIGURE 5.24).
LAA THRU LAK	ALAA THRU ALAK	IN	PERIMETER LENGTH OF SECTOR LA FOR A REFERENCE PLANE. INPUT ON CARD SET NUMBER 20.
λ	ALAMDA	RADIANS	ANGLE BETWEEN MOTOR AXIS AND A LINE FROM CENTER OF TORUS GENERATING CIRCLE TO OUTSIDE ELEMENT OF SURFACE INCREMENT ON TOROIDAL END AREA IN ZONE B OF END SECTION STRAIGHT THROUGH GRAIN. (FIGURE 5.23)
λ_{min}	ALAMIN	RADIANS	ANGLE BETWEEN MOTOR AXIS AND A LINE FROM CENTER OF TORUS GENERATING CIRCLE TO INSIDE ELEMENT OF SURFACE INCREMENT ON TOROIDAL END AREA IN ZONE B OF END SECTION STRAIGHT THROUGH GRAIN. (FIGURE 5.23)
L _B	ALB		INITIAL LENGTH OF SECTOR 4. DETERMINED IN SUBROUTINE PLNCNS (FIGURE 5.24)
LBA THRU LBK	ALBA THRU ALBK	IN	PERIMETER LENGTH OF SECTOR LB FOR A REFERENCE PLANE. INPUT ON CARD SET NUMBER 21.
L _C	ALC	IN	INITIAL LENGTH OF SECTOR 6. DETERMINED IN SUBROUTINE PLNCNS (FIGURE 5.24).

MATH SYMBOL	PROGRAM SYMBOL	UNIT	DESCRIPTION
L_D	ALD	IN	INITIAL LENGTH OF SECTOR 12. DETERMINED IN SUBROUTINE PLNCNS (FIGURE 5.24).
L_E	ALE	IN	INITIAL LENGTH OF SECTOR 10. DETERMINED IN SUBROUTINE PLNCNS (FIGURE 5.24).
LEA THRU LEK	ALEA THRU ALEK	IN	PERIMETER LENGTH OF SECTOR LE FOR A REFERENCE PLANE. INPUT ON CARD SET NUMBER 22.
L_P	ALP	IN	TOTAL PERIMETER LENGTH OF CURRENT INCREMENT DIVIDING PLANE CROSS SECTION FOR A SEGMENT.
	ALPHI	IN	TOTAL PERIMETER LENGTH OF UPSTREAM INCREMENT DIVIDING PLANE CROSS SECTION FOR A SEGMENT.
	ALPPLA THRU ALPPLK	IN	REFERENCE PLANE GEOMETRY TABLE PORT PERIMETER (DEPENDENT VARIABLE). INPUT ON SUBSET CARD NUMBER 40-7.
L_Q	ALQ	IN	ARC LENGTH ON PSEUDOELLIPSOID. DETERMINED IN SUBROUTINE SCTOR1 (FIGURE 5.4).
L_R	ALR	IN	LENGTH TO A POINT ON BURNING SURFACE PERIMETER IN ANY SECTOR AT THICKNESS τ MEASURED ALONG PERIMETER FROM END OF SECTOR NEAREST MOTOR AXIS. DETERMINED IN SUBROUTINE ALRSUB. (FIGURE 5.22)
L_{Pmax}	ALRMAX	IN	LENGTH OF PART OF BURNING SURFACE PERIMETER IN ANY ZONE AT THICKNESS τ MEASURED FROM END OF SECTOR NEAREST MOTOR AXIS TO END OF SECTOR OR ZONE WHICH EVER IS SMALLER. DETERMINED IN SUBROUTINE AESUB. (FIGURE 5.21).

MATH SYMBOL	PROGRAM SYMBOL	UNIT	DESCRIPTION
L _{RI}	ALRI	IN	LENGTH TO THE LOWEST POINT ON BURNING SURFACE PERIMETER IN ANY ZONE AT THICKNESS TAU. MEASURED ALONG PERIMETER FROM END OF SECTOR NEAREST MOTOR AXIS DETERMINED IN SUBROUTINE AESUB (FIGURE 5.21)
L _{RS}	ALRS	IN	LENGTH OF CHORD DETERMINED IN SUBROUTINE ARSSUB. (FIGURE 5.22).
L _X	ALSUBX	IN	LENGTH OF A SECTOR AT THICKNESS TAU DETERMINED IN SUBROUTINE AFSUB (FIGURE 5.21).
L _{TA}	ALTA	IN	ARC LENGTH BETWEEN POINTS PRA AND PSA (FIGURE 5.2)
L _{TB}	ALTB	IN	ARC LENGTH BETWEEN POINTS PRB AND PSB (FIGURE 5.2)
LS1A THRU LS1K	ALS1A THRU ALS1K	IN	LENGTH FROM WEB TO INNER GRAIN POINT OF REFERENCE PLANE. INPUT ON CARD SET NUMBER 11.
LS2A THRU LS2K	ALS2A THRU ALS2K	IN	LENGTH FROM WEB TO OUTER GRAIN POINT OF REFERENCE PLANE. INPUT ON CARD SET NUMBER 12
AL ₇	AL7	IN	PERIMETER LENGTH OF ANISOTROPIC PROPELLANT IN SECTOR 7 DURING TAIL-OFF.
AL ₈	AL8	IN	PERIMETER LENGTH OF ANISOTROPIC PROPELLANT IN SECTOR 8 DURING TAIL-OFF.
PM	ANW	--	PRESENT TIME VALUE OF PROPELLANT GAS MOLECULAR WEIGHT.

MATH SYMBOL	PROGRAM SYMBOL	UNIT	DESCRIPTION
	AMWG	- - -	TABULAR INPUT VALUE OF PROPELLANT GAS MOLECULAR WEIGHT.
NITW	ANITW	- - -	NUMBER OF TIME INCREMENTS BEFORE FIRST WEB BURNOUT. INPUT ON CARD SET NUMBER 43.
NN	ANN	- - -	NUMBER OF NOZZLES. INPUT ON CARD SET NUMBER 31.
	ANGLE	RADIANS	CENTRAL ANGLE THAT DEFINES INTERSECTION OF ISOTROPIC PROPELLANT ARC LENGTH WITH CASE WALL IN SECTOR 7 DURING MOTOR TAIL-OFF.
	ANI	- - -	FLOATING POINT NUMBER OF TOTAL INCREMENT DIVIDING PLANES.
NOA THRU NOK	ANOI THRU ANOK	- - -	REFERENCE PLANE NUMBER OF GRAIN CROSS SECTION SYMMETRICAL PARTS. INPUT ON CARD SET NUMBER 3.
N2	AN2	DEGREES	NOZZLE EXPANSION CONE HALF-ANGLE. INPUT ON CARD SET NUMBER 31.
α_{01}	AOA(1) THRU AOK(1)	DEGREES	REFERENCE PLANE ANGLE OF SLOPE LAA WHICH DEFINES INITIAL GRAIN GEOMETRY. INPUT ON CARD SET NUMBER 6.
α_{02}	AOA(2) THRU AOK(2)	DEGREES	REFERENCE PLANE ANGLE OF SLOPE LBA WHICH DEFINES INITIAL GRAIN GEOMETRY. INPUT ON CARD SET NUMBER 7.
α_{03}	AOA(3) THRU AOK(3)	DEGREES	REFERENCE PLANE ANGLE OF SLOPE LCA WHICH DEFINES INITIAL GRAIN GEOMETRY. INPUT ON CARD SET NUMBER 8.

MATH SYMBOL	PROGRAM SYMBOL	UNIT	DESCRIPTION
α_{04}	AOA(4) THRU AOK(4)	DEGREES	REFERENCE PLANE ANGLE OF SLOPE LDA WHICH DEFINES INITIAL GRAIN GEOMETRY. INPUT ON CARD SET NUMBER 9.
α_{05}	AOA(5) THRU AOK(5)	DEGREES	REFERENCE PLANE ANGLE OF SLOPE LEA WHICH DEFINES INITIAL GRAIN GEOMETRY. INPUT ON CARD SET NUMBER 10.
A0E	A0E	IN	LENGTH OF SEMI-MAJOR AXIS OF INNER ELLIPSE (FIGURE 5.7)
α_{0Hmax}	AOHM	DEGREES	ANGLE BETWEEN TANGENT TO FORE-HEAD ELLIPSE AND MOTOR CENTERLINE. INPUT ON CARD SET NUMBER 29.
α_{0Nmax}	AONM	DEGREES	ANGLE BETWEEN TANGENT TO AFT-HEAD ELLIPSE AND MOTOR CENTERLINE. INPUT ON CARD SET NUMBER 30.
A_p	AP	SQ IN	PORT AREA OF CURRENT INCREMENT DIVIDING PLANE FOR A SEGMENT.
	APHI	SQ IN	PORT AREA OF UPSTREAM INCREMENT DIVIDING PLANE FOR A SEGMENT.
	APORTA THRU APORTK		INITIAL PORT AREA OF A REFERENCE PLANE. INPUT ON SUBSET CARD NUMBERS 40-4.
A_R	AR	SQ IN	AREA OF SECTOR BCD IN ZONE A OF THE AFT END BURNING SURFACE (FIGURE 5.22)
α_{rc0}	ARCO	RADIANS	ANGLE BETWEEN Y-AXIS AND NORMAL LINE THROUGH PO (FIGURE 5.4). USED IN SUBROUTINE SCTOR1 FOR THE HEAD-END WITH WEB BLOCK 2A ANALYSIS

MATH SYMBOL	PROGRAM SYMBOL	UNIT	DESCRIPTION
α_{rci}	ARC1	RADIANS	ANGLE BETWEEN Y-AXIS AND NORMAL LINE THROUGH P1 (FIGURE 5.4). USED IN SUBROUTINE SCTOR1 FOR THE HEAD-END WITH WEB BLOCK 2A ANALYSIS
A_{RO}	ARO	SQ IN	AREA OF SECTOR AEF IN ZONE A OF THE AFT END BURNING SURFACE (FIGURE 5.22)
	ASE	SQ IN	END SECTION BURN AREA. COMPUTED IN SUBROUTINE ASESUB.
	ASI	SQ IN	BURNING SURFACE AREA OF AN INCREMENTAL STRIP DETERMINED IN THE BLOCK 2A ANALYSIS OF THE HEAD END WITH WEB IN SUBROUTINE SCI (FIGURE 5.4)
A_{slvr}	ASLVR	SQ IN	INCREMENT DIVIDING PLANE INERT SLIVER AREA FOR ONE GRAIN CROSS SECTION SYMMETRICAL PART.
A_T	AT	SQ IN	EXHAUST NOZZLE THROAT AREA.
A_{TO}	ATO	SQ IN	AREA IN ZONE A OF THE AFT END BURNING SURFACE BETWEEN THE CHORD LRS AND THE CIRCULAR ARC LR (FIGURE 5.22)
A_{tslot}	ATSLOT	SQ IN	TOTAL BURNING SURFACE AREA OF ALL SLOTS.
A_{TT}	ATT	SQ IN	THE POSITIVE OR NEGATIVE VALUE OF ATO DEPENDING ON RT. NEGATIVE IF RT IS NEGATIVE AND POSITIVE IF RT IS POSITIVE.
	AWE	SQ IN	TOTAL BURNING SURFACE AREA OF WEB ZONE (SECTOR 8 PLUS AFT FACE) OF THE AFT END BURNING SURFACE AT THICKNESS TAU DETERMINED IN SUBROUTINE AWESUB.

MATH SYMBOL	PROGRAM SYMBOL	UNIT	DESCRIPTION
BE	BE	IN	LENGTH OF SEMI-MINOR AXIS OF END SECTION. FORE-HEAD (H) OR AFT-HEAD (N).
β_H	BH	--	FORE-HEAD CASE ELLIPSE RATIO. INPUT ON CARD SET NUMBER 29.
β_N	BN	--	AFT-HEAD ELLIPSE RATIO. INPUT ON CARD SET NUMBER 30.
BOE	BOE	IN	LENGTH OF SEMI-MINOR AXIS OF INNER ELLIPSE OF HEAD-END WITH WEB.
	BRNOUT	--	PROGRAM CONTROL FLAG FOR WEB BURNOUT.
β_{OE}	BTAOE	--	RATIO OF HEAD END WEB ELLIPSE AXIS NORMAL TO MOTOR AXIS TO ELLIPSE AXIS PARALLEL WITH MOTOR AXIS. INPUT ON CARD SET NUMBER 29.
	BVX	RADIANS	ANGLE OF INERT SLIVER IN SECTOR 7.
	BVXX	RADIANS	ANGLF OF INERT SLIVER IN SECTOR 6.
	BV2	RADIANS	ANGLE THAT DEFINES PERIMETER LENGTH OF PROPELLANT IN SECTOR 7.
	BV2P	RADIANS	ANGLE THAT DEFINES PERIMETER LENGTH OF ISOTROPIC PROPELLANT ONLY IN SECTOR 7.
β_{71max}	B71M	RADIANS	GEOMETRY CONSTANT DETERMINED IN SUBROUTINE PLNCNS (FIGURE 5.25)
β_{72max}	B72M	RADIANS	GEOMETRY CONSTANT DETERMINED IN SUBROUTINE PLNCNS (FIGURE 5.25)

MATH SYMBOL	PROGRAM SYMBOL	UNIT	DESCRIPTION
β_{g1max}	B91M	RADIANS	GEOMETRY CONSTANT DETERMINED IN SUBROUTINE PLNCNS (FIGURE 5.25)
β_{g2max}	B92M	RADIANS	GEOMETRY CONSTANT DETERMINED IN SUBROUTINE PLNCNS (FIGURE 5.25)
	CAE	- - -	CONSTANTS USED IN CALCULATION OF COEFFICIENT FOR FOURTH-DEGREE EQUATION FOR SOLUTION OF INTERSECTION OF TOROIDAL SURFACE AND END SECTION ELLIPSE. DETERMINED IN SUBROUTINE ENDCSB.
	CBE	- - -	
	CCCE	- - -	
	CCVE	- - -	
	CDCE	- - -	
	CDVE	- - -	
	CECE	- - -	
	CEVE	- - -	
C_{FO}	CFO	- - -	THRUST COEFFICIENT DETERMINED FROM MOMENTUM EXCHANGE ONLY WITHOUT EXPANSION FROM EXIT PRESSURE TO AMBIENT PRESSURE.
	CKDUMP(1)	SEC	LOWER TIME LIMIT FOR A DIAGNOSTIC PRINT IN SUBROUTINE MNCHN4
	CKDUMP(2)	SEC	UPPER TIME LIMIT FOR DIAGNOSTIC PRINT IN SUBROUTINE MNCHN4.
	CM	- - -	NOZZLE EFFICIENCY. INPUT ON CARD SET NUMBER 31.
	CMPTME	- - -	STORAGE ARRAY FOR INTERNAL CLOCK PRINTOUT.
	COM	- - -	BLOCK NAME IN COMMON (DIMENSIONED 6600) FOR VARIABLE STORAGE

2

MATH SYMBOL	PROGRAM SYMBOL	UNIT	DESCRIPTION
CKP	CRP	- - -	CONVERGENCE VALUE FOR NON-STEADY FLOW DISCHARGE PRESSURE AT EXIT OF EACH MASS ADDITION REGION. INPUT ON CARD SET NUMBER 41.
CRT	CRT	- - -	CONVERGENCE VALUE FOR NON-STEADY FLOW DISCHARGE GAS TEMPERATURE AT EXIT OF EACH MASS ADDITION REGION. INPUT ON CARD SET NUMBER 41.
CRV	CRW	- - -	CONVERGENCE VALUE FOR NON-STEADY FLOW TO COMPARE FLOW RATES AT EXIT OF GRAIN TO THAT WHICH CAN BE DISCHARGED THROUGH NOZZLE BOTH AT SAME TOTAL PRESSURE. INPUT ON CARD SET NUMBER 41.
C*	CSTAK	FT/SEC	PROPELLANT GAS CHARACTERISTICS VELOCITY. INPUT ON CARD SET NUMBER 36.

MATH SYMBOL	PROGRAM SYMBOL	UNIT	DESCRIPTION
	CSTR	FT/SEC	TABULAR INPUT VALUE OF CHARACTERISTIC VELOCITY FOR PROPELLANT GAS (DEPENDENT VARIABLE). INPUT FOLLOWING CARD SET NUMBER 31.
D_E	DE	IN	NOZZLE EXIT DIAMETER. INPUT ON CARD SET NUMBER 31.
ρ_f	DEL F	LB/CU IN	PROPELLANT DENSITY. INPUT ON CARD SET NUMBER 38.
ΔL	DELL	IN	INCREMENTAL PERIMETER LENGTH USED IN APPROXIMATE INTEGRATION OF SURFACE AREAS (FIGURE 5.23)
ΔL_o	DELLO	IN	DISTANCE BETWEEN POINTS P_0 AND P_1 USED TO OBTAIN SURFACE AREA OF BLOCK 1 ANALYSIS OF HEAD-END WITH WEB.
ΔR	DELR	IN	DISTANCE BETWEEN POINTS P_0 AND P_1 USED TO OBTAIN SURFACE AREA OF BLOCK 2 B AND VOLUME IN BLOCK 3 OF HEAD-END WITH WEB.
Δt	DELT	SEC	CURRENT VALUE OF TIME INCREMENT
ρ	DELTA	LB/CU IN	PROPELLANT GAS DENSITY.
Δt_{ss}	DELTSS	SEC	FIXED TIME INCREMENT FOR STEADY STATE. INPUT ON CARD SET NUMBER 42.
Δt_{st}	DELTST	SEC	FIXED TIME INCREMENT USED DURING START TRANSIENT. INPUT ON CARD SET NUMBER 42.
Δt_{to}	DELTO	SEC	FIXED TIME INCREMENT FOR TAIL-OFF OR SHUTDOWN. INPUT ON CARD SET NUMBER 42.

MATH SYMBOL	PROGRAM SYMBOL	UNIT	DESCRIPTION
ΔZ	DELZ	IN	MAXIMUM LENGTH OF MASS ADDITION REGIONS IN GRAIN SEGMENTS. INPUT ON CARD SET NUMBER ONE. AT TIME=0, AN INCREMENT DIVIDING PLANE WILL BE PLACED EVERY DELZ INCHES DOWN EACH GRAIN SEGMENT BEGINNING AT THE FORWARD TANGENT PLANE OR AT THE AFT FACE OF A SLOT AND TERMINATING AT THE AFT TANGENT PLANE OR THE FORWARD FACE OF A SLOT.
D_{E1}	DE1	IN	CASE OPENING DIAMETER (H) FORE-HEAD OR (N) AFT-HEAD. INPUT ON CARD SETS 29 AND 30.
C_{H1}	DH1	IN	FORE-HEAD CASE OPENING DIAMETER. INPUT ON CARD SET NUMBER 29.
$\frac{\Delta L}{R_f}$	DLRF	- - -	DELTA-L OVER R _f , WHERE DELTA-L = INCREMENT SIZE USED FOR THE BURNING SURFACE AREA CALCULATIONS, MEASURED ALONG THE INTERNAL PERIMETER IN THE ADJACENT REFERENCE PLANE. INPUT ON CARD SET NUMBER 30.
D_{N1}	DN1	IN	AFT-HEAD CASE OPENING DIAMETER. INPUT ON CARD NUMBER 30.
	DO3	IN	DISTANCE BETWEEN POINTS P0 AND P3. DETERMINED IN SUBROUTINE SCI FOR HEAD-END WITH WEB ANALYSIS
ΔP_o	DPO	PSIA	TOTAL PRESSURE LOSS IN NOZZLE END SECTION FROM MASS ADDITION.
	DPR	IN	DISTANCE BETWEEN POINTS P0A AND P0B. DETERMINED IN SUBROUTINE SCI FOR HEAD-END WITH WEB ANALYSIS.

MATH SYMBOL	PROGRAM SYMBOL	UNIT	DESCRIPTION
	DPS	IN	DISTANCE BETWEEN POINTS POA AND POB. DETERMINED IN SUBROUTINE SCI FOR HEAD-END WITH WEB ANALYSIS
$\frac{\Delta R_v}{R_f}$	DRVRF -		DELTA-RV OVER DELTA-RF, WHERE DELTA-RV = OUTSIDE PROPELLANT RADIUS OF ADJACENT REFERENCE PLANE. INPUT ON CARD SET NUMBER 30.
D_T	DT	IN	INITIAL NOZZLE THROAT DIAMETER. INPUT ON CARD SET NUMBER 31.
	DS	IN	DISTANCE BETWEEN POINTS P0 AND P1 WHEN P1 IS LOCATED ON THE CASE ELLIPSE (FIGURE 5-6-2) DETERMINED IN SUBROUTINE S2SK FOR HEAD-END WITH WEB ANALYSIS
ΔT	DTAUA THRU DTAUK	IN	INCREMENTAL SIZE OF REFERENCE PLANE DISTANCE BURNED TO EVALUATE GEOMETRY TABLES. INPUT ON CARD SET NUMBER 27.
ΔT_w	DTAUWA THRU DTAUWK		INCREMENTAL SIZE OF REFERENCE PLANE DISTANCE BURNED BEYOND WEB THICKNESS TAUW TO EVALUATE GEOMETRY TABLES. INPUT ON CARD SET NUMBER 28.
	DTTOR	- - -	RATIO OF TIME INCREMENT SIZE DURING TAIL-OFF TO NOMINAL TIME INCREMENT SIZE BEFORE FIRST WEB BURNOUT. INPUT ON CARD SET NUMBER 43.
	DTWBR	- - -	RATIO OF TIME INCREMENT SIZE DURING WEB BURNOUT TO NOMINAL TIME INCREMENT SIZE BEFORE FIRST WEB BURNOUT. INPUT ON CARD SET NUMBER 43.
ΔV	DV	CU IN	INCREMENTAL PROPELLANT VOLUME USED TO DETERMINE INITIAL PROPELLANT VOLUME IN END SECTIONS IN SUBROUTINE ASESUB.

MATH SYMBOL	PROGRAM SYMBOL	UNIT	DESCRIPTION
$\frac{dV}{dt}$	DVDT	CU IN/SEC	RATE OF CHANGE OF SLOT VOLUME WITH RESPECT TO TIME. COMPUTED IN SR SEGSUB FROM TSLOT AND RSLOT.
\dot{m}	DWDOT	LB/SEC	PROPELLANT GAS GENERATED IN SEGMENT OR MASS ADDITION REGION.
$\frac{dW}{dt}$	DWDT	LB/SEC	STORED PROPELLANT GAS IN SEGMENT OR CONTROL VOLUME.
$\frac{dV_{slot}}{dt}$	DWDTS	LB/SEC	MASS OF STORED GAS IN A SLOT FOR ONE COMPUTING INTERVAL.
\dot{m}_s	DWSLOT	LB/SEC	MASS FLOW GENERATED IN A SLOT.
ϵ_c	EC	LB/SQ IN	AVERAGE VALUE OF CASE MODULUS OF ELASTICITY INPUT ON CARD SET NUMBER 46.
ϵ_g	EG	LB/SQ IN	GRAIN MODULUS OF ELASTICITY. INPUT ON CARD SET NUMBER 46.
ϵ_{CA}	EPCA	- - -	MEASURED CASE STRAIN AT FORWARD TANGENT PLANE. INPUT FOLLOWING CARD SET NUMBER 46.
ϵ_{CN}	EPCN	- - -	MEASURED CASE STRAIN AT AFT TANGENT PLANE. INPUT FOLLOWING CARD SET NUMBER 46.
η_1	ETA1	RADIANS	ANGLE FROM R5 RADIUS POINT THAT DEFINES INTERSECTION OF ANISOTROPIC PROPELLANT WITH CASE WALL IN SECTOR 7 DURING MOTOR TAIL-OFF.
η_2	ETA2	RADIANS	ANGLE FROM R5 RADIUS POINT THAT DEFINES INTERSECTION OF ANISOTROPIC PROPELLANT WITH ISOTROPIC PROPELLANT IN SECTOR 7 DURING MOTOR TAIL-OFF.

MATH SYMBOL	PROGRAM SYMBOL	UNIT	DESCRIPTION
η_{11}	ETA11	RADIANS	CENTRAL ANGLE THAT DEFINES INTERSECTION OF ANISOTROPIC PROPELLANT WITH CASE WALL IN SECTOR 7 DURING MOTOR TAIL-OFF.
η_{22}	ETA22	RADIANS	CENTRAL ANGLE THAT DEFINES INTERSECTION OF ANISOTROPIC PROPELLANT WITH ISOTROPIC PROPELLANT IN SECTOR 7 DURING MOTOR TAIL-OFF.
γ	GAMA	- - -	PROPELLANT GAS SPECIFIC HEAT RATIO. INPUT ON CARD SET NUMBER 38.
γ_G	GAMAG	- - -	TABULAR INPUT VALUE OF PROPELLANT GAS SPECIFIC HEAT RATIO (DEPENDENT VARIABLE). INPUT FOLLOWING CARD SET NUMBER 39.
γ_R	GAMAR	RADIANS	ANGLE BETWEEN RADIAL VECTOR RA AND BISECTOR OF PRIMARY OR SECONDARY PROPELLANT TIP. (FIGURE 5.23)
γ_{R0}	GAMAR0	RADIANS	ANGLE BETWEEN RADIAL VECTOR RAO AND BISECTOR OF PRIMARY OR SECONDARY PROPELLANT TIP. (FIGURE 5.22)
γ_T	GAMAT	RADIANS	ANGLE SUBTENDED AT CENTER OF RADIUS RT BY CHORD LRS (FIGURE 5.20 AND 5.21)
γ_1	GAMA1	RADIANS	ANGLE BETWEEN NORMAL LINE TO PERIMETER OF GRAIN CONFIGURATION AND NORMAL LINE TO THE LINE SEGMENT RAT (FIGURE 5.6) DETERMINED IN SUBROUTINE GAMSUB
γ_2	GAMA2	RADIANS	ANGLE BETWEEN Y-AXIS AND NORMAL LINE TO INNER ELLIPSE (FIGURE 5.7) DETERMINED IN SUBROUTINE GAMA2S.

MATH SYMBOL	PROGRAM SYMBOL	UNIT	DESCRIPTION
	GEOM	-- --	CYLINDRICAL SECTION GEOMETRY TABLE FLAG. INPUT ON CARD SET NUMBER 40. = 1.0 ONLY END SECTION(S) ARE INPUT = 2.0 ALL SECTIONS ARE INPUT
g_o	GNOT	FT/SQ SEC	GRAVITATIONAL CONSTANT
H_{CO}	HCO	IN	LENGTH OF CYLINDRICAL SECTION. INPUT ON CARD SET NUMBER 1.
h_E	HE	IN	LENGTH OF A GENERAL ELEMENT OR LENGTH OF LONGER EDGE OF ELEMENT USED IN CALCULATION OF BURNING SURFACE AREA FOR THE END SECTION ANALYSIS. DETERMINED IN SUBROUTINE HESUB.
h_{EO}	HEO	IN	GEOMETRICAL LENGTH OF END SECTION. DETERMINED IN SUBROUTINE ENDCSB. (FIGURE 5.35)
h_{ER}	HER	IN	REFERENCE LENGTH OF END SECTION. DETERMINED IN SUBROUTINE ENDCSB. (FIGURE 5.35)
h_{EI}	HEI	IN	LENGTH OF END SECTION CONIC SECTION. DETERMINED IN SUBROUTINE ENDCSB (FIGURE 5.35)
h_{E2}	HE2	IN	LENGTH OF END SECTION ELLIPTIC SECTION. DETERMINED IN SUBROUTINE ENDCSB (FIGURE 5.35)
	HOLDR	IN	PREVIOUS ITERATIVE VALUE OF PERIMETER LENGTH ALONG CURRENT SECTOR. INITIALIZED IN SUBROUTINE SCI FOR THE BLOCK 1 ANALYSIS OF THE HEAD-END WITH WEB.
	IDMOI(1) THRU IDMOI(12)	-- --	ALPHANUMERIC IDENTIFICATION OF MOMENTS OF INERTIA TABLES. INPUT ON SUBSET CARD NUMBER 40-2 FOLLOWING IDTAB.

MATH SYMBOL	PROGRAM SYMBOL	UNIT	DESCRIPTION
	IDTAB(1) THRU IDTAB(12)	- - -	ALPHANUMERIC IDENTIFICATION OF GEOMETRY TABLES. INPUT ON SUBSET CARD NUMBER 40-2
	IFLAG	- - -	CONTROL FLAG IN SUBROUTINE AIBST TO INDICATE ITERATION PASSES FOR FALSE POSITION ITERATION.
	IIS	- - -	CURRENT SLOT NUMBER. USED AS A SUBSCRIPT FOR THE SLOT VARIABLES.
	IIZ	- - -	SUBSCRIPT OF RBZ TO INDICATE DIVIDING PLANE LOCATION.
	ISET(I)	- - -	INPUT CONTROL FLAG TO SUBROUTINE INPT TO INDICATE WHICH CARD SETS ARE TO BE READ.
	ISI	- - -	NUMBER OF INCREMENT DIVIDING PLANE THAT IS LOCATED JUST DOWNSTREAM OF SLOT FORWARD INTERFACE. USED IN SR SEG SUB TO OBTAIN STATIC PRESSURE AT SLOT INLET.
	ISZ	- - -	NUMBER OF INCREMENT DIVIDING PLANE THAT IS LOCATED JUST UPSTREAM OF SLOT AFT INTERFACE. USED IN SR SEG SUB TO STORE SLOT DISCHARGE STATIC PRESSURE FOR NEXT GRAIN SEGMENT.
	KMOICG	- - -	MOMENT OF INERTIA CALCULATION SUPPRESSION FLAG. A NON-ZERO VALUE WILL SUPPRESS THE MOI AND CG CALCULATION. INPUT ON CARD SET NUMBER 41.
	NACCEL	- - -	NUMBER OF TABLE INPUT VALUES OF ACCELERATION -TIME CURVE. INPUT ON CARD SET NUMBER 47.

MATH SYMBOL	PROGRAM SYMBOL	UNIT	DESCRIPTION
	NAKRST	- - -	NUMBER OF TABLE INPUT VALUES OF ANISOTROPIC PROPELLANT BURN RATE COEFFICIENT TABLE. INPUT ON CARD SET NUMBER 45.
	NAKSTR	- - -	NUMBER OF TABLE INPUT VALUES OF PROPELLANT GAS PROPERTIES FOR CSTR, GAMAG, AMUG, TCOMB, AND PRESS TABLES. INPUT ON CARD SET 39.
	NEPS	- - -	NUMBER OF TABLE INPUT VALUES OF MEASURED CASE STRAIN DATA TABLE. INPUT ON CARD SET NUMBER 46.
	NGEOHD	- - -	NUMBER OF FORE-HEAD GEOMETRY TABLE VALUES. INPUT ON SUBSET CARD NUMBER 40-3.
	NGEOMA THRU NGEOMK	- - -	NUMBER OF REFERENCE PLANE GEOMETRY TABLE VALUES. INPUT ON SUBSET CARD NUMBERS 40-3.
	NGEOMN	- - -	NUMBER OF AFT-HEAD GEOMETRY TABLE VALUES. INPUT ON SUBSET CARD NUMBER 40-3.
	NI	- - -	INTEGER NUMBER OF TOTAL INCREMENT DIVIDING PLANES.
	NINCP/L	- - -	DESIRFD INCREMENT DIVIDING PLANE NUMBER TO DETERMINE BURN RATE COEFFICIENT TABLE INDEPENDENT VARIABLE, TAUAKR. INPUT ON CARD SET NUMBER 44.
	NPH	- - -	NUMBER OF TABLE INPUT VALUES OF HEAD END PRESSURE TABLE. INPUT ON CARD SET NUMBER 44.
	NSLOT	- - -	INTEGER NUMBER OF TOTAL SLOTS. THIS VARIABLE IS DECREMENTED IN SUBROUTINE TISUB EVERY TIME A GRAIN SEGMENT BURNS OUT Laterally.

MATH SYMBOL	PROGRAM SYMBOL	UNIT	DESCRIPTION
	NTABH	- - -	NUMBER OF HEAD END TABLE VALUES.
	NTABN	- - -	NUMBER OF NOZZLE END TABLE VALUES.
	NTME	- - -	NUMBER OF COMPUTED VALUES OF ANISOTROPIC PROPELLANT BURN RATE COEFFICIENT TABLE.
P_a	PA	PSIA	ATMOSPHERIC PRESSURE. INPUT ON CARD SET NUMBER 31.
	PCTAB	- - -	PERCENT CHANGE, RELATIVE TO 1.0, IN TOTAL BURN AREA REQUIRED TO CONVERGE SOLUTION TO DESIRED VALUE OF HEAD END PRESSURE AND BURN RATE COEFFICIENT. PROGRAM WILL CLOSE ON PCTAB AT EACH TIME INCREMENT FOR SET VALUE OF PH AND AKRST AS A FUNCTION OF TIME FROM INPUT TABLES.
	PCTWB	- - -	WEB TIME CONSTANT. RATIO OF INCREMENT DIVIDING PLANES BURNED OUT AT WEB TIME TO TOTAL NUMBER OF INCREMENT DIVIDING PLANES. INPUT ON CARD SET NUMBER 43.
P_D	PD	PSIA	PRESENT TIME DISCHARGE PRESSURE OF INCREMENT DIVIDING PLANE. COMPUTED IN SUBROUTINE AIBST.
P'_D	PDPR	PSIA	PREVIOUS TIME DISCHARGE PRESSURE OF INCREMENT DIVIDING PLANE. INITIALIZED IN SUBROUTINE MNCHN4
P_{HI}	PHI	PSIA	INITIAL GUESS OF FORE-HEAD PRESSURE FOR FIRST TIME INCREMENT. INPUT ON CARD SET NUMBER 41.
	PHST	PSIA	DEPENDENT VARIABLE OF HEAD-END PRESSURE CURVE FIT FOR START TRANSIENT.

MATH SYMBOL	PROGRAM SYMBOL	UNIT	DESCRIPTION
π	PI	- - -	MATHEMATICAL CONSTANT.
$\frac{\pi}{2}$	PIO2	- - -	PI DIVIDED BY TWO.
	PLANES	- - -	NUMBER OF CYLINDRICAL SECTION GEOMETRY PLANE TABLES INPUT. INPUT ON CARD SET NUMBER 40.
	PMOIH	SLUG-SQ IN	FORE-HEAD GEOMETRY TABLE POLAR MOMENT OF INERTIA (DEPENDENT VARIABLE). INPUT ON SUBSET CARD NUMBER 40-5.
	PMOIN	SLUG-SQ IN	AFT-HEAD GEOMETRY TABLE POLAR MOMENT OF INERTIA (DEPENDENT VARIABLE). INPUT ON SUBSET CARD NUMBER 40-6.
P_o		- - -	POINT ON A PLANE USED IN THE BLOCK 1 ANALYSIS OF THE HEAD-END WITH WEB. LOCATED ON THE INNER ELLIPSE ALONG A LINE PARALLEL WITH THE Y-AXIS AND NORMAL TO THE FORWARD TANGENT PLANE AT A POINT IN A SECTOR ALONG THE GRAIN INITIAL PERIMETER (FIGURE 5.1)
			OR
P_{ra} or P_{rb}		- - -	POINT ON THE PSEUDOELLIPSOID USED IN THE BLOCK 2A, 2B, AND 3 ANALYSIS OF THE HEAD-END WITH WEB (FIGURE 5.4)
		- - -	POINT IN PLANE A OR B DEFINING RADIAL BURNING FROM POINT P0 (FIGURE 5.2) PR IS A FUNCTION OF TAU. IF TAU IS GREATER THAN OR EQUAL TO D03, THEN THE PLANE HAS BURNED OUT. IF TAU IS GREATER THAN D02, THEN PR IS LOCATED ON THE CURVE BETWEEN THE POINTS P2 AND P3. IF TAU IS LESS THAN OR EQUAL TO D02, THEN PR IS LOCATED ON THE LINE SEGMENT BETWEEN POINTS P0 AND P2.

MATH SYMBOL	PROGRAM SYMBOL	UNIT	DESCRIPTION
	PRESS	PSIA	PROPELLANT GAS PROPERTY TABLE INDEPENDENT VARIABLE. INPUT FOLLOWING CARD SET NUMBER 39.
	PRNT	- - -	STORAGE ARRAY FOR EXPANDED INCREMENT DIVIDING PLANE PRINTOUT VARIABLES.
	PRNTAB	- - -	GEOMETRY TABLE PRINT FLAG. INPUT ON CARD SET NUMBER 40. = 0.0 DO NOT PRINT GEOMETRY TABLES = 1.0 PRINT GEOMETRY TABLES.
	PRIFLG	- - -	CONTROL FLAG FOR EXPANDED PRINTOUT. INPUT ON CARD SET NUMBER 41. = 0.0 NO EXPANDED PRINT = 1.0 EXPANDED PRINT
P_{sa} or P_{sb}		- - -	POINT IN PLANE A OR B DEFINING RADIAL BURNING FROM POINT P0 (FIGURE 5.2) PS IS A FUNCTION OF TAU. IF TAU IS GREATER THAN OR EQUAL TO D03, THEN THE PLANE HAS BURNED OUT. IF TAU IS GREATER THAN D01, THEN PS IS LOCATED ON THE LINE SEGMENT BETWEEN POINTS P1 AND P3. IF TAU IS LESS THAN OR EQUAL TO D01, THEN PS IS LOCATED ON THE LINE SEGMENT BETWEEN POINTS P0 AND P1.
P_{st}	PST	PSIA	MAXIMUM START TRANSIENT PRESSURE. USED AS OPTION IN SUBROUTINE MNCHN4 TO TERMINATE START TRANSIENT CALCULATIONS. INPUT ON CARD SET NUMBER 41.
	PUNTAB	- - -	GEOMETRY TABLE PUNCH FLAG. INPUT ON CARD SET NUMBER 40. = 0.0 DO NOT PUNCH GEOMETRY TABLES = 1.0 PUNCH GEOMETRY TABLES

MATH SYMBOL	PROGRAM SYMBOL	UNIT	DESCRIPTION
P_1		-- --	POINT ON A PLANE USED IN THE BLOCK 1 ANALYSIS OF THE HEAD-END WITH WEB. (FIGURES 5.1 AND 5.10) LOCATED IN THE Y-Z PLANE ALONG A LINE NORMAL TO THE GRAIN PERIMETER AT P_0 .
			OR
P_2		-- --	POINT ON THE PSEUDOELLIPSOID USED IN THE BLOCK 2A, 2B, AND 3 ANALYSIS OF THE HEAD-END WITH WEB. LOCATED AT THE DISTANCE $DELL$ FROM POINT P_0 . (FIGURE 5.4)
P_3		-- --	POINT ON A PLANE USED IN THE BLOCK 1 ANALYSIS OF THE HEAD-END WITH WEB. LOCATED ON THE OUTER ELLIPSOID ALONG A LINE NORMAL TO THE INNER ELLIPSOID AT P_0 . (FIGURES 5.1 AND 5.10)
		-- --	POINT ON A PLANE USED IN THE BLOCK 1 ANALYSIS OF THE HEAD-END WITH WEB. LOCATED IN THE Y-Z PLANE ON THE OUTER ELLIPSOID AND IN THE PLANE FORMED BY POINTS P_0, P_1 , AND P_2 (FIGURES 5.1 AND 5.10)
	R	FT/DEG RANKIN	PROPELLANT GAS CONSTANT. INPUT ON CARD SET NUMBER 38.
r_{Amax}	R_{AMAX}	IN	RADIAL DISTANCE FROM MOTOR AXIS TO EITHER- 1. OUTSIDE LIMIT OF A SECTOR IN A ZONE 2. OUTSIDE LIMIT OF AN INCREMENTAL AREA (SEE FIGURES 5.21 THRU 5.23)
R_{Amin}	R_{AMIN}	IN	RADIAL DISTANCE FROM MOTOR AXIS TO EITHER- 1. INSIDE LIMIT OF A SECTOR IN A ZONE 2. INSIDE LIMIT OF AN INCREMENTAL AREA (SEE FIGURES 5.21 THRU 5.23)

MATH SYMBOL	PROGRAM SYMBOL	UNIT	DESCRIPTION
R_{AO}	RAO	IN	RADIAL DISTANCE FROM MOTOR AXIS TO A POINT ON PERIMETER OF ANY SECTOR AT THICKNESS TAU AND LENGTH L=0 (FIGURE 5.21) DETERMINED IN SUBROUTINE AESUB.
R_{AT}	RAT	IN	RADIAL VECTOR FROM MOTOR AXIS TO A POINT IN A SECTOR FOR THE BLOCK 1 ANALYSIS OF THE HEAD-END WITH WEB, (FIGURE 5.21) AND 5.6) DETERMINED IN SUBROUTINE RAB.
R_{AX}	RAX	IN	RADIAL DISTANCE FROM MOTOR AXIS TO A POINT ON PERIMETER OF ANY SECTOR AT THICKNESS TAU AND LENGTH L=LX FOR THE STRAIGHT THROUGH GRAIN END SECTION ANALYSIS. (FIGURE 5.21) DETERMINED IN SUBROUTINE AESUB.
R_B	RB	IN/SEC	PROPELLANT BURNING RATE OF ISOTROPIC PROPELLANT.
	RBFLAG	- - -	BURNING RATE EQUATION CONTROL FLAG FOR AKR(2) AND AKR(36). INPUT ON CARD SET NUMBER 44. IF RBFLAG = 0.0, AKR(2) AND AKR(36) ARE INPUT IF RBFLAG = 1.0, AKR(2) AND AKR(36) = AKRST AT STEADY STATE.
	RBHI	IN/SEC	ISOTROPIC PROPELLANT BURNING RATE OF UPSTREAM INCREMENT DIVIDING PLANE
R_{Bslot}	RBSLOT	IN/SEC	BURNING RATE IN A SLOT.
	RBZTO	IN/SEC	INCREMENT DIVIDING PLANE ANISOTROPIC BURN RATE FOR SECTOR. VALUE IS EQUAL TO SECTOR 8 ANISOTROPIC BURN RATE DURING MOTOR TAIL-OFF.

MATH SYMBOL	PROGRAM SYMBOL	UNIT	DESCRIPTION
R ₈₇	RB7	IN/SEC	ANISOTROPIC PROPELLANT BURNING RATE IN SECTOR 7 DURING MOTOR TAIL-OFF.
R ₈₈	RB8	IN/SEC	ANISOTROPIC PROPELLANT BURNING RATE IN SECTOR 8 DURING MOTOR TAIL-OFF.
R _{E1}	RE1	IN	END SECTION CASE OPENING RADIUS DETERMINED IN SUBROUTINE ENDCS8. (RN1) AFT-HEAD (RH1) FORE-HEAD (FIGURE 5.35)
R _{E2}	RE2	IN	RADIAL DISTANCE FROM MOTOR AXIS TO INTERSECTION OF ELLIPTIC AND CONIC SECTION DETERMINED IN SUBROUTINE ENDCS8 (FIGURE 5.35)
R _f	RF	IN	OUTER RADIUS OF PROPELLANT.
	RFA THRU RFK	IN	REFERENCE PLANE OUTSIDE RADIUS OF PROPELLANT. INPUT ON CARD SET NUMBER 4.
R _{IG}	RIG	IN	IGNITER OPENING RADIUS. INPUT ON CARD SET NUMBER 29.
	RMOIHD	SLUG-SQ IN	FORE-HEAD GEOMETRY TABLE RECTANGULAR MOMENTS OF INERTIA (DEPENDENT VARIABLE). INPUT ON SUBSET CARD NUMBER 40-5.
	RMCIN	SLUG-SQ IN	AFT-HEAD GEOMETRY TABLE RECTANGULAR MOMENT OF INERTIA (DEPENDENT VARIABLE). INPUT ON SUBSET CARD NUMBER 40-6.
p ₁	ROE1		RADIUS OF CURVATURE OF POINT P1 DETERMINED IN SUBROUTINE ROE1SB FOR THE BLOCK 2A ANALYSIS OF HEAD-END WITH WEB.

MATH SYMBOL	PROGRAM SYMBOL	UNIT	DESCRIPTION
R ₀₃	R03	IN	RADIAL DISTANCE FROM MOTOR AXIS TO ORIGIN OF R3 FILLET RADIUS (FIGURE 5.26) DETERMINED IN SUBROUTINE PLNCNS.
R ₀₅	R05	IN	RADIAL DISTANCE FROM MOTOR AXIS TO ORIGIN OF R5 FILLET RADIUS (FIGURE 5.26) DETERMINED IN SUBROUTINE PLNCNS
R ₀₇	R07	IN	RADIAL DISTANCE FROM MOTOR AXIS TO ORIGIN OF R7 FILLET RADIUS (FIGURE 5.26) DETERMINED IN SUBROUTINE PLNCNS.
R ₀₉	R09	IN	RADIAL DISTANCE FROM MOTOR AXIS TO ORIGIN OF R9 FILLET RADIUS (FIGURE 5.26) DETERMINED IN SUBROUTINE PLNCNS
R ₀₁₁	R011	IN	RADIAL DISTANCE FROM MOTOR AXIS TO ORIGIN OF R11 FILLET RADIUS (FIGURE 5.26) DETERMINED IN SUBROUTINE PLNCNS.
R _{p1} thru R _{p13}	RP1 THRU RP13	IN	RADIAL DISTANCES DEFINING SECTOR BOUNDARIES FOR BLOCK 28 ANALYSIS OF HEAD-END WITH WEB. DETERMINED IN SUBROUTINE SCTOR1 (FIGURE 5.15)
R _{slotA}	RSLOTA	IN	RADIUS OF CASE AT SLOT AFT INTERFACE LOCATION AT PRIOR TIME INCREMENT. USED IN SR SLOT TO OBTAIN SLOT VOLUME.
R _{slotF}	RSLOTF	IN	RADIUS OF CASE AT SLOT FORWARD INTERFACE LOCATION AT PRIOR TIME INCREMENT. USED IN SUBROUTINE SLOT TO OBTAIN SLOT VOLUME.

MATH SYMBOL	PROGRAM SYMBOL	UNIT	DESCRIPTION
R _T	RT	IN	RADIUS OF CURVATURE OF PERIMETER IN ANY ZONE AT THICKNESS TAU. POSITIVE WHEN CENTER LIES INSIDE ZONE, NEGATIVE WHEN CENTER LIES OUTSIDE ZONE, AND ZERO WHEN PERIMETER HAS NO CURVATURE (FIGURES 5.20 THRU 5.22) DETERMINED IN SUBROUTINE ASESUB.
R ₁	R1	IN	RADIUS OF CURVATURE FROM MOTOR AXIS TO INNER STAR POINT. (FIGURE 5.25) DETERMINED IN SUBROUTINE PLNCNS.
R _{2A} thru R _{2K}	R2A THRU R2K	IN	RADIUS OF INNER GRAIN POINT OF REFERENCE PLANE. INPUT ON CARD SET NUMBER 13.
R _{3A} thru R _{3K}	R3A THRU R3K	IN	FILLET RADIUS BETWEEN SLOPES LA AND LB FOR A REFERENCE PLANE. INPUT ON CARD SET NUMBER 14.
R _{4A} thru R _{4K}	R4A THRU R4K	IN	FILLET RADIUS BETWEEN SLOPES LB AND LC FOR A REFERENCE PLANE. INPUT ON CARD SET NUMBER 15.
R _{5A} thru R _{5K}	R5A THRU R5K	IN	FILLET RADIUS BETWEEN SLOPE LC AND THE WEB FOR A REFERENCE PLANE. INPUT ON CARD SET NUMBER 16.
R _{6A} thru R _{6K}	R6A THRU R6K	IN	FILLET RADIUS BETWEEN THE WEB AND SLOPE LD FOR A REFERENCE PLANE. INPUT ON CARD SET NUMBER 17.
R _{7A} thru R _{7K}	R7A THRU R7K	IN	FILLET RADIUS BETWEEN SLOPES LD AND LE FOR A REFERENCE PLANE. INPUT ON CARD SET NUMBER 18.

MATH SYMBOL	PROGRAM SYMBOL	UNIT	DESCRIPTION
R8A thru R8K	R8A THRU R8K	IN	FILLET RADIUS BETWEEN FORKS OF FORKED WAGON WHEEL FOR A REFERENCE PLANE. INPUT ON CARD SET NUMBER 19.
R9	R9	IN	RADIUS OF CURVATURE FROM MOTOR AXIS TO OUTER STAR POINT (FIGURE 5.25) DETERMINED IN SUBROUTINE PLNCNS.
	SCUR	IN	CURRENT LOCATION OF THE SLOT INTERFACE FROM THE FORWARD TANGENT PLANE. SCUR(IIS,1) IS THE FORWARD INTERFACE AND SCUR(IIS,2) IS THE AFT INTERFACE LOCATION.
	SLTFLG	- - -	PROGRAM CONTROL FLAG TO INDICATE STATUS OF THE CURRENT SLOT WITH RESPECT TO THE CURRENT INCREMENT DIVIDING PLANE. 1 - THE CURRENT INCREMENT DIVIDING PLANE AND/OR THE Y REFERENCE PLANE ARE DOWNSTREAM OF THE CURRENT SLOT FORWARD INTERFACE. THE PROGRAM WILL SET THE WORKING INCREMENT DIVIDING PLANE TO THE SLOT FORWARD INTERFACE AND CHECK THE LOCATION OF THE Y REFERENCE PLANE. 2 - THE PROGRAM IS SEARCHING FOR THE Y REFERENCE PLANE THAT IS LOCATED DOWNSTREAM OF THE CURRENT SLOT FORWARD INTERFACE. 3+4 - THE PROGRAM IS SEARCHING FOR THE Y REFERENCE PLANE THAT IS LOCATED DOWNSTREAM OF THE CURRENT SLOT AFT INTERFACE. 5 - THE X AND Y REFERENCE PLANES HAVE BEEN UPDATED FOR THE AFT SLOT DETERMINE THE SLOT MASS BALANCE.

MATH SYMBOL	PROGRAM SYMBOL	UNIT	DESCRIPTION
	STDYST	--	CONTROL FLAG TO INDICATE STEADY STATE. INPUT ON CARD SET NUMBER 42.
	STFLAG	--	PROGRAM CONTROL FLAG FOR START TRANSIENT CALCULATIONS. IF STFLAG = 1.0, PERFORM TRANSIENT CALCULATIONS. INPUT ON CARD SET NUMBER 41.
	S1A THRU S11A	IN	SLOT FORWARD INTERFACE LOCATION FROM FORWARD TANGENT PLANE. INPUT ON CARD SET NUMBER 24 AND STORED IN SCUR(IIS,1).
	S1B THRU S11B	IN	SLOT AFT INTERFACE LOCATION FROM FORWARD TANGENT PLANE. INPUT ON CARD SET NUMBER 25 AND STORED IN SCUR(IIS,2).
	T	DEG RANKIN	COMBUSTION GAS STATIC TEMPERATURE.
	TAUAKR	IN	ANISOTROPIC BURN RATE COEFFICIENT TABLE INDEPENDENT VARIABLE. INPUT FOLLOWING CARD SET NUMBER 45.
τ_{EO}	TAUEO	IN	MAXIMUM BURNING DISTANCE IN STRAIGHT THROUGH GRAIN END SECTION (FIGURE 5.35) DETERMINED IN SUBROUTINE ENDCSE
τ_{EI}	TAUEI	IN	MAXIMUM BURNING DISTANCE IN STRAIGHT THROUGH GRAIN FND SECTION CONIC SECTION. (FIGURE 5.35) DETERMINED IN SUBROUTINE ENDCSR.
	TAUHD	IN	FORE-HEAD GEOMETRY TABLE INDEPENDENT VARIABLE (DISTANCE BURNED). INPUT ON SUBSET CARD NUMBER 40-5.

MATH SYMBOL	PROGRAM SYMBOL	UNIT	DESCRIPTION
τ_{max}	TAUM	IN	MAXIMUM BURNING DISTANCE FOR A REFERENCE PLANE. DETERMINED IN SUBROUTINE ENDCSB FROM THE GEOMETRY PLANE CONSTANTS.
	TAUN	IN	AFT-HEAD GEOMETRY TABLE INDEPENDENT VARIABLE (DISTANCE BURNED). INPUT ON SUBSET CARD NUMBER 40-6.
	TAUPLA THRU TAUPLK	IN	REFERENCE PLANE GEOMETRY TABLE DISTANCE BURNED (INDEPENDENT VARIABLE). INPUT ON SUBSET CARD NUMBER 40-7.
τ_{T0}	TAUTO	IN	ANISOTROPIC PROPELLANT THICKNESS. CALCULATED AT END OF START TRANSIENT IN SUBROUTINE SEGSUB. EQUAL TO TAUAKR (NTME).
	TAUTOV	IN	TEMPORARY VALUE FOR TAU0 IN SUBROUTINES LPDAPS AND AFPSUB
	TAUTOZ	IN	ANISOTROPIC PROPELLANT THICKNESS OVER INERT SLIVER IN SECTORS 3 AND 7.
	TAUWA THRU TAUWK	IN	REFERENCE PLANE WEB THICKNESS. INPUT ON CARD SET NUMBER 5.
	TAUWDP	IN	INCREMENT DIVIDING PLANE WEB THICKNESS.
	TAUX	IN	DISTANCE BURNED AT FORWARD REFERENCE PLANE. USED IN SR SEGSUB TO INTERPOLATE FOR INCREMENT DIVIDING PLANE DISTANCE BURNED.
	TAUXTO	IN	ANISOTROPIC PROPELLANT DISTANCE BURNED AT FORWARD TANGENT PLANE.

MATH SYMBOL	PROGRAM SYMBOL	UNIT	DESCRIPTION
	TAUY	IN	DISTANCE BURNED AT AFT REFERENCE PLANE.
	TAUYTO	IN	ANISOTROPIC PROPELLANT DISTANCE BURNED AT AFT TANGENT PLANE.
	TAUZTO	IN	TOTAL DISTANCE BURNED OF ANISOTROPIC PROPELLANT IN SECTORS 7 AND 8 DURING MOTOR TAIL-OFF.
	TCO _{0.9}	°R RANKIN	TABULAR INPUT VALUE OF COMBUSTION TEMPERATURE OF PROPELLANT GAS (DEPENDENT VARIABLE). INPUT FOLLOWING CARD SET NUMBER 39.
	TDMAX	IN	MAXIMUM BURNING DISTANCE IN THE FORE-HEAD WITH A HEAD-END WEB. DETERMINED IN SUBROUTINE SCIDUF NG THE INITIAL INTEGRATION FOR THE BURNING SURFACE AREA IN THE BLOCK 1 ANALYSIS. EQUAL IN VALUE TO TAUMA OR DO3 FOR AN INTEGRATION PLANE.
θ_o	THO	RADIANS	CENTRAL ANGLE OF SLOTTED- CONE GRAIN CONFIGURATION TO DEFINE LOCATION OF ONE-HALF OF SLOT IN ONE GRAIN CROSS SECTION SYMMETRICAL PART.
θ_{oA} thru θ_{oK}	THOA THRU THOK	DEGREES	REFERENCE PLANE SLOTTED-CONE GRAIN CONFIGURATION CENTRAL ANGLE. INPUT ON CARD SET NUMBER 23.
	THOW	RADIANS	WORKING INCREMENT DIVIDING PLANE SLOTTED-CONE GRAIN CONFIGURATION CONTRAL ANGLE.
θ_R	THR	RADIANS	ANGLE BETWEEN Z-AXIS AND A RADIAL VECTOR FROM MOTOR AXIS TO A POINT ON A SECTOR. DETERMINED IN SUBROUTINE THETAR (FIGURE 5.3)

MATH SYMBOL	PROGRAM SYMBOL	UNIT	DESCRIPTION
θ_{R1}	THR1	RADIANS	ANGLE BETWEEN Z-AXIS AND A RADIAL VECTOR FROM MOTOR AXIS TO A POINT ON A SECTOR. DETERMINED IN SUBROUTINE XRTHR (FIGURE 5.16)
θ_{R0}	THR0	IN	ANGLE BETWEEN Z-AXIS AND RADIAL VECTOR RAO.
θ_{slv}	THSLV	DEGREES	HALF ANGLE OF INERT SLIVER SECTOR OF INCREMENT DIVIDING PLANE IN SUBROUTINE SEGSUB
θ_{slva} thru θ_{slvk}	THSLVA THRU THSLVK	DEGREES	REFERENCE FRAME INERT SLIVER SECTOR HALF ANGLE.
	THSLVV	DEGREES	INCREMENT DIVIDING PLANE INERT SLIVER SECTOR HALF ANGLE IN SUBROUTINE AFPSUB.
	THSLVX AND THSLVY	DEGREES	REFERENCE FRAME SECTOR HALF ANGLE IN SUBROUTINE SEGSUB.
θ_1	TH1	RADIANS	GEOMETRY CONSTANT DETERMINED IN SUBROUTINE PLNCNS (FIGURE 5.25)
θ_2	TH2	RADIANS	GEOMETRY CONSTANT DETERMINED IN SUBROUTINE PLNCNS. (FIGURE 5.25)
θ_3	TH3	RADIANS	GEOMETRY CONSTANT DETERMINED IN SUBROUTINE PLNCNS. (FIGURE 5.25)
θ_4	TH4	RADIANS	GEOMETRY CONSTANT DETERMINED IN SUBROUTINE PLNCNS. (FIGURE 5.25)
	TIMAX	SEC	MAXIMUM VALUE OF TIME. IF TIME IS GREATER THAN OR EQUAL TO TIMAX, PROGRAM EXECUTION WILL TERMINATE FOR THE CASE. INPUT ON CARD SET NUMBER 41.

MATH SYMBOL	PROGRAM SYMBOL	UNIT	DESCRIPTION
	TIMEAC	SEC	ACCELERATION-TIME CURVE INDEPENDENT VARIABLE. INPUT FOLLOWING CARD SET NUMBER 47.
	TIMEPH	SEC	HEAD END PRESSURE CURVE INDEPENDENT VARIABLE. INPUT FOLLOWING CARD SET NUMBER 44.
	TIMEPS	SEC	MEASURED CASE STRAIN DATA TABLE INDEPENDENT VARIABLE. INPUT FOLLOWING CARD SET NUMBER 46.
	TITL	- - -	STORAGE ARRAY FOR CASE TITLE FIELD DATA CODE. INPUT ON CARD SET NUMBER 50.
T_o	TO	DEG RANKIN	PROPELLANT GAS COMBUSTION TEMPERATURE. INPUT ON CARD SET NUMBER 38.
	TOFLAG	- - -	PROGRAM CONTROL FLAG TO SIGNAL SUBROUTINE RBSUB TO COMPUTE BURN RATE FROM ANISOTROPIC BURN RATE COEFFICIENT TABLE. SET IN SUBROUTINE SEG SUB TO COMPUTE BURN RATE OVER INERT SLIVER IN SECTORS 6 AND 7 AND SET IN SUBROUTINE MNCHN4 TO COMPUTE BURN RATE IN FORE AND AFT DOMES DURING TAIL-OFF.
	TPR	- - -	PRESSURE RATIO OF NOZZLE TOTAL PRESSURE TO HEAD END TOTAL PRESSURE. USED IN SUBROUTINE RBSTSB TO DETERMINE FIRST ITERATION VALUE OF AKRST FOR EACH TIME INCREMENT. INPUT ON CARD SET NUMBER 44.
τ_{slotA}	TSLOTA	IN	ONE PAST TIME VALUE OF LATERAL DISTANCE BURNED IN A SLOT FORWARD INTERFACE. USED IN CONJUNCTION WITH SKA TO DEFINE SLOT INTERFACE LOCATION AND TO DETERMINE DV/DI OF A SLOT.
τ_{slotF}	TSLOTF	IN	ONE PAST TIME VALUE OF LATERAL DISTANCE BURNED IN A SLOT FORWARD INTERFACE.

MATH SYMBOL	PROGRAM SYMBOL	UNIT	DESCRIPTION
	TSLVR	IN	INERT SLIVER RADIUS FROM R5 FILLET TO INERT SLIVER IN SUBROUTINE SEG SUB.
	TSLVRA THRU TSLVRK	IN	DISTANCE FROM CORE INTERFACE TO INERT SLIVER FOR A REFERENCE PLANE. INPUT ON CARD SET NUMBER 26.
	TSLVRN	IN	SLIVER RADIUS OF REFERENCE PLANE ADJACENT TO NOZZLE SECTION. DETERMINED BY SUBROUTINE SEG SUB FOR USE IN SUBROUTINE TISUB TO LIMIT TAUZTQ(NI) TO SLIVER RADIUS.
	TSLVRV	IN	INERT SLIVER RADIUS OF INCREMENT DIVIDING PLANE IN SUBROUTINE AFPSUB.
	TSLVRX	IN	INERT SLIVER RADIUS OF CURRENT REFERENCE PLANE IN SUBROUTINE SEG SUB.
	TSLVRY	IN	INERT SLIVER RADIUS OF NEXT REFERENCE PLANE IN SUBROUTINE SEG SUB.
	TST	SEC	START TIME. USED AS OPTION IN SUBROUTINE MNCHN4 TO TERMINATE START TRANSIENT INTERVAL. INPUT ON CARD SET NUMBER 41.
	TV6PR	IN	REFERENCE PLANE SLOTTED-CONE GRAIN CONFIGURATION GEOMETRY CONSTANT. DISTANCE BETWEEN SIDE LC AND CASE WALL MEASURED ALONG A PERPENDICULAR LINE TO LC AT THE INTERSECTION OF LC WITH RADIUS R5.
	TV7PR	IN	REFERENCE PLANE SLOTTED-CONE GRAIN CONFIGURATION GEOMETRY CONSTANT. DISTANCE ALONG LINE TV6PR WHERE SIDE LC DISAPPEARS AS A RESULT OF PROGRESSION OF BURNING SURFACE OF SLOTTED-CONE.

MATH SYMBOL	PROGRAM SYMBOL	UNIT	DESCRIPTION
T_{2max}	T2M	IN	MAXIMUM BURNING DISTANCE FOR A SECTOR DETERMINED IN SUBROUTINE PLNCNS (FIGURE 5.25)
.	T4M		
.	T5M		
.	T6M		
	T7M		
	T9M		
	T10M		
T_{12max}	T12M		
	U	FT/SEC	VELOCITY OF GAS IN CONTROL VOLUME.
	V	CU IN	PRESENT TIME GAS VOLUME OF INCREMENT DIVIDING SECTION. USED IN SUBROUTINE AIBST TO COMPUTE PD.
V_{CE}	VCE	CU IN	VOLUME OF CASE IN REFERENCE END SECTION DETERMINED IN SUBROUTINE ENDCSB.
	VCHINP	CU IN	VOLUME OF FORE-HEAD CASE. INPUT ON CARD SET NUMBER 40.
	VCNINP	CU IN	VOLUME OF AFT-HEAD CASE. INPUT ON CARD SET NUMBER 40.
V_{EH}	VEH	CU IN	INITIAL VOLUME OF PROPELLANT BETWEEN TWO OBLATE SPHEROIDS. DETERMINED IN SUBROUTINE VOLSUB FOR THE BLOCK 3 ANALYSIS OF THE HEAD-END WITH WEB.
V_{FH0}	VFHO	CU IN	INITIAL PROPELLANT VOLUME IN FORE-HEAD. INPUT ON CARD SET NUMBER 40.
V'_{FH}	VFHPR	CU IN	PREVIOUS TIME VALUE OF HEAD-END FUEL VOLUME.
	VFI	CU IN	VOLUME OF FUEL IN INCREMENT DIVIDING PLANE.

MATH SYMBOL	PROGRAM SYMBOL	UNIT	DESCRIPTION
V_{fno}	VFNO	CU IN	INITIAL PROPELLANT VOLUME IN AFT-HEAD. INPUT ON CARD SET NUMBER 40.
	VOLCH	CU IN	TOTAL HEAD END VOLUME CONSUMED.
	VOLCHO	CU IN	PREVIOUS TIME VALUE OF HEAD END VOLUME CONSUMED.
	VOLCN	CU IN	TOTAL NOZZLE END VOLUME CONSUMED.
	VOLCNO	CU IN	PREVIOUS VALUE OF NOZZLE-END TOTAL VOLUME CONSUMED.
	VPH	CU IN	FREE GAS VOLUME OF HEAD END SECTION.
	VPN	CU IN	FREE GAS VOLUME OF NOZZLE END SECTION.
V'	VPR	CU IN	PREVIOUS TIME VALUE OF INCREMENT DIVIDING SECTION GAS VOLUME.
V_{slvr}	VSLVR	CU IN	VOLUME OF INERT SLIVER.
\dot{W}_D	WDOTD	LB/SEC	TRANSIENT DISCHARGE WEIGHT FLOW FROM INCREMENT DIVIDING SECTION.
\dot{W}_{Dslot}	WDSLOT	LB/SEC	DISCHARGE MASS FLOW OF A SLOT.
\dot{W}_{Islot}	WISLOT	LB/SEC	INLET MASS FLOW OF A SLOT.
	XCGHD	IN	FORE-HEAD GEOMETRY TABLE CENTER OF GRAVITY LOCATION FROM FORWARD TANGENT PLANE (DEPENDENT VARIABLE). INPUT ON SUBSET CARD NUMBER 40-5.
	XCGN	IN	AFT-HEAD GEOMETRY TABLE CENTER OF GRAVITY LOCATION FROM AFT TANGENT PLANE (DEPENDENT VARIABLE). INPUT ON SUBSET CARD NUMBER 40-6.

MATH SYMBOL	PROGRAM SYMBOL	UNIT	DESCRIPTION
		IN	X-COORDINATE OF ORIGIN OF CIRCULAR ARC USED IN CALCULATION OF AFT-END SECTOR AREA IN SUBROUTINE ASESUB
X03	X03	IN	X-COORNDINATE OF R3 FILLET RADIUS (FIGURE 5.26) DETERMINED IN SUBROUTINE PLNCNS.
X05	X05	IN	X-COORDINATE OF R5 FILLET RADIUS (FIGURE 5.26) DETERMINED IN SUBROUTINE PLNCNS.
X07	X07	IN	X-COORDINATE OF R7 FILLET RADIUS (FIGURE 5.26) DETERMINED IN SUBROUTINE PLNCNS.
X09	X09	IN	X-COORDINATE OF R9 FILLET RADIUS (FIGURE 5.26) DETERMINED IN SUBROUTINE PLNCNS.
X011	X011	IN	X-COORDINATE OF R11 FILLET RADIUS (FIGURE 5.26) DETERMINED IN SUBROUTINE PLNCNS.
X _R	XR	IN	X-COORDINATE OF A POINT ON THE PERIMETER OF A SECTOR. DETERMINED IN SUBROUTINE XRSUR FOR THE END SECTION STRAIGHT THROUGH GRAIN ANALYSIS
X _{ra}		IN	X-COORDINATE OF A POINT ON THE PERIMETER OF A SECTOR FOR THE BLOCK 1 ANALYSIS OF THE HEAD-END WITH WEB. (FIGURE 5.3) DETERMINED IN SUBROUTINE XRSUBB.
X _{rf}		IN	X-COORDINATE OF A POINT ON THE PERIMETER OF A SECTOR FOR THE BLOCK 2R ANALYSIS OF THE HEAD-END WITH WEB (FIGURE 5.16) DETERMINED IN SUBROUTIN XRSUBB.

MATH SYMBOL	PROGRAM SYMBOL	UNIT	DESCRIPTION
X_{Rmin}		IN	X-COORDINATE OF A POINT ON THE PERIMETER OF ANY SECTOR AT THICKNESS TAU AND RA=RAMIN(FIGURE 5.21)
X_{RO}	XRO	IN	X-COORDINATE OF THE POINT ON THE PERIMETER OF ANY SECTOR AT THICKNESS TAU AND RA=RAO. (FIGURE 5.21)
X_{RX}		IN	X-COORDINATE OF A POINT ON THE PERIMETER OF ANY SECTOR AT THICKNESS TAU AND RA=RAX. (FIGURE 5.21)
X_{45}	X45	IN	GEOMETRY CONSTANT WHICH DEFINES THE X-COORDINATE OF THE POINT LOCATED ALONG LINE 16 MAX AT THE DISTANCE R5 FROM SIDE LC (FIGURE 5.25) DETERMINED IN SUBROUTINE PLNCNS
X_{76}	X76	IN	GEOMETRY CONSTANT WHICH DEFINES THE X-COORDINATE OF THE POINT LOCATED ALONG LINE 112 MAX AT THE DISTANCE R6 FROM SIDE LD (FIGURE 5.25) DETERMINED IN SUBROUTINE PLNCNS
Y_{Amax}		IN	Y-COORDINATE CORRESPONDING TO XRMAX (FIGURE 5.21)
Y_{AmIn}		IN	Y-COORDINATE CORRESPONDING TO XRMIN (FIGURE 5.21)
Y_{AO}		IN	Y-COORDINATE CORRESPONDING TO XRO (FIGURE 5.21)
Y_{AX}		IN	Y-COORDINATE CORRESPONDING TO XRX (FIGURE 5.21)

PATH SYMBOL	PROGRAM SYMBOL	UNIT	DESCRIPTION
Y _{NO}	YNO	IN	Y-INTERCEPT OF LINE NORMAL TO INNER ELLIPSE AT RADIUS RIG WHICH IS USED TO DETERMINE ANGLE BETWEEN Y-AXIS AND NORMAL LINE IN SUBROUTINE AIGSUR (FIGURE 5.14)
Y _{0A}	Y0A	IN	Y-COORDINATE OF THE P0 POINT FOR PLANE A.
Y _{0B}	Y0B	IN	Y-COORDINATE OF THE P0 POINT FOR PLANE B.
		IN	Y-COORDINATE OF ORIGIN OF CIRCULAR ARC USED IN CALCULATION OF AFT-END SECTOR AREA IN SUBROUTINE ASESUR.
Y ₀₃	Y03	IN	Y-COORDINATE OF R3 FILLET RADIUS (FIGURE 5.26) DETERMINED IN SUBROUTINE PLNCNS
Y ₀₅	Y05	IN	Y-COORDINATE OF R5 FILLET RADIUS (FIGURE 5.26) DETERMINED IN SUBROUTINE PLNCNS
Y ₀₇	Y07	IN	Y-COORDINATE OF R7 FILLET RADIUS (FIGURE 5.26) DETERMINED IN SUBROUTINE PLNCNS
Y ₀₉	Y09	IN	Y-COORDINATE OF R9 FILLET RADIUS (FIGURE 5.26) DETERMINED IN SUBROUTINE PLNCNS
Y ₀₁₁	Y011	IN	Y-COORDINATE OF R11 FILLET RADIUS (FIGURE 5.26) DETERMINED IN SUBROUTINE PLNCNS.
Y ₄₅	Y45	IN	GEOMETRY CONSTANT WHICH DEFINES THE Y-COORDINATE OF THE POINT LOCATED ALONG LINE T6 MAX AT THE DISTANCE R5 FROM SIDE LC (FIGURE 5.25) DETERMINED IN SUBROUTINE PLNCNS.

MATH SYMBOL	PROGRAM SYMBOL	UNIT	DESCRIPTION
r_{76}	r_{76}	IN	GEOMETRY CONSTANT WHICH DEFINES THE Y-COORDINATE OF THE POINT LOCATED ALONG THE LINE T12 MAX AT THE DISTANCE R6 FROM SIDE LD (FIGURE 5.25) DETERMINED IN SUBROUTINE PLNCNS.
	ZCALC(I)	IN	STOREAGE ARRAY OF INCREMENT DIVIDING PLANE LOCATIONS.
z_{1a}	z_{1a}	IN	(1) DISTANCE FROM CENTER OF ELLIPSE TO POINT ON OUTER ELLIPSE (FIGURE 5.6) (2) CODE USED IN SUBROUTINE P3SUB.
α_v		RADIANS	ANGLE BETWEEN BISECTOR OF PROPELLANT TIP AND STRAIGHT SIDE SECTOR USED IN CALCULATION OF AFT-END SECTOR AREA IN SUBROUTINE ASESUB.

The major modifications to the original Thiokol Chemical Corporation (TCC) program made by Boeing were done during the HIBEX program. HIBEX stands for "High G Boost Experiment." Because of its extreme flight environment and a new stapled high burning rate propellant, it was not known if the internal ballistics of the HIBEX motor would be affected, i.e., ignition transient interval, maximum chamber pressure, motor burn time, and shape of the chamber pressure-time trace. Accordingly, program modifications were made as discussed in Section 1.1.

Resulting predictions using these modifications were compared with measured results. The dimensionless fore-head pressure-time traces are shown in Figure 7.1. The prediction indicates good agreement with the results of three full scale motor firings. During the HIBEX program, various grain configurations, propellant formulations, and nozzle throat sizes were used. The three firings for which data are shown in Figure 7.1 are from identical motor configurations.

Security classification of the HIBEX program prohibits the discussion of specific numerical results in this unclassified report. Initial analysis that was conducted is reported in Reference 4, and an updated analysis using an anisotropic burning rate model developed from small scale "Forty-Pound Charge" (FPC) motor firings to predict the traces shown in Figure 7.1 is discussed in Reference 5.

Figure 7.2 shows the influence of internal gas flow along the propellant grain and the propellant burning rate model on ballistic predictions. Curve A is based on steady internal flow and isotropic burning. Curve B is based on non-steady internal flow and isotropic burning. Curve C represents use of the complete program capability except for an accelerating reference system. It is based on non-steady, internal flow and anisotropic burning during ignition and talloff. The method of solution for these and other program options are discussed in Section 8.1.

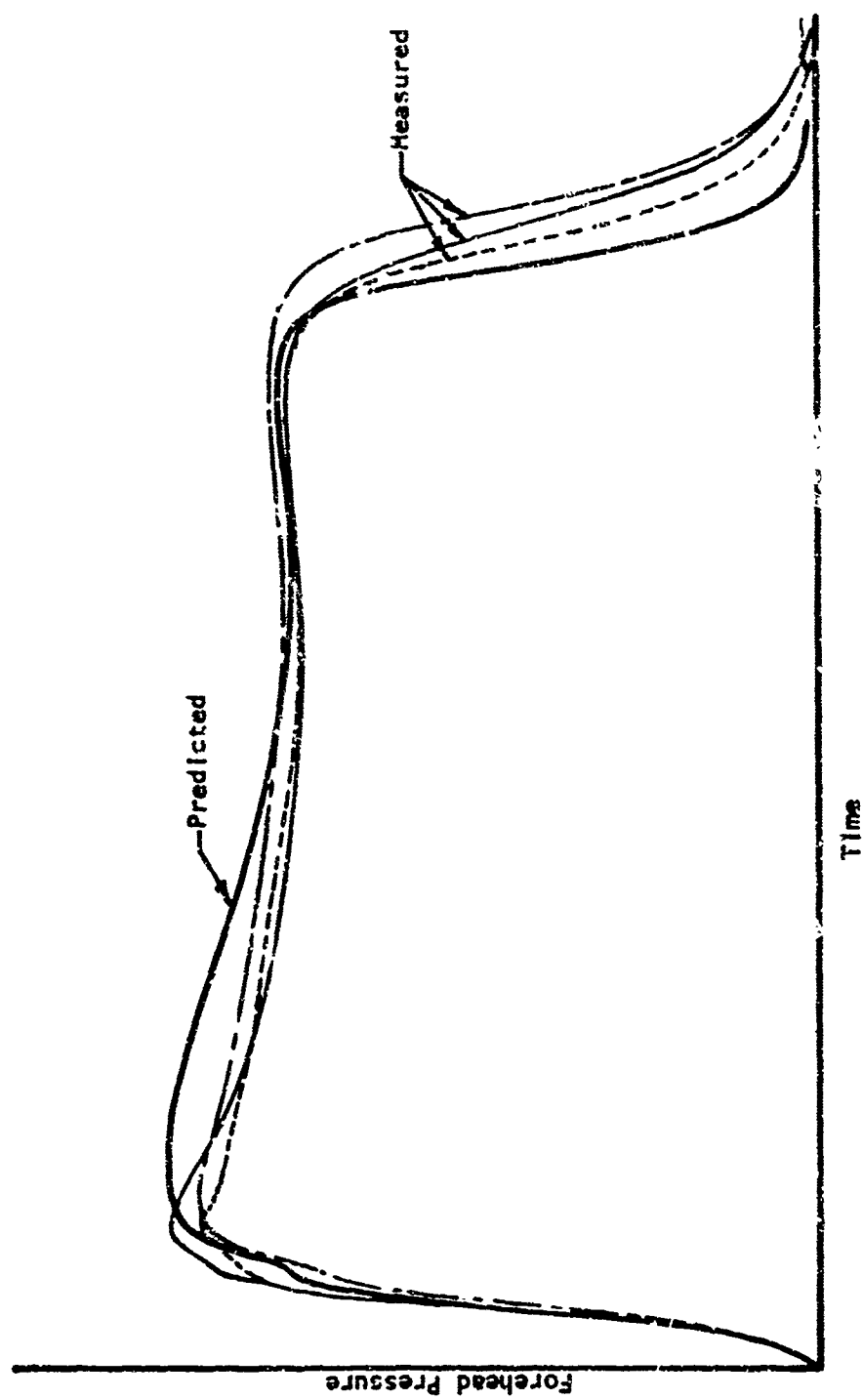


Figure 7.1. HIBEX Forehead Chamber Pressure Trace

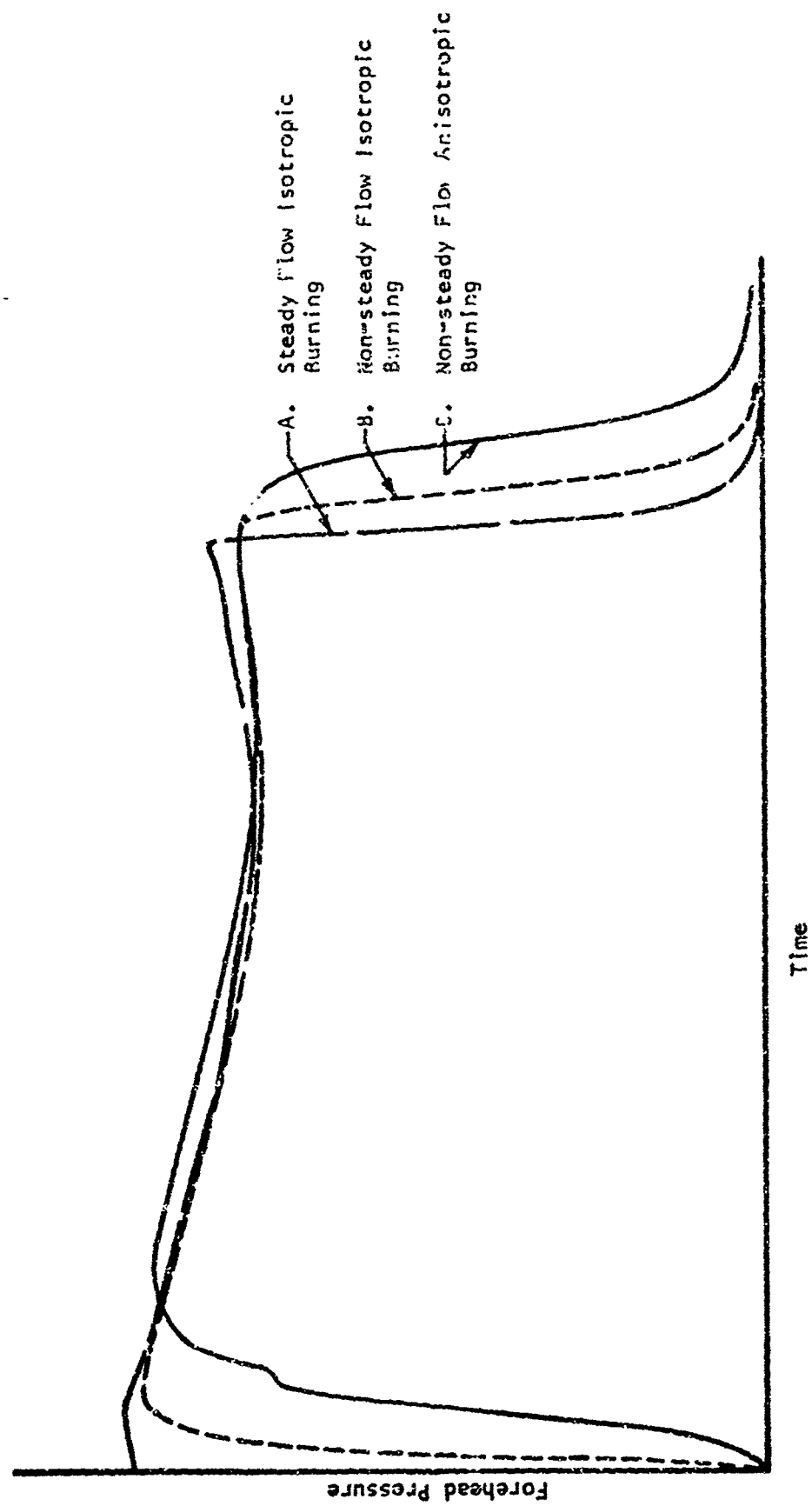


Figure 7.2. Influence of Internal Flow and Burning Rate Model